Harnessing Biological half reactions for organic synthesis



A thesis submitted to the Board of the Faculty of Physical Sciences, for

the degree of Doctor of Philosophy, University of Oxford

Charlotte Hancox

The Queens College

Acknowledgements

Firstly, I would like to thank Professor Kylie Vincent for the opportunity to be part of her exciting research. Special thanks to Dr Tim Sudemeier, a brilliant and inspirational chemist who supported me and guided my project thorughout the pandemic. Thanks also to Dr Beatriz Dominguez and Dr Sarah Montgomery at Johnson Matthey for their supervision and supporting my project.

A particular mention has to go to my amazingly supportive family for putting up with me throughout my DPhil journey. My husband Chris for his unwavering support, without which I would be unable to do any of this. A big thanks to my wonderful children Georgia, Milly, Adam and Evalyn, I love you all and none of this would have been possible without you.

Huge thanks to Dr Holly Reeve for being the most inspirational woman I have ever had the pleasure to work with. Thank you for all of your support throughout my DPhil, for knowing when I needed a kick, and when I needed picking me up. For always being so positive and encouraging. To Dr Sara Cleary for so many things, not least for sharing her organic chemistry knowledge (which is vast), I look forward to sharing a Sassi's with you soon! Dr Non Evans for her advice, friendship and support. Special thanks go to the whole team at HydRegen, I loved working with you all.

A massive thank you to my good friend Cath Brown who has been instrumental to my success throughout both my undergraduate degree and DPhil. Thank you for your advice, help and for always being there to listen. I appreciate you more than you will ever know.

To Kelly Britton, who has shared both my OU Journey an d my Oxford University journey, I could not have done this without you. You have been at my side throughout, to motivate me when I am

flagging, give me a kick when I need it and drag me to many social events that I would otherwise not have gone to! I thank you from the bottom of my heart.

To my dear friend Dr Julia Vallejo - the most brilliant inorganic chemist. Thank you for all of constant support throughout my DPhil journey. You are the person who picked me up when the going was tough and always believed in me – even when I doubted myself.

To my favourite twins Lois and Kathryn for their friendship, support and for always being on hand to say the right thing and make me smile. Both of you have always given me encouragement and the belief that I could do this, even though neither of you have a clue what it is I'm doing!

There are so many people to thank at the Open University, for making this dream possible for me and I give thanks in no particular order. I had some fantastic tutors, but those that deserve a particular mention are Dr Jenny Faulkner for supporting me through my final year, I would not be where I am without you. Dr Sarah Howcutt the tutor who inspired me to study chemistry in the first place. Dr Sue Armstrong for answering my endless queries and always pushing me that little bit further. To Professor Eleanor Crabb for constant support throughout my OU journey. Dr Nick Chatterton for taking a chance on me and supervising me during my first summer internship and the first person to ever make me believe I was capable of doing a PhD. Then of course Dr Simon Collinson for all of his help and support through my final couple of years of study. For his supervision during my summer internship and presenting at my first conference, not to mention his guidance during my PhD applications.

Many many other people have helped me along the way, and to all of you I give my heartfelt thanks.

Abstract

The work in this Thesis addresses one of the challenges associated with incorporating biocatalysis into industrial processes. This project develops a new way of implementing biocatalysis for industrial biotechnology in clean electrochemical reactors. Enzymes dependent on the cofactor NAD(P)H are used widely in industrial chemical synthesis, particularly for the manufacture of fine chemicals and pharmaceuticals where single enantiomers are often required. This is due to their ability to catalyse reactions with exquisite selectivity and they operate until mild aqueous conditions. One of the limitations to implementing redox biocatalysis for industrial applications is the requirement for a reducing equivalent, usually in the form of expensive nicotinamide cofactors NAD(P)H, which are required in stoichiometric quantities.

Existing cofactor regeneration methods require the use of a second enzyme to recycle the cofactor requiring stoichiometric quantities of a sacrificial substrate such as glucose or isopropanol. This not only creates difficulties around product separation but generates large amounts of carbon-based waste which is undesirable when companies are looking to make processes cleaner. In order to provide more sustainable routes to implementing biotechnology, improved cofactor recycling systems are crucial. Electroenzymatic NAD(P)H and $NAD(P)^+$ recycling represents one attractive alternative for greener chemistry because it uses electrons as a clean reductant. If adopted for industrial applications, this could harness green electricity sources such as solar and wind power. Another approach developed here skips NAD^+ and supplies enzymes with electrochemically reduced flavin instead. A third approach uses cofactor-free biocatalytic hydrogenation for nitro-group reductions. These methods would offer a more sustainable way to synthesise small molecules.

Abbreviations

ADH	alcohol dehydrogenase
BP	Carbon black pearl 2000
CE	counter electrode
CV	cyclic voltammogram
DMSO	dimethyl sulfoxide
E	electrode potential
e	charge of an electron
E. coli	*Escherichia coli*
ee	*enantiomeric excess*
F	Faraday's constant = 96,485 C mol^{-1}
FAD	flavin adenine dineucliotide
FMN	flavin mononucleotide
GDH	glucose dehydrogenase
HoxFU	NAD^+-reducing subunits of the soluble hydrogenase
Hox~~HY~~FU	varient of the soluble hydrogenase with inactive hydrogenase dimer
HPLC	high performance liquid chromotography
K_M	Michaelis constant
KP_i	potassium phosphate buffer
LDH	lactate dehydrogenase
N_A	Avagadro constant
NAD^+	nicotinamide adenine dinucleotide (oxidised)
NADH	nicotinamide adenine dinucleotide hydride (reduced)
$NADP^+$	nicotinamide adenine dinucleotide phosphate (oxidised)
NADPH	nicotinamide adenine dinucleotide phosphate hydride (reduced)
PFE	protein film electrochemistry
PG	pyrolytic graphite
PGE	pyrolytic graphite 'edge'
Q	charge
R	the gas constant = 8.314 J K^{-1} mol^{-1}
R. eutropha (*R. e*)	*Ralstonia eutropha*
RDE	rotating disk electrode
RE	reference electrode
RF	riboflavin
r_t	retention time
SCE	saturated calomel electrode
SH	soluble hydrogenase
SHE	standard hydrogen electrode
TOF	turnover frequency (number of product generated per second per enzyme)
TN	turnover number (moles product generated per mole cofactor used)
TTN	total turnover number (number of product generated per

	enzyme)
U mg^{-1}	units mg^{-1} = µmole min^{-1} mg^{-1}
UV-Vis	ultraviolet-visible
WE	working electrode
WT	wild type
ε	extinction coefficient

Table of Contents

Biological half reactions for organic synthesis **1**

Acknowledgements **3**

Abstract ..... **vii**

Abbreviations ..... **ix**

Table of Contents ..... **xi**

1 Introduction **1**

1.1 Electrosynthesis 4

1.2 Flow Chemistry 4

1.2.1 Biocatalytic synthesis in flow 5

1.3 Redox biocatalysis 6

1.3.1 Using stoichiometric sacrificial reductants 6

1.4 Cofactors 7

1.4.1 Nicotinamides 7

1.4.2 Flavins 8

1.5 Existing methods for cofactor regeneration 10

1.5.1 H_2-driven NADH regeneration 11

1.5.2 Methods for NADPH regeneration 13

1.5.3 H_2-driven flavin recycling 14

1.5.4 Electrochemical NAD^+ reduction 15

1.5.5 Direct electrochemical reduction 16

1.6 The concept of this project 17

Chapter 1 Bibliography **20**

2 Theory and Methods **25**

2.1 Electrochemistry 26

2.1.1 The Nernst equation 27

2.1.2 Standard Hydrogen Electrode 27

2.1.3 Protein Film Electrochemistry[2,3] 27

2.2 Electrochemical setup 31

2.2.1 Three-electrode system 31

2.2.2 Working electrodes – for analytical electrochemistry 32

2.2.3 Reference electrodes 34

2.2.4 Counter electrode 35
2.2.5 Electrochemical cells 36
2.3 Electrochemical techniques 37
2.3.1 The electrode-solution interface 37
2.3.2 The electrical double layer 37
2.3.3 The diffuse layer 38
2.3.4 Cyclic voltammetry 39
2.3.5 Chronoamperometry 41
2.4 High surface area electrodes 42
2.4.1 Materials used for high surface area electrodes 42
2.4.2 Protocol for enzyme-modified particles 43
2.5 Enzyme kinetics and electrochemical analysis 44
2.5.1 Affinity constant (K_M) 44
2.6 Ultraviolet-visible spectroscopy (UV-Vis) 46
2.6.1 Electronic transitions in cofactor molecules 46
2.6.2 Concentration determination using the Beer Lambert Law 49
2.7 Gas Chromatography-Flame Ionisation Detection (GC-FID) 50
2.8 Reagents 52
2.8.1 Buffers 52
2.8.2 Cofactors 53
2.9 Enzyme samples 53
Chapter 2 Bibliography 54
3 Preliminary electrochemistry 59
3.1 Introduction 60
3.2 Isolation of the Ht HoxFU moiety 61
3.3 Electrochemical characterisation 61
3.4 NAD+/NADH cycling 61
3.5 Michaelis-Menten kinetics 63
3.5.1 Determination of the affinity constant K_M with NAD^+ 63
3.5.2 Control experiment 65
3.6 pH dependence 66
3.6.1 Cyclic voltammetry pH experiments in mixed buffer 67
3.6.2 Shift in thermodynamic potential 67
3.6.3 Measuring the catalytic current 68

3.7 Temperature 71
3.8 Stability 73
3.8.1 Stability over an extended time period 74
3.9 Solvent tolerance of *Ht* HoxFU 75
3.10 Methods for electrochemically testing solvent tolerance 76
3.11 Sodium inhibition of *Ht* HoxFU 80
3.12 Electrosynthesis of NADH 81
3.12.1 High surface area electrodes 81
3.13 Quantifying the synthesis of NADH 82
3.14 Scope for NADPH recycling 84
3.14.1 C=N reduction via imine reductases 85
3.15 Mutagenesis of Ht HoxFU 86
3.15.1 Activity assays for mHoxFU 88
3.16 Catalytic activity of mHoxFU with NAD(P)H 89
3.17 Electrochemical characterisation of mHoxFU 90
3.18 Confirming $NADP^+$ reduction 91
3.19 Comparison of mHoxFU to Ht HoxFU 92
3.20 Developing an H_2-driven NADPH generation catalyst 93
3.20.1 Comparison of HoxFU activities 94
3.21 NADPH generation and optimising [$NADP^+$] 96
3.22 The effect of temperature on mHoxFU-Hyd1 particles 98
3.22.1 The ratio of mHoxFU-Hyd1 to carbon 100
3.22.2 Reduction of acetophenone in batch 101
3.22.3 Coupling Acetophenone reduction to NADPH recycling 104
3.23 H_2-driven imine reductions 105
3.24 Imine reduction in an NADPH recycling system 108
3.25 Summary 111

Chapter 3 Bibliography 112

4 Evaluation of electrochemical flavin recycling 115

4.1 Introduction 116
4.2 Electrochemical flavin reduction 116
4.3 Preliminary flavin reduction 117
4.4 Preliminary electrochemical characterization of FMN and FAD 119
4.5 Chronoamperometry experiments to determine if electrochemically FMNH2 and FADH2

are biologically active. 121
4.6 Evolution of the crude electrochemical cell 122
4.7 Electrochemical FAD reduction on carbon felt with ex situ spectroscopy 125
4.8 Considerations for recycling FMN 127
4.9 Electrochemical reduction of FMN 129
4.9.1 Coupling electrochemical $FMNH_2$ regeneration to a biocatalytic hydrogenation using ENE-108 131
4.9.2 Increasing the concentration of substrate 132
4.10 Riboflavin 134
4.10.1 Preliminary electrochemical testing of riboflavin 135
4.10.1 Complete electrochemical reduction of riboflavin 136
4.11 Coupling electrochemical riboflavin reduction to ENE-red 137
4.12 Summary 139
Chapter 4 Bibliography 140
5 Scale-up of flavin recycling 143
5.1 Introduction 144
5.2 Optimise conditions in batch 145
5.3 Solvent control experiments. 145
5.3.1 Investigating the effect of applied potential on the reaction 148
5.3.2 Dosing experiments to improve conversion 150
5.4 Bespoke electrochemical cell 152
5.1.1 Results from RedoxMe cell experiments 153
5.1.2 Scale up of electrochemical flavin-driven ENE-reduction in batch 156
5.5 Electrosynthesis in flow 159
5.5.1 Electrochemical cofactor recycling in flow 160
5.5.2 Development of high surface area electrodes 160
5.5.3 Immobilising ENE-reductase enzyme on an electrode 164
5.5.3.i Using polymyxin as co-adsorbate 165
5.6 Electrochemical recycling of riboflavin in flow 168
5.7 Summary and further work 170
Chapter 5 Bibliography 172
6 Library Building tool for Medicinal Chemists 173
6.1 Introduction 174
6.2 Compound selection and analytics 177

6.2.1 Compound selection 177
6.3 Solubility 180
6.4 Analytical methods 181
6.4.1 UV-Vis spectroscopy for nitro-to-amine conversions 181
6.4.2 High Performance Liquid Chromatography (HPLC) 182
6.5 NMR 185
6.6 Continuous synthesis of aminophenol 185
6.7 Continuous flow of successive compounds as a semi-preparative screening tool. 188
6.8 Control experiment 193
6.9 Catalyst loading 195
6.10 Catalyst stability 197
6.11 Intermediates 199
6.12 Increasing solubility of hydrophobic compounds 201
6.13 Effect of flow rate on conversion. 202
6.14 Effect of concentration on conversion. 204
6.15 Increasing catalyst 205
6.16 Optimising tricky compounds 207
6.17 Mesalazine 210
6.18 Selecting an appropriate buffer 211
6.19 Optimisation experiments 212
6.20 Scale up of mesalazine synthesis 212
6.21 Isolated yield of mesalazine 215
6.22 Conclusion and future work 216

Chapter 6 Bibliography 219

7 Conclusion 221

7.1 Conclusion 222

Introduction

Biocatalysis is now a go-to method for generating stereoselective small molecules. The reaction scope for biocatalytic processes has been broadened enormously by large-scale genetic engineering efforts, and enormous advances have been made in molecular biology in the last 10 years.[1–3] Implementation of biocatalytic oxidations and reductions is still compromised by the need for expensive nicotinamide cofactors which must be recycled, in ways which, for many processes is prohibitively expensive. [4]

Organic synthesis is widely used in the pharmaceutical industry for the manufacture of drug precursors and fine chemicals, where single enantiomers are often required. Industrial chemical synthesis can generate large amounts of hazardous waste (e.g., organic solvents) and often the synthetic steps generate a poor yield. Increasingly, biocatalysis is being used as a tool in the organic chemist's kit for the generation of stereoselective chiral alcohols and amines, and asymmetric reduction of alkenes. Advantageously these reactions are usually carried out in an aqueous environment. During industrial biocatalytic transformations, NADH or NADPH are recycled via coupled enzymatic reactions, typically linked to the sacrificial oxidation of isopropanol to acetone or glucose to gluconolactone, raising issues around product separation and poor atom economy.[5]

Electrochemical NAD^+ reduction or NADH oxidation at standard electrodes has proved impractical because these electrodes generate chemically-incorrect cofactor forms that are no longer enzyme active, and lead to large overpotential energy losses.[6] However, electrosynthesis can almost be considered reagentless as it uses electrons as a clean reductant. It has benefits to being implemented in industrial processes as greener electricity sources such as solar and wind power could be incorporated.

Greener chemistry is becoming increasingly important, with scientists focusing on environmentally friendly reaction conditions which lessen the impact on the planet: reducing waste, eliminating environmental pollution, increasing the selectivity of reactions and lowering the temperature at which reactions are carried out. [5]

The work in this Thesis will explore alternative options for supplying reducing equivalents that would allow biocatalytic hydrogenations to be incorporated more widely to industrial processes. A brief overview is shown in Figure 1-1.

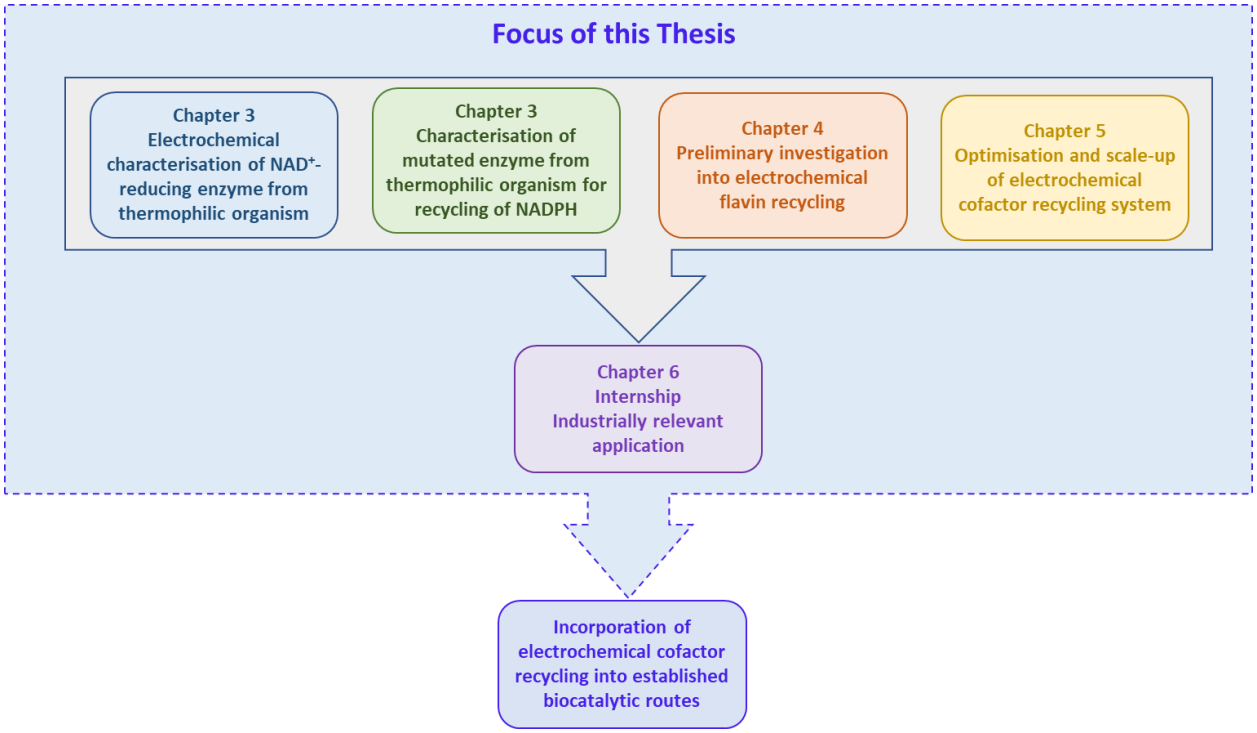


Figure 1-1: The work in this Thesis looks primarily at electrochemical cofactor recycling to provide reducing equivalents for biocatalytic reactions that would ultimately lead to their wider industrial incorporation.

The work in this Thesis will incorporate some of the merits of emerging techniques such as electrosynthesis and flow chemistry which will be discussed briefly below.

1.1 Electrosynthesis

Electrosynthesis has been performed for almost 200 years and has been the subject of much research.[7] It uses electrons as a clean reductant with no other reagents reaquired.[8] From a sustainability perspective, electrochemical synthesis can harvest renewable energy sources to generate the electricity required.[9] However at present it has not been widely adopted for industrial applications, due to fluctuations in green electricity which can lead to non-productive time during the operation day. Much research is currently underway to develop innovative energy storage systems to combat these difficulties.[10,11]

Electrosynthesis can either be direct electrolysis where the reaction takes place at the surface of the electrode, or indirect electrolysis where a mediator is used as an electron source.[12] Often electrochemical reduction is non-selective and can proceed via single-electron transfers which generate the incorrect enantiomer. In order to ensure that the second electron in a two-electron process is transferred fast enough to generate the correct product, a very negative potential is required, which can lead to electrode fouling and the production of undesirable side-products.[13-14] Biocatalytic electrosynthesis will be discussed further in section 1.5.4.

1.2 Flow Chemistry

Flow chemistry is a technique that has seen an increase in industrial implementation in recent years, offering a sustainable more efficient alternative to batch production. Reagents are pumped through the flow cell where the catalyst is immobilised in a continuous reaction.[15–17] The focus of the work in this Thesis is not primarily with flow chemistry, so it will only be discussed briefly here. However, some of the merits of flow chemistry were incorporated into the electrochemical synthesis work discussed in Chapter 5) and the medicinal chemistry screening tool developed in Chapter 6.

There are many advantages to flow such as precise control over reaction parameters such as the temperature and pressure of a reaction.[15] Automation of chemical processes and in-line analysis allows real-time feedback which can speed up the intensification process.[18,19] Heat and mass transfer efficiency are much better in flow systems than in batch, thus minimising reaction times and reducing energy usage for a more efficient chemical process. Flow systems offer consistent product formation and easy methods of scale up which is advantageous for industrial application.[20]

1.2.1 Biocatalytic synthesis in flow

Until recently biocatalysts were only really used in continuous flow while in solution, which still offers the advantages listed above, plus mass transport limitation or enzyme inhibition, can be overcome by the constant removal of reaction solution in biocatalytic flow systems.[21,22] One of the drawbacks however is that separation of the enzymes from the product at the end can be costly and difficult.[23]

In 2020, former Vincent Group DPhil Student, Barnabas Poznansky demonstrated carbon as a support for the conversion of pyruvate to lactate with *in situ* cofactor recycling using coadsorbed lactate dehydrogenase and formate dehydrogenase.[24] This work demonstrated high conversion to product and good stability of the enzyme on the support, which overcame many of the challenges faced during biocatalysis in flow. This built on previous work carried out by Thompson *et al.* to support enzymes on carbon nanotubes for use in a flow system.[25]

For hydrogenations, safer use of H_2 is another benefit of flow chemistry. The commercially available ThalesNano H-Cube provides an excellent solution to this problem with its in-built electrolytic H_2 generator. In 2021 Poznansky *et al.* were able to demonstrate the use of H_2-driven biocatalysis in the H-cube. This method opened up opportunities for the asymmetric reduction of C=X bonds in the

synthesis of chiral alcohols and amines which are highly desired in both the pharmaceutical and fine chemicals industries.[22,26]

1.3 Redox biocatalysis

Industrial scale biocatalysis is now increasing in scale, to catalyse reactions with exquisite selectivity under aqueous conditions without the presence of the heavy metals or toxic reagents that can have a huge environmental impact.[27] There is also the added benefit of decreased production costs due to less waste and lower temperatures providing more efficient synthetic pathways.[28–30] Large scale efforts in bioengineering are bringing down the cost of enzymes and producing industrially desirable activities at an economically viable cost.[31]

1.3.1 Using stoichiometric sacrificial reductants

The most significant challenge to commercially incorporating biocatalytic processes lies in the requirement for cofactor recycling. The majority of enzymes used in biocatalytic C=X reductions are dependent on the reduced cofactor NADH (or NADPH) required for hydride transfer. Stoichiometric addition of cofactor is not economically viable.[32,33]

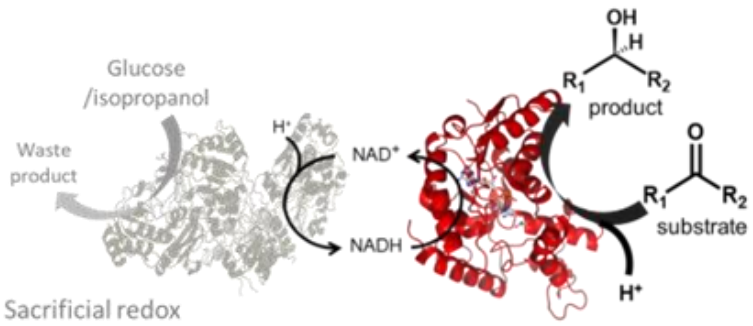


Figure 1-2 **biocatalytic NADH regeneration systems require a sacrificial redox reaction generating carbon-based waste and resulting in difficulty separating product.**

Enzymatic cofactor recycling systems are essential for industrial scale-up, however, many of these rely on super-stochiometric addition of sacrificial reducing equivalents as shown in Figure 1-2 such as glucose or isopropanol, resulting in increased costs and generating unnecessary carbon waste.33–36 This limits the posibilities of NADH driven biocatalysis, and prompts development of more atom efficient methods for cofactor recycling relying on either H2 or an electrode which will be discussed in section 1.5.

1.4 Cofactors

Cofactors are helper molecules that are essential to catalyse biological reactions.[37] Metal ions in various oxidation states can act as cofactors, however, 80% of all oxidoreductase enzymes rely on organic cofactors for their catalytic activity.[38,39] The cofactors relevant to the work in this Thesis will be introduced below:

1.4.1 Nicotinamides

Two of the most important and well-studied cofactors are Nicotinamide Adenine Dinucleotide (NAD^+) and Nicotinamide Adenine Dinucleotide Phosphate ($NADP^+$). These are abundant in nature and the most widely used in biocatalysis. Nicotinamides strictly undergo a two-electron transfer to form the reduced species NADH and NADPH. The chemical structures for the nicotinamide cofactors are shown in Figure 1-3 in their oxidised forms (red) and the reduced forms (blue). It is the reduced forms that aid hydride transfer in enzyme catalysis, which is essential for the reduction to occur. All biological organisms can synthesise $NADP^+$ from NAD^+, however the two cofactors have key biological roles so enzymes have evolved specificity for one particular cofactor.[40] This is relevant for the work carried out in this Thesis as some of the Johnson Matthey (JM) enzymes used for biocatalysis are specifically driven by NADPH. Reeve *et al.* developed a successful H_2-driven NADH

recycling system, however if this could be extended to recycle NADPH this could vastly increase the scope of biocatalytic reductions possible.

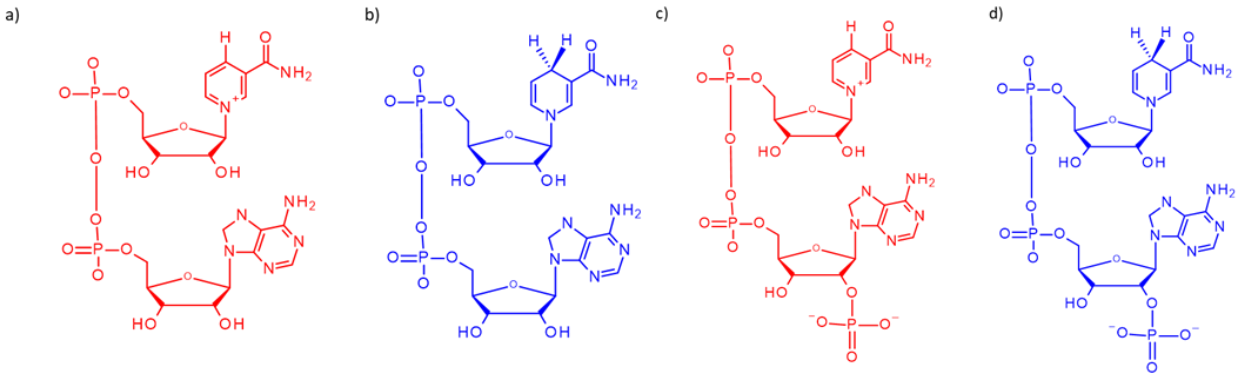


Figure 1-3: Chemical structures of (a) NAD^+, (b) NADH, (c) $NADP^+$, (d) NADPH

1.4.2 Flavins

Flavins are a large class of cofactors, widely used in biocatalysis, although rarely exploited in industrial biotechnology. In 2021, Srinivasan *et al.* demonstrated a H_2-driven flavin regeneration system that could be used to drive alkene hydrogenation using Ene-reductase enzymes (discussed further in chapter 4).[41,42] Flavins can undergo either a one or two-electron process, unlike the nicotinamide cofactors mentioned above. The main flavins used in the work in this Thesis will be introduced below:

1.4.2.1 Flavin mononucleotide (FMN) and Flavin adenine dinucleotide (FAD)

Flavin mononucleotide (FMN) and flavin adenine dinucleotide (FAD) are found as prosthetic groups in many biocatalytic enzymes, ene-reductases and hydrogenases to name the two relevant to this Thesis. These enzymes catalyse many reductions relevant to both the fine chemicals and pharmaceuticals industries.[43]

In their reduced forms (see Figure 1-4 (b) $FMNH_2$ and (d) $FADH_2$) these molecules serve as electron donors for a broad range of biological redox reactions that are relevant in organic synthesis.[44] At the

core of each flavin is an isoalloxazine ring which is able to stabilise the three redox states: oxidised (highlighted in red in (a) and (c) in Figure 1-4), radical and the reduced form (highlighted in red in (b) and (d) in Figure 1-4).[43]

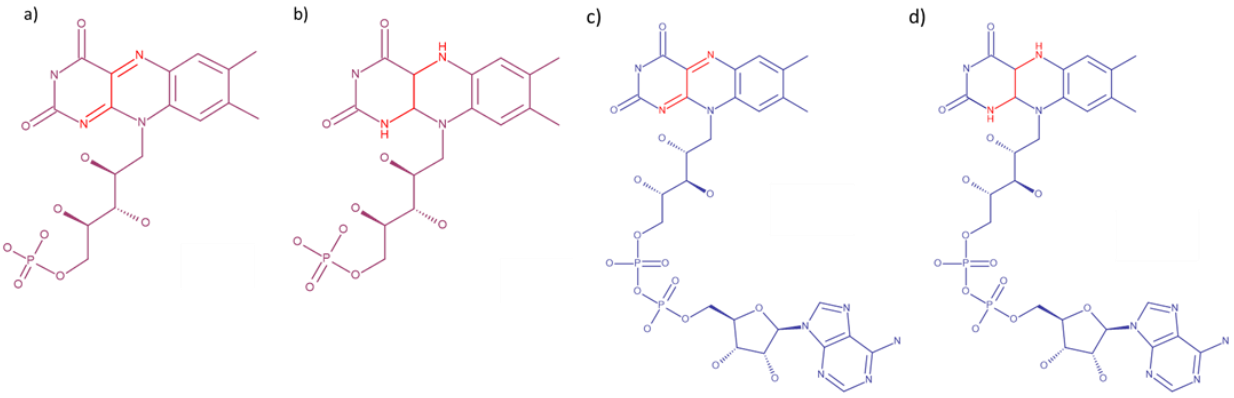


Figure 1-4: Chemical structures of (a) FMN, (b) $FMNH_2$, (c) FAD and (d) $FADH_2$

Flavins in nature have evolved to be excited by light and also to react with O_2 which allows them to perform biological oxidations and light-sensing.[45] These properties create additional challenges when attempting to use them to drive biocatalytic reactions, which generally expose them to both light and to O_2.

1.4.2.2 Riboflavin (RF)

Riboflavin (RF), also known as vitamin B2 is an essential micronutrient used to convert carbohydrates into glucose in order to produce energy for a cell. It is a precursor molecule to both FMN and FAD which are essential for energy metabolism, cellular respiration and growth and repair of all biological organisms, and is often sold as a dietary supplement or added to foods.[46] Due to its large-scale production (>9000 tonne per annum) it is widely available and significantly cheaper than the other flavins.[47]

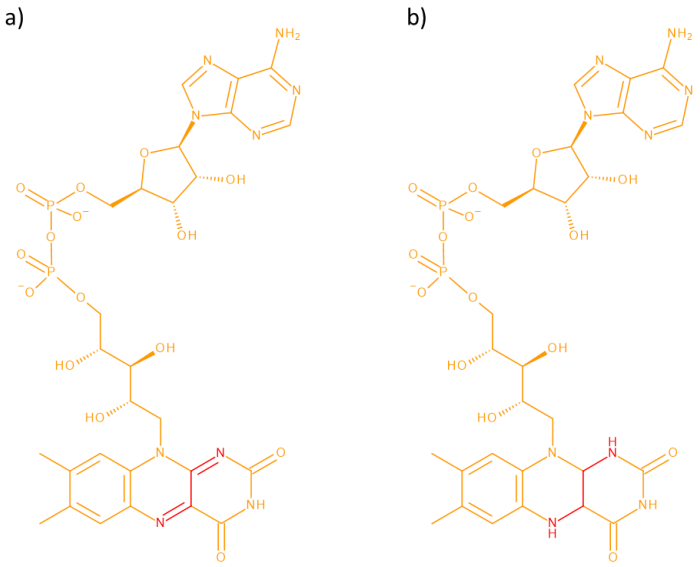


Figure 1-5: Chemical structures of (a) RF, (b) RF^{2-}

The structure of RF and its reduced form RF^{2-} is shown in Figure 1-5 highlighting the isoalloxazine ring in red to demonstrate the two desirable redox states for RF-driven biocatalysis.

1.5 Existing methods for cofactor regeneration

As discussed in section 1.3, a significant limitation to using enzymes as catalysts for reduction reactions, is their requirement for electrons in the form of the expensive cofactors NADH or NADPH. In order to be viable for most industrial processes a continuous cofactor regeneration system is essential. Any regeneration system implemented should allow each cofactor molecule to be cycled between 1000 and 10,000 times, (referred to as the turnover number (TN) in moles of product generated per mole of cofactor used).[48,49]

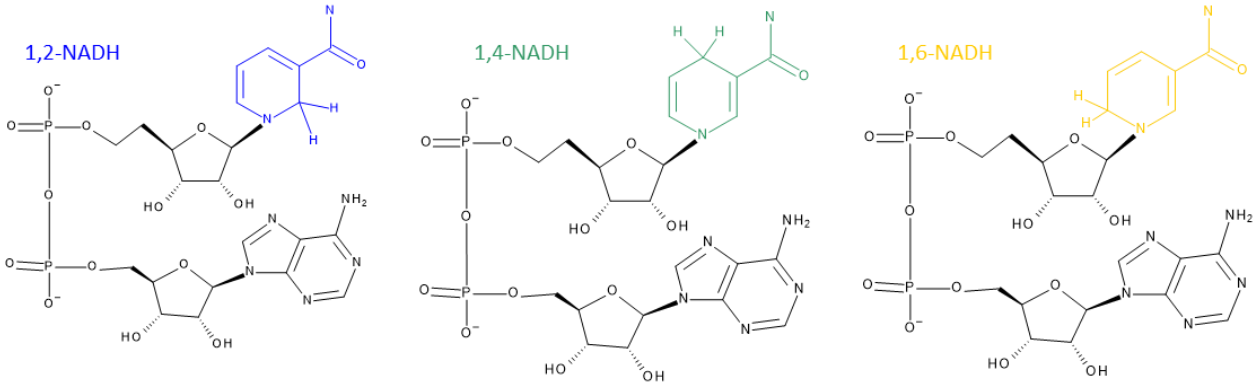


Figure 1-6: The 3 structural forms of NADH; 1-2-NADH (blue), biologically active 1,4-NADH (green) and 1,6-NADH (yellow)

At present, methods used on an industrial scale involve the use a second enzyme for cofactor regeneration, in order to form the biologically active 1,4-NADH (Figure 1-6 in green). The other two forms of the cofactor are not enzyme-active and cannot drive biocatalytic reactions.

1.5.1 H_2-driven NADH regeneration

The work in this Thesis builds on work previously carried out by Dr Holly Reeve during her time in the Vincent Group.[50,51] In fact, this technology was the basis behind Oxford spin-out company HydRegen, with whom the industrial placement project detailed in Chapter 6 was carried out. Both Vincent and Lenz Groups have demonstrated successful cofactor recycling using NAD+ reducing soluble hydrogenase from Ralstonia eutropha (SH).[21,52,53] Before explaining the technology behind the H2-driven NADH recycling system, it is first necessary to describe the enzyme moiety used as the catalyst for the recycling system.

1.5.1.1 Soluble NAD^+-reducing hydrogenase

Natively the bacterium *Ralstonia eutropha* (now known as *Cupriavidus necator*) is able to use H_2 as its sole energy source.[54] One of the hydrogenase enzymes it makes is the soluble hydrogenase (SH). A simplified schematic representation of the two moieties of interest for this project are shown in

Figure 1-7. This enzyme couples H_2 oxidation to the reduction of NAD^+, and in doing so supplies the cell with the reducing equivalent, NADH.[55,56] Molecular hydrogen enters the active site of the HoxHY subunit and is split into two protons and two electrons. The electrons are carried along the chain of iron-sulfur clusters (FeS) to the active site of the HoxFU moiety. The flavin molecule at the centre of the active site aligns with the cofactor and allows a hydride transfer to occur that always results in the biologically active form 1,4-NADH being generated.[57]

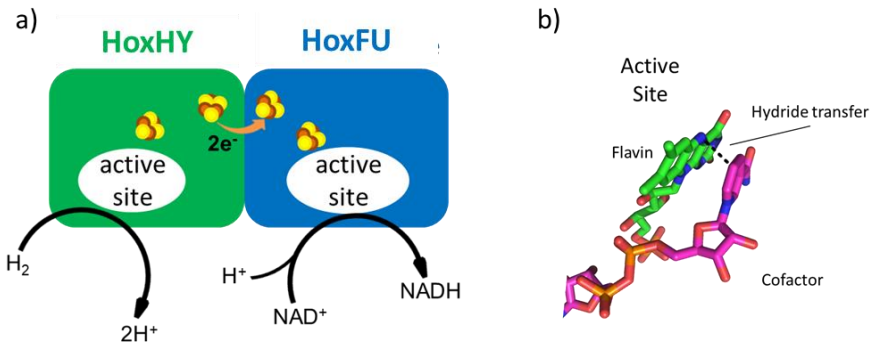


Figure 1-7: (a) A schematic representation of the Soluble Hydrogenase from *Ralstonia eutropha*. The hydrogenase subunits (HoxHY), shown in green; molecular H_2 is split into two protons and the electrons carried along the chain of FeS clusters (shown as spheres in elemental colours) to the active site of the NAD^+-reducing subunits (HoxFU), which is shown in blue. There is an FMN molecule in the active site of the HoxFU which performs a hydride transfer to the NAD^+ to produce biologically active NADH. (b) A close up of the FMN and NADH interaction.

In nature, the NAD^+-reductase moiety (HoxFU), uses the electrons from H_2 transferred from the hydrogenase dimer (HoxHy) as an electron source. This means that the HoxFU would allow direct electron transfer to or from an electrode to which it was adsorbed. This allowed analysis work to be carried using protein film electrochemistry (PFE) techniques.[58] These techniques are explored in Chapter 3 when a HoxFU moiety from a thermophilic organism *Hydrogenophilus thermoluteolus* is electrochemically characterised.

In 2015, Reeve *et al* were able to demonstrate a catalyst system that comprised both the hydrogenase and NAD-reductase moieties described above, coadsorbed with an alcohol

dehydrogenase enzyme (ADH) to carbon black particles (BP2000). Electrons for the reduction of NAD^+ were provided by the oxidation of H_2 through the carbon particle. The NADH generated was then used to drive the ADH to convert acetophenone to phenylethanol.

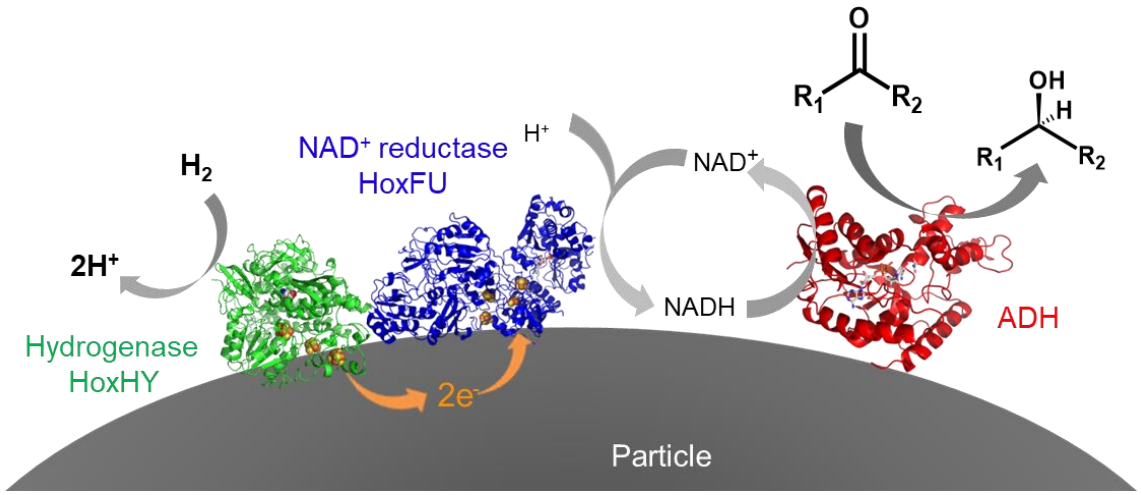


Figure 1-8: Schematic representation of the H_2-driven particle system for NADH-dependent biocatalysis. Oxidation of H_2 by the Hydrogenase (HoxHY) transfers electrons to the carbon particle where they can be carried to the NAD^+-reductase (HoxFU) to generate NADH to drive the ADH (red) enzyme to perform the catalytic reduction of a ketone to chiral alcohol.

A number of other NADH regeneration systems have been investigated over recent years including photochemical routes but so far these are not competitive for commercial applications due to the low TN they achieve.[59] There has been research into the use of transition metal complexes for H_2-driven NADH generation. However, the results lacked the selectivity achieved by biocatalysis.[60–62]

1.5.2 Methods for NADPH regeneration

There are currently fewer systems avaialble for NADPH recycling, however, some reductase and monooxygenase enzymes have a specificity for NADPH. NADPH is less stable than NADH and significantly more expensive.[63] Currently it is recycled in using the sacrificial reductant methods outlined in section 1.3.1, but industrial applications would benefit from a more atom-efficient way of recycling this cofactor.

1.5.2.1 Electrochemical leaf NADPH recycling

One NADPH-recycling system that had achieved very high turnover numbers (TON) and worthy of noting here is the electrochemical leaf.[64–66] Armstrong *et al.* developed a very successful system for NADPH recycling using ferredoxin-$NADP^+$reductase (FNR) loaded into the nanopores of a highly porous conducting metal oxide-coated electrode. FNR transduces electron and hydride transfer through the unidirectional recycling of NADPH, which is then coupled to a dehydrogenase and a cascade of enzymes. These are linked by channelling the cofactors and intermediates through the nanopores of the metal oxide layer. In this way, the system mimics the conditions under which enzymes operate in living cells, allowing the enzymes to stay active for many days.[67] Whilst this system has many advantages and shows great promise, at the moment it is still being researched at laboratory scale. In addition, the metal oxide electrode coating may cause interactions with specific substrates, causing undesirable side reactions.

1.5.2.2 Engineered O_2 tolerant hydrogenase

In 2020, Preissler *et al.* engineered the NAD^+ binding pocket of an O_2-tolerant NAD^+-linked soluble [NiFe]-hydrogenase so that it could bind $NADP^+$.[68] This development allowed the genetically engineered enzyme moiety to reduce $NADP^+$ and was shown to have a K_M of 3.4 mM (K_M is the Michaelis-Menten constant is explained in Chapter 2 (section 2.5), which shows a reasonable affinity to the substrate, though still too high for industrial application.

1.5.3 H_2-driven flavin recycling

Previous work carried out in the Vincent Group involved the development of an H_2-driven flavin recycling system to drive the asymmetric reduction of alkenes.[41,69] Flavins were introduced in section 1.4.2, and Shiny Joseph Srinivasan achieved excellent results using these to drive NAD(P)H-dependent ENE-reductase enzymes.[70]

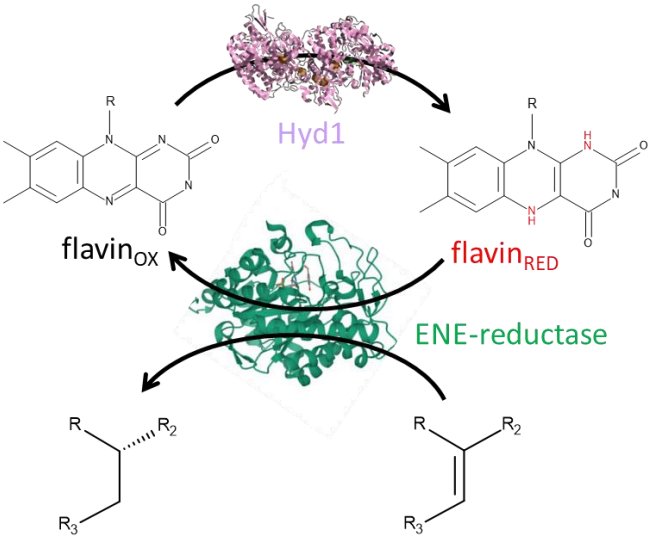


Figure 1-9: Schematic representation of the H_2-driven flavin recycling system used to drive the asymmetric reduction of an alkene.[69]

Flavin recycling shows promise for biocatalytic reactions as it achieves a high atom efficiency and an FMN TN of 240 was achieved for a reaction that ran for more than 5 days.[70] This showed good stability of the system, although there is limited data for comparison in the literature, this was the highest FMN TN recorded.

1.5.4 Electrochemical NAD^+ reduction

Electrochemical reduction of NAD^+ to NADH uses electrons a a clean reductant (Equation [1-1]).

$$NAD^+ + H^+ + 2e^- \rightarrow NADH \qquad [1\text{-}1]$$

This method is attractive because, as previously mentioned it can be powered by green energy sources, however, at present much of the electricity available is not renewable. The UK government have set targets for all electricity to come from 100% zero-carbon generation by 2035, making electrochemical processes more desirable and cost effective.[71]

A drawback to electrode-driven synthesis is that the reaction takes place at the surface of the electrode, requiring the bulk solution to be delivered to the electrode for an efficient reaction. This would be alleviated by a flow system as discussed in section 1.2.

1.5.5 Direct electrochemical reduction

Although direct electrochemical reduction of NAD^+ at the surface of an electrode would seem like an ideal solution, this occurs at Faradaic efficiencies of between 1-30 % and often leading to the generation of the incorrect cofactor form.[72] The direct electrochemical process occurs in two steps:

$$NAD^+ + e^- \rightarrow NAD^\bullet \qquad [1\text{-}2]$$

$$NAD^\bullet + H^+ + e^- \rightarrow NADH \qquad [1\text{-}3]$$

The overpotential required for eqn. [1-3] is large compared to the first step in eqn. [1-2].[73] The overpotential is defined as the difference between the thermodynamic potential for the reaction and the potential at which reduction is seen electrochemically, a large overpotential not only requires high energy inputs but can lead to electrode fouling.[74] The second step of the reaction (eqn. [1-3]) can not only yield the desired 1,4-NADH, but also the two biologically inactive forms 1,2-NADH and 1,6-NADH. There is also a high possibility on a bare metal electrode of yielding the enzymatically inactive dimer NAD_2.[73,75,76] This is shown in eqn. [1-4]:

$$NAD^\bullet + NAD^\bullet \rightarrow NAD_2 \qquad [1\text{-}4]$$

The NAD_2 formation occurs more rapidly than the addition of a second electron and a proton, so some researchers have looked at preventing the formation of the dimer by increasing the availability of protons on the surface of the electrode. [6] Ali *et al.* showed the formation of 100 % biologically active 1,4-NADH, at an optimum potential of *ca.* -1 V *vs* SHE. However, at this overpotential there is

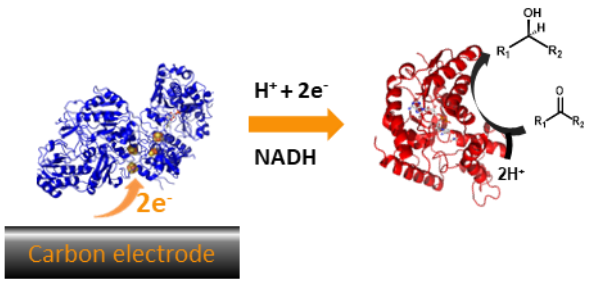
a high risk of undesirable side-reactions of the desired substrate which ultimately decreases selectivity of the final product.[6]

1.6 The concept of this project

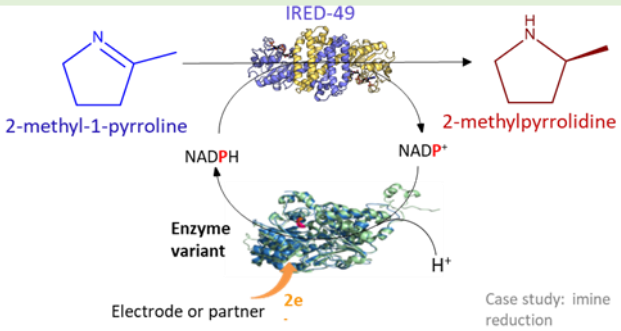
The aim for this project is to develop a clean and sustainable method for electrochemical cofactor recycling, and establishing electrochemical methods to drive enzymatic reactions which avoid the need for NAD(P)H. The Vincent Group have already established a clean and efficient method for reducing NAD^+ using H_2 by immobilising an NAD^+-reductase enzyme on a carbon particle to generate NADH to a range of cofactor-dependent dehydrogenase enzymes. Building on this technology to allow electricity to be used to control the reaction in order to harvest renewable electricity sources to drive the reaction. A schematic overview to the project is shown in Figure 1-10.

In Chapter 3 a new enzyme moiety from a thermophilic organism will be electrochemically characterised. This moiety has been expressed in *E. coli* which allows mutations to be easily introduced. Based on the research by Preissler *et al.* electrochemical characterisation is carried out on a mutant form of the enzyme moiety, generated with the aim of changing selectivity to allow reduction of $NADP^+$ in addition to NAD^+. This will then be used to drive NADPH-dependent imine reductase enzymes.

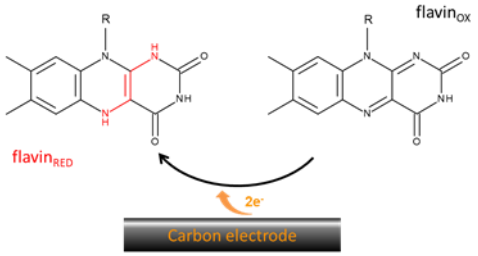
Chapter 3: Electrochemical analysis of enzyme moiety from thermophilic organism expressed in *E. coli*



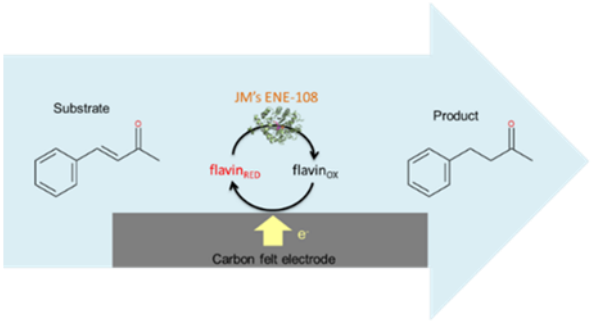
Chapter 3: Mutation of enzyme moiety to recycle NADPH together with preliminary imine reduction



Chapter 4: Preliminary electrochemical flavin reduction



Chapter 5: Scale up of electrochemical flavin recycling to drive asymmetric alkene reduction



Chapter 6: Industrial placement at HydRegen to develop library building tool for medicinal chemists

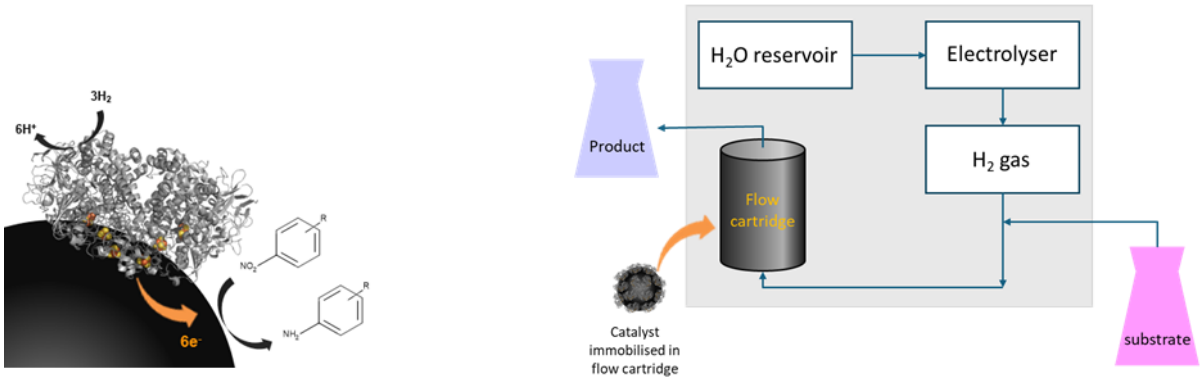


Figure 1-10: Overview of the methods developed in this work to provide reducing equivalents for biocatalytic synthesis. Electrochemical NADH recycling (blue), NAD(P)H recycling using H_2 or an electrode as an electron source (green), electrochemical flavin reduction (orange), electrochemically recycled flavin-driven hydrogenation(yellow), H_2-driven bio-electrocatalyst for nitro to amine reduction (purple).

Chapter 4 builds on work carried out in the Vincent Group by Dr Shiny Joseph Srinivasan, who successfully developed an H_2-driven flavin recycling system. This will be developed to be electrochemically reduce flavins, including the much cheaper riboflavin cofactor. In Chapter 5, the scale up of asymmetric alkene reductions will be scaled up to aim to achieve a TN of at least 100. This would demonstrate an industrially relevant cofactor recycling system that could be implemented to achieve a cheaper and more sustainable way to synthesise small molecules for pharmaceutical and fine chemicals industries.

In Chapter 6, the application of these technologies will be developed in an industrially relevant project carried out during a 16-week internship at University of Oxford spinout company HydRegen. Here a library building tool designed for medicinal chemists to synthesise small quantities of multiple different amines will be developed.

Chapter 1 Bibliography

1 Hanefeld, U. Cao L. and Magner E., Chem. Soc. Rev., 2013, **42**, 6211–2.

2 Wheeldon, S. D. Minteer, S. Banta, S. C. Barton, P. Atanassov and M. Sigman, Nat. Chem., 2016, **8**, 299–309.

3 Wan, R. S. Heath, B. Siritanaratkul, C. F. Megarity, A. J. Sills, M. P. Thompson, N. J. Turner and F. A. Armstrong, *Green Chem*., 2019, **21**, 4958–4963.

4 Bolivar, M., Rocha, R. A., North, A. J., Speight, R. E., Williams C. C. and Scott, C., *Catalysts*, 2022, **12**, 1454

5 Castiello, P. Junghanns, A. Mergel, C. Jacob, C. Ducho, S. Valente, D. Rotili, R. Fioravanti, C. Zwergel and A. Mai, *Green Chem*., 2023, **25**, 2109-2169

6 Ali, A. Gill and S. Omanovic, *J. Chem. Eng.*, 2012, **188**, 173–180

7 Lund, H., Hammerich, O., *Organic Electrochemistry*, 4th edn., 2001

8 Sequeira, M. F., and Santos, C. A. C., *J. Braz. Chem*. Soc., 2009, **20**, 387–406

9 Ganiyu, O. and Martínez-Huitle, C. A., *Curr. Opin. Electrochem*., 2020, **22**, 211–220

10 Montiel, D. Valero, F. Gallud, V. García-García, E. Expósito and J. Iniesta, *Echem Water Treat.*, 2018, 513-541

11 Zhang, M. Xie, V. Adamaki, H. Khanbareh and C. R. Bowen, *Chem. Soc. Rev*, 2017, **46**, 7757

12 Francke, R. and Little, R. D., *Chem. Soc. Rev*., 2014, **43**, 2492-2521

13 Elving J. and Leone, J. T., *J. Am. Chem. Soc*., 1958, **80**, 1021–1029

14 Mairanovskii, G., Rubinskaya, T. Y., Gul'tyai, V. P. and Proskurovskaya, I. V., *Bull. Acad. Sci. USSR Div. Chem. Sci.*, 1976, **25**, 2203–2205

15 Plutschack, B., Pieber, B., Gilmore, K. and Seeberger, P. H., *Chem. Rev*., 2017, **18**, 11796-1189

16 Bogdan, R., and Dombrowski, A. W., *J. Med. Chem*., 2019, **62**, 6422–6468

17 Thompson, P., Peñafiel, I., Cosgrove, S. C. and Turner, N. J., *Org. Process Res. Dev*., 2019, **23**, 9–18.

18 Britton, J., Majumdar, S., and Weiss, G. A., *Chem. Soc. Rev*., 2018, **47**, 5891–5918

19 Britton, S., and C. L. Raston, *Chem. Soc. Rev*., 2017, **46**, 1250–1271.

20 Cravotto, W. Bonrath, S. Tagliapietra, C. Speranza, E. C. Gaudino and A. Barge, *Chem. Eng. Process.*, 2010, **49**, 930–935

21 A. Thompson, J. S. Rowbotham, J. H. Nicholson, M. A. Ramirez, C. Zor, H. A. Reeve, N. Grobert and K. A. Vincent, ChemCatChem, 2020, 12, 3913-3918

22 Tamborini, P. Fernandes, F. Paradisi and F. Molinari, *Trends Biotechnol*., 2018, **36**, 73–88

23 Coloma, Y. Guiavarc', P.-L. Hagedoorn and U. Hanefeld, *Chem. Commun*., 2021, **57**, 11416.

24 Poznansky, B., Cleary, S.C., Thompson, L. A., Warren, S. A., Reeve, H. A. and Vincent, K. A., *Chem. Soc. Rev.* 2018, **47**, 5891-5918

25 Thompson, A., Rowbotham, J. S., Reeve, H. A., Zor, C., Grobert, N. and Vincent, K. A., *Methods in Enzymology*, 2020, **630**, 303–325

26 Savile, K. , Janey, J. M., Mundorff, E. C., Moore, J. C., Tam, S., Jarvis, W. R., Colbeck, J. C., Krebber, A., Fleitz, F. J., Brands, J., Devine, P. N., Huisman, G. W. and Hughes, G. J. *Science*, 2010, **329**, 305–309

27 Sheldon, A. and Woodley, J. M., Chem. Rev., 2018, **118**, 801–838

28 Kharisov, I., Kharissova, O. V Máximo, C., González, O., Peña Méndez ,Y. and López, I., R. Soc. Open Sci, 2019, **11**, 191378

29 Desai, A. Angew. *Chemie, Int. Ed.*, 2011, **50**, 1974–1976.

30 Bommarius, S., Blum, J. K. and Abrahamson, M. J., *Curr. Opin. Chem. Biol*., 2011, **15**, 194–200

31 Sakhuja, D., Ghai, H., Ranju, R., Rathour, K., Bhatia, K., 3 Biotech, 2021, **11**, 280.

32 Wu, H., Tian, C., Song, X., Liu, C., Yang, D. and Jiang, Z., *Green Chem.*, 2013, **15**, 1773–1789

33 Lauterbach, L., Lenz, O. and Vincent, K. A., *FEBS J*., 2013, **280**, 3058–3068.

34 Marcus A. and Sutin, N., BBA Rev. Bioenerg., 1985, **811**, 265–322.

35 Reeve, H. A., Lauterbach, L., Ash, P. A., Lenz O. and Vincent, K. A., *Chem. Commun.*, 2012, **48**, 1589–1591.

36 Zor, C., Reeve, H. A., Quinson, J., Thompson, L. A., Lonsdale, T. H., Dillon, F., Grobert, N. and Vincent, K. A., *Chem. Commun.*, 2017, **53**, 9839–9841

37 Fischer, D., Holliday, G. L., Rahman, S. A. and Thornton, J. M., *J. Mol. Biol.*, 2010, **403**, 803–824

38 Richter, M., *Nat. Prod.Rep.,* 2013, **10**, 1324-1345

39 Holliday, G. L., Fischer, J. D., Mitchell, J. B. O. and Thornton, J. M., FEBS, 2011, **20**, 3835 - 3845

40 Agledal, L., Niere, M. and Ziegler, M., Redox Rep., 2010, **15**, 2–10.

41 Joseph Srinivasan, S, Cleary, S. E., Ramirez, M. A., Reeve, H. A., Paul C. E.and Vincent, K. A., *Fron. Catal.*, 2020, **2**, 906694

42 Joseph Srinivasan, S., Cleary, S. E., Ramirez, M. A., Reeve, H. A. , Paul, C. E. and Vincent, K. A., *Angew. Chemie - Int. Ed.*, 2021, **60**, 13824–13828

43 De Gonzalo, G. and Fraaije, M. W*., ChemCatChem.*, 2012, **5**, 403-415

44 Romero, E., Rubén, J., Gómez, R., Castellanos, G., Gadda, G., Fraaije, M. W. and Mattevi, A., *Chem. Rev.* 2018, **118,** 1742–1769

45 Joosten, V. and van Berkel, W. J., *Curr. Opin. Chem. Biol.*, 2007, **11**, 195–202

46 Dainty, J. R., Bullock, N. R., Hart, D. J., Hewson, A. T., Turner, R., Finglas, P. M. and Powers, H. J., *Am. J. Clin. Nutr.*, 2007, **85**, 1557–1564

47 Schwechheimer, S. K., Park, E. Y., Revuelta, J. L., Becker, J. and Wittmann, C., *Appl. Microbiol. Biotechnol*., 2016, **100**, 2107–2119

48 van der Donk W. A. and Zhao, H. M., *Curr. Opin. Biotechnol.*, 2003, **14**, 421–426.

49 Liu, W. F. and Wang, P. *Biotechnol. Adv.,* 2007, **25**, 369–384

50 Reeve, H. A., DPhil Thesis, University of Oxford, 2015.

51 Reeve, H. A., Lauterbach, L., Lenz, O. and Vincent, K. A., *ChemCatChem,* 2015, **7,** 3480–3487.

52 Lauterbach, L., Liu, J., Horch, M., Hummel, P., Schwarze, A., Haumann, M., Vincent, K. A., Lenz O. and Zebger, I., *Eur. J. Inorg. Chem.*, 2011, **2011**, 1067–1079

53 Lauterbach, L. Idris, Z., Vincent, K. A. and Lenz, O., *PLoS One*, 2011, **6**

54 Burgdorf, T., Lenz, O., Buhrke, T., van der Linden, E., Jones, A. K., Albracht, S. P. J. and Friedrich, B., *J. Mol. Microbiol. Biotechnol*., 2005, **10**, 181–196

55 Horch, M., Lauterbach, L., Lenz, O., Hildebrandt, P. and Zebger, I., *FEBS Lett*., 2012, **586**, 545-556

56 Schneider, K. an dSchlegel, H. G., *Biochim. Biophys. Acta,* 1976, **452**, 66–80.

57 Reeve, H. A., Lauterbach, L., Lenz O. and Vincent, K. A. *ChemCatChem*, 2015, **7**, 3480–3487.

58 Lauterbach, L. Idris, Z., Vincent, K. A. and Lenz, O., *PLoS One*, 2011 **10**

59 De Wildeman, S. M. A , Sonke, T., Schoemaker, H. E. and May, O*., Acc. Chem. Res*. 2007, **40**, 12, 1260–1266

60 Maenaka, Y., Suenobu, T. and Fukuzumi, S., *J. Am. Chem. Soc*., 2012, **134**, 367–74

61 Hembre, R. T., Penney, J. M. and Wagenknecht, P. S., *Patent*, 2007, **1**, 7867

62 Betanzos-Lara, S., Habtemariam, Z. Liu, A, Pizarro, A. M., Qamar, B. and Sadler, P. J., *Angew. Chem. Int. Ed. Engl.*, 2012, **51**, 3897–900

63 Schneider, K. and Schlegel, H. G., *Biochem. J.*, 1981, **193**, 99–107.

64 Preissler, J., Reeve, H. A., Zhu, T., Nicholson, J., Urata, K., Lauterbach, L., Wong, L. L., Vincent, K. A. and Lenz, O., ChemCatChem, 202, **19**, 4853-4861

65 Megarity, C. F., Siritanaratkul, B., Cheng, B., Morello, G., Wan, L., Sills, A. J., Heath, R. S., Turner, N. J. and Armstrong, F. A., *ChemCatChem*, 2019, **11**, 5662–5670

66 Siritanaratkul, B. and Megarity, C. F. , *Curr. Opin. Electrochem.*, 2024, **47**, 101565

67 Armstrong, F. A., Cheng, B., Herold, R. A., Megarity, C. F. and Siritanaratkul, B., 2023, **123**, 5421-5458

68 Herold, R, Armstrong, , F. A.,, Reinbold, R., Schofield, C., *Proc. Natl. Acad. Sci*., 2022, **120**

69 Ramirez, M. A., Joseph Srinivasan, S., Cleary, S. E., Todd, P. M. T., Reeve H. A. and K. A. Vincent, *Front. Catal.*, 2022, **2**, 15.

70 S. J. Srinivasan, 2021

71 National Grid ESO, 2023, 1–224

72 Aamer, E., Thöming, J., Baune, M., Reimer, N., Dringen, R., Romero, M. and Bösing, I., *Sci. Reports*,

2022, **12,** 16380

73 Jaegfeldt, H., J. *Electroanal. Chem. Interfacial Electrochem*., 1981, **128**, 355–370

74 DevauxBasseguy, R., Bergel, A. and Comtat, M., *Enzyme Microb. Technol.*, 1997, **20**, 248–258

75 Azem, A., Man, F. and Omanovic, S., *J. Mol. Catal. A Chem.,* 2004, **219**, 283–299.

76 Moiroux, J. and Elving, P. J., *J. Electroanal. Chem. Interfacial Electrochem.*, 1979, **102**, 93–108

Theory and Methods

The experimental work described in this Thesis uses a range of techniques both to drive bio-electrochemical synthesis and analyse redox enzyme catalysis. This chapter explores these methods and the theory behind them. Future chapters expand on these concepts and refer back to this chapter where non-standard experimental techniques are developed.

2.1 Electrochemistry

Electrochemistry is used throughout this Thesis both to drive electrochemical synthesis and as an analytical tool to understand what is happening at the surface of an electrode during a redox reaction, and can give information on both the kinetics and thermodynamics of the system.

Electrode potential is the driving force behind a redox reaction where an oxidation takes place at the anode and a reduction at the cathode. The electrode potential governs the availability of electrons which can flow between the surface of the electrode and the species being oxidised/reduced, and this flow is recorded as a current. The faster the flow of electrons, the larger the magnitude of current observed.

In any redox reaction, the electron donor and the electron acceptor are referred to as the redox couple. The thermodynamic potential of the couple is obtained by measuring the difference between a standard hydrogen electrode (SHE) and the tendency of the couple to gain or lose electrons and this is measured in Volt. The onset of catalytic current in a reaction may not be at the thermodynamic redox potential if there is a kinetic barrier which means the reaction would need an overpotential to provide additional energy.

2.1.1 The Nernst equation

The Nernst equation[1] can be used to determine the redox potential of an electrochemical reaction when not performed under standard conditions. A redox reaction must consist of both a reduction and an oxidation half reaction to enable a flow of electrons. For the reaction:

$$Ox + ne^- \rightleftarrows Red \qquad [2\text{-}1]$$

the Nernst equation is written as:

$$E = E^{\Theta} + \frac{RT}{nF} ln \frac{[Ox]_{eq}}{[Red]_{eq}} \qquad [2\text{-}2]$$

where E is the thermodynamic potential, E^{Θ} is the standard reduction potential of the redox couple (under standard conditions), *R* is the gas constant, *T* is the absolute temperature, *F* is the Faraday constant, *n* is the number of electrons, $[Ox]_{eq}$ and $[Red]_{eq}$ are the concentration of species on the left and right side to the power of their stoichiometric coefficient.

2.1.2 Standard Hydrogen Electrode

The standard reduction potential for a redox couple can be determined experimentally relative to an electrode of known or defined potential. The work in this Thesis is referenced to the Standard Hydrogen Electrode (SHE).

$$2H^+_{(aq)} + 2e^- \rightleftharpoons H_{2(g)} \qquad [2\text{-}1]$$

The SHE is defined to be 0 V at 1 bar H_2 and pH 0.

2.1.3 Protein Film Electrochemistry[2,3]

Protein film electrochemistry (PFE) is a technique used to study certain redox enzymes, by immobilising them in a mono or sub-monolayer on the surface of a working electrode.[4] The

technique requires the enzyme to be directly adsorbed to the surface of the electrode in order that electrons can transferred to the redox centre of the enzyme, so is not applicable to all enzymes. The soluble hydrogenase (SH) or HoxFU used in this Thesis can adsorb to the carbon electrode where they form a stable film with access to their redox centre, allowing electrons to pass from the electrode to the chain of FeS clusters inside the structure to the active site of the protein.[5] This technique allows analysis of a very small quantity of enzyme, typically picomoles. [6]

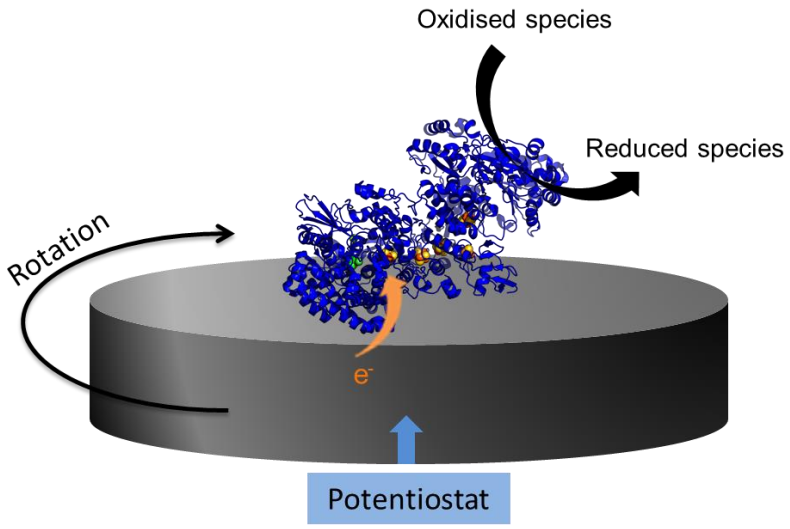


Figure 2-1: Schematic representation of an enzyme adsorbed to a pyrolytic graphite working electrode.

Figure 2-1 shows an enzyme immobilised on the surface of a pyrolytic graphite edge (PGE) electrode which is used for this technique. The gas environment can be controlled, as can the temperature and pH of the solution within the electrochemical cell. Rotation of the electrode allows fresh solution to be brought to the surface of the electrode, and for any product to be swept away, preventing mass transport limitations.

2.1.1.1. Protein film preparation

Comparison of protein films is difficult due to differences in coverage during application. In order to achieve reproducible results, a certain protocol was established. All PFE experiments were carried out in triplicate to minimise any experimental error. Application of the enzyme to the electrode was important to the results of the experiment. Each enzyme has its own surface properties and adsorbs to the electrode differently, so a technique that has been used for one enzyme will not always apply to another. It was determined through trial and error over the first few experiments that for the *Ht* HoxFU, good adherence to the RDE required the surface of the electrode to be 'roughened' after polishing. This was done by pressing the RDE on the surface of clean P800 sandpaper and turning 180°. When spotting the enzyme onto the electrode, it is important to deposit the enzyme in the centre of the carbon surface so that the enzyme does not spread beyond the carbon (Figure 2-2c). If the protein comes into contact with the resin on the outside of the carbon, this causes the enzyme to spread over the surface of the electrode pin where it cannot adsorb. It appears that when a poorly prepared protein film is immersed in the cell, there is significant film loss, possibly from buffer entering the edge of the film where it is not properly adsorbed to the electrode.

Orientation of the enzyme on a film can also be a significant limitation to PFE. It is hard to tell how much enzyme is immobilised on the electrode, even using the same technique to apply a set amount each time. It is also unclear how much of the enzyme is able to exchange electrons with an electrode.[7]

Panel (b) shows an example of a set of CVs with a correctly prepared protein film, the magnitude of the current changes little between scans and NAD^+ reduction is taking place. There is minimal protein loss between scans. If there is a significant decline in current observed between the forward

and back scan of the CV, the protein film may not be well adsorbed and in this case it would be necessary to reapply.

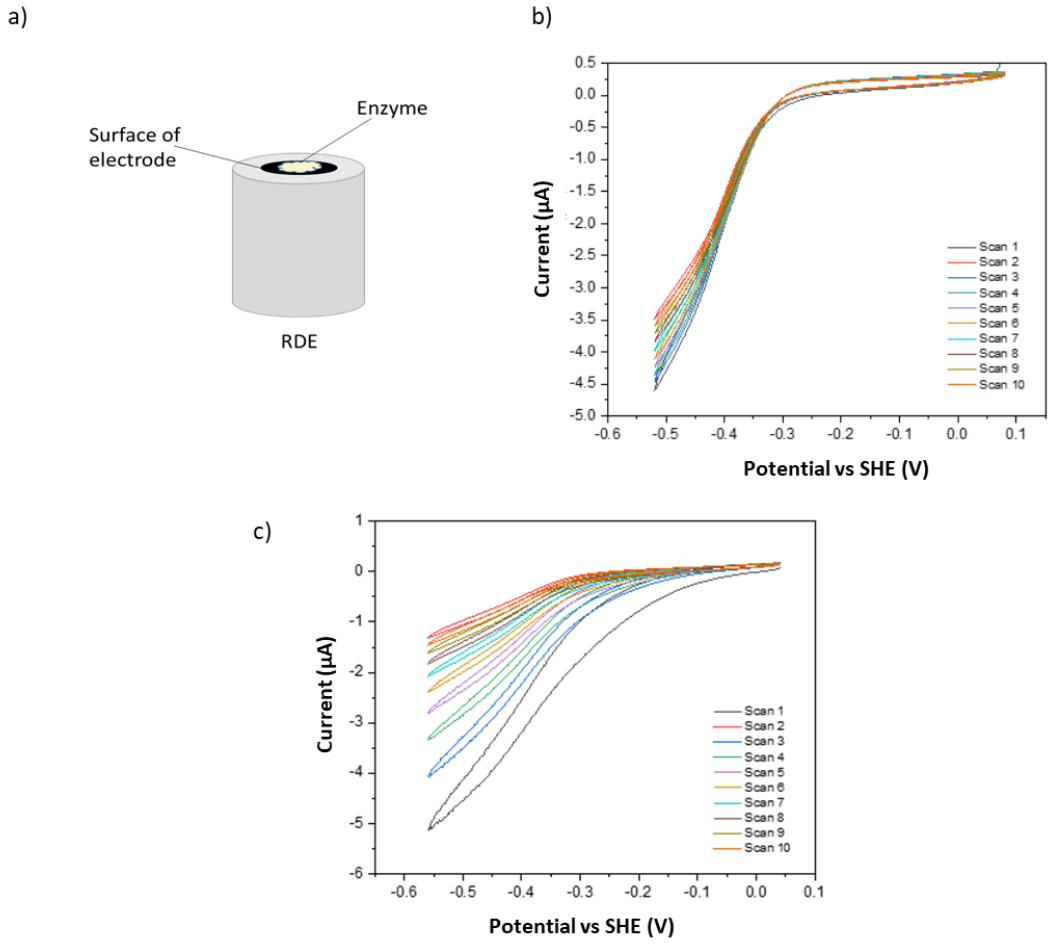


Figure 2-2: (a) Schematic representation of surface of the electrode showing the ideal place to 'spot' an electrode with enzyme. (b)Set of CVs recorded with a correctly-applied enzyme film showing minimal protein loss between films. (c) example of a set of CVs recorded with O_2 present (possibly in buffer), the onset potential for the reduction of O_2 masks that of NAD^+ plus there is significant film loss between cycles as the O_2 destabilises the protein film. Both CVs used 0.5 µL *Ht* HoxFU on a freshly polished electrode. Cell contained 50 mM Tris-HCl, pH 8, with 1 mM NAD^+ and 1 mM NADH. Scan rate 10 mV s^{-1}, rotation 2000 rpm.

It is also important to exclude O_2 from the system and panel (c) shows a set of CVs that are contaminated with O_2, possibly from insufficient degassing of buffer prior to starting the experiment. Here the reduction of O_2can be observed at approximately -0.2 V vs SHE which masks the reduction of NAD^+ as it adds to the negative current. This highlights the importance of keeping all experiments completely anaerobic when working at potentials where O_2 can be reduced at the electrode.

2.2 Electrochemical setup

Electrochemical experiments in this Thesis use a three electrode system as described in section 2.2.1.

2.2.1 Three-electrode system

The electrochemical experiments carried out in this Thesis use a three-electrode system shown in Figure 2-3 . The working electrode (WE) is where the reaction of interest takes place. During the reaction a potential is applied between this and a reference electrode (RE) (see section 2.2.3.) which has a known constant potential. If electron transfer occurs then current will flow through the system, and so that the RE maintains a constant potential, most of the current generated at the WE will pass through a counter electrode (CE).

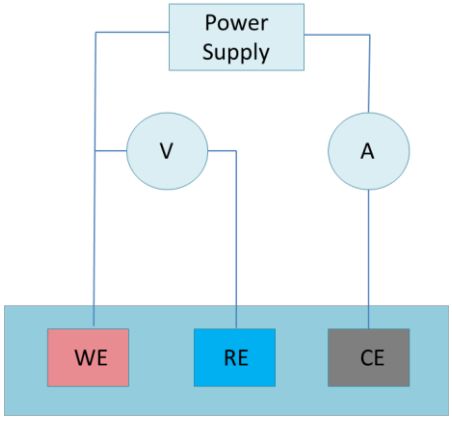


Figure 2-3 : schematic representation of the three-electrode system used in this Thesis. A potential is applied between the working electrode (WE) and the reference electrode (RE), the current generated passes through the counter electrode (CE).

The standard electrochemical setup is shown in Figure 2-3. A PalmSens potentiostat with associated PS Trace software was used both control the applied potentials and record the current. With the

exception of the flow experiments performed in Chapter 5 where an Autolab PGstat128N with Nova software was used.

2.2.2 Working electrodes – for analytical electrochemistry

For analytical electrochemistry the enzyme films were prepared on a pyrolytic graphite edge (PGE) rotaring disk electrode (RDE). Carbon is a suitable material for enzyme immobilisation and known to adsorb to proteins well. The PGE electrode has high surface area exhibiting defects which electrostatically attract regions on the surface of the protein. Polishing the surface of the electrode prior to applying the protein film is essential to increase the number of defect sites and roughness of the surface to assist in adsorption.[8–10]

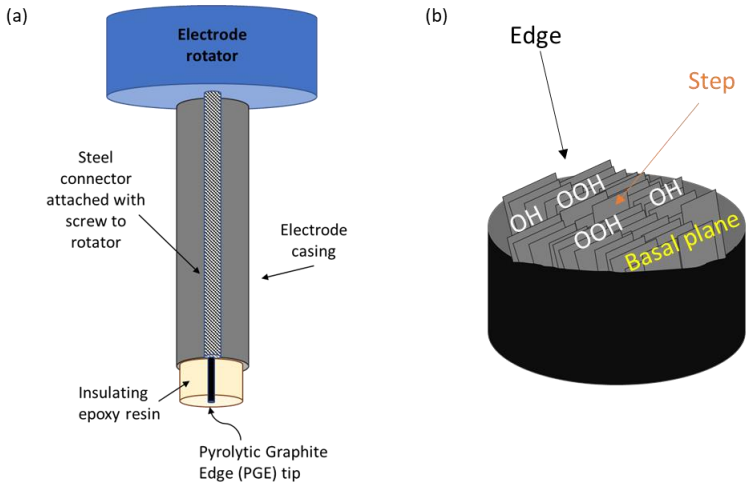


Figure 2-4: Schematic representation of the (a) pyrolytic graphite edge (PGE) rotating disk electrode (RDE) used for the analytical experiments in this Thesis. (b) structure of the pyrolytic graphite with edge and basal plane labelled. Polishing the surface of the PGE forms 'steps' with exposed functional grous which aid enzyme adsorption.

Carbon electrodes are also 'electrochemically silent' in aqueous conditions at the potential used in this Thesis (-0.6 to +0.5 V *vs* SHE); this simplifies analysis of electrochemical data.[11] All experiments were performed in a N_2 atmosphere using a glove box (MBraun or Glove Box Technology Ltd, < 0.1

ppm O_2), since O_2 reduction occurs at carbon electrodes at *ca* -0.2 V, this was to prevent complication of catalytic currents by direct O_2 reduction at the electrode.

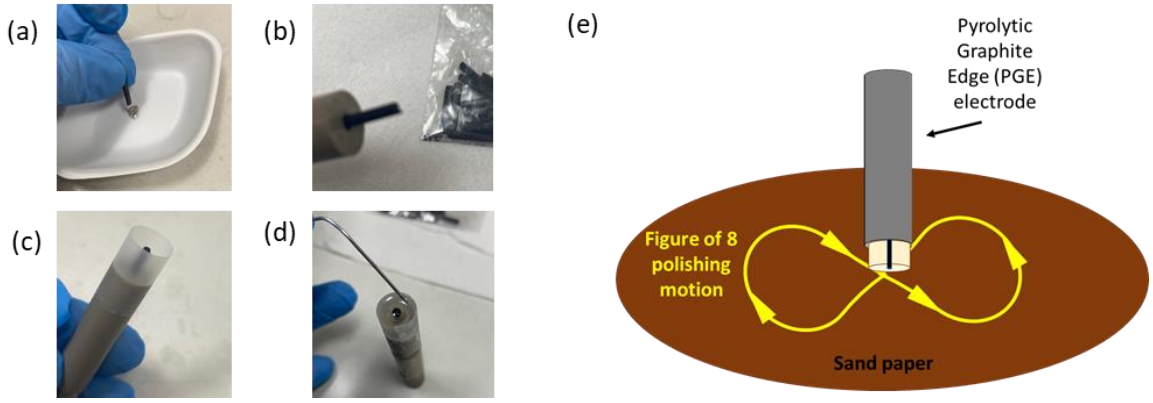


Figure 2-5: Technique for making the PGE RDE. (a) carefully cementing the pyrolytic graphite rod in place using RS Pro silver epoxy resin (b) carbon rod cemented in place (c) using Scotch brand tape to create a mould for epoxy resin (d) removing any air bubbles with a pin. (d) Schematic representation of how to prepare the PGE by polishing and roughening up the surface of the electrode on sandpaper using a figure of 8 motion to prevent the surface of the electrode becoming slanted and uneven.

The working electrodes were prepared as shown in Figure 2-5 (a) taking a cylindrical pyrolytic graphite rod (Momentive Performance Materials) with a diameter of 2 mm and dipping it in to silver loaded epoxy glue (RS) being careful not to allow any epoxy onto the sides of the rod as they can contaminate the electrochemistry experiments with Ag. (b) The carbon rod was then sealed into a Delrin rotating disk electrode case with *ca* 0.5 cm of carbon protruding from the end. (c) A circular mould was made around the edge of the electrode case using Scotch tape. It is crucial to ensure that the mould is circular, as any irregularities would affect the stirring when the electrode is rotated. (d) Insulating epoxy resin (Aradur hardener and Araldite resin, Robnor Resins) was prepared and poured carefully into the mould of the PGE so that only the edge surface of the carbon rod tip was exposed. A pin was used to carefully remove any bubbles from the wet epoxy. The electrode was then allowed to cure for at least 48 hours before being polished with several grades of sand paper starting from 80 grit (coarse) paper to 440 grit (fine) and then finally polishing with RS Pro P800 very fine sanding sheets in a 'figure of 8' motion as shown in Figure 2-5 (e). This technique ensures that the surface

of the electrode is even and not slanted, which would alter the surface area of the WE, and leaves exposed a graphite 'edge' disk of surface area 0.03 cm^2.

The electrode was connected to an electrode rotator (EG&G model 636) and prior to every electrochemical experiment the surface was polished using the 'figure of 8' technique on P800 paper. This generates a rough 'stepped' surface as shown in Figure 2-4(b) which has polar fuctionalities exposed which facilitate enzyme adsorption.[12,13] The electrode was then rinsed in MilliQ water before being sonicated for at least 30 seconds to remove any loose carbon dust from the sand paper. The electrode was allowed to dry or was dried gently using a dust free tissue.The electrode was then abraded using sand paper to create an electrode finish more similar to a pyrolytic graphite particle, then followed by a further 30 seconds sonication before drying.

To prepare the enzyme film an aliquot of enzyme solution (~ 0.5 µL) was spotted onto the PGE electrode tip as shown in Figure 2-2(c). This was then allowed to partially dry for approximately 10 to 15 seconds (depending on the enzyme and the concentration of the solution). The electrode was then attached to the electrode rotator and placed into the electrochemical cell (section 2.2.5) which was prefilled with the appropriate buffer. The electrode rotator was connected to the potentiostat allowing electrochemical control over the working electrode.

2.2.3 Reference electrodes

For the majority of analytical experiments in this Thesis, a saturated calomel electrode (SCE) was used as a reference and the potential for all experiments corrected to SHE using equation 2-2, and depending on temperature was adjusted using a linear correction of -67 mV / °C.[14]

$$E_{SHE} = E_{SCE} + 0.244 \text{ V at } 25°C \qquad [2\text{-}2]$$

For experiments carried out using the RedoxMe cell and the electrochemical flow cell (Chapter 5), a Ag/AgCl reference electrode was used. Once again potentials were converted to SHE using equation 2-3 below:

$$E_{SHE} = E_{Ag/AgCl} + 0.205 \text{ V at } 25°C \quad [2\text{-}3]$$

Where necessary these were also corrected for the temperature of the experiment using a linear correction of - 0.73 mV / ^{o}C.[14]

2.2.4 Counter electrode

In the three-electrode system described in section 2.2.1, a counter electrode (CE) is required to complete the circuit. This was achieved by using a platinum wire (Surepure Chemetals, 99.95%, 0.4 mm diameter) as it is inert and has high conductivity and catalytic activity. For the reactions in this Thesis, the reduction taking place at the CE likely includes the oxidation of water, resulting in the evolution of O_2 at the surface of the CE.

For the analytical experiments in this Thesis, which are short with low currents, this reaction is not a concern. However, to ensure the kinetics of the reaction taking place at the CE do not affect the reaction taking place at the WE, the surface area of the CE must be larger than the WE. For the electrochemical synthesis experiments, high surface area carbon electrodes were used and the experiments were carried out for a prolonged period of time. To ensure the CE had sufficient surface area to support the currents involved the Pt wire was coiled tightly. It was therefore necessary to isolate this reaction from the rest of the system by using a fritted compartment for the Pt wire to sit in. For the electrochemical experiments in Chapter 4 a glass tube with a sintered glass frit from IJ Cambria was used, and this was filled with saturated potassium chloride solution (KCl). The RedoxMe cell used in Chapter 5 was separated with an Aquivion membrane to separate the anode and

cathode compartments. This material is similar to Nafion and allows proton exchange but prevents any gases or undesirable by-products from contaminating the experiment in the WE compartment.

2.2.5 Electrochemical cells

Analytical electrochemical experiments were performed in a specialised, gas tight, electrochemical cell Figure 2-6.

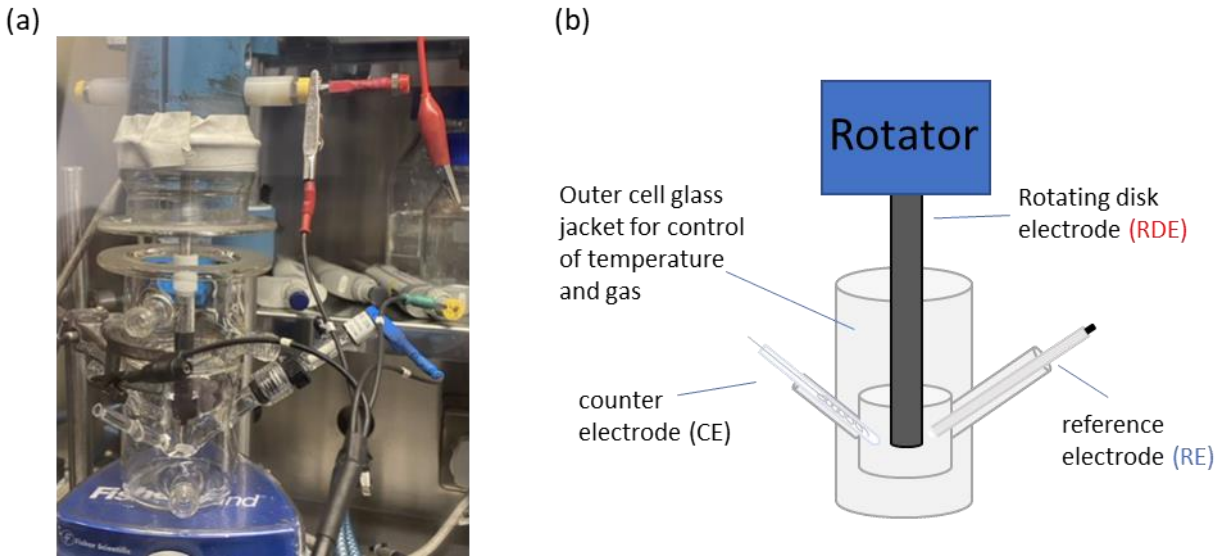


Figure 2-6: (a) A gas tight glass electrochemical cell with a water jacket for temperature control and gas inlet and outlet for control of the gas atmosphere. The cell seals around the electrode rotator allowing use of a pyrolytic graphite edge (PGE) rotating disc electrode (RDE). Sealed side arms allow the use of a RE, CE and syringe for injecting substrates. (b) schematic representation of electrochemical cell.

This cell allowed precise control over the temperature via the water jacket which could be attached to a water bath. Stirring is controlled via the rotation of the WE and and substrate can be injected via a small side-arm.

2.3 Electrochemical techniques

This work in this Thesis used cyclic voltammetry (CV) and chronoamperometry to investigate and characterise enzyme activity. Chronoamperometry was also used to drive enzyme catalysed synthesis reactions.

2.3.1 The electrode-solution interface

Where the surface meets the solution is known as the electrode-solution interface which contain the double and diffuse layers and understanding these is crucial to interpreting what the electrochemistry experiments.

2.3.2 The electrical double layer

The surface of the carbon electrode is in contact with the solution. When a potential is applied, the surface of the electrode becomes charged (positive or negative) at its surface and this has an effect on the solution it is in contact with. The potential applied is not the same as that of the bulk solution contained in the cell, so the charge at the surface of the electrode, will have an effect at the electrode-solution interface.[15]

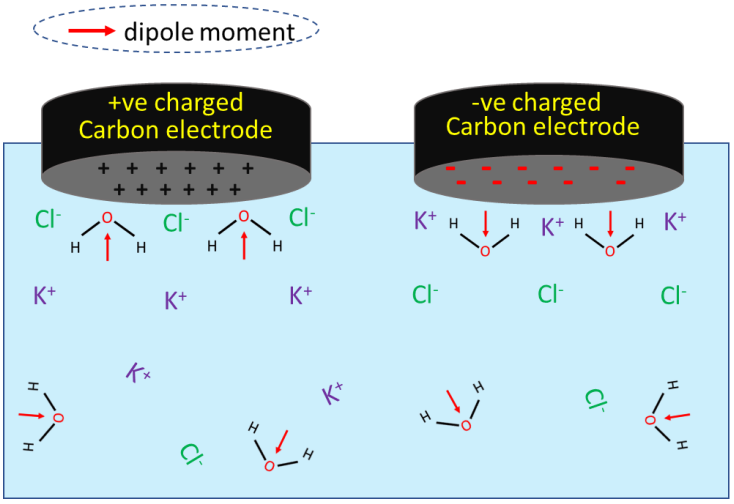


Figure 2-7: Schematic representation of electric double-layer; Change in electrode polarity causes a re-orientation of molecules and ions in solution at the electrode-surface interface.

The molecules in the bulk solution are randomly oriented, and even without stirring these molecules will be moving due to Brownian motion. The charge on the surface of the electrode causes the molecules to rearrange themselves so that their permanent dipole attracts/repels this charge. Together with any ions in solution, they align themselves in a layer near the interface of the electrode as shown in Figure 2-7. This layer of orderly solvent molecules and ions is known as the electrical double layer.

2.3.3 The diffuse layer

The electrical double layer formed at the electrode-solution interface acts to oppose the charge of the electrode and essentially cancel the charge. However, molecules in solution under Brownian motion will disrupt the layer as shown in Figure 2-8 causing an excess of oppositely charged ions to collect in a so-called diffuse layer. This causes a change in potential over the distance of the layer.

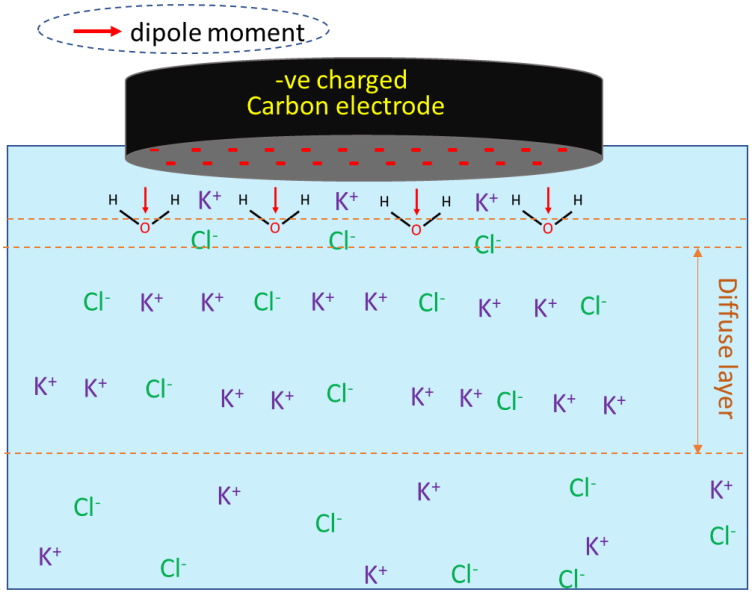


Figure 2-8: Schematic representation of the diffuse layer which forms when Brownian motion disrupts the molecules in the electrical double layer at the surface of the electrode. This causes an excess of cations (in this example of a negatively charged electrode) to form the diffuse layer where there is a change in potential.

When the polarisation of the electrode is changed, the ions and solvent molecules in the electrochemical cell will respond to this change which can be observed as a sharp change in the magnitude of the current seen in the chronoamperometry graphs in Chapters 4 and 5. Any additional substrate/cosolvent that is injected during an experiment can cause a temporary change in polarity which disrupts the double layer causing a spike on the chronoamperometry graph.

2.3.4 Cyclic voltammetry

Cyclic voltammetry is a powerful tool for analysing what is happening at the surface of the electrode. During a cyclic voltammogram (CV) as shown in Figure 2-9, the potential of the WE is swept between two potentials (E_1 and E_2) and any change in current is recorded.

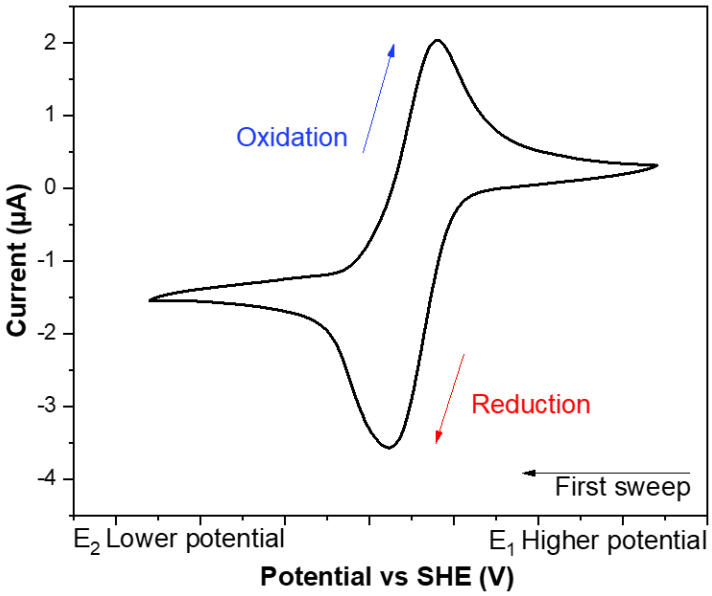


Figure 2-9: Cyclic voltammetry for analysis of redox enzymes. A potential is applied (E_1) and swept to a more negative potential (E_2) before being swept back to E_1 and the current recorded on the y-axis.

As the applied potential is changed, so is the charge on the electrode which rearranges the electrical double layer leading to a flow of ions, giving a non-redox (non-Faradaic) current. When a redox reaction takes place at the surface, electrons are transferred between the electrode and the redox active species and a Faradaic current is observed. At the start of each experiment, a blank CV is recorded under the same conditions but in the absence of any catalyst or substrate. This shows that any peaks in the CV are contributions from the species being investigated.

The magnitude of the non-Faradaic (capacitive) current is dependent on a number of factors including surface area of the electrode, scan rate and temperature. To ensure accuracy in the experiments, the conditions for the blank were the same as conditions for the main experiment. A scan rate of 10 mV s^{-1} was used as standard for CV experiments, unless otherwise stated. At the start of each CV, the starting potential is held for 10 seconds to allow the double layer to equilibrate, this prevents a large initial capacitive current.

2.3.5 Chronoamperometry

For a chronoamperometry experiment, the potential applied to the WE is kept constant for the duration of the experiment. After the initial reorganisation of the double layer when the potential is applied (approximately 10 – 15 seconds), there is no significant non-Faradaic contribution to the current. Chronoamperometry monitors the activity of the enzyme under a set of conditions that the enzyme is exposed to (temperature, potential, rpm, gas atmosphere) whilst other parameters such as substrate concentration are changed

In the work in this Thesis, chronoamperometry was also used to drive electro-enzymatic synthesis by applying a fixed potential to the system to drive the redox catalysis. The chronoamperometry plots the change in current (I) over time (t_i to t_f) and this plot can be integrated to calculate the charge passed (Q) using equation [2-4]:

$$Q = \int_{t_i}^{t_f} I \, \mathrm{d}t \qquad [2\text{-}4]$$

This can then be used to determine the number of electrons passed

In Equation [2-5], Faraday constant, F, e is the charge on an electron (1.60×10^{-19} C) and N is the Avagadro constant (6.022×10^{23} mol^{-1}).

$$F = eN = 96{,}485 \text{ C mol}^{-1} \qquad [2\text{-}5]$$

This can used to determine the current efficiency: moles of product generated (which in this thesis is quantified by GC analysis) per moles electrons passed. For both the reduction of NAD(P)$^+$ to NAD(P)H and flavin$_{ox}$ to flavin$_{red}$ is a two electron process, so the number of electrons should be

divided by 2.

As catalysis is taking place at the surface of the electrode only, any substrate at the surface of a stationary electrode will be consumed and there will be a build-up of product. To prevent mass transport limitations, the solution at the surface of the electrode must be removed and replaced. This is achieved by either the rotation of the electrode or by stirring the solution in the cell. The stirring speed (or rotation) should be increased until there is no increase observed in the magnitude of current.

2.4 High surface area electrodes

Much of the work in Chapter 3 of this Thesis involved analytical work, for which the PGE RDE was used. However, much of the work in Chapters 4 – 6 required larger quantities of enzyme to be used, and for this, higher surface area electrodes were required.

2.4.1 Materials used for high surface area electrodes

Various types of carbon electrodes were used for the work in this Thesis. For most of the synthesis work in Chapters 4 and 5, carbon felt was used due to its high surface area with good porosity that can provide an abundance of redox reaction sites.[16] The carbon felt used for this work was 3.18 mm thickness and was attached to the potentiostat via a 10 cm length of carbon yarn.

For the development of high surface-area electrodes for use in the flow cell in Chapter 5, carbon paper (CP) was used. CP is made from interwoven carbon fibres and is commonly used for fuel cells.[17] In the work in this Theisis it is used for the direct adsorption of NAD^+-reductase or for the adsorption of enzyme-modified particles described in Chapter 5, 160 5.5.2 .

2.4.2 Protocol for enzyme-modified particles

Carbon black nanoparticles (BP2000), Cabot Corporation, were used to create the high surface-area nanoparticle electrodes in Chapter 5. These particles range in diameter from 17 nm to 31 nm and have a specific surface area (BET) of 1332 ± 22 $m^2 g^{-1}$.[18] The pores in these particles have a diameter of 4.7 nm and a volume of 1.36 $cm^3 g^{-1}$. The particles act as a conductive surface onto which many enzymes will adsorb, and they have been demonstrated as a heterogeneous H_2-driven NAD^+-recycling system by Reeve *et al.*[19]

The general protocol for preparation of the enzyme modified nanoparticles is:

- Carbon particles were added to aqueous buffer in an Eppendorf tube to give a concentration of ca 20 mg mL^{-1}.

- This mixture was sonicated for at least 30 minutes to aid dispersion, then a small pipette tip was used to thoroughly mix the slurry before sonicating for a further 30 mins.

At this stage the particles are suitable for using to pipette directly onto the surface of an electrode and allowed to dry. This technique was used in the synthesis of NADH experiments in Chapter 3.

However, most of the experimental work involved adsorbing the enzyme to the particles to create enzyme-modified electrodes. For this the following additional step was performed:

- An aliquot of BP2000 slurry was added to the required enzyme (or mixture of enzymes) and allowed to incubate at 4 °C for at least 30 minutes.

The quantity of enzyme and particles used is detailed in the relevant results chapters.

2.5 Enzyme kinetics and electrochemical analysis

The work presented in this Thesis requires an understanding of enzyme kinetics to develop and optimise experiments. Enzymes that catalyse the same reactions behave differently under the same conditions since they have different structures and roles *in vivo*. In Chapter 3 HoxFU from *H. thermoluteolus* was electrochemically characterised with side-by-side comparison to soluble hydrogenase from *R. eutropha* (which has previously been used extensively within the group).

2.5.1 Affinity constant (K_M)

The Michaelis-Menten kinetic model gives an algebraic expression that relates the activity of an enzyme to the concentration of its substrate.[20,21] This is shown in [2-6] where an enzyme (*E*) and a substrate (*S*) form a complex (*ES*) with a rate of k_1. This complex can either dissociate with a rate constant of k_{-1} or react to form the product (*P*) with rate constant k_2. The product can also dissociate to form ES, but for the systems described in this Thesis, this happens so rarely that the contribution of k_{-2} is negligible.

$$E + S \underset{k_{-1}}{\overset{k_1}{\rightleftharpoons}} ES \xrightarrow{k_2} E + P \qquad [2\text{-}6]$$

If the formation of the product is the rate limiting step the rate of reaction (*v*) is equivalent to expression [2-7].

$$v - k_2[\mathrm{ES}] \qquad [2\text{-}7]$$

If the formation and dissociation of [*ES*] occur at equal rates, the steady-state approximation can be applied to the enzyme-substrate complex (Equation [2-8]) to derive Michaelis-Menten constant (K_M) Equation [2-9]:

$$\frac{d[ES]}{dt} = k_1[E][S] - (k_{-1} + k_2)[ES] = 0 \quad [2\text{-}8]$$

$$[ES] = \frac{k_1[E][S]}{k_{-1} + k_2} = \frac{[E][S]}{K_{\mathrm{M}}}, K_M = \frac{k_{-1} + k_2}{k_1} \quad [2\text{-}9]$$

Throughout a reaction the total enzyme concentration ([E_{total}]) is equal to [E] + [ES], by substituting for [E] the equation can be re-written to give Equation [2-10]:

$$[ES] = \frac{([E_{total}] - [ES])\,[S]}{K_{\mathrm{M}}}, [ES] = \frac{[E_{total}][S]}{(K_{\mathrm{M}} + [S])} \quad [2\text{-}10]$$

At the maximum rate of reaction, v_{max}, all of the enzyme will have substrate bound meaning [ES] is equivalent to [E_{total}], Equation [2-11].

$$v_{max} = k_2[\mathrm{E}]_{\mathrm{total}} \quad [2\text{-}11]$$

By substituting the expression for [ES] from Equation [2-10] into Equation [2-7] and combining with Equation [2-11] the Michaelis-Menten equation is reached:

$$v = \frac{v_{max}[S]}{[S] + K_{\mathrm{M}}} \quad [2\text{-}12]$$

When the substrate concentration is equal to the K_{M}, the rate is half the maximum. The Michaelis-Menten constant therefore indicates the enzymes affinity for a particular substrate. An enzyme with a low K_{M} has a higher affinity to the substrate compared to an enzyme with a high K_{M}.

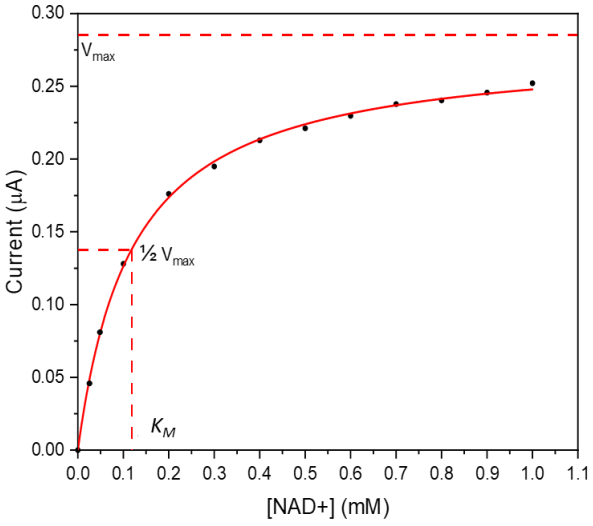


Figure 2-10: A typical plot of substrate concentration, [NAD^+], vs current. This is then fitted to the Michaelis Menten equation. fit applied.

The K_M for an enzyme can be determined electrochemically (Chapter 3, section 3.5.1). A constant potential is applied (chronoamperometry) and the current recorded. Aliquots of substrate are injected into the electrolyte. Since the magnitude of the current is proportional to the rate of catalytic turnover by the adsorbed enzyme film, the current can be plotted against the concentration of substrate and a Michaelis-Menten fit applied. A typical plot is shown in Figure 2-10, with v_{max} and K_M labelled on the plot. The value of K_M can be compared across multiple enzyme films to obtain an average, as this technique is independent of the amount of enzyme used.

2.6 Ultraviolet-visible spectroscopy (UV-Vis)

2.6.1 Electronic transitions in cofactor molecules

The cofactor recycling experiments performed in Chapters 3 to 4 of this Thesis used ultraviolet-visible (UV-Vis) spectrophotometry to determine if oxidised/reduced cofactors were present. This type of analysis used UV light in the region 200-800 nm. The absorptions in this region are due to electronic transitions shown in equation 2-13:

$$\sigma \rightarrow \sigma^* > n \rightarrow \sigma^* > \boldsymbol{\pi} \rightarrow \boldsymbol{\pi}^* > n \rightarrow \boldsymbol{\pi}^* \quad [2\text{-}13]$$

These transitions are caused by the excitation of electrons from an occupied molecular orbital to an unocucupied one. The σ → σ transitions are too high in energy to be seen in the UV-Vis region. However, molecules that contain aromatic rings have conjugated systems where the **π** → **π** *and n → **π*** transitions absorb in the UV-Vis region.

2.1.1.1.Nicotinamides – NAD(P)⁺ and NAD(P)H

The **π** → **π** *transition in the adenine ring of nicontinamide cofactors (shown in red in Figure 2-11) have a absorb in the 240-275 nm region of the UV spectrum, with λ_{max} = 260 nm:, both the reduced and oxidised cofactors absorb in this region.

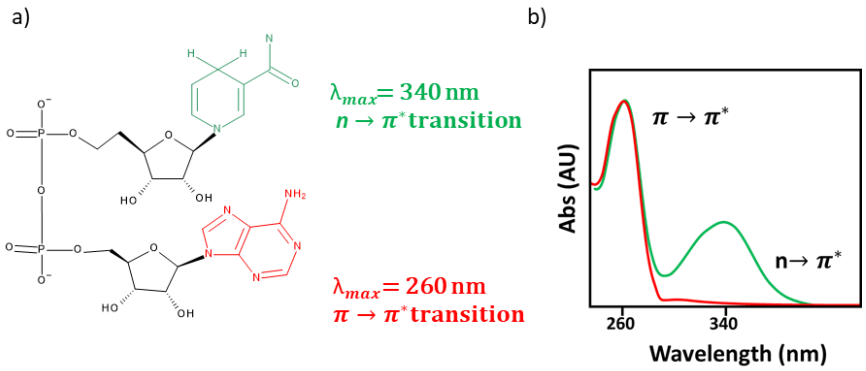


Figure 2-11: The UV-Vis active regions of the nicotinamide cofactors (a) the adenine ring (shown in red) absorbs strongly in the 260 mn region due to a π → π * transition. The oxidised nicotinamide ring has a weak π → π * transition in the 260 nm region, this is lost upon the addition of a hydride to form the reduced species NADH. The addition of two electrons causes a **n→** π * transition at 340 nm. (b) A typical UV-Vis spectra of NAD^+ (red) and NADH (green).

A diagnostic peak for the reduced species appears at λ_{max} = 340 nm, this is due to an n → **π*** transition in the NAD(P)H, involving the electrons from the non-bonding nitrogen in the carboxyamide group (shown in green in Figure 2-11).

2.1.1.2. Flavins – FAD and $FADH_2$, FMN and $FMNH_2$ and Riboflavin[22–25]

In a flavin molecule, the isoalloxazine moiety is the chromophore where electronic transitions occur that give rise to UV-Vis absorption.[24] The isoalloxazine ring is also the centre for redox catalysis, and can exist in 3 redox states, as shown in Figure 2-12:

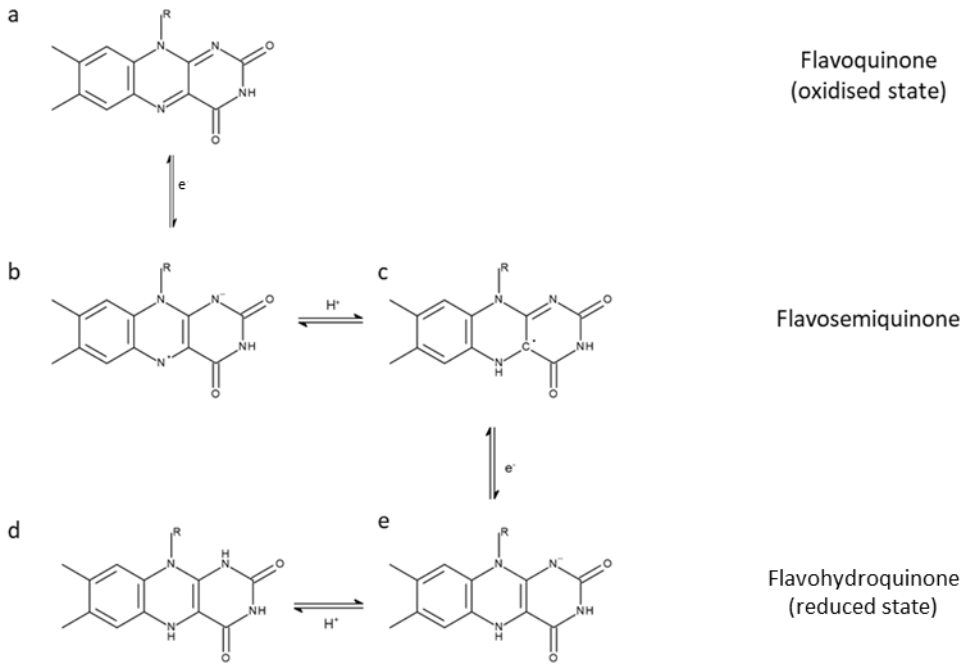


Figure 2-12: The different redox states of flavin molecules; (a) oxidised flavin, (b) anionic flavin semiquinone, (c) neutral flavin semiquinone, (d) anionic flavin hydroquinone, (e) neutroal flavin hydroquinone.

Spetroscopically, the flavins can be identified by UV-Vis due to the electronic transitions occurring in the isoalloxazine ring. In its oxidised form, the isoalloxazine ring absorbs UV-visible light at wavelengths of *c.a.* 450 nm and 375 nm. The absorbance at 450 nm is attributed to a $\pi \rightarrow \pi^*$ transition, whereas the absorbance peak at 375 nm is an overlap of two transitions; $\pi \rightarrow \pi^*$ and $n \rightarrow \pi^*$transition, where the $n \rightarrow \pi^*$ transition is a result of the the non-bonding nitrogen in the carboxyamide group.[26] A typical spectrum is shown in Figure 2-13 in blue.

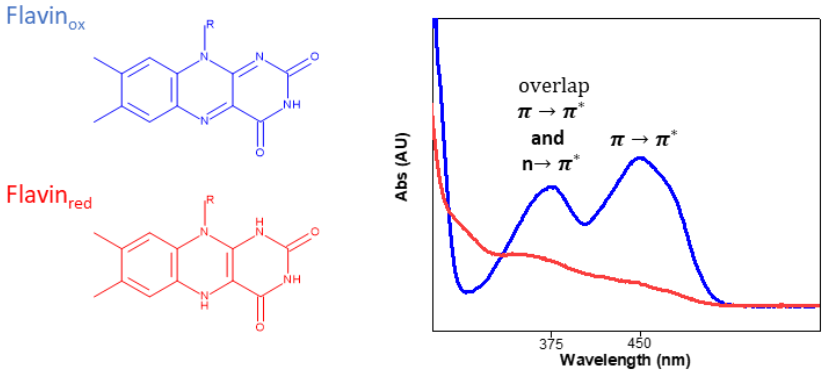


Figure 2-13: A typical UV-Vis spectra of oxidised flavins (blue); the isoalloxiazine absorbs strongly in the 450 mn region due to a $\pi \rightarrow \pi^*$ transition. There is also a peak at 375 mn due to an overlap in the $\pi \rightarrow \pi^*$ transition of the C-C and the $n \rightarrow \pi^*$ transition due to the non-bonding nitrogen in the carboxyamide. The hydroquinone or reduced flavin (red) displays a smaller peak in the 320 – 340 nm region due to a weak $\pi \rightarrow \pi^*$ transition.

The reduced flavin (hydroquinone, shown in red in Figure 2-13) shows no absorption at 450 nm as it has a fully occupied π orbital, therefore no transitions are observed. A $\boldsymbol{\pi \rightarrow \pi^*}$ transition is observed in the UV region between 320 – 340 nm where a $\boldsymbol{\pi \rightarrow \pi^*}$ transition is observed.

2.6.2Concentration determination using the Beer Lambert Law

The UV-Vis spectrophotometer routinely used in this work was the Cary 60 (Agilent). This uses a cuvette with a path length of 1 cm which allows quantitative analysis of samples using the Beer-Lambert Law (eqn. 2-14):

$$A = \varepsilon c l \qquad [2\text{-}14]$$

Where the absorbance (A) is equal to the extinction coefficient (ε) multiplied by the concentration of the solution multiplied by the path length (l).

Table 2-1: Literature values for extinction coefficients (ε) for the flavin[24,27–29] and nicotinamide cofactors, [30] together with the values obtained experimentally for NAD^+ and NADH within the Vincent group. [31]

Cofactor	λ_{max} *(nm)*	Literature ($mM^{-1}\ cm^{-1}$)	Experimental ($mM^{-1}\ cm^{-1}$)
NAD^+	260	17.4	15.1
	340	N/A	*N/A*
NADH	260	14.1	*N/A*
	340	6.22	*5.5*
FAD	375	9.3	N/A
	450	11.3	N/A
FMN	373	10.4	N/A
	445	12.5	N/A
RF	365	12.9	N/A
	450	N/A	N/A

The literature values for the cofactors used in this Thesis are shown in Table 2-1. The extinction coefficients for NAD^+ and NADH were higher than experimental values determined by Dr Zul Idris, during experiments carried out in the Vincent Group.[30] This is possibly due to interactions between the cofactor and the buffers used, so where relevant, experimental values were used.

2.7 Gas Chromatography-Flame Ionisation Detection (GC-FID)

The alkene reactions studied in Chapter 4 were analysed using Gas Chromatography- flame ionisation detection. This is a technique used to separate and analyse organic compounds by combustion of the compounds in the sample to produce ions which are then detected when they pass between two electrodes causing a potential difference. The current induced is proportional to the reduced carbon ions hitting the detector. All analysis was performed on ThermoScientific Trace

1310 GC. Conversion to corresponding products were calculated on the area of their respective peaks.

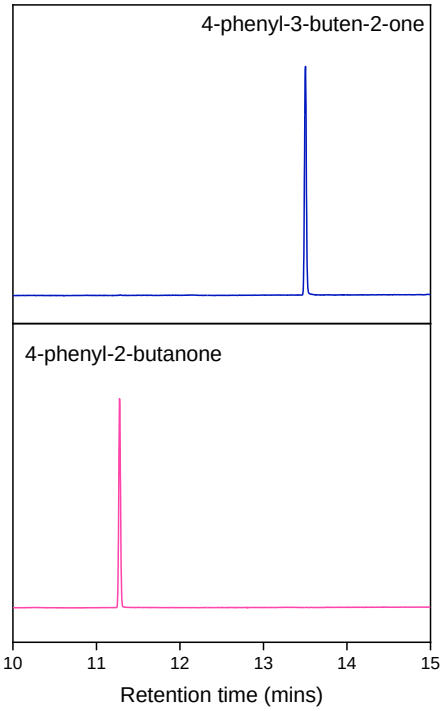


Figure 2-14: Example GC-FID chromatogram of 4-phenyl-3-buten-2-one (blue, commercially available) and 4-phenyl-2-butanone (pink), commercially available) standards.

Instrument: ThermoScientific Trace 1310 GC

Column CP-Chirasil-Dex CB (Agilent). Length 25 m,

Inlet: Temperature: 200 °C, split flow: 60 mL min^{-1}, splitless time 0.8 min, purge flow 5 mL min^{-1}, injection volume: 0.1 μL.

Carrier gas: H_2 constant pressure 170 kPa.

Oven program: Initial temp = 70 °C, hold for 5 mins, heat at 10 °C min^{-1} to 165 °C, heat at 50 °C min^{-1} to 200 °C, hold at 200 °C for 5 mins. Overall oven program was 108 minutes.

Detector: FID, temperature = 250 °C.

Gas chromatography (GC) was used to characterise the products of the reductions by comparing their retention times with those of pure commercially-bought standards. To prepare the sample for GC analysis, ethyl acetate was used to extract the reaction components (substrate and products) from the aqueous mixture. The organic layer was dried with anhydrous Na_2SO_4 before transferring 100 μL of the dried sample to a glass insert within a glass vial and diluting if necessary with more ethyl acetate.

Conversion to the products (%) was calculated using the relative peak areas according to Equation 2-15.

$$\text{Conversion (\%)} = \frac{\text{Product peak area}}{\text{Product peak area + Starting material peak area}} \times 100 \quad [2\text{-}15]$$

2.8 Reagents

In most cases, the reagents and methods for their use are discussed in the relevant Chapters. Where not specified, any substrates and products for the enzymes used purchased from Sigma.

2.8.1 Buffers

All experiments carried out in this Thesis were performed in buffered solutions. Electrochemical experiments require salts to increase the ionic conductivity of the solution and also buffers to control the pH of the solution to within a particular range suitable for the enzymes being used. The buffers used for work in this Thesis are shown in Table 2-2.

Buffers were prepared to a concentration of 50 mM (unless otherwise stated) by dissolving an appropriate mass of buffer salt in Milli-Q water. This buffer solution was then titrated to the desired pH using either concentrated HCl or KOH.

Table 2-2: Buffers used in this Thesis with their respective pk_a values.

pH	Buffer	pK_a (25 °C)
7	KP_i	6.8-7.2
8	Tris-HCl	8.1
5-10	Mixed buffer	-

The phosphate buffer (KP_i) was prepared by titrating K_2HPO_4 (Sigma, > 99 %) and KH_2PO_4 (Sigma, > 99 %) of the same concentration together. The mixed buffer system contained CHES, TAPS, HEPES, MES and Sodium Acetate (at 15 mM) and KCl (100 mM). The buffer was titrated to the chosen pH using KOH and HCl.

2.8.2 Cofactors

The cofactors (NAD^+, NADH, $NADP^+$ and NADPH) were all purchased from Sigma, stock solutions of 100 mM were made up in buffer as required. It is widely accepted that commercially available cofactors tend to contain impurities (adenosine diphosphate ribose and adenosine triphosphate). Dr Idris determined that the effect of these impurities on the activity of the NAD^+-reductase enzymes is only significant at concentrations above ~1 mM.[31] The work carried out in this Thesis only used cofactor concentrations of <2 mM, so the effect of these (<1 %) would be negligible. All cofactors were freshly made up before use as they tend to be unstable. In particular, the reduced cofactors are unstable with respect to oxidation, high pH, high temperature and buffer systems.[32]

2.9 Enzyme samples

A range of redox enzymes are used in the experimental work carried out in this Thesis. Some of these enzymes were made within the Vincent Group. Others were kindly provided by my industrial partners Johnson Matthey and some were commercially available.

The soluble hydrogenase from *Ralstonia eutropha (Re*SH) and the HoxFU from *Hydrogenophilus Thermoluteolus* (*Ht* HoxFU) were produced and purified Dr Miguel Ramierez from the Vincent Group.

Chapter 2 Bibliography

1 P. Atkins, J. de Paula and J. Keeler, Oxford University Press, 2022.

2 C. F. Blanford, *Chem. Commun*., 2013, **49**, 11130–2

3 M. Eddowes and Hill, *Nature*., 1980, **285**, 673-674

4 G. Morello, B. Siritanaratkul, C. F. Megarity and F. A. Armstrong*, ACS Catal*., 2019, **9**, 11255–11262

5 P. A. Ash and K. A. Vincent, *Chem. Commun*., 2012, **48**, 1400–9

6 K. A. Vincent, A. Parkin and F. A. Armstrong, *Chem. Rev*., 2007, **107**, 4366–4413

7 C. Leger, A. K. Jones, S. P. J. Albracht and F. A. Armstrong, *J. Phys. Chem. B*, 2002, **106**, 13058–13063

8 N. D. J. Yates, M. A. Fascione and A. Parkin, *Chem. - A Eur. J*., 2018, **24**, 12164–12182

9 C. F. Megarity, J. Esselborn, S. V Hexter, F. Wittkamp, U.-P. Apfel, T. Happe and F. A. Armstrong, *J. Am. Chem. Soc*., 2016, **138**, 15227–15233

10 F. A. Armstrong, *J. Chem. Soc., Dalton Trans.*, 2001, 661-671

11 R. M. Evans and F. A. Armstrong, *J. Am. Chem. Soc*. 2018, **140**, 10208–10220

12 J. Hirst and F. A. Armstrong, *Anal. Chem*., 1998, **70**, 5062–5071

13 C. Leger, S. J. Elliott, K. R. Hoke, L. J. C. Jeuken, A. K. Jones and F. A. Armstrong, *Biochemistry*, 2003, **42**, 8653–8662

14 D. T. Sawyer, A. Sobkowiak and J. L. Roberts, Wiley-Interscience New York, 1995

15 A.J. Bard and L. R. Faulkner, Wiley-Interscience New York, 2000

16 T. X. Huong Le, M. Bechelany and M. Cretin, *Carbon N. Y*., 2017, **122**, 564–591

17 D. Bevers, M. Wöhr, K. Yasuda and K. Oguro*, J. Appl. Electrochem*., 1997, **27**, 1254–1264

18 J. Quinson, R. Hidalgo, P. A. Ash, F. Dillon, N. Groberta and K. A. Vincent, *Chem. Electro. Chem.,* 2016, **3**, 2179-2188

19 H. A. Reeve, L. Lauterbach, O. Lenz and K. A. Vincent, *ChemCatChem*, 2015, **7**, 3480–3487

20 A. Cornish-Bowden, *Fundamentals of Enzyme Kinetics,* Portland Press Ltd, 2004

21 J. M. Berg, J. L. Tymoczko and L. Stryer, *Biochemistry, New* York, 2006.

22 K. Schwinn, N. Ferré and M. Huix-Rotllant, *Phys. Chem.*, 2020, **22**, 12447–12455.

23 P. Mondal, K. Schwinn and M. Huix-Rotllant, *J. Photochem. Photobiol. A Chem*., 2020, **387**, 112164

24 P. Macheroux, S. K. Chapman, G. A. Reid, S. K. Chapman and G. A. Reid, *Methods in molecular biology,* 1999, **131,** 1-7

25 R. Bartzatt, *J. Sci. Res. Reports*, 2014, **3**, 799–809

26 P. F. Heelis, *Chem. Soc. Rev.*, 1982, **11**, 15-39

27 C. Visvanathan, X. Li, S. Shi, L. A. Averianova, L. A. Balabanova, O. M. Son, A. B. Podvolotskaya and L. A. Tekutyeva, *Front. Bioeng. Biotechnol*, 2020, **8**, 570828

28 I. Ahmad, Q. Fasihullah, A. Noor, I. A. Ansari and Q. N. M. Ali, *Int. J. Pharm*., 2004, **280**, 199–208

29 R. Bartzatt, and T. Wol, *International scholarly research notices,* 2014, **2014**, 453085

30 E. Hald, P. Lehmann and J. Ziegenhorn, *Clinc. Chem.,* 1975, **21**, 884–887

31 Z. Idris, DPhil Thesis, University of Oxford, 2012

32 L. Rover, J. C. B. Fernandes, G. de O. Neto, L. T. Kubota, E. Katekawa and S. H. P. Serrano, *Anal. Biochem*., 1998, **260**, 50–55

33 L. Lauterbach, J. Liu, M. Horch, P. Hummel, A. Schwarze, M. Haumann, K. A. Vincent, O. Lenz and I. Zebger, *Eur. J. Inorg. Chem*., 2011, **2011**, 1067–1079

34 Lauterbach, Z. Idris, K. A. Vincent and O. Lenz, *PLoS One*, 2011, **10**, e25939

Preliminary electrochemistry

Protein film electrochemical (PFE) is an excellent tool for understanding redox enzymes that are capable of electron transfer with an electrode, such as NAD^+ reductase that cycles NAD^+ and NADH at a flavin-active site and shuttles electrons to the protein surface via a chain of FeS clusters. Previous work undertaken in the Vincent Group has demonstrated implementation of the NAD^+-reductase from *Ralstonia eutropha* (*Re* SH) in a novel approach to cofactor recycling, with significant insights drawn from PFE experiments.[1,2] However, this NAD^+-reductase is hard to manipulate using molecular biology techniques due to lack of tools for working in *Ralstonia*, leading to evaluation of an NAD^+ reductase recombinant expressed in E. coli, which could then be rapidly modified using standard techniques.

3.1 Introduction

The focus of this chapter is to compare the electrochemical characterisation of *Re* SH with a NAD^+-reductase moiety native to the thermophilic organism *Hydrogenophilus thermoluteolus* expressed recombinantly in *E. coli (Ht* HoxFU). It was presumed that this enzyme may be more thermostable and generally robust than SH, and being expressed in *E. coli* may mean mutations could be made to change selectivity to allow recycling of the related cofactor, NADPH.

Experimental work focussed on the preliminary electrochemical characterisation of *Ht* HoxFU, in terms of:

- Establishing whether the enzyme moiety could accept electrons from an electrode to reduce NAD^+ and/or oxidise NADH.
- Electrochemical characterisation of the *Ht* HoxFU moiety to determine under which conditions it operates optimally.

- Electrochemical synthesis of NADH to establish whether *Ht* HoxFU can be employed as an electrocatalyst for the recycling of NAD^+.
- Study of a genetically mutated version of *Ht* HoxFU for use in an $NADP^+$ recycling system.

Findings from electrochemical study were then used to develop a system for using electrochemically generated NADPH to drive a biocatalytic reaction.

3.2 Isolation of the Ht HoxFU moiety

All samples of *Ht* HoxFU were prepared by Dr Miguel Ramirez in the Vincent Group

3.3 Electrochemical characterisation

Electrochemical studies of the NAD^+-reducing subunits of the soluble hydrogenase of thermophilic organism *H. thermoluteolus* expressed in *E. coli (Ht* HoxFU) were carried out alongside a batch of soluble hydrogenase from *Ralstonia eutropha* (*Re* SH) which has been well studied within the group. This was to act as a positive control and also for comparison purposes to see if the *Ht* HoxFU is more thermostable and generally robust than the *Re* SH.

3.4 NAD+/NADH cycling

Before carrying out any characterisation experiments, it was for necessary to establish that *Ht* HoxFU was able to exchange electrons with an electrode (Figure 3-1a) and catalyse both the oxidation of NADH and the reduction of NAD^+. For each experiment, an aliquot of enzyme (0.5 µL) was spotted onto a freshly polished PGE RDE and allowed to partially dry for a few seconds. The enzymes used in this chapter were from the same batch and were flash frozen in aliquots of 4 µL by submersing in liquid nitrogen. This allowed a fresh aliquot to be removed from the freezer for each triplicate of experiments, ensuring that the enzyme was 'fresh' for each set of experiments. This

enzyme-modified electrode was then placed into the electrochemical cell containing buffer with either NAD^+ (Figure 3-1b) or NADH (Figure 3-1c). The potential was swept from a value where no catalysis was expected to a potential where catalysis was thermodynamically favourable. The CVs in Figure 3-1 show the current recorded at the surface of the electrode. A sharp increase/decrease in the magnitude of the current can be observed at -0.32 V vs SHE for NAD^+ reduction and -0.45 V vs SHE for NADH oxidation. This is due to exchange of electrons from the electrode to the enzyme and from the enzyme to the electrode. This confirms that cofactor is being cycled by the *Ht* HoxFU. The difference in the magnitude of current recorded for NAD^+ cycling compared to NADH suggests a strong bias towards the reduction of NAD^+ by the *Ht* HoxFU.

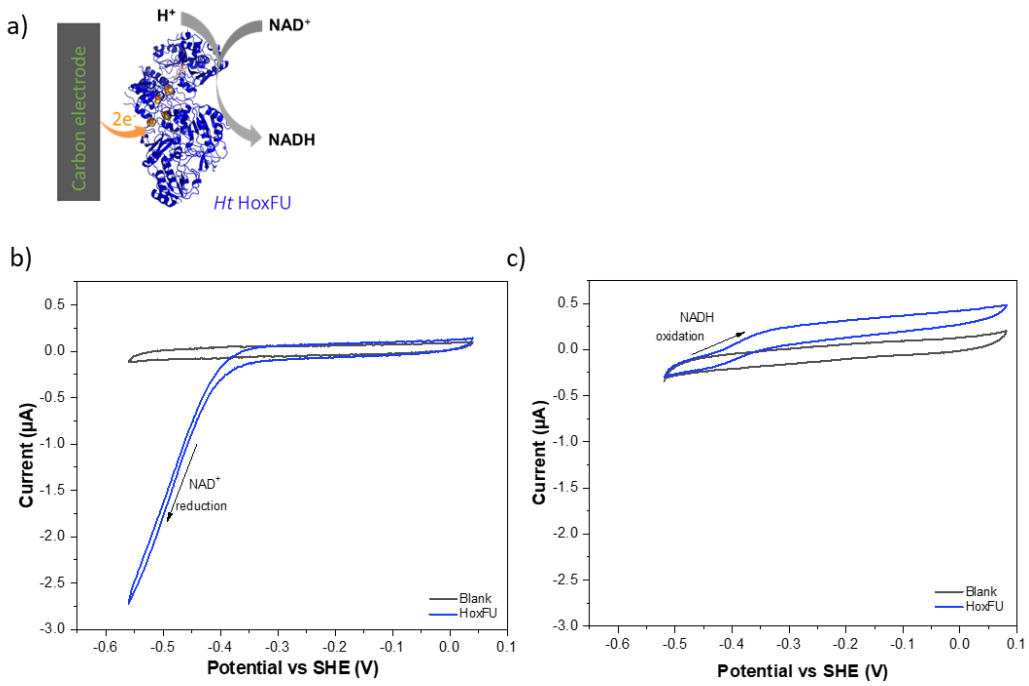


Figure 3-1: (a) Schematic representation of Ht HoxFU moiety adsorbed to a carbon electrode showing how electrons are accepted directly from the electrode and travel along the Fe-S clusters to the active site where NAD+ reduction takes place. (b) Cyclic voltammetry confirming that the Ht HoxFU is able to catalyse the reduction of NAD+ and b) the oxidation of NADH. Experiments performed in Tris-HCl buffer, pH 8, at 29°C with (a) 1 mM NAD^+ and (b) 1 mM NADH in solution. The arrows denote the direction of the first potential sweep. A scan in the absence of cofactor is shown in black. The electrode was rotated at 2000 rpm to prevent mass transport limitations. Protein Film Electrochemistry[3,4]

3.5 Michaelis-Menten kinetics

Michaelis-Menten kinetics were introduced in Chapter 2, section 2.5.1 and determines the affinity of the NAD^+-reductase towards NAD^+ and NADH. Chronoamperometry was the electrochemical technique used to determine the K_M. A low K_M value means that an enzyme has a high affinity for the substrate (in this case NAD^+ or NADH). It is desirable for the *Ht* HoxFU to have a high affinity towards NAD^+ reduction, as this would mean that the enzyme could achieve high activity at low substrate concentration. This would be desirable not only because the cofactor is expensive, but also if concentrations of cofactor could be minimised, it would avoid the need for additional purification steps.

3.5.1 Determination of the affinity constant K_M with NAD^+

All chronoamperometry experiments in this section were performed 8 times each for both *Re* SH and *Ht* HoxFU (an example plot is shown in Figure 3-2, this example has been selected as the K_M is close to the mean). Performing the experiments multiple times helps to minimise error.

The experiments were performed using a PGE electrode that had been modified with NAD^+-reductase (either *Re* SH or *Ht* HoxFU) in Tris HCl pH 8 buffer. A potential for the chronoamperometry experiments was selected from the catalytic region of the CV. This potential had been chosen by other members of the Vincent group when performing similar characterisation experiments, so it was useful to use the same for comparison.[5,6] At the potential selected, (-0.41 V vs SHE) there is significant current for the reduction of NAD^+, and it can be observed from the CV that there are no other unwanted redox reactions taking place at the surface of the electrode.

A chronoamperometry plot from one of the kinetic experiments is shown in Figure 3-2a. A fixed potential was applied and the current allowed to settle, this should be around 0 A since there is no substrate in the solution. Any current observed at the start is due to residual capacitance, and this value is subtracted from the data. Aliquots of NAD^+ were injected at intervals (indicated by the arrows) and the magnitude of the current increase was recorded. Catalytic current is directly proportional to the activity of the enzyme; so, this can be plotted against the concentration of substrate, NAD^+, and a Michaelis-Menten fit applied (Figure 3-2b). The example shown in this figure was selected as it had a K_M value close to the mean. The Michaelis-Menten equation can be used to determine the K_M, which is shown on the plot.

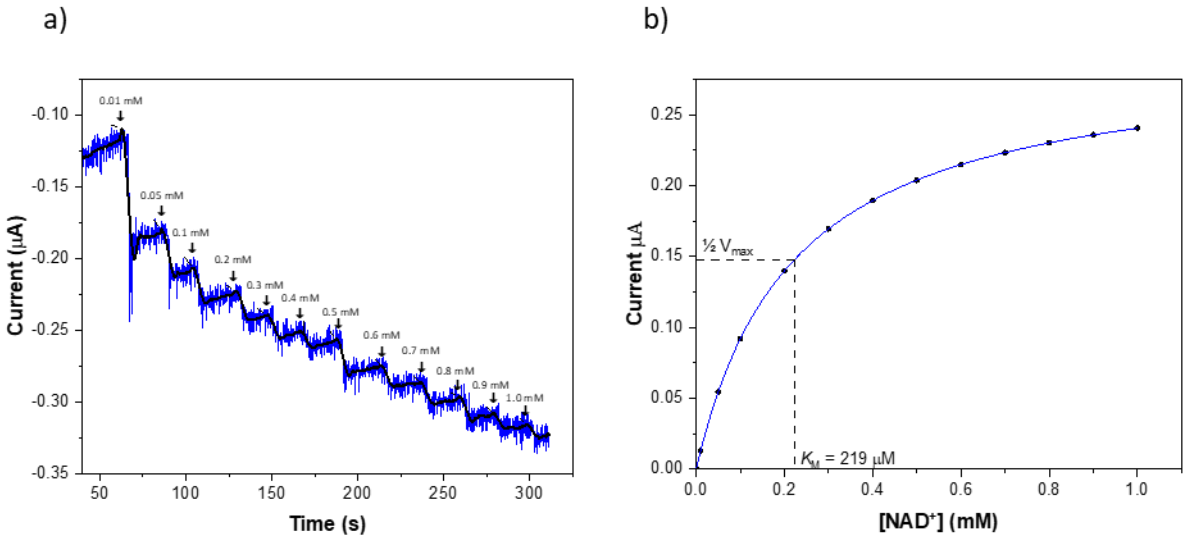


Figure 3-2: (a) Typical plot from a chronoamperometry experiment used to determine the K_M of the NAD^+-reductase (Ht HoxFU used in this example). A 0.5 µL aliquot of *Ht* HoxFU is spotted onto a freshly polished RDE which is then poised at -0.41 V vs SHE. Aliquots of NAD^+ (concentrations shown in the figure) were injected over time and the current recorded. (b) The magnitude of the increase in current from (a) can be plotted *vs* the concentration of NAD^+ and a Michaelis-Menten fit applied to give the K_M for NAD^+. Experiments performed in Tris-HCl, pH 8 at 30 °C, with electrode rotation of 2000 rpm.

The results of all 9 experiments, each using a fresh protein film and performed on both NAD+-reductases to find an average K_M; for *Re* SH this was found to be 103 ± 9 µM and for *Ht* HoxFU the KM was electrochemically determined to be 219 ± 18 µM, these values compare well with the values

Dr Zulkifli Idris on his experiments using *Re* SH and Dr Holly Reeve obtained from the HoxFU from *Rhodococcas opacus*.[5–7]

3.5.2 Control experiment

To ensure that any change in current from the chronoamperometry experiments in section 3.5 were due to the addition of NAD^+, a control experiment was carried out. All experimental conditions were kept the same (temperature, pH, rpm). The surface of the RDE was freshly polished and an aliquot of enzyme applied (experiments were carried out using both *Re* SH and *Ht* HoxFU). A fixed potential of -0.41 V vs SHE was applied and the current allowed to stabilise. Aliquots of Tris-HCl buffer were added at 10 second intervals, these are indicated by the arrows in Figure 3-3, and the current recorded. It can be seen from the graph that there is no current response to these aliquots. At the end of the experiment 0.1 mM NAD^+ was injected as a positive control; this produced a small increase in current magnitude, indicating the enzyme was active.

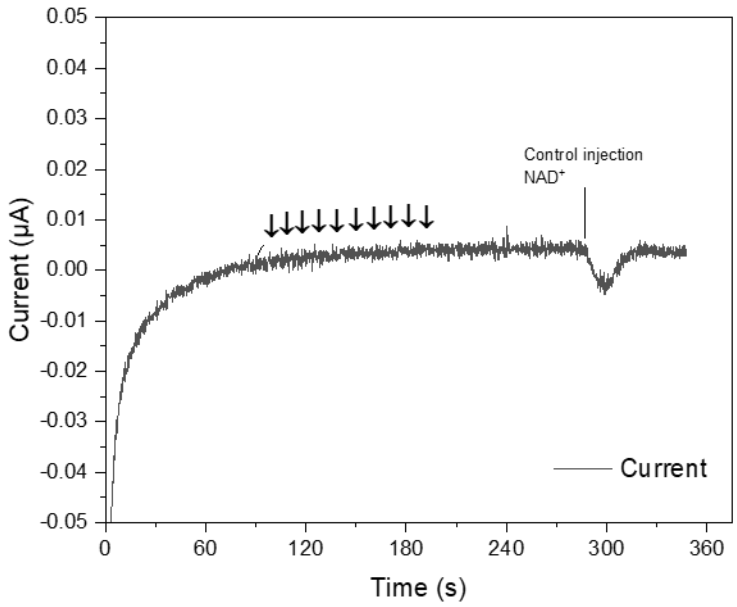


Figure 3-3: Chronoamperometry experiment using an RDE modified with 0.5 µL SH. A fixed potential of -0.41 V vs SHE was applied. Aliquots of Tris-HCl were injected at approximately 10 second intervals (indicated by the arrows) and the current recorded. A control injection of NAD^+ was made at the end of the experiment to ensure the enzyme was active. Experiments performed in tris-HCl, pH 8 at 25 °C with electrode rotation of 2000 rpm.

The control experiment indicates that any increase in the magnitude of the current is due to the enzyme accepting electrons from the electrode to reduce the NAD^+ in solution, injecting Tris-HCl buffer has no effect on the current.

3.6 pH dependence

The pH of the electrolyte has a profound effect on both the stability of the enzyme on the electrode and also its catalytic activity. The pH can change the ionisation states of amino acids in the active site which can affect conformation and the ability to bind substrates.[8] At extreme pH the enzyme may denature and the protein structure can be compromised. This can affect the ability of the enzyme to bind with the substrate and therefore prevent catalysis. Preissler *et al.* determined that for *Re* SH from *Hydrogenophilus thermoluteolus* the optimum pH was 6.5, however Lauterbach *et al.* found *Ht* HoxFU isolated from *Re* had highest activity at pH 10. [9,10]

It is possible that *Ht* HoxFU being native to a thermophilic organism may enable the enzyme to operate over a wider pH range than *Re* SH. The experiments in this section investigate the activity of the enzyme moiety over a range of pH conditions from 5 – 9. Experiments performed at pH 10 proved unsuccessful as the HoxFU is quite unstable at this pH.[10] Lauterbach *et al.* noted that although maximum activity for HoxFU was reached at pH 10, the protein was unstable after only 30 seconds. A CV performed on *Ht* HoxFU confirmed this with high current activity observed on the first scan, but almost no activity seen on the second scan of the experiment. For this reason, all experiments in this section are confined to the pH range 5 – 9.

3.6.1 Cyclic voltammetry pH experiments in mixed buffer

Experiments to determine the optimum pH conditions for electrochemical reduction of NAD^+ and oxidation of NADH were performed in a mixed buffer system, in which the pH could be varied from 5.0 – 9.0. This minimises any effect due to changing the buffer components. A fresh protein film was prepared for each experiment before immersing in mixed buffer containing 1 mM NAD^+ and 1 mM NADH and all experiments were performed in triplicate.

3.6.2 Shift in thermodynamic potential

The temperature for all pH experiments in this chapter was 25 °C (298 K). The shift in E due to pH can be seen in Figure 3-4 where CVs from three pH experiments have been overlaid to demonstrate how the onset potential for both the reduction and the oxidation is more negative at a higher pH.

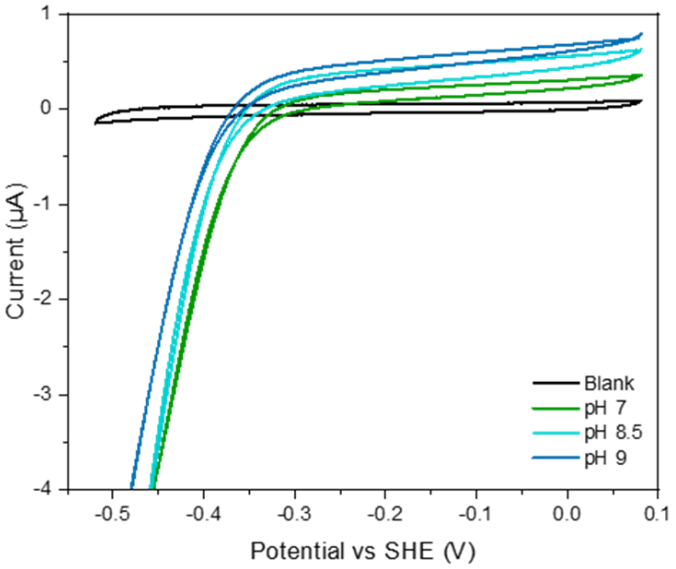


Figure 3-4. Cyclic voltammograms taken at three different pHs were recorded in mixed buffer containing 1 mM NAD^+ and 1 mM NADH, rotation 2000 RPM at 25 °C using a PGE RDE modified with *Ht* HoxFU. Blank scan recorded using unmodified PGE RDE (black trace). The colours of the pH traces on this graph correspond to those in Figure 3-5(a).

The thermodynamic redox potential (E) for the NAD^+/NADH couple is dependent upon both temperature and pH according to the Nernst equation (section 2.1.1) and this is demonstrated by the graphs in Figure 3-5. Graph (a) shows how E shifts to a more negative potential with higher pH. The reaction is dependent on protons in solution, so therefore as the pH increases there are less protons available and the reaction will require a more negative potential to drive it. The temperature of an electrochemical reaction also affects E and this is shown in graph (b) with all temperatures shown in Kelvin (K). Higher temperatures increase the rate of reaction which will increase the flow of electrons leading to a more negative E. Increasing the temperature also lowers the activation energy making it easier for reactants to overcome the energy barrier and this increases the voltage.

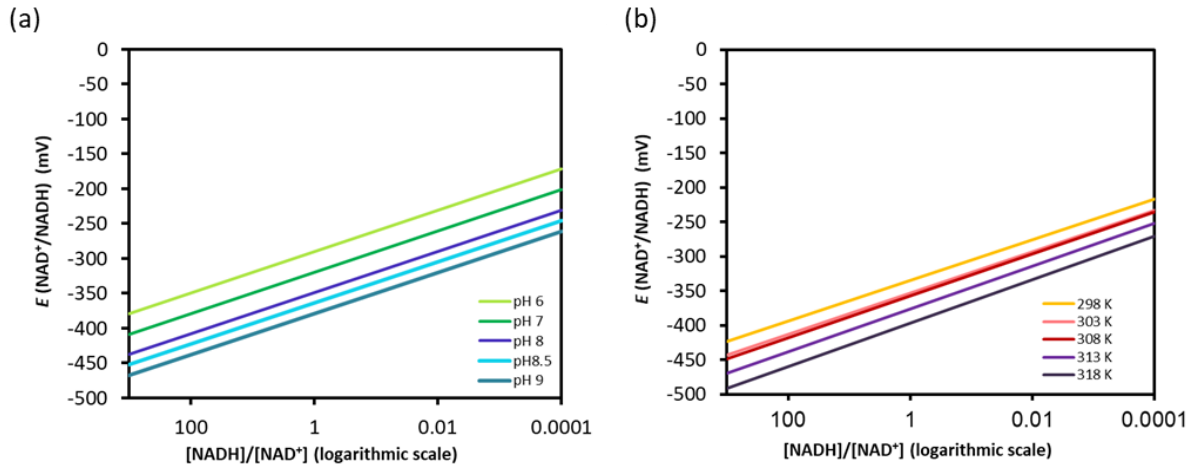


Figure 3-5(a) the thermodynamic redox potential for the [NADH]/[NAD^+] couple at a range of pH conditions all at 298 K (25 °C). (b) the thermodynamic redox potential for the [NADH]/[NAD^+] couple at a range of different temperatures (shown in Kelvin) all at pH 8.

3.6.3 Measuring the catalytic current

Each experiment was performed using a freshly prepared protein film and fresh NAD^+/NADH solution in the cell. There is variation between films due to application, so the magnitude of current is not always indicative of the absolute activity. Therefore, a way of consistently measuring both the

oxidation current and the reduction current needed to be established that would allow consistency across the experiments. It was shown in section 3.6.2 that the thermodynamic potential for the NAD^+/NADH couple shifts with pH, this was also taken into consideration when devising a method for measuring the current.

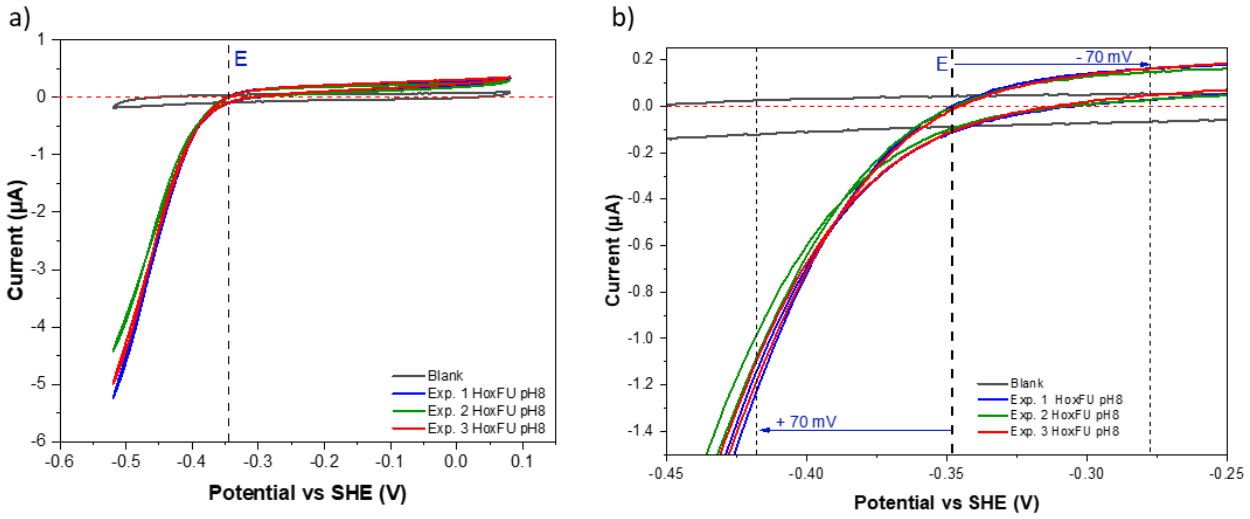


Figure 3-6: Method of determining the pH optimum for the electrochemical reduction of NAD^+ and oxidation of NADH. (a) CVs were recorded in mixed buffer made up with K^+ salts, containing 1 mM NAD^+ and 1 mM NADH. (b) an enlarged section of the CV's taken at pH 8 showing where the current was measured at -70 mV from the thermodynamic potential for NAD^+ reduction (an average of the forward and backward scan was used) and at +70 mV from the thermodynamic potential (dotted black line) for NADH oxidation. Blank scan with an unmodified PGE RDE recorded in mixed buffer pH 8 shown in black. All experiments recorded using an RDE modified with *Ht* HoxFU, rotation 2000 rpm, scan rate 10 mV s^{-1}

The thermodynamic redox potentials were first calculated for each of the pH conditions used in this section, then a point 70 mV either side was selected as shown in Figure 3-6b. The points where the measurements were taken are marked on this enlarged section of the CVs taken at p H8. These points are selected as they are in the catalytic region of the CV, with minimal mass transport limitations. An average measurement was taken of the forward and backward scan for each experiment, and triplicate experiments were performed at each pH.

The results of the mean current were then plotted against pH (and the experiments repeated using Re SH and these are shown in Figure 3-7. For the *Ht* HoxFU NAD^+ reduction experiments the optimum pH can be estimated to be around pH 8.5, which is higher than previous experiments carried out on *Re* HoxFU in the group, which had determined the optimum pH to be pH 6.5.[11] The optimum pH for NADH oxidation seems to be around pH 9, and significantly more activity is seen at this pH than others. There is very little activity seen at pH 5 for either oxidation or reduction using *Ht* HoxFU, although the *Re* SH at this pH shows no activity at all. This suggests that neither enzyme is active at a low pH.

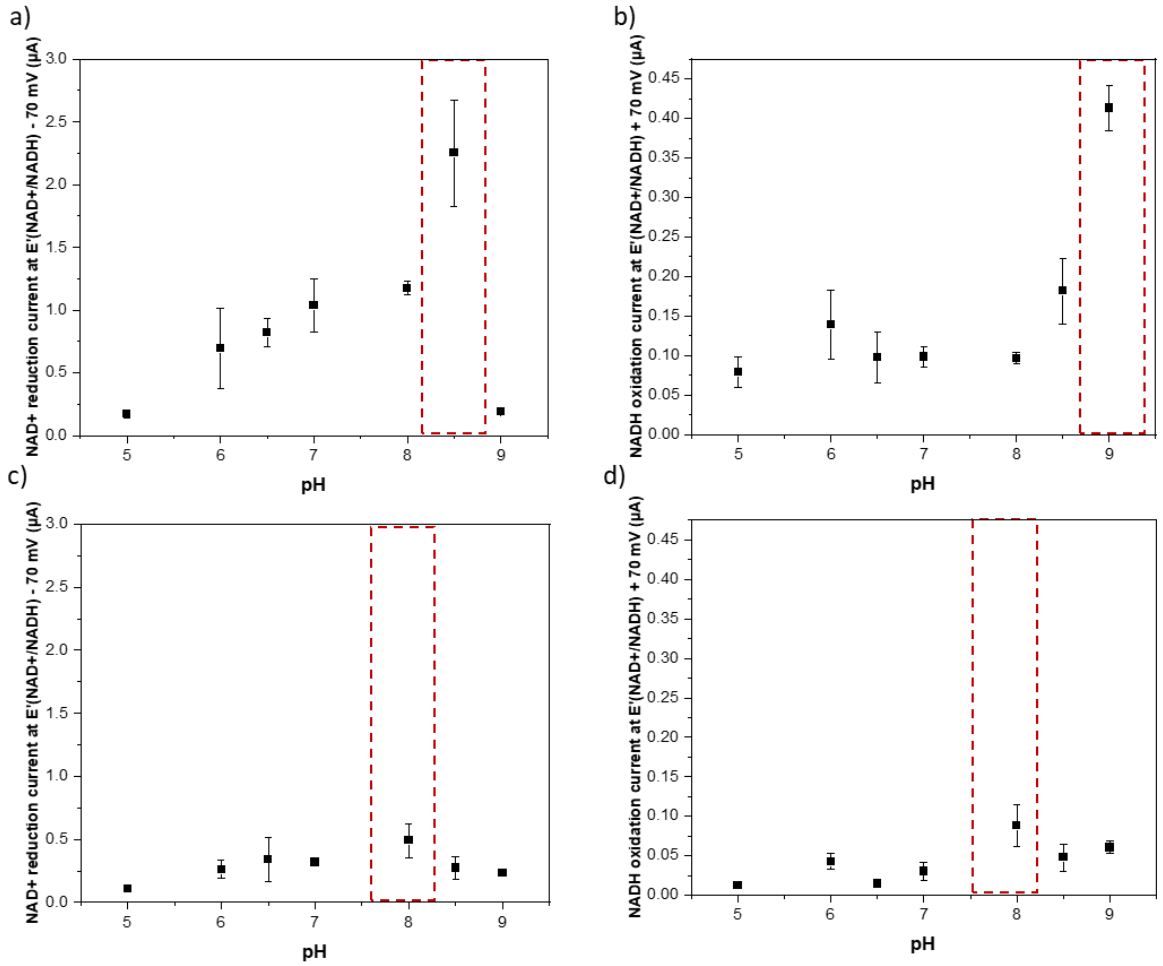


Figure 3-7: Overview of pH experiments for (a) and (b) *Ht* HoxFU and (c) and (d) *Re* SH. The catalytic current was measured at -70 mV from the thermodynamic potential for NAD^+ reduction (a) and (c) and +70 mV for the NADH oxidation (b) and (d).

Stability of the *Ht* HoxFU on the electrode prevented investigation at higher pH. It is possible however, that when used in solution or adsorbed to BP2000, the enzyme may operate at higher pH.

3.7 Temperature

As *Hydrogenophilus thermoluteolu*s is a thermophilic organism that natively grows at temperatures of 50 - 70°C,[12,13] it was presumed that it may be catalytically active at higher temperatures than the *Re* SH. Experiments were carried out at elevated temperatures to establish whether the catalyst was active. Increasing the temperature will affect the potential of the reaction according to the Nernst equation (section 2.1.1). It may be beneficial for some reactions to be carried out at higher temperatures, for example to assist with solubility of substrates or to speed up a reaction.

Experiments were performed at temperatures of 30 °C, 45 °C, 55 °C and 65 °C, each using a freshly prepared protein film. It was immediately apparent, even at 45 °C that there was significant film loss throughout the 20-minute duration of the CV. At 45 °C the catalytic current was 1.5 µA at the start of the experiment and 0.65 µA after 20 minutes. Experiments performed at higher temperatures suffered with more significant film loss, as can be seen in Figure 3-8 (a) where the current at the start of the experiment was ~1.1 µA and after only 3 minutes had dropped to ~0.5 µA.

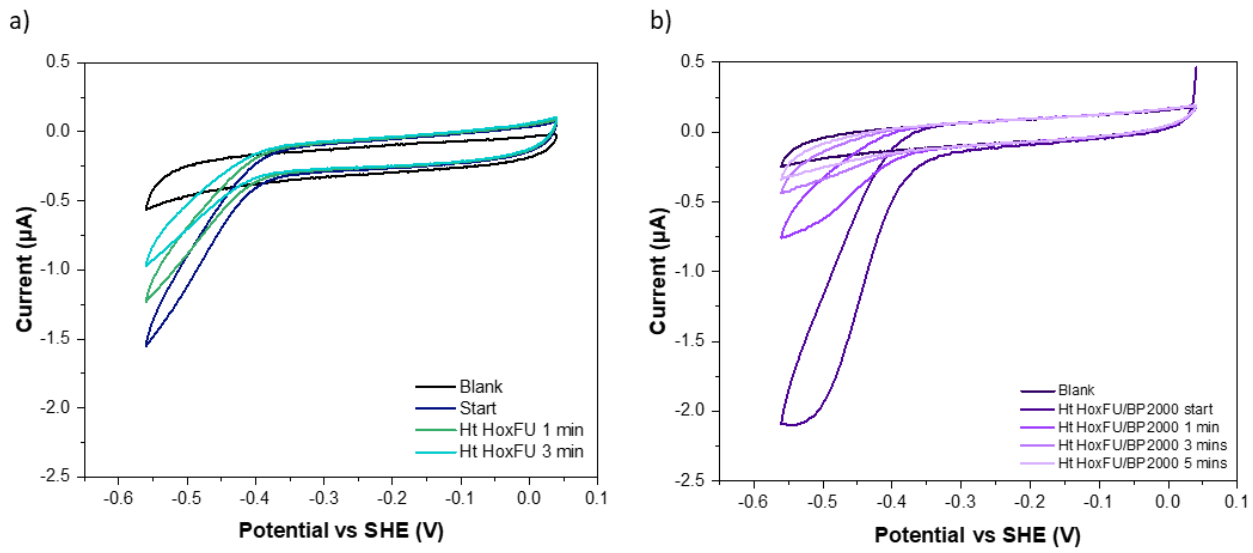


Figure 3-8: Protein film stability on the electrode at elevated temperatures. CVs recorded at 65 °C with a freshly polished PGE RDE spotted with (a) *Ht* HoxFU and (b) *Ht* HoxFU-modified particles. In both cases the enzyme starts off quite active but the current rapidly drops with each successive scan, due to either film loss or the enzyme being denatured. Cell contains 50 mM Tris-HCl, pH 8 buffer, rotation 1000 rpm.

Investigating whether the *Ht* HoxFU on supported on carbon black particles (B2000) would be more stable was then explored (*Ht* HoxFU-modified particles are discussed further in 3.12.1). These particles were then adsorbed to the surface of a freshly polished PGE RDE (see section 2.1.1.1). The results of the CV from the Ht HoxFU-modified particles can be seen in Figure 3-8 (b) where there is an increase in the magnitude of current for the first scan due to the increased enzyme-loading. However, the current rapidly drops within 5 minutes until there is barely any catalytic current observed. It is important to note that in this experiment there is significant mass transport limitation observed in the first scan (dark purple, labelled Start). Increasing the rotation of the RDE would alleviate this issue, however, increased rotation was shown to increase film loss (deterioration of the protein film either due to loss of protein film or loss of acticity of enzyme) in 3.12.1. For the purpose of this experiment the rotation was limited to 1000 rpm, so any film loss observed would not be due to the rotation speed.

The catalyst seemed to be active over a range of temperatures up to 65 °C, but only for a short period of time before activity diminished or was lost altogether. This could be due to the increased temperatures increasing film loss, but could also be due to the protein denaturing.

3.8 Stability

For the electrochemical synthesis experiments, not only is it important to have an enzyme with high activity, but also good stability. The aim of this project was to create metalloenzyme electrodes that recycle cofactor to drive a biocatalytic reaction. It is therefore important that the enzyme should have good stability on the electrode.

A drop in catalytic current can occur as a result of dissociation of the protein film, so an experiment was performed to test the stability of the *Ht* HoxFU protein film over time (Figure 3-9).[10]

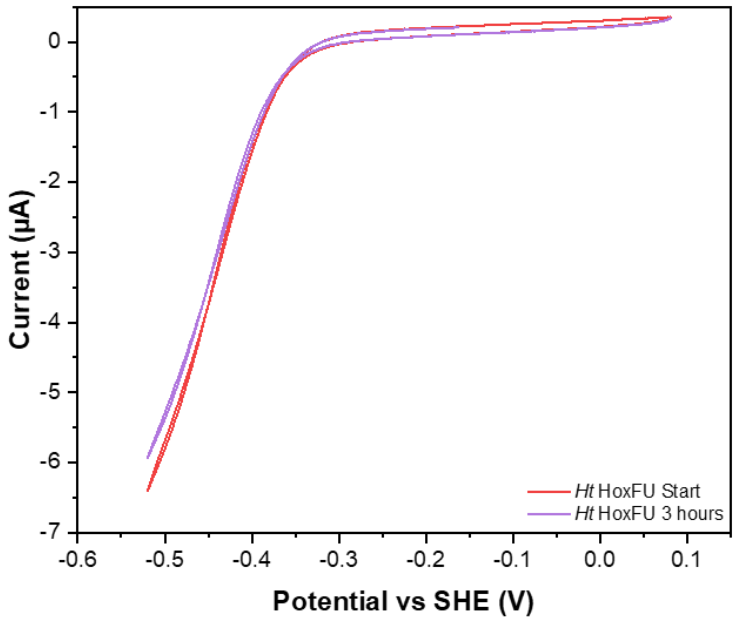


Figure 3-9: Cyclic voltammograms taken over a 3-hour period to show the stability of *Ht* HoxFU protein film on the electrode over time. The red trace was the second scan taken at the start of the experiment and the purple scan recorded 3 hours later. Experiment performed in 50 mM Tris-HCl, pH 8 containing 1 mM NAD^+ and 1 mM NADH, rotation 3000 RPM at 30 °C using a PGE RDE modified with *Ht* HoxFU. Slightly higher rotation and temperature used for this experiment to test stability of the protein film over time.

The CV shown in Figure 3-9 shows very little loss of catalytic current during the experiment, despite performing the experiment at 30 °C and using a rotation of 3000 rpm. This shows that the *Ht* HoxFU adsorbs well to the electrode and the protein film is stable throughout the experiment.

3.8.1 Stability over an extended time period

An interesting observation on the stability of *Ht* HoxFU was made one day when setting up the electrochemical cell. An old enzyme-modified electrode from an experiment almost 2 weeks earlier had been put away on a shelf without cleaning. This electrode was placed into the cell to check the potentiostat was connected and working. When running a test CV, it could be observed that there was some catalytic activity from the old, dried protein film that had not been removed. An aliquot of NAD^+ was injected into the cell and a second CV recorded and this is shown in Figure 3-10 of a screenshot taken of the software where the pink trace shows an increase in current. This indicates that even after two weeks drying out in the glovebox, the enzyme retained some activity.

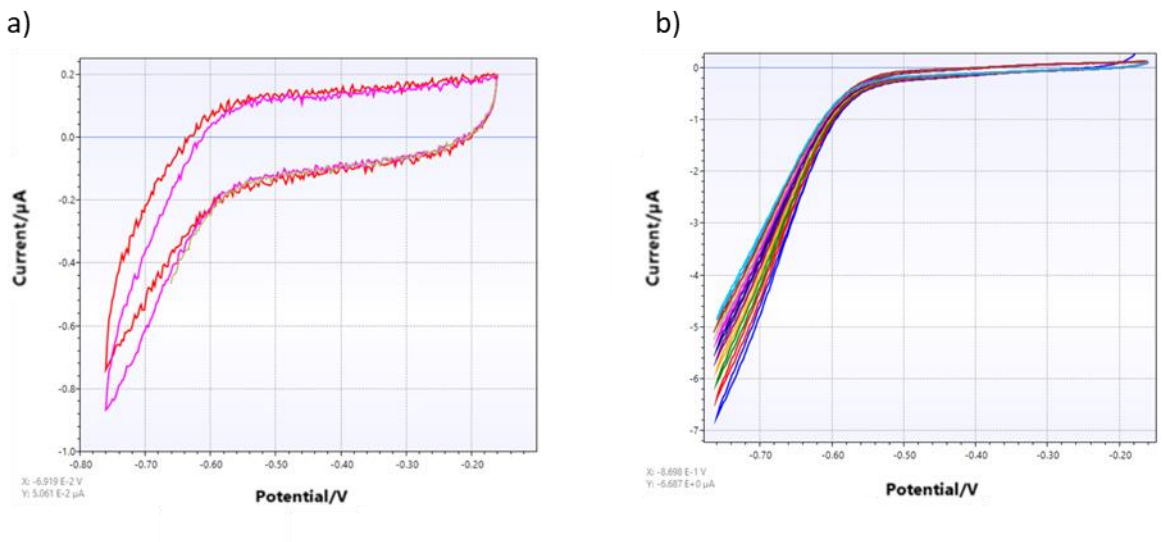


Figure 3-10(a): CV performed on an *Ht* HoxFU-modified electrode that had been left for over 2 weeks in the dry N_2 atmosphere of the glovebox. The scan in red was performed when testing the electrochemical set-up and upon noticing some catalytic current, an aliquot of NAD^+ was injected into the cell and the pink scan recorded, which clearly shows an increase in current and indicates that the enzyme was still active. (b) shows CV performed on the same electrode when the protein film was fresh, showing activity has significantly decreased in (a) but enzyme is still active. Cell contained 8 mL 50 mM Tris-HCl buffer, 1 mM NAD^+ (red scan) and ~2 mM NAD^+ (pink scan). Rotation 2000 rpm

3.9 Solvent tolerance of *Ht* HoxFU

So far, the experiments have focussed on establishing whether the *Ht* HoxFU is effective as a catalyst by investigating its performance through PFE. This provides some useful insight into how the enzyme behaves in a range of conditions. As part of a cofactor recycling system, the *Ht* HoxFU will be required drive another enzymatic reaction, so in addition to the NAD^+ substrate used so far, other compounds will be added to the cell. Often the substrates used for such reactions are not water soluble, which can be a problem in aqueous systems. To mitigate this, a cosolvent can be used to increase the solubility of hydrophobic compounds in aqueous solution. Organic solvents can have a profound effect on both the function and activity of the enzyme.[14] The experiments in this section will explore how well the *Ht* HoxFU tolerates a range of commonly used cosolvents such as acetonitrile (MeCN), dimethyl sulfoxide (DMSO) and ethanol (EtOH).

3.10 Methods for electrochemically testing solvent tolerance

In order to test for solvent tolerance, it was first necessary to devise a method that would give clear and reliable results. There are a number of parameters that can affect the protein film on the surface of the electrode: pH, temperature, atmospheric O_2, electrode rotation. Each of these parameters can cause deterioration of the protein film over time, so quantifying the effect of the cosolvent will be difficult to achieve. The chosen method needs to enable the effect of the cosolvent to be clearly observed.

Initially a chronoamperometry technique was trialled. A fixed potential of -0.38 V vs SHE was applied, this is a lower potential than the previous experiments; this was selected as the aim is not NADH generation, so high catalytic activity is not required. An example of a chronoamperometry experiment is shown in Figure 3-11, this was to determine the effect of MeCN. Initially a control injection of buffer was added at 400 s to ensure that any effect on the current was not simply due to additional volume being added to the cell. There was no current response to the control injection. Two aliquots of MeCN were then added at 600 s and 800 s taking the overall % by volume of MeCN to 1% and 2% respectively. Once again, no change in current could be observed, although there is a steady decrease in current consistent with NADH generation by the *Ht* HoxFU. Larger aliquots were added at 1000 s and 1420 s taking the overall concentration of MeCN to 5 % and 10 % by volume.

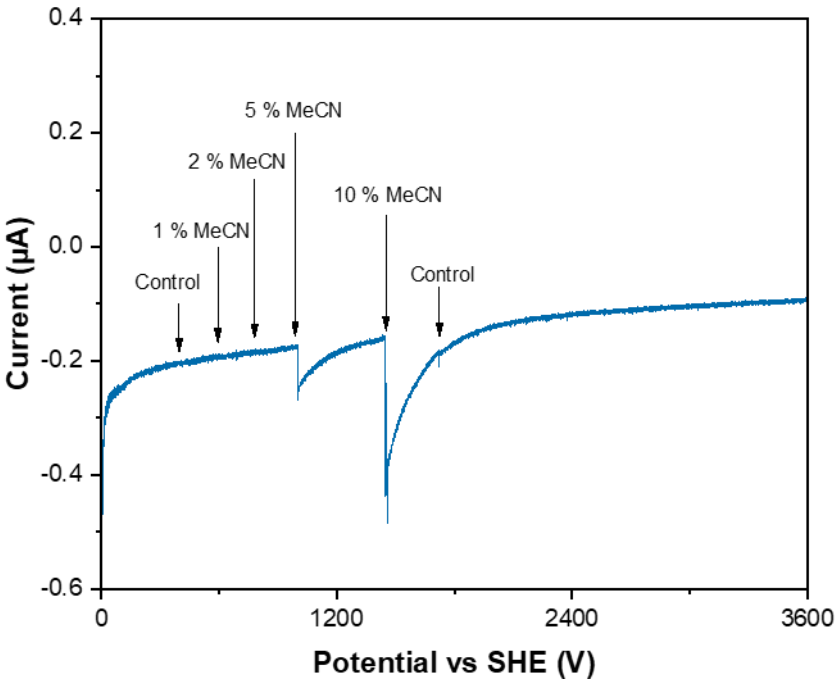


Figure 3-11: Chronoamperometry experiment to determine effect of a cosolvent. A fixed potential of -0.38 V vs SHE was applied and the current allowed to stabilise. Aliquots of MeCN were injected at intervals denoted by arrows. These show that there was no effect on the addition of the lower doses, a sharp increase in current was seen for the addition of 5 and 10% MeCN. A control injection of 100 µL Tris HCl was injected and shows no effect on the current. Cell contains 8 mL 50 mM Tris-HCl, pH8, with 1 mM NAD^+ at 25 °C, rotation 2000 rpm

A sharp increase in the current magnitude could be observed upon injection, although the current rapidly stabilised. At 1710 s a 500 µL aliquot of the cell contents was removed and re-injected to ensure that the spike in currents observed with the previous two injections were not simply due to the increased volume being added to the cell. There was no response to this injection. The results from this experiment seemed to suggest there was an initial effect on the *Ht* HoxFU from larger percentages of MeCN being added, but that this was short-lived. This could be due to a change in capacitance due to the solvent polarity near the electrode surface. It was also difficult to measure the impact of the cosolvent as it was not clear what the cause of the increase in current was and whether the enzyme returned to its normal activity when the current settled.

Two further chronoamperometry traces can be seen in Figure 3-12 which looked at the effect of (a) MeCN and (b) DMSO. Graph (a) shows an increase in current of approximately 1.1 µA with the

addition of 5% MeCN which is similar to the current spike in (b) upon the addition of 20% DMSO which is approximately 0.9 µA. In both cases the current takes approximately 300 s to stabilise.

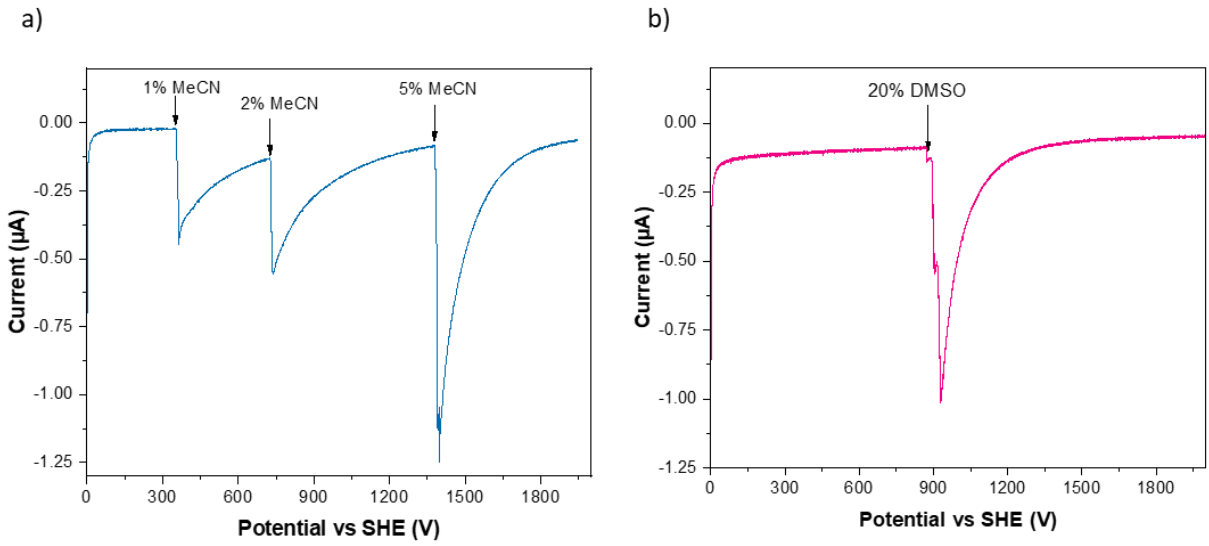


Figure 3-12: Chronoamperometry experiments to determine effect of cosolvents (a) MeCN and (b) DMSO. A fixed potential of -0.38 V vs SHE was applied and the current allowed to stabilise. Aliquots of cosolvent were injected at intervals denoted by arrows. Cell contains 8 mL 50 mM Tris-HCl, pH8, with 1 mM NAD^+ at 25 °C, rotation 2000 rpm.

These results suggest that DMSO has less of an effect on the *Ht* HoxFU than MeCN, but doesn't really give much more information on the impact on the enzymes activity. To give a clearer picture on how active the enzyme was both before and after the addition of the cosolvent, cyclic voltammetry was used. An example of one of the experiments is shown in Figure 3-13. At the start of the experiment, an *Ht* HoxFU-modified electrode is placed in the electrochemical cell with Tris-HCl and 1 mM NAD^+ and the red scan recorded. This scan has a current of approximately 3 µA (after subtracting capacitive current) for both (a) and (b). In experiment (a) an aliquot of 10% v/v MeCN is injected and a scan recorded after 20 mins and for (b) an aliquot of 30% MeCN v/v. The current recorded on the CV's was 2.5 µA and 2.0 µA respectively, suggesting that the higher percentage of MeCN had more of an impact on the enzyme's activity. The electrodes were then removed from the cell and washed with Milli-Q before being replaced into a cell of fresh Tris-HCl with 1 mM NAD^+ and

another CV recorded. This final CV should give an idea of how well the enzyme recovers from exposure to the organic solvent. In experiment (a) the current was approximately 1.9 µA whereas for the 30% MeCN experiment the recovery CV was approximately 1.5 µA.

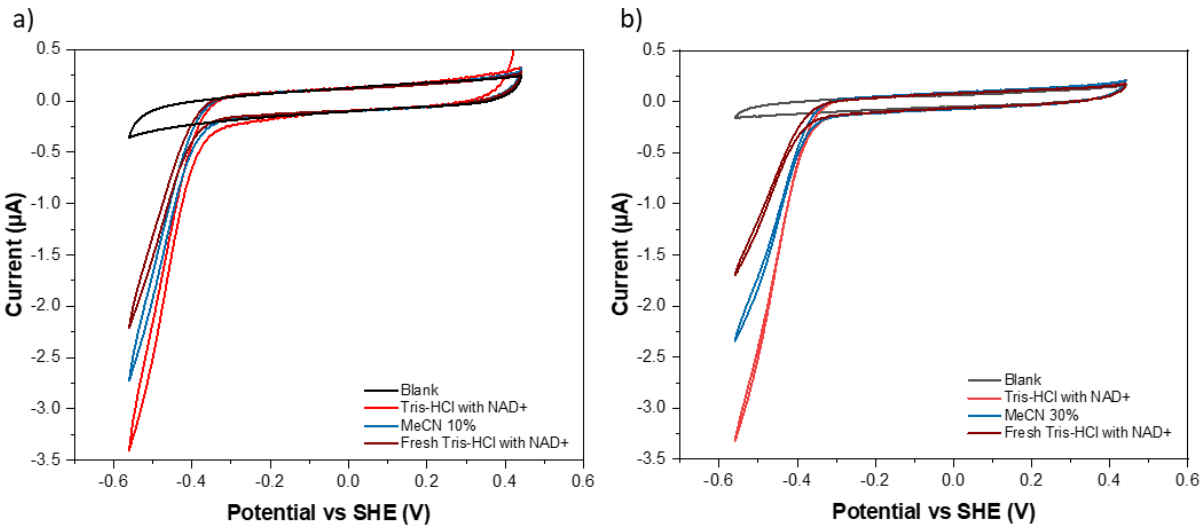


Figure 3-13: Cyclic voltammogram of a solvent tolerance experiment using *Ht* HoxFU and acetonitrile (MeCN). Black trace shows a blank unmodified electrode. The RDE is then spotted with 0.5 µL HoxFU and allowed to almost dry. Red trace shows the CV scan of HoxFU in 50 mM Tris-HCl, pH 8 at 25 °C with 1 100 mM NAD^+, rotation 2000 rpm. The blue trace shows the CV taken 20 mins after injecting MeCN. After exposure to the solvent, the RDE was removed from the solution and rinsed before being replaced in a cell containing fresh 50 mM Tris-HCl, pH 8 with 1 mM NAD^+ (dark red trace).

Whilst these results are not quantitive, they show clearly that the enzyme remains quite active even after 20 mins exposure to MeCN up to a percentage of 30%. This experiment was repeated for DMSO and EtOH using concentrations of 1%, 2%, 5%, 10%, 20% and 30%. The results from the CVs for all solvents indicated no noticeable drop in activity for 1% 2% and 5% of all cosolvents. A small loss in activity corresponding with approximately 10% drop in current was observed for 10% MeCN and EtOH but only around 7% drop in current for 10 and 20% DMSO. There was around a 30% drop in current observed for 30% MeCN and EtOH, but only a 15% loss of current with 30% DMSO. These results suggest that the *Ht* HoxFU is most tolerant to DMSO, but can tolerate all three solvents up to 30% v/v and remain active. It is important to note that with any PFE experiments, there is always

some film loss over time (section 3.8), so not all of the loss in activity can be attributed to the cosolvents used.

3.11 Sodium inhibition of *Ht* HoxFU

In research carried out in 1976, Schneider and Schlegel reported that high ionic strength resulted in the inhibition of SH, with the most pronounced effects being seen using 0.2 M sodium salts, which resulted in enzyme inhibition of up to 70%.[15] In biotechnology involving the SH, the use of sodium salts when making buffers has generally been avoided, although there is limited research into the effect of Na^+ on hydrogenase enzymes. Alongside the pH experiments carried out in section 3.6 using mixed buffer made up with K^+ salts, parallel experiments were carried out with buffer made up with Na^+ salts for comparison.

The results from the Na^+ inhibition experiments can be seen in Figure 3-14 in red, they have been overlaid onto the results from the *Ht* HoxFU experiments carried out using K^+ salts for comparison.

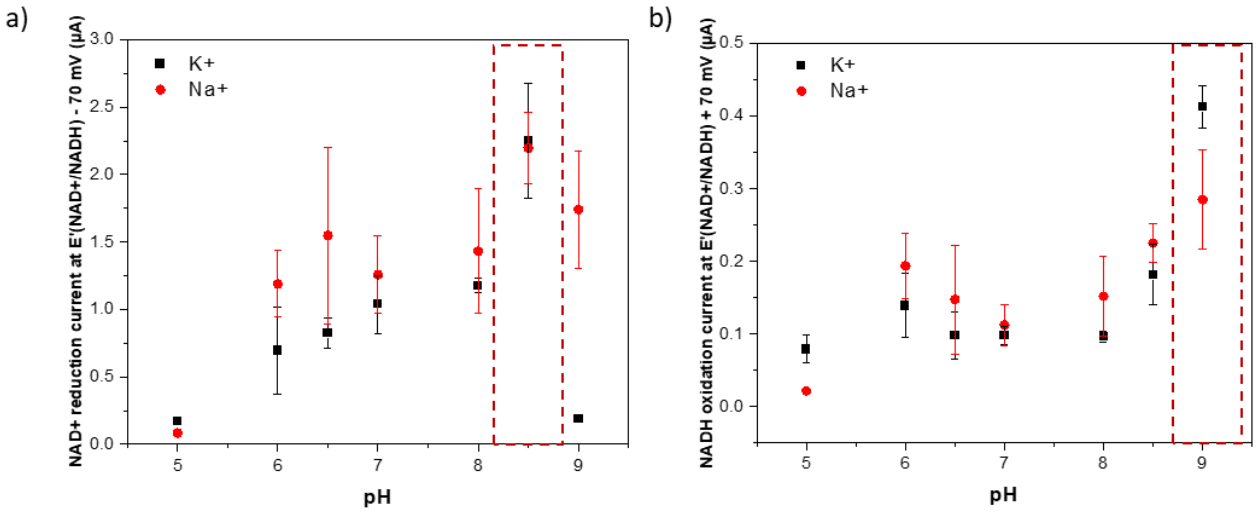


Figure 3-14: The catalytic current measured at a) -70 mV from the thermodynamic potential for NAD^+ reduction and b) at +70 mV for NADH oxidation in the experiments shown in has been plotted against the pH to give an indication of the activity of *Ht* HoxFU in mixed buffer made up with Na^+ salts (red) and K^+ salts (black) at the various pH's. The red dotted line outlines the pH with the most activity.

The results from pH experiments using buffer prepared with Na^+ salts follow the same general trend as the experiments carried out using K^+ salts. The error bars are quite large for some of the experiments, but this is probably due to differences in the protein film as discussed earlier in this chapter. The results show little difference in activity between the two salts, with the Na^+ results in general having slightly more activity. This suggests that the *Ht* HoxFU is not inhibited by Na^+.

3.12 Electrosynthesis of NADH

The purpose of the electrochemical characterisation experiments performed so far in this chapter was to gain an insight to how effective *Ht* HoxFU would be in a cofactor recycling system. It has been established that *Ht* HoxFU has a high affinity for NAD^+ and can operate in a range of different conditions, which could be used to optimise a particular reaction of interest. Ultimately however, the enzyme could be used to develop metalloenzyme electrodes for electrosynthesis. It would therefore be useful to quantify the NADH produced electrochemically and determine the efficiency of *Ht* HoxFU as an electrocatalyst.

3.12.1 High surface area electrodes

Electrochemical characterisation experiments were performed using a PGE RDE as *Ht* HoxFU adsorbs well to the surface and allows electrons to flow from the electrode to the enzyme and vice versa. However, for synthesis of NADH, a larger surface electrode is required. The development of high surface area electrodes will be discussed further in Chapter 5. For the purpose of the NADH synthesis experiments, the PGE RDE was used in the same electrochemical cell that has been used throughout this chapter. The surface area of the PGE RDE can be increased, without increasing its geometrical area, by adsorbing enzyme-modified particles to the electrode.[5] Carbon black

nanoparticles (BP2000) have a very large surface area, *ca* 1500 $m^2 g^{-1}$, which allows them to support a high enzyme loarding.[16]

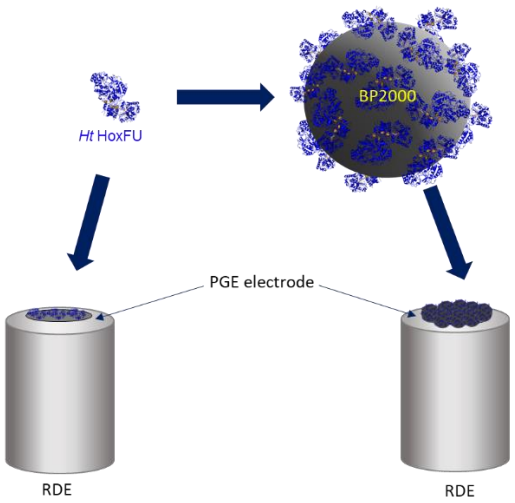


Figure 3-15: Schematic representation of high surface-area metalloenzyme electrodes prepared by adsorbing *Ht* HoxFU to BP2000 before dropping onto the surface of a freshly polished PGE RDE

A schematic representation of the high surface-area metalloenzymes is shown in Figure 3-15, the *Ht* HoxFU were first adsorbed to the BP2000 following the procedure outlined in section 2.4. A slurry of the enzyme-modified particles was spotted onto a freshly polished electrode and allow to adsorb for a few minutes without drying before being placed into the electrochemical cell.

3.13 Quantifying the synthesis of NADH

Overnight chronoamperometry experiments were performed by applying a fixed potential of - 0.51 V vs SHE was applied and the cell sealed to prevent evaporation. Traces for these experiments are shown in Figure 3-16(a) for the electrodes modified with *Ht* HoxFU and Figure 3-16 (b) for the electrodes modified with *Re* SH. The black line shows the current over time for the experiments. This graph can then be integrated to give the charge passed in Coulombs, which is then used to calculate the theoretical yield of NADH (shown as dotted blue line).

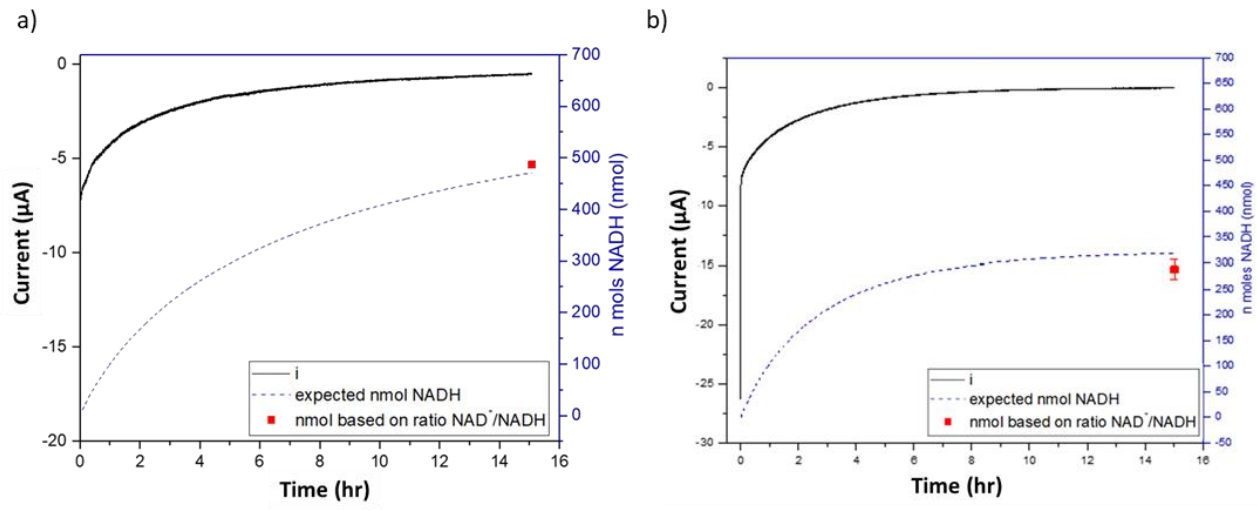


Figure 3-16: Chronoamperometry experiment (black trace) to synthesise NADH for quantification using (a) *Ht* HoxFU-modified electrode and (b) *Re* SH. The dotted line is the predicted amount of NADH generated during the experiment. The red spot is the actual amount of NADH calculated at the end of the experiment by UV-Vis spectroscopy. A freshly polished RDE was spotted with 0.5 µL enzyme-particles. The enzyme-modified electrode was allowed to almost dry before being immersed into the cell which contained 5.5 mL of 50 mM Tris-HCL buffer, pH 8, with 1 mM NAD^+ in solution. A fixed potential of -0.51 V vs SHE was applied. Electrode was rotated at 1000 rpm

After 15 hours, the experiment was stopped and a sample of the cell solution was analysed by UV-Vis spectroscopy. The concentration of NADH could then be calculated using a calibration curve and this is shown as a red dot on the graph.

This experiment indicates a current efficiency of 85.4% for the *Re* SH and 90.3% for the *Ht* HoxFU, almost all of the charge passed is being used to synthesise NADH. These experiments demonstrate an effective way to electrochemically generate NADH and this could be easily adapted to recycle NADH to drive a reaction of interest. The metalloenzyme electrodes offer a simple way to scale up the reaction and adapt for use in a flow cell, this is discussed further in Chapter 5.

Next the mutation of *Ht* HoxFU for use as an NADPH recycling catalyst will be considered.

3.14 Scope for NADPH recycling

The experiments in this chapter were predominantly carried out by Part II student Zipporah Hodder under my guidance.

Many of the oxidoreductase enzymes widely used in biocatalysis require NADH as a cofactor, or can be driven by either NADH or NADPH. However, some enzymes, such as certain alcohol dehydrogenase (ADH) and imine reductase enzymes (IRED) will only operate using NADPH as their hydride source for catalysing C=O or C=N reduction.[17] In comparison to the well-developed H_2 driven NADH recycling system that has been described in chapter 1, an efficient NADPH recycling system that could easily scale up to industrial applications is yet to be established.[18] The electrochemical leaf NADP(H) recycling system that has been developed Armstrong et al., although achieving high TN, is still on a laboratory scale. The GDH/glucose-driven system is the widely adopted industrial method for recycling NADPH. The disadvantages of this system were discussed in Chapter 1.

There have been recent attempts to recycle NADPH to catalyse C=X bond reductions *in vitro* using $NADP^+$-linked SH. However, these proved unsuccessful at efficient NADPH recycling. [19] Kwan *et al.* demonstrated successful reduction of $NADP^+$ using $NADP^+$-linked [Ni-Fe]-hydrogenase from *Pyrococcus furiosus* (*Pf* SHI) under H_2.[20] Unfortunately, electrochemical assays carried out at 25 °C showed that enzyme activity drops to zero when exposed to less than 1% O_2. This would be a problem for industrial scale-up as the reactions would require strictly anaerobic conditions.

Promising work by Priessler *et al.* demonstrated NADPH recycling both *in-vitro* and *in-vivo* using a rationally designed, $NADP^+$-reducing system based on the SH from *R. eutropha*.[7] An oxygen-tolerant NADPH-active enzyme was developed by genetically modifying the wild-type WT *Re* SH (wt*Re*SH). The wt*Re*SH (which is highly specific for NAD^+) underwent a double amino acid substitution at the NAD^+ binding site. The resulting mutant SH (mReSH) was able to support IRED reductions by

supplying H_2-driven NADPH recycling in an O_2-dependent biocatalytic process. However, genetic engineering in *R. eutropha* is much more complex than mutagenesis using a bacterium such as *E. coli*; which has established site-directed mutagenesis routes. [21]

The results obtained in section 3.3using *Ht* HoxFU demonstrate a simple and effective electrochemically-driven recycling system for NADH using an isolated enzyme moiety expressed in *E. coli*. This opens up the possibility of emulating the mutagenesis carried out by Preissler *et al.* in the *Ht* HoxFU expressed in *E. coli* (details in 3.15).

3.14.1 C=N reduction via imine reductases

The synthesis of chiral amines would be highly desirable as API's, however their alicyclic imine substrates are generally unstable in aqueous solutions,[22] which limits the application of IREDs in biocatalysis.[22] Until recently, the substrate-scope was limited to cyclic imines, but there has been some recent success of IREDs reducing ketones to amines, and also chiral amines formed in cascade reactions.[23] With this broadening substrate scope, there is increasing demand for a cleaner NADPH-recycling system to facilitate these reactions. The general mechanism for an IRED catalysed reduction of imine to amine is shown in Figure 3-17.

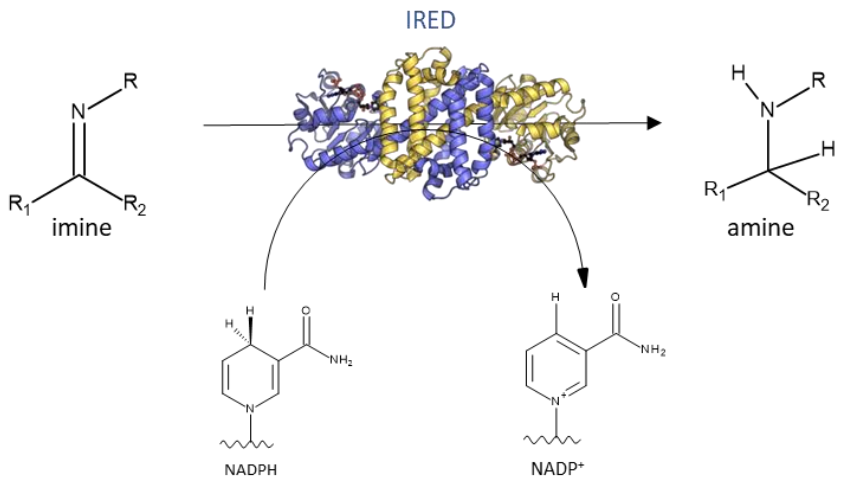


Figure 3-17: Biocatalytic imine reduction using IRED and NADPH.

Attempts have been made by researchers to engineer the cofactor specificity of IREDs from NADPH to NADH, as generally the former is more expensive and unstable.[24,25] NADPH degrades more rapidly than NADH under the same conditions, this is due to the rate of degradation being more dependent upon temperature and hydronium ion concentration. Attempts by Cahn *et al.* demonstrated a loss of activity when engineering the enzymes selectivity.[26] A further disadvantage is that each IRED enzyme would need to be engineered to be driven by NADH which would be expensive and time consuming.

3.15 Mutagenesis of Ht HoxFU

The mutagenesis experiments in this section were performed by Part II student Zipporah Hodder under guidance of Dr Miguel Ramirez.

Preissler *et al.* had identified a double mutation in the HoxFU subunit of *Re*SH that gave the enzyme moiety increased specificity towards $NADP^+$ (Figure 3-18) based on both steric and electrostatic reasoning. This is due to interactions between amino acid residues at the active site making binding more favourable.

```
Re      MDSRITTILERYRSDRTRLIDILWDVQHEYGHIPDAVLPQLGAGLKLSPLDIRETASFYH      60
Ht      ------MTTERQRTAPGLLAALHQARSRFGRPLDAQALAELSTAFSLPPGEIAATASFYH
                ** *:    *  :    .:    :   .*.:*.:.:.*.* :*  ******

Re      FFLDKPSGKYRIYLCNSVIAKINGYQAVREALERETGIRFGETDPNGMFGLFDTPCIGLS      120
Ht      FFQTPP-ARYQIHFVDHVVDHHAGVAALCNHLCAAFAIQPGQRTADARLFVGWTACAGLS
        **   * .:*:*:: : *: :  *  *: : *    .*: *:  .:. : :  *.* ***

Re      DQEPAMLIDKVVFTRLRPGKITDIIAQLKQGRSPAEIANPAGLPSQDIAYVDAMVESNVR      180
Ht      DQAPAALINGRPMPRLDAARIDALIEKIQ-----------AQIPMDQWPTEWFAVTNAIH
        ** ** **:   :.** ..:*  :* :::           * :* :: .     * . ::

Re      TKGPVFFRG-RTDLRSLLDQCLLLKPEQVIETIVDSRLRGRGGAGFSTGLKWRLCRDAES      239
Ht      RHGPLLTWLDTTPAEAVFEHPTAHDPDAILQAVTDAGLRGRGGAGFPTATKWRFCRENAD
         :**::     *  .:::::    .*: ::::::.*: *********.*. ***:**:  .

Re      EQKYVICNADEGEPGTFKDRVLLTRAPKKVFVGMVIAAYAIGCRKGIVYLRGEYFYLKDY      299
Ht      PERFLICNADEGEPGTFKDRVLLTRYPEHLFAGMILAARAIGADKAILYLR----YEYQY
         ::::******************** *:::*.**::** ***. *.*:***    *  :*

Re      LERQLQELREDGLLGRAIGGRAGFDFDIRIQMGAGAYICGDESALIESCEGKRGTPRVKP      359
Ht      LLPQLEAARERIASAQATVPQAER-VTLEIALGAGAYVCGEESALIESLEGKPGRPRVRP
        *  **:  **    .:*   :*   . :.* :*****:**:******* *** * ***:*

Re      PFPVQQGYLGKPTSVNNVETFAAVSRIMEEGADWFRAMGTPDSAGTRLLSVAGDCSKPGI      419
Ht      PYPVTQGYLGHPTVVNNVETLVAVAAIVGNGAAWWRALGTPDSSGPKLFCVSGDVAQPGL
        *:** *****:** ******:.**: *: :** *:**:*****:*.:*:.*:** ::**:

Re      YEVEWGVTLNEVLAMVGARDAR-AVQISGPSGECVSVAKDGERK-LAYEDLSCNGAFTIF      477
Ht      YEFPYGVALGDVVTAARPLGTRYAVQVSGPSGTLLPATPEQLARPLAFEALPCNGTVMVF
        **. :**:*.:*:: . . .:* ***:*****  :..: :   : **:* *.***:. :*

Re      NCKRDLLEIVRDHMQFFVEESCGICVPCRAGNVDLHRKVEWVIAGKACQKDLDDMVSWGA      537
Ht      DVRRDPVAIVHHFARFFAHESCGFCTPCRVGTQLIAKTFEKIAAGYATRFDLERLAPALE
        : :** : **:.. :**..****:*.***.*.  : :..* : ** * : **: :..

Re      LVRRTSRCGLGATSPKPILTTLEKFPEIYQNKLVRHEGPLLPSFDLDTALGGYEKALK--      595
Ht      AMRLASNCGFGLSAGNPVRDLIAHFRQQLEAQLQPHD--FIPAFSLDAELAATRRLTGRD
         :* :*.**:* :: :*:   : :* :  : :*  *:  ::*:*.**: *.. .:

Re      ---------DLEEVTR
Ht      DPHAHLAQFEQPEVTR
                :  ****
```

Figure 3-18: Sequence alignment of HoxFU subunits of the *Re* SH and *Ht* SH: * = single, fully conserved residue, : = conservation between groups of strongly similar properties, . = conservation between groups of weakly similar properties. The highlighted amino acids correspond to the residues mutated in the article by Preissler *et. al*.[7]

The mutagenesis was carried out by Dr Miguel Ramirez who provided all samples of mHoxFU, the protein sequence after mutagenesis is shown in Figure 3-19.

(a)

```
wild-type   AAAGCAATCCTGTATCTGCGCTATGAATATCAGTATCTGCTGCCGCAGCTGGAAGCCGCA
mutant      AANNCAATC-TGTATCTGCGCTATGAATATCAGTATCTGCTGCCGCAGCTGGAAGCCGCA
            **  ***** **************************************************

wild-type   CGTGAACGTATTGCAAGCGCACAGGCAACCGTT-CCGCAGGCAGAACGTGTTACCCTGGA
mutant      CGTGAACGTATTGCAAGCGCACAGGCAACCGTTTCCGCAGGCAGAACGTGTTACCCTGGA
            ********************************* ************************

wild-type   AATTGCATTAGGTGCCGGTGCGTATGTTTGTGGTGAAGAAAGTGCCCTGATTGAATCACT
mutant      AATTGCATTAGGTGCCGGTGCGTATGTT------GAAGCGCGTGCCCTGATTGAATCACT
            ****************************      ****   ********************

wild-type   GGAAGGCAAACCGGGTCGTCCTCGTGTTCGTCCGCCTTATCCGGTTACACAGGGTTATCT
mutant      GGAAGGCAAACCGGGTCGTCCTCGTGTTCGTCCGCCTTATCCGGTTACACAGGGTTATCT
            ************************************************************

wild-type   GGGTCATCCGACAGTTGTTAATAATGTTGAAACCCTGGTTGCAGTTGCAGCCATTGTTGG
mutant      GGGTCATCCGACAGTTGTTAATAATGTTGAAACCCTGGTTGCAGTTGCAGCCATTGTTGG
            ************************************************************
```

(b)

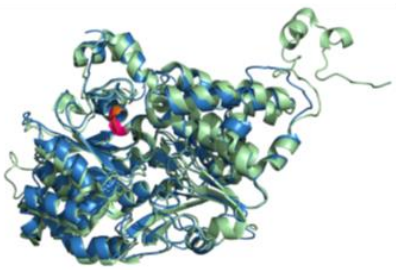


Figure 3-19: (a) The sequences of the wtHoxFU and the mHoxFU at DNA level after mutagenesis. (b) Visual representation of sequence alignment of the HoxFU subunits of the *Re* SH (green) and *Ht* SH (blue). The pink (glutamic acid) and orange (serine) section highlights the amino acids substituted in the mutagenesis.

3.15.1 Activity assays for mHoxFU

Upon completion of the mutagenesis and subsequent protein expression and purification, the first step was to carry out characterisation assays to test whether the mHoxFU was catalytically active. This was done by performing a standard assay using the redox mediator benzyl viologen (BV^{2+}), the protocol for which was outlined in Chapter 2. The HoxFU moieties lack the HoxHY subunit, so H_2-driven $NAD(P)^+$ reduction cannot be tested using just this protein. However, the oxidation of NAD(P)H can be used to reduce BV^{2+} and the results analysed by UV-Vis.

The reduction of BV^{2+} leads to the formation of a radical monocation which absorbs at 550 nm. The increase in absorbance at this wavelength can therefore be used to measure the activity of the enzyme moiety. These assays were carried out in the glovebox under an inert dinitrogen atmosphere, as O_2 can abstract electrons from $BV^{\bullet+}$ distorting the results. An example UV-Vis spectrum is shown in Figure 3-20 using the m*Re*SH developed by Preissler *et al.* the increasing absorbance at 550 nm indicates catalytic activity.[7]

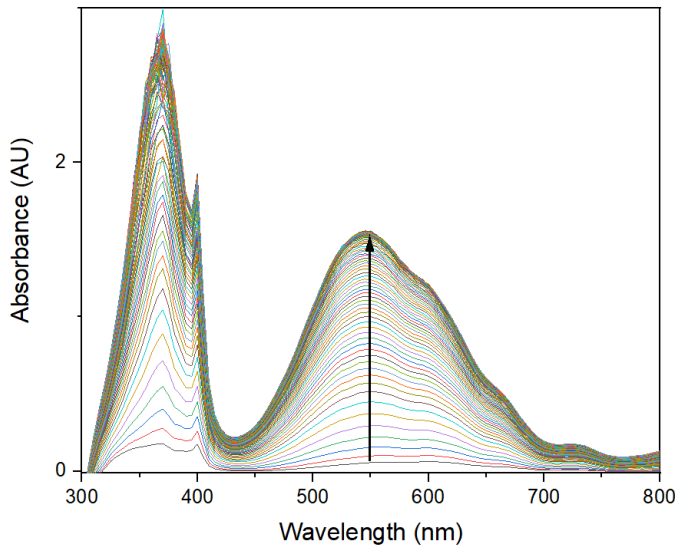


Figure 3-20: UV-vis spectra showing the results of activity assay for the reduction of 0.2 mM solution of BV^{2+} using 0.1 mM NADPH and 60 µg mReSH. Increasing absorbance at 550 nm indicates catalytic activity.

It is important to note that the $BV^{\bullet+}$ also gives the solution a bright blue colour, which can be observed to intensify during the reaction.

3.16 Catalytic activity of mHoxFU with NAD(P)H

Activity assays were performed using m*Re*SH, *Ht*HoxFU and *mHt*HoxFU showing the activity towards both NADH and NADPH, and the results analysed using UV-Vis Abs_{550} which can be seen in Figure 3-20.

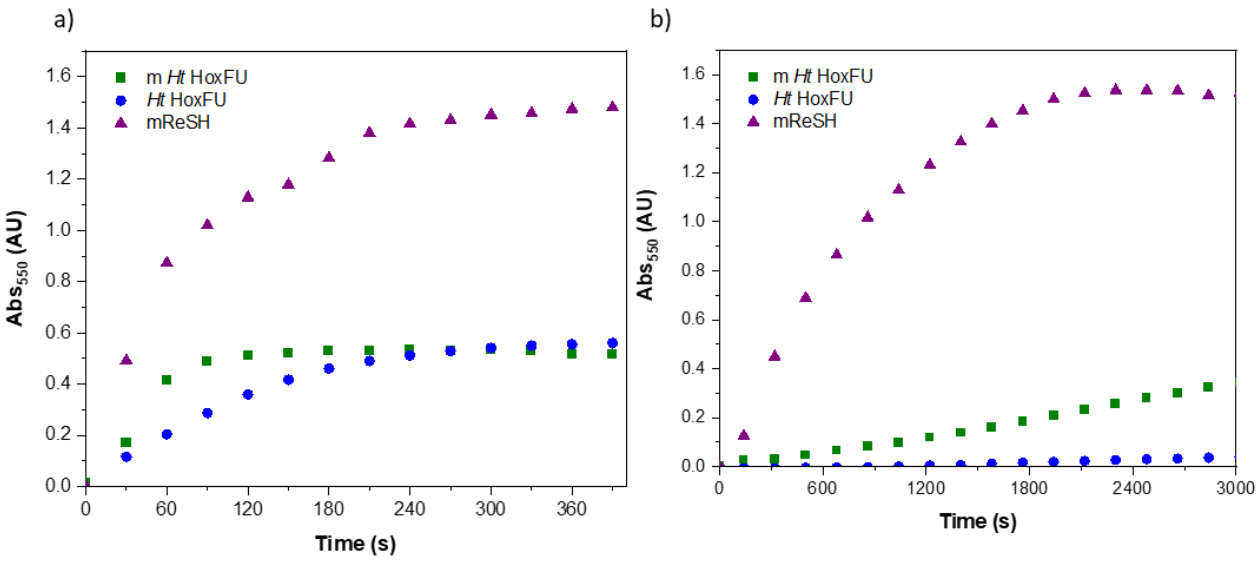


Figure 3-21: Abs_{550} recorded over time for (a) NADH-driven and (b) NADPH-driven BV^{2+} reductions using m*Re*SH, m*Ht*HoxFU and *Ht*HoxFU. The linear region of the graph (used to calculate the initial rate) is taken as 0-60 s.

The m*Re*SH was considerably more responsive to NADH-driven BV^{2+} reduction than the *Ht* HoxFU variants. Both the *Ht*HoxFU and the m*Ht*HoxFU showed similar activity towards NADH, indicating that the mutagenesis had not switched the selectivity of the cofactor binding unit from NAD(H) to NADP(H), but that the active site is now accepts both cofactors. It is important to note that the cofactors were not purified and may have contained trace impurities of oxidised/reduced cofactor

species (also NAD^+ containing traces of $NADP^+$), this would influence the activity assays. This is discussed in Chapter 2.

Rates were calculated using the Beer-Lambert law, where $\varepsilon_{exp\ (BV2+)} = 15.39 \times 10^3\ M^{-1}\ cm^{-1}$ measured at 340 nm, and these are summarised in Table 3-1. Gradients of the initial, linear portion of the curves in Figure 3-21 were used to calculate the initial rates in terms of BV^{2+} reduction. The NADPH-driven BV^{2+} reductions were notably slower than the NADH equivalents.

Table 3-1: Initial rates for NAD(P)H-driven BV^{2+} reduction using mReSH, mHoxFU, and mReSH

	Cofactor	mReSH	m *Ht* HoxFU	*Ht* HoxFU
Initial slope (10^{-3} U s^{-1})	NADH NADPH	16 1.8	8.1 0.12	2.9 0.019
Initial rate (10^{-3} mM s^{-1})	NADH NADPH	1.1 0.12	0.52 0.0076	0.19 0.0012
Initial rate (10^{-3} mM min^{-1})	NADH NADPH	63 7.2	32 0.45	12 0.075

3.17 Electrochemical characterisation of mHoxFU

After establishing that the mHoxFU was capable of acting on NADPH, electrochemical experiments were used to investigate the $NAD(P)^+$ activity of the mHoxFU under a range of conditions to establish whether the enzyme would be suitable for electrochemically-driven NADPH cycling.

Cyclic voltammograms were recorded for a 1 mM solution of $NADP^+$ (Figure 3-22a) and 1 mM NAD^+ (Figure 3-22b). The onset potential for the mHoxFU with $NADP^+$ is approximately -0.3 V vs SHE less negative than the mHoxFU in NAD^+ (approximately -0.33 V vs SHE). The notable difference however is between the magnitudes of the current produced, with an observably larger current being

observed for the mHoxFU in NAD^+; approximately 1.1 µA after subtracting the capacitive current of 0.4 µA.

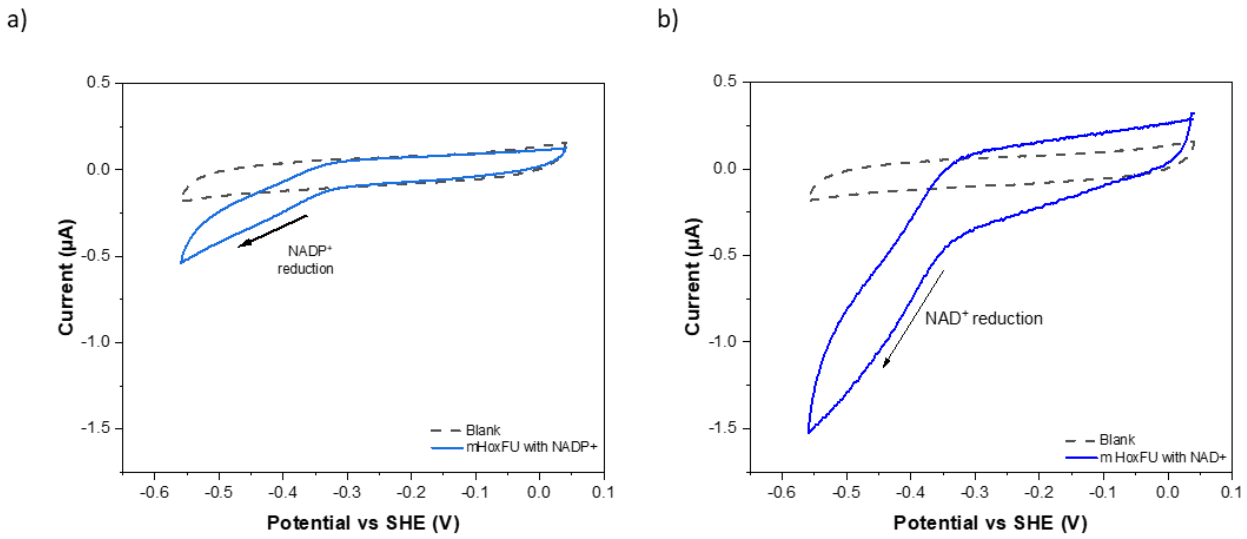


Figure 3-22: CVs of electrodes modified with mHoxFU (blue trace) in a cell containing (a) 1 mM $NAPD^+$ and (b) 1 mM $NAP^{+\cdot}$ Unmodified electrode is shown as a dotted black trace. Cell contained 50 mM Tris-HCl, pH 8, 3000 rpm.

Whilst there is certainly some catalytic activity for the mHoxFU in $NADP^+$ (approximately 0.3 µA for the mHoxFU in $NADP^+$), it is important to note that the cofactor was not purified. It is known that commercially purchased $NADP^+$ contains traces of NAD^+ contaminants.[27] For this reason, further electrochemical experiments were carried out to confirm that the activity seen in the mHoxFU CV is due to $NADP^+$.

3.18 Confirming $NADP^+$ reduction

The CV in Figure 3-23 has been recorded using an electrode modified with mHoxFU to assess its selectivity towards $NADP^+$ (green trace) and fractional levels of NAD^+ that mimic the level of contaminant which could be present in $NADP^+$. The current is very low at 0.01 mM or 0.1 mM NAD^+, so even at 10% contaminant, background from NAD^+ would be low (purity is stated as 97.6%).

Comparing the green trace to the red trace (0.01 mM NAD^+) confirms the mHoxFU's activity is due to the reduction of $NADP^+$.

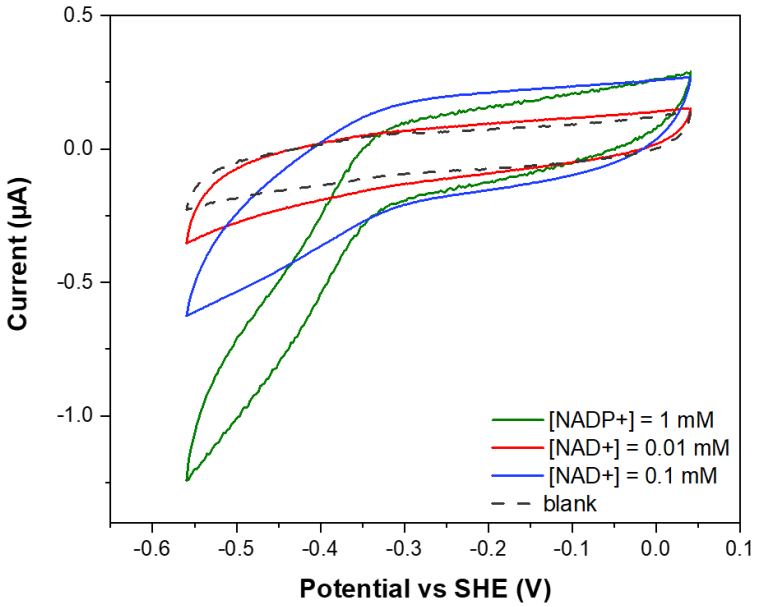


Figure 3-23: Cyclic voltammogram showing the difference in activity of mHoxFU towards 1 mM $NADP^+$ and two concentrations of NAD^+. These concentrations exceed the typical contaminants in commercially purchased $NADP^+$. Electrode has been modified with mHoxFU (unmodified electrode shown as black dotted trace). Experiments performed in 50 mM Tris-HCl, pH8 at 30°C. The electrode was rotated at 2000 rpm.

This confirms the affinity of mHoxFU towards $NADP^+$ and sets the foundation for section 3.20 which will look at preparing the mHoxFU for use as an H_2-driven NADPH recycling system.

3.19 Comparison of mHoxFU to Ht HoxFU

It is important when considering the mHoxFU as a potential candidate for electrochemical cofactor recycling, to compare the results against those achieved for the *Ht* HoxFU obtained in section 3.3. The CVs shown in Figure 3-24 were recorded under similar pH/temperature conditions and have been overlaid for comparison purposes.

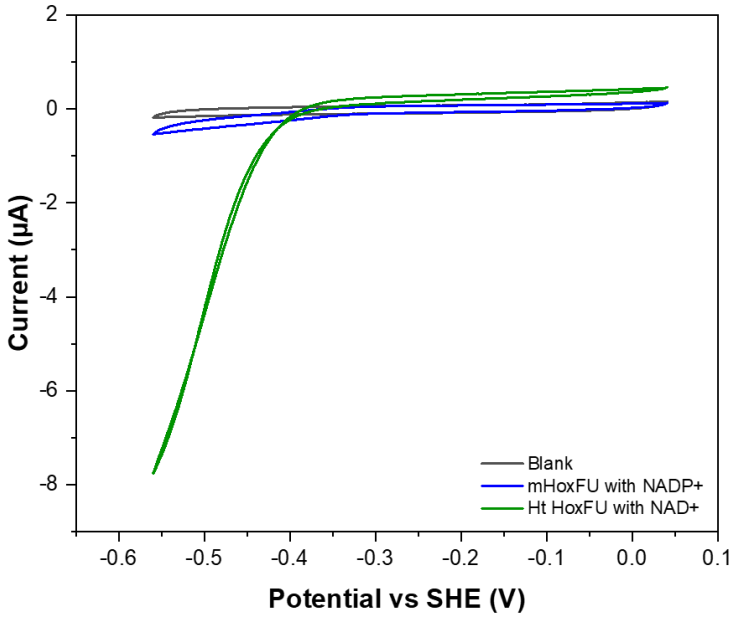


Figure 3-24: CVs of electrodes modified with mHoxFU (blue trace) in 1 mM $NADP^+$ and *Ht* HoxFU (green trace) in 1 mM NAD^+. Unmodified electrode is shown as a dotted black trace. Cell contained 50 mM Tris-HCl, pH 8, performed at 30 °C with rotation 3000 rpm.

The green trace on the CV shows the current recorded at a PGE electrode that has been modified with *Ht* HoxFU and the blue trace shows mHoxFU. The difference in the magnitude of catalytic current between the two enzymes/substrates is significant, and it is important to note that these currents were typical of multiple experiments carried out. This indicates that the mHoxFU would not be a good candidate for electrochemical cycling of NADPH, and further mutation would likely be needed.

3.20 Developing an H_2-driven NADPH generation catalyst

Following on from the experiments carried out in sections 3.18 and 3.19, the mHoxFU was then tested for use with hydrogenase as an H_2-driven NADPH catalyst, by co-adsorbing the enzyme with Hyd1 on carbon nanoparticles (BP2000) based on the method developed by Reeve *et al.* in the Vincent Group for recycling NADH.[28] The full procedure for this is detailed in Chapter 2, section 2.4. The Hyd1 is required for this process as the mHoxFU moiety has been isolated and does not contain

the HoxHY hydrogenase subunit. A schematic representation of the mHoxFU-Hyd1-modified particle is shown in Figure 3-25. The Hyd1 moity is shown in green and splits molecular hydrogen into two protons and two electrons. The electrons are carried along the chain of Fe-S clusters into the carbon where they can be transferred to the co-adsorbed mHoxFU. The electrons travel to the flavin active site where a hydride transfer is performed on an NADP+ molecule in solution. The resulting NADPH can then be used drive a reaction of interest, during which the NADP+ will be regenerated and the process can continue.

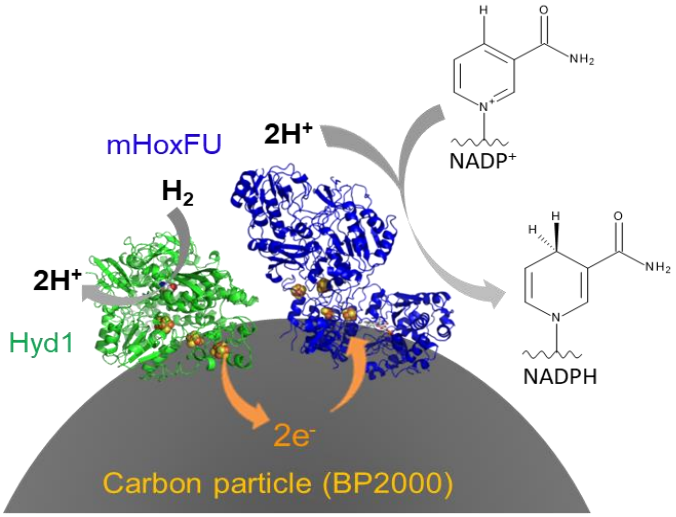


Figure 3-25: Schematic representation of NADPH regeneration by mHoxFU coadsorbed to BP2000 with Hyd1 acting as an electron source for the reduction. Based on the system developed in the Vincent Group by Reeve *et al.*[28]

3.20.1 Comparison of HoxFU activities.

Due to the disappointing results of the electrochemical experiments using mHoxFU, it is not possible to establish the K_M for the enzyme electrochemically. To get an idea of how active the enzyme is, an assay was performed to generate NADH from the enzyme-modified particles for both mHoxFU and wtHoxFU. A 20 mg mL^{-1} slurry of BP2000 was made up in 50 mM Tris-HCl buffer and sonicated for 1 hour. An aliquot of the BP2000 slurry was then placed into an Eppendorf tube together with an aliuot of Hyd-1 and an aliquot of the HoxFU (either mHoxFU or wtHoxFU) in a ratio of 2:0.7:0.3 by mass. The mixture was then incubated in a fridge for 1 hour at 4°C. The enzyme-modified particles

were then centrifuged fo 3 minutes at 12,000 g and the supernatant removed. Assays were then performed to reduced a 0.1 mM solution of NAD^+ by both mHoxFU-Hyd1-modified particles and wtHoxFU-Hyd1-modified particles over a period of 30 minutes. UV-Vis spectra were recorded and for both experiments and these are shown in Figure 3-26b for the mHoxFU, and Figure 3-26c for the wtHoxFU. The Abs_{340} has been plotted over time and this is shown in Figure 3-26a.

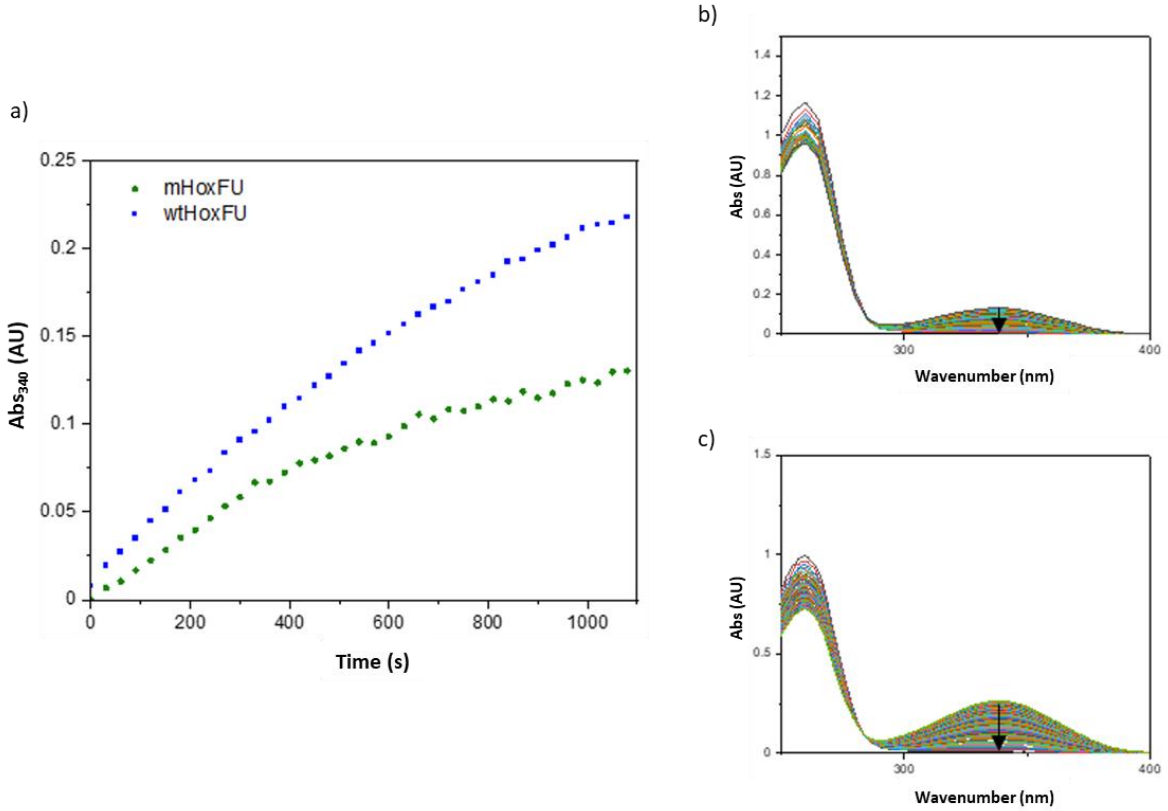


Figure 3-26: (a) Abs_{340} against time for the first 20 mins of the reaction to reduce a 0.1 mM solution of NAD^+ by enzyme-modified particles; mHoxFU (green) and wtHoxFU (blue) (b) UV-Vis spectra for the mHoxFU reaction and (c) UV-Vis spectra of the wtHoxFU reaction. Arrows denote the direction of change of Abs_{340}.

The Beer-Lambert Law was then used to calculate the initial rate of NADH production using the experimental value for the extinction coefficient (15.1 mM^{-1} cm^{-1}).[6,29] The initial rates were determined to be 2.76 x 10^{-3} mM min^{-1} for wtHoxFU and 2.3 x 10^{-3} mM min^{-1} for the mHoxFU. These rates are equivalent to specific activities for wtHoxFU of 0.55 µmol min^{-1} mg^{-1} and for mHoxFU of 0.46 µmol min^{-1} mg^{-1}.

3.21 NADPH generation and optimising [$NADP^+$]

Similar assays to those carried out in the previous section were repeated with mHoxFU using a range of $NADP^+$ concentrations. No NADPH was generated from experiments using 0.1 – 0.5 mM $NADP^+$ so the concentration was increased to 1 mM and above. The Abs_{340} was plotted over time for two assays of mHoxFU-Hyd1-modified particles and this is shown in Figure 3-27 for 3 mM NAD^+ (purple) and 3 mM $NADP^+$ (green). The rate of NADH generation by the mHoxFU-Hyd1-modified particles is 5.8 x 10^{-3} mM min^{-1} (specific activity 1.2 µmol min^{-1} mg^{-1}) and for NADPH is 1.1 x 10^{-3} mM min^{-1} (specific activity 0.2 µmol min^{-1} mg^{-1}) which is over four times slower than the rate for NADH generation.

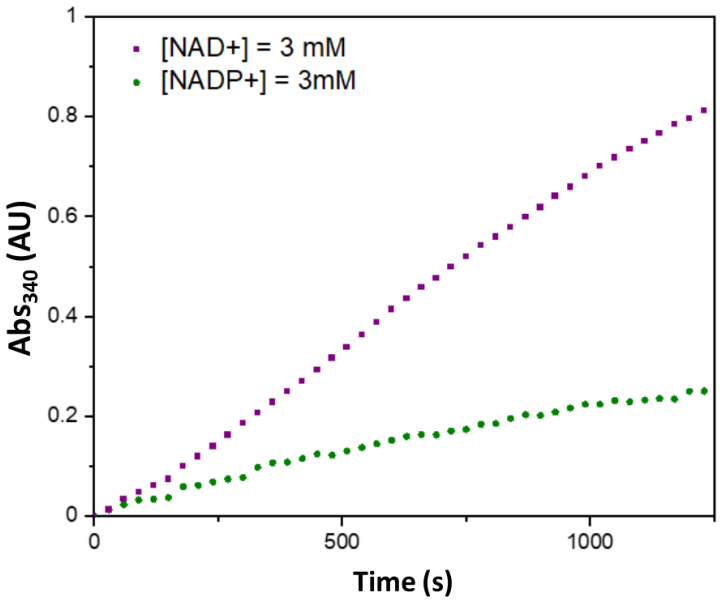


Figure 3-27: Abs_{340} against time for NADH and NADPH generation by mHoxFU-Hyd1-modified particles. Starting concentrations of $NAD(P)^+$were 3 mM. Both Abs_{340} traces started to plateau after 2400 seconds.

Following on from these experiments, further assays were carried out to establish the best concentration of $NADP^+$ for optimum generation of NADPH. It is important to note that these assays are carried out to explore the generation of NADPH using just the particles. Once the particles are

implemented into a recycling system, there is the possibility of substrate inhibition affecting the rate, and also a consideration of the affinity of the downstream enzyme for NADPH. This will be considered further in 3.22.2.

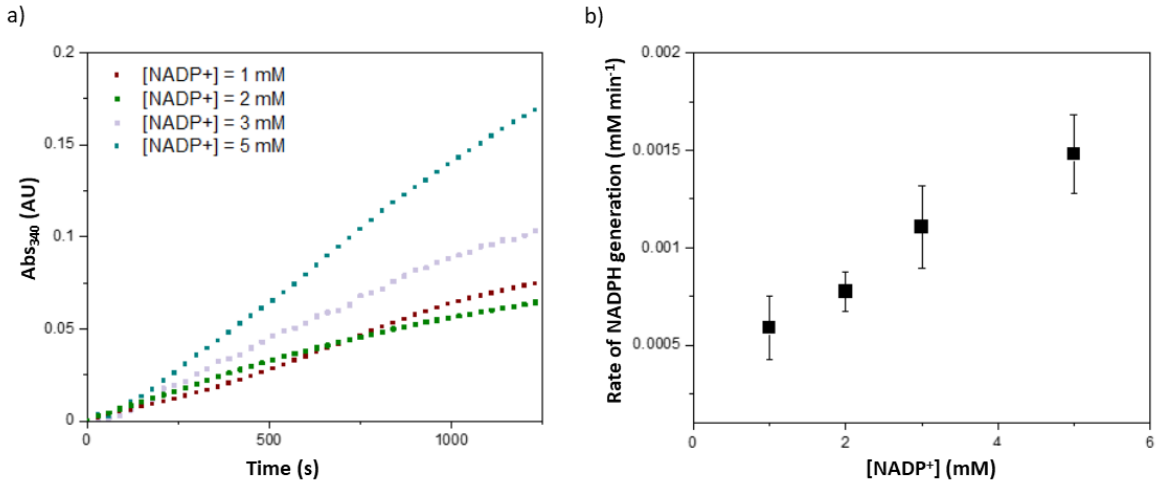


Figure 3-28: (a) Abs_{340} plotted against time for the generation of NADPH at different concentrations of $NADP^+$. (b) Corresponding initial rates for each concentration of $NADP^+$. Experiments performed in triplicate and error bars represent the mean ± one standard deviation of uncertainty. Assays performed in Tris-HCl buffer, pH8 using mHoxFU-Hyd1-modified particles.

A plot of the Abs_{340} over time for mHoxFU-Hyd1-modified particles is shown in Figure 3-28a and from these data the initial rate of NADPH generation was calculated and plotted against concentration (Figure 3-28b). The specific activity for each concentration has been calculated, and this is shown in

Table 3-2.

Table 3-2: Concentration of $NADP^+$ and the equivalent mean specific activity values of the mHoxFU-Hyd1-modified particles

[$NADP^+$] (mM)	Specific activity (µmol min^{-1} mg^{-1})
1	0.12
2	0.16
3	0.22
5	0.30

This clearly shows that as the substrate is increased, the activity increases. However, in practice it is not economically viable to use concentrations of 5 mM $NADP^+$.

3.22 The effect of temperature on mHoxFU-Hyd1 particles

The temperature of a reaction has a significant effect on the rate of the reaction according to the Nernst equation (Chapter 2, section 2.1.1). As *Hydrogenophilus thermoluteolu*s is a thermophilic organism, it was presumed that *Ht* HoxFU might operate over a wider range of temperatures. It was observed in section 3.7 that the *Ht* HoxFU was catalytically active at temperatures up to 65 °C. At higher temperatures there was a significant loss of activity over a time period of only 5 minutes.

The mHoxFU-Hyd1-modified particles were assayed in 3 mM $NADP^+$ at 20 °C, 30 °C and 40 °C and the results are shown in Figure 3-29. The enzyme operates at increased temperature and the rate of reaction is enhanced.

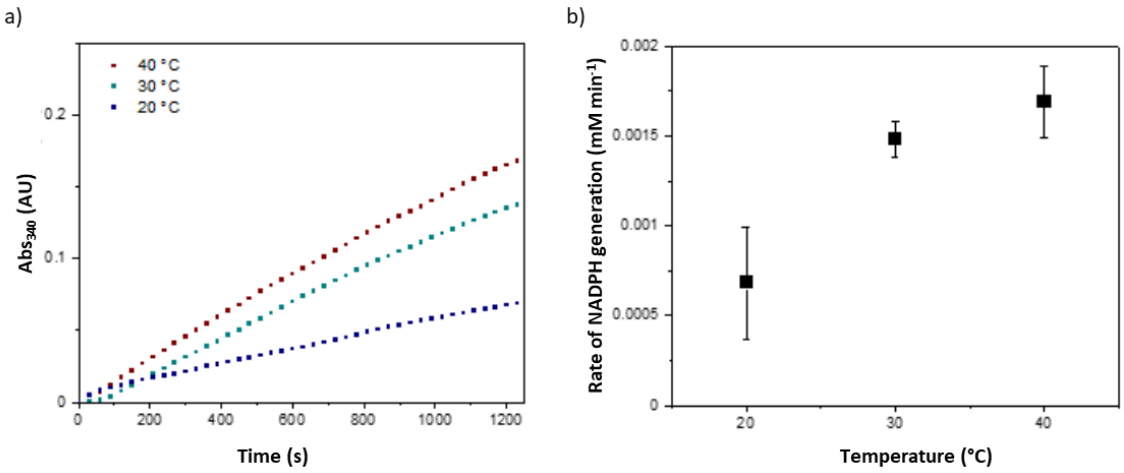


Figure 3-29: (a) Abs_{340} plotted against time for the generation of NADPH where [$NADP^+$] = 3 mM at 20 °C, 30 °C and 40 °C. (b) Corresponding initial rates at each temperature. Experiment carried out in triplicate and error bars represent the mean ± one standard deviation of uncertainty. Assays performed in Tris-HCl buffer, pH8 using mHoxFU-Hyd1-modified particles.

A summary of the mean specific activities obtained at each temperature is shown in Table 3-3

Table 3-3: The effect of temperature on the mean specific activity values of MHoxFU-Hyd1-modified particles. Conditions [$NADP^+$] = 3 mM, H_2 saturated environment

Temperature (°C)	Mean specific activity (µmol min^{-1} mg^{-1})
20	**0.13**
30	**0.29**
40	**0.34**

The specific activity at 30 °C is more than double that at 20 °C, so even a small increase in temperature could have quite a big impact on the activity of the enzyme and the rate of reaction.

3.22.1 The ratio of mHoxFU-Hyd1 to carbon

In the presence of H_2 and $NADP^+$ the mHoxFU-Hyd1-modified particles are able to generate NADPH, the particle acting as an 'electrode' for each half reaction; the oxidation of H_2 and the reduction of $NADP^+$. It is likely that composition of the particles in terms of catalyst loading could change the equilibrium potential of the particle, and therefore affect the availability of electrons for $NADP^+$ reduction.

To test this theory, varying ratios of Hyd1 and mHoxFU were immobilised onto BP2000. The overall total mass of enzyme was kept the same for each experiment to allow for comparison. Previously, higher masses of enzyme had been tested, but had not shown any improved results. Different ratios of carbon:Hyd1: mHoxFU were assayed at 40 °C in a 3 mM solution of $NADP^+$, and the results are shown in Figure 3-30.

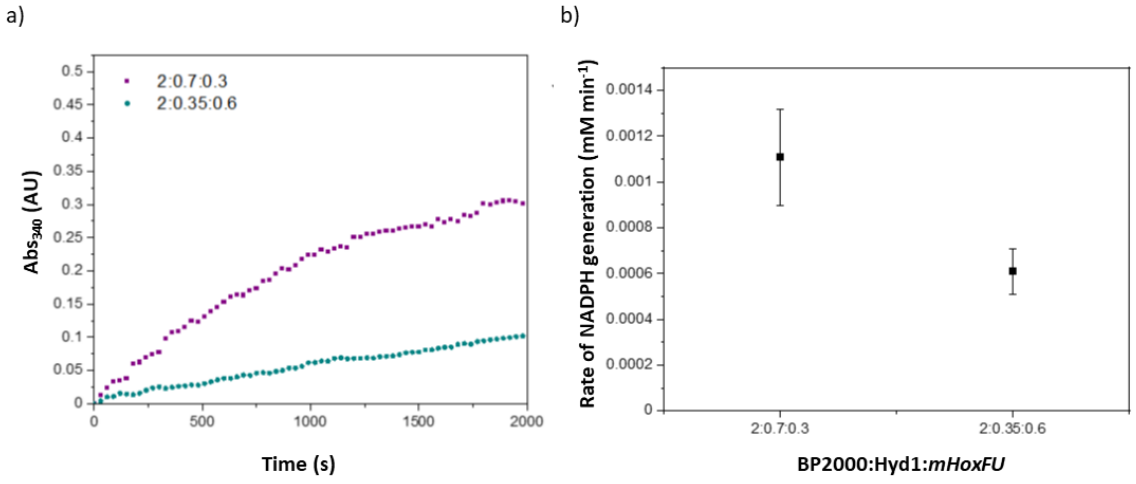


Figure 3-30: Comparison of initial rates when varying quantities of Hyd1 and mHoxFU on carbon. Ratios are given by mass of carbon (BP2000): Hyd1: mHoxFU. Experiment carried out in triplicate and error bars represent the mean ± one standard deviation of uncertainty. Assays performed in Tris-HCl buffer, pH8.

It can be seen from graph a that the ratio of 2:0.7:0.3 of carbon: Hyd1: mHoxFU gives much better results. Increasing the rate of NADPH generation to almost double that of the particles with ratio 2:0.35:0.6. The mean specific activity of this ratio was 0.11 µmol min^{-1} mg^{-1} compared to the 2:0.7:0.3 ratio which had a mean specific activity of 0.23 µmol min^{-1} mg^{-1}. These results indicate that increasing the loading of mHoxFU does not offer any advantage to the rate of NADPH generation.

H_2-driven NADPH recycling to drive a biocatalytic hydrogenation

Having somewhat optimised the conditions for effective NADPH generation, it was then appropriate to study the activity of the particles when coupled to a C=X reduction. One reaction that has been well studied within the Vincent Group is the reduction of acetophenone to 1-phenylethanol but Johnson Matthey's ADH-101, so this reaction was selected to test the NADPH recycling system.

3.22.2 Reduction of acetophenone in batch

Before coupling with the NADPH recycling system, a stoichiometric NAD(P)H-driven acetophenone reduction was completed to get an idea of substrate and enzyme quantities. The reaction scheme is shown in Figure 3-31. and comprises of only acetophenone, ADH-101 and NADPH.

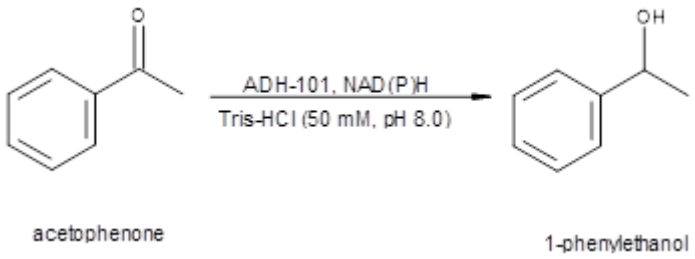


Figure 3-31: Reaction scheme for the reduction of acetophenone to 1-phenylethanol by ADH-101, driven by NAD(P)H *in situ*.

Although ADH-101 has a preference for NADPH, it can also use NADH as its hydride source. Assays were prepared and analysed by UV-Vis spectroscopy. Comparison of the NADH-driven and NADPH-driven acetophenone reduction is shown in Figure 3-32.

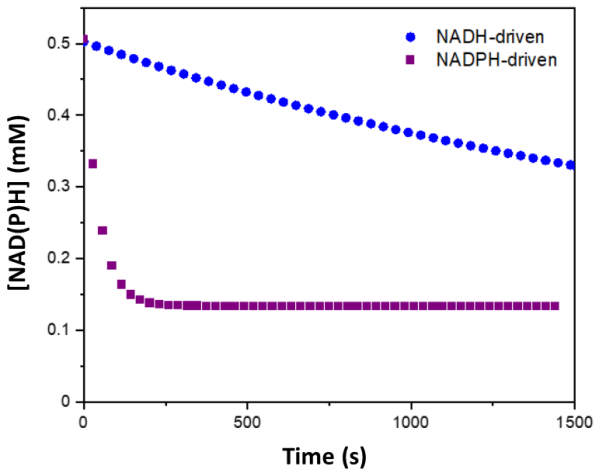


Figure 3-32: Consumption of a 0.5 mM solution of NADPH vs NADH over time in an ADH-101 catalysed acetophenone reduction.

In section 3.21 the concentration of $NADP^+$ for fastest NADPH generation was found to be between 1 and 5 mM (for the concentrations tested). However, as NADPH is consumed in the recycling system, $NADP^+$ is regenerated. High concentrations of $NADP^+$ could cause substrate inhibition at the active site of ADH-101 as well as unbalancing the equilibrium. To test how much $NADP^+$ the ADH can tolerate, a number of assays were carried out with various concentrations of $NADP^+$ as contaminants. The results of the UV-Vis spectroscopy analysis are shown in Figure 3-33 (a-c) and the [NADPH] is plotted over time and shown in Figure 3-33d. The rate of reaction determined from the slope in Figure 3-33d slows down with the increase in $NADP^+$.

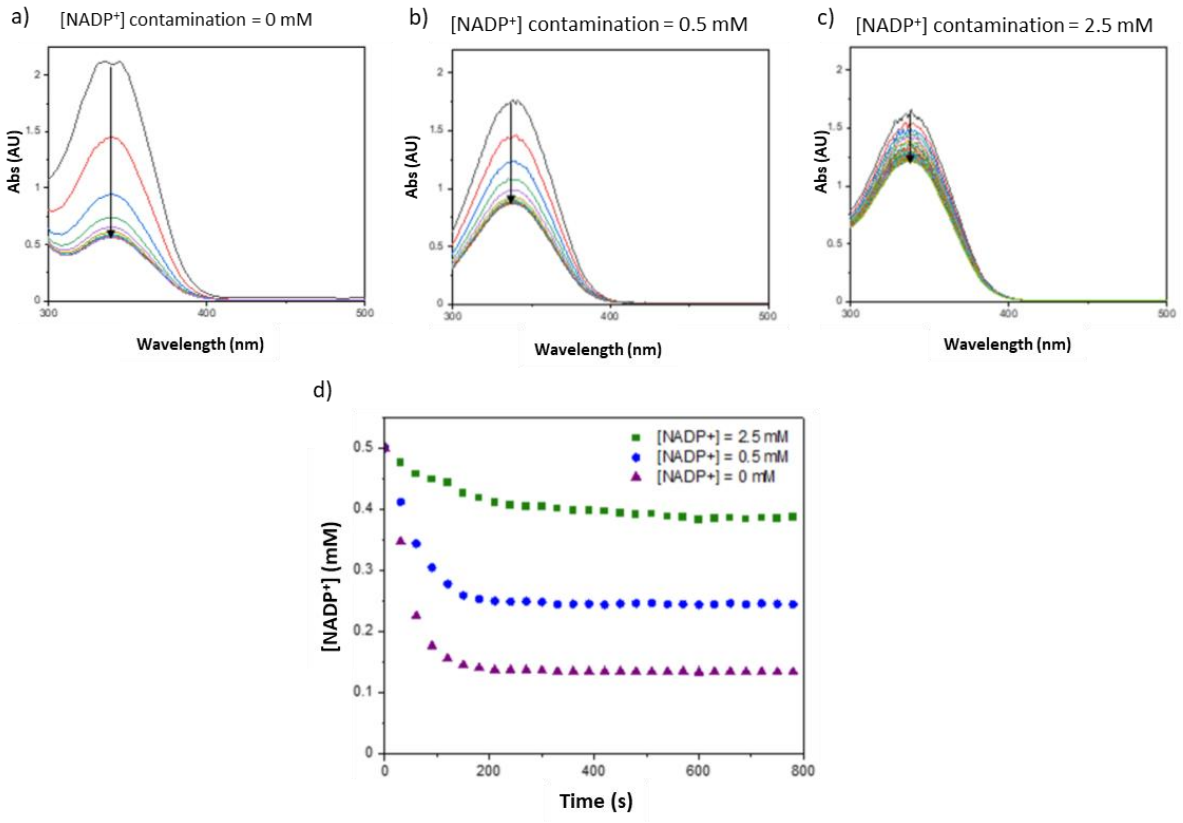


Figure 3-33: NADPH-driven reduction of acetophenone by ADH-101 under different conditions (arrows denote decreasing Abs_{340} throughout the course of the reaction: (a) without $NADP^+$ contamination, (b) 0.5 mM $NADP^+$ contamination (c) 2.5 mM $NADP^+$ contamination (d) Initial rates of all reactions plotted over time. Experiments performed in Tris-HCl buffer, pH 8 with ADH-101 10 mg mL^{-1}. Initial concentration of NADPH were 3 mM

The effect of the contaminants on the rate of NADPH consumption are summarised in Table 3-4.

Table 3-4: The effect of $NADP^+$ contaminants on the rate of NADPH consumption in terms of the specific activity values of mHoxFU-Hyd1-modified particles

[$NADP^+$] contaminant (mM)	Specific activity (µmol min-1 mg-1)
0	0.11
1	0.059
2.5	0.0085

These results show a large drop in the specific activity with the increase in $NADP^+$. From these results it was established that a good starting concentration for $NADP^+$ should be 1 mM. This ensures sufficient NADPH is generated, whilst minimising inhibition of ADH-101 by $NADP^+$.

3.22.3 Coupling Acetophenone reduction to NADPH recycling

Generation of an H_2-driven NADPH-Hyd1-modified particle system was introduced in section 3.20 and here this will be coupled to the ADH-101 reduction of acetophenone previously described. A schematic representation of this is shown in Figure 3-34 where the Hyd1 and mHoxFU are coadsorbed to BP2000. The experiment commenced with just the particles in Tris-HCl with the acetophenone present. $NADP^+$ was added and the reaction bubbled with H_2 for just over an hour to allow the system to build up a supply of NADPH.

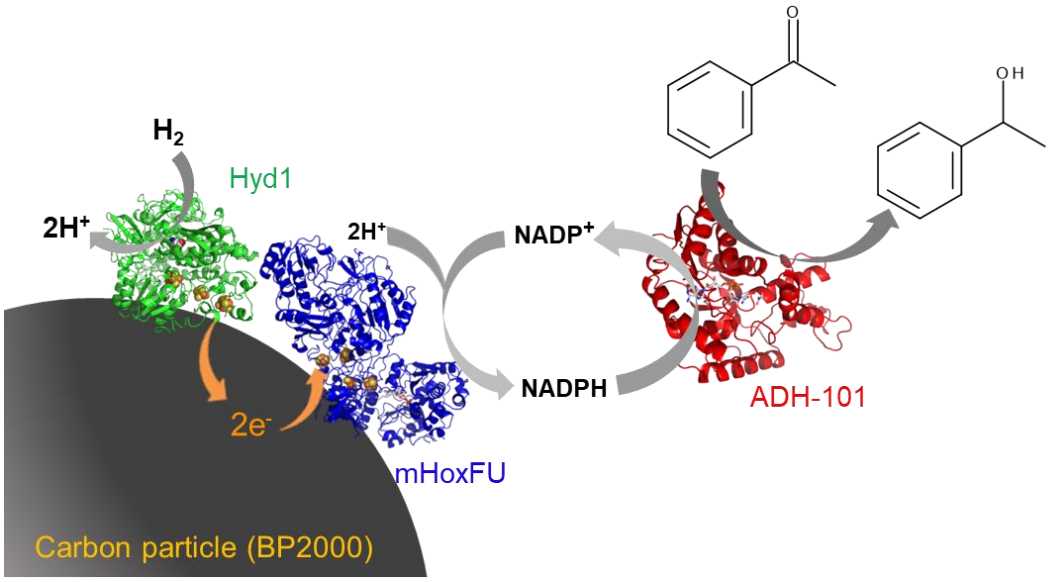


Figure 3-34: schematic representation of mHoxFU-Hyd1-particle system to recycle NADPH to drive the ADH-101 reduction of acetophenone.

The results of the experiment were analysed by *in-situ* UV-Vis spectroscopy and the results of this can be seen in Figure 3-35a. The Abs_{340} was plotted over time and this is shown in Figure 3-35b. There is a steep increase in the absorbance at around 2000 s, this is due to stirring which led to an increase in $NADP^+$ reduction. An injection of ADH-101 was added at around 4000 s, and here a sudden drop in Abs_{340} can be observed, due to the ADH-101 consuming the NADPH which has been generated during the reaction.

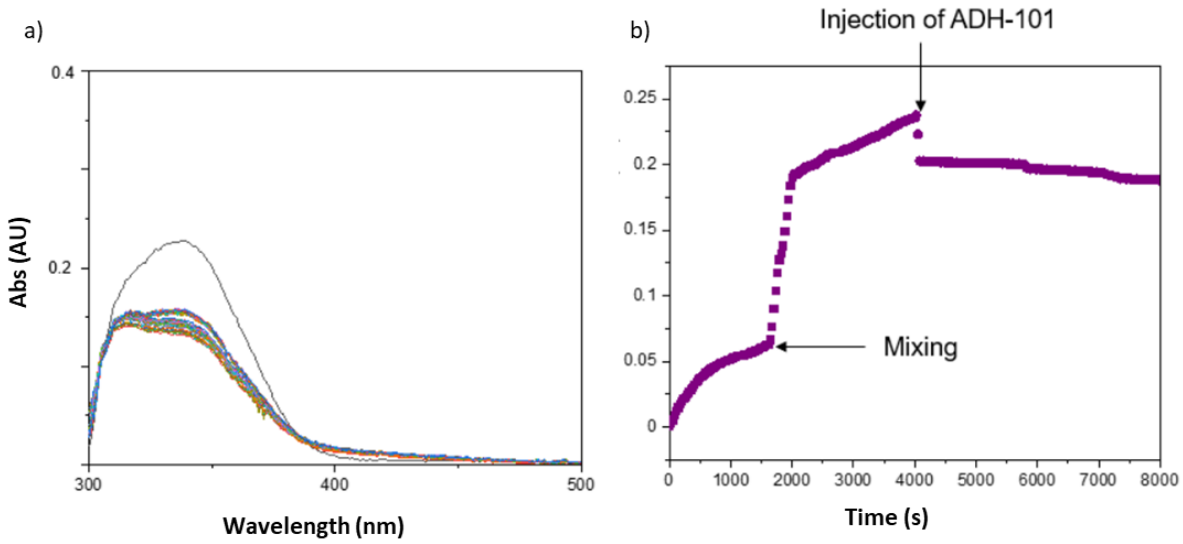


Figure 3-35: (a) UV-Vis spectra for the ADH-101 catalysed reduction of acetophenone recorded *in-situ*. (b) Abs_{340} plotted against time for the generation of NADPH and subsequent consumption throughout the acetophenone reduction. ADH-101 is added to the reaction mixture at 4000s, a sudden drop in [NADPH] is observed, suggesting that 1-phenylethanol is being produced.

3.23 H_2-driven imine reductions

Imine reductases (IREDs) catalyse the reduction of imines. However, unlike the ADH-101 which can be driven by NADH, IREDs are highly selective for NADPH as their hydride source. [24,25] Investigating the activity of the mHoxFU with an NADPH-dependent enzyme will confirm the success of the mutagenesis and show it can be effectively used in a cofactor recycling system.

As was previously done in section 3.22.2 with the ADH, the IRED reduction was carried out with NADPH in a reduction assay. The reduction of 2-methyl-1-pyrrolidine was performed using Johnson

Matthey's IRED-49 with a stoichiometric quantity of NADPH to gauge ideal substrate and mHoxFU-Hyd1-modified particle quantities. The reaction scheme is shown in Figure 3-36.

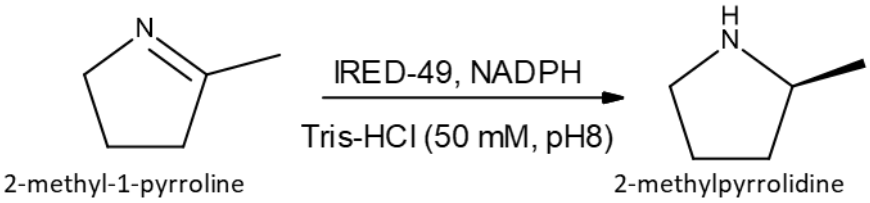


Figure 3-36: Reaction scheme for the reduction of 2-methyl-1-pyrroline to 2-methylpyrolidine by NADPH-driven IRED-49

To ensure that the IRED is selective for NADPH, an assay was performed using a stoichiometric quantity of NADH for comparison. The assays were analysed *in-situ* by UV-Vis spectroscopy and these results used to calculate the concentration of cofactor to determine its consumption. The concentration of cofactor over time has been plotted in Figure 3-37 and clearly shows a steady consumption of NADPH, whilst the concentration of NADH remains constant at the level it started at. This confirms the IRED-49 is selective for NADPH.

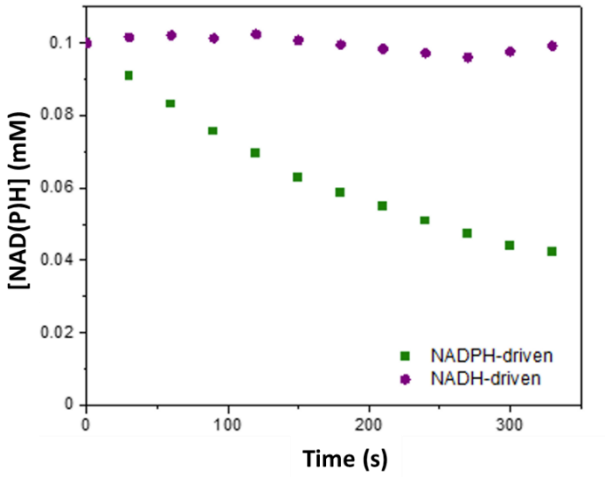


Figure 3-37: Consumption of cofactor over time for the reduction of 2-methyl-1-pyrroline by IRED-49. The specific activity of the NADPH-driven imine reduction was 0.035 ± 0.01 µmol min^{-1} mg^{-1}. No activity was observed for the NADH-driven reaction.

It was also essential to determine whether the high concentration $NADP^+$ desirable for good NADPH generation by mHoxFU-Hyd1-modified particles would inhibit the reaction. Assays were performed both with and without a 0.9 mM $NADP^+$ contaminant and the results analysed *in-situ* with UV-Vis spectroscopy. The Abs_{340} was used to calculate the concentration of NADPH (confirmed by a calibration curve) in the reaction and these were plotted over time and are shown in Figure 3-38. The reaction without $NADP^+$ contaminant progresses well whereas the contaminated assay makes little progress. The specific activity of the mHoxFU-Hyd1 particles with contaminant were 0.0045 µmol min^{-1} mg^{-1} which was significantly less than the 0.035 µmol min^{-1} mg^{-1} for the non-contaminated reduction. Once again, a balance needs to be met between a high concentration of $NADP^+$ to drive an efficient recycling system and keeping the concentration of $NADP^+$ low in order to prevent inhibition and keep the redox balance in favour of reduction.

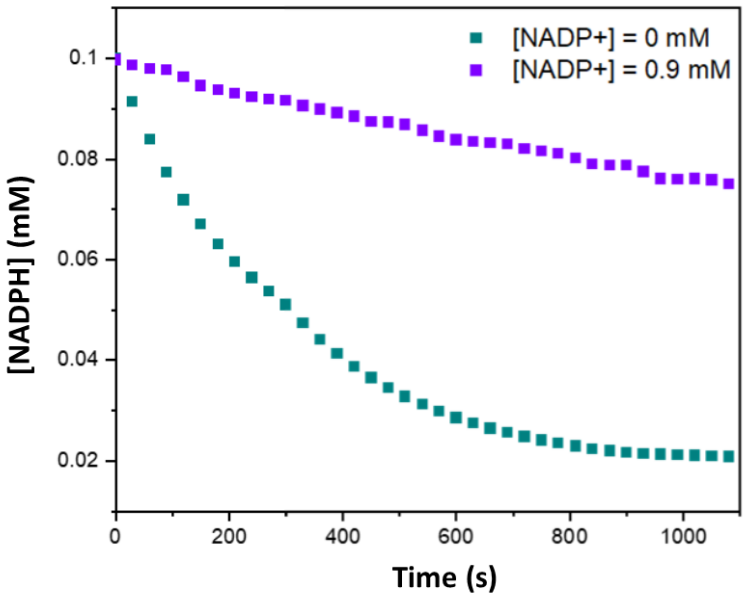


Figure 3-38: Concentration of NADP plotted over time throughout the reduction of 2-methyl-1-pyrroline. The blue trace shows the progress of the reaction without contaminant while the green trace shows the progress of a reaction that has been contaminated with 0.9 mM $NADP^+$.

Although these results indicate that higher concentrations of $NADP^+$ achieve higher conversion, it is not economically viable to use high concentrations of cofactor. Therefore the decision was made to use 1 mM $NADP^+$ for the H_2-driven mHoxFU-Hyd1-modified particle recycling system to drive the IRED reduction.

3.24 Imine reduction in an NADPH recycling system

Having optimised the conditions for the NADPH recycling system a reaction was set up (reaction scheme shown in Figure 3-39).

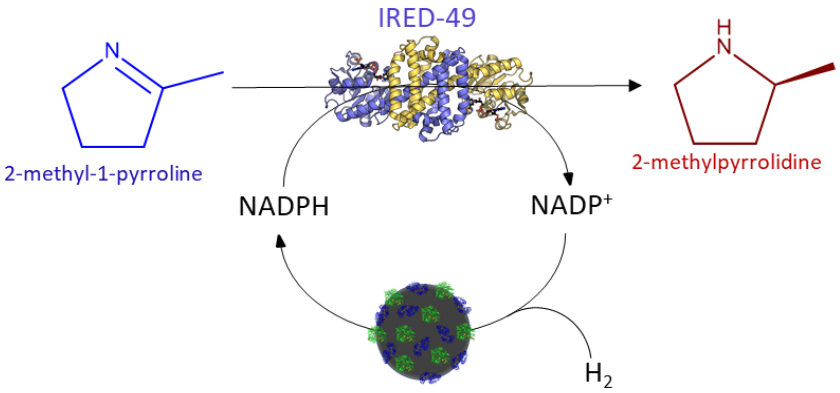


Figure 3-39: Reaction scheme for the IRED-49 reduction of 2-methyl-1-pyrroline with NADPH recycling.

A reaction mixture of mHoxFU-Hyd1-modified particles together with 1 mM $NADP^+$ in 50 mM Tris-HCl, pH8 were added to the reaction vessel together with 3 mg mL^{-1} IRED-49 and the substrate 2-methyl-1-pyrroline, and the reaction was left to run for 48 hrs under 2 bar H_2 pressure. Three different reactions were run, each under slightly different conditions, detailed in Table 3-5.

Table 3-5: Compositions of reactions for the reduction of 2-methyl-1-pyrroline by IRED-49.

Experiment Number	[IRED-49] (mM)	Mass of Hyd1-HoxFU-modified particles (µg)	[2-methyl-1-pyrroline] (mM)
1	3	40	10
2	6	40	10
3	3	60	10

Samples from each experiment were taken after 48 hours and analysed by GC and the results are shown in Figure 3-40 where it can be seen that each of the experiments produced the *S* enantiomer when compared to product standards of both enantiomers.

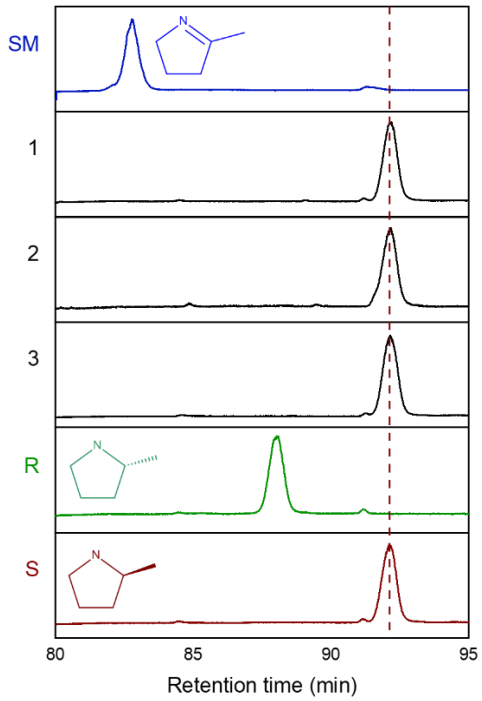


Figure 3-40: GC-FID traces (from top to bottom); starting material (SM) 2-methyl-1-pyrrolidine (blue trace), reaction samples taken after 48 hours (labelled 1, 2 and 3 according to experiment number corresponding to those in Table 3-5 and Table 3-6), enantiomeric product standards labelled *R* (green) and *S* (red). The dotted line marks the retention time of the peak of the *S* enantiomeric standard and this lines up with the peaks of the 3 experiment samples confirming the results are all the *S* enantiomer.

The conversion to product is shown in Table 3-6 which shows almost full conversion to product after 48 hours and shows that IRED-49 maintains excellent stereoselectivity. The specific activities for each of the three experiments was calculated to 0.42 µmol min^{-1} mg^{-1}. This demonstrates that the mHoxFU-Hyd1-modified particles can be used in an H_2-driven NADPH recycling system.

Table 3-6: Conversion to product (%) and enantiomeric excess given for each of the 2-methyl-1-pyrroline reductions by IRED-49

Experiment Number	Conversion at 48 h (%)	*S* enantiomer (%)
1	98	>99
2	97	>99
3	98	>99

3.25 Summary

The work carried out in this chapter has demonstrated *Ht* HoxFU to be a robust enzyme that can tolerate a range of temperatures and pH conditions and can be used with a number of cosolvents. It accepts electrons readily from a carbon electrode and is therefore suitable for use in an electrochemical NADH recycling system.

The mutation of *Ht* HoxFU produced a moiety that has activity for both NAD^+ and $NADP^+$. However, the K_M of mHoxFU is probably in the mM range, and only able to support NADPH recycling at ~1 mM concentration. Although this was suitable for small scale use as an H_2-driven NADPH recycling system, this would not be acceptable for use as an industrial catalyst.

Although the mHoxFU showed disappointing results when used electrochemically, this could serve as a base mutant for further genetic engineering to improve affinity for $NADP^+$. As one of the main aims of this project was to develop an electrochemical cofactor recycling system, this was an important factor when considering whether to pursue this moiety for further development.

Further mutagenesis would be required to increase the specific activity of the enzyme, and as it is expressed in *E. coli* this simplifies this process. However, the mutagenesis work required to develop the enzyme for use in larger scale reductions would be beyond the scope of this project.

Chapter 3 Bibliography

1 H. A. Reeve, P. A. Ash, H. S. Park, A. Huang, M. Posidias, C. Tomlinson, O. Lenz and K. A. Vincent, *Biochem. J.*, 2017, **474**, 215–230

2 H. A. Reeve, J. Nicholson, F. Altaf, T. H. Lonsdale, J. Preissler, L. Lauterbach, O. Lenz, S. Leimkühler, F. Hollmann, C. E. Paul and K. A. Vincent*, Chem. Commun*., 2022, **58**, 10540–10543.

3 C. F. Blanford, *Chem. Commun*., 2013, **49**, 11130–2.

4 M. Eddowes and Hill, *Nature*., 1980, **285**, 673-674

5 H. A. Reeve, DPhil Thesis, University of Oxford, 2015

6 Z. Idris, DPhil Thesis, University of Oxford, 2012

7 J. Preissler, H. A. Reeve, T. Zhu, J. Nicholson, K. Urata, L. Lauterbach, L. L. Wong, K. A. Vincent and O. Lenz, *ChemCatChem*, 2020, **12**, 4852-4861

8 J. S. Shindler and K. F. Tipton, *Biochem. J.,* 1977, **167**, 479–482

9 J. Preissler, S. Wahlefeld, C. Lorent, C. Teutloff, M. Horch, L. Lauterbach, S. P. Cramer, I. Zebger and O. Lenz, *Biochim. Biophys. Acta - Bioenerg*., 2018, **1859**, 8–18

10 L. Lauterbach, Z. Idris, K. A. Vincent and O. Lenz, PLoS One, 2011, **6**, e25939

11 T. H. Lonsdale, DPhil Thesis, University of Oxford, 2017

12 J. O. Eberly and R. L. Ely, *Crit. Rev. Microbiol*., 2008, **34**, 117–130

13 S. Fujii, M. Masanari, H. Inoue, M. Yamanaka, S. Wakai, H. Nishihara and Y. Sambongi, *Biosci. Biotechnol. Biochem*., 2013, **77**, 1677–1681

14 H. Zhao, *Biotechnol*. *Adv*., 2020, **45**, 107638

15 K. Schneider and H. G. Schlegel, *Biochim. Biophys. Acta - Enzymol*., 1976, **452**, 66–80

16 J. Wang, G. Yin, Y. Shao, S. Zhang, Z. Wang and Y. Gao, *J. Power Sources*, 2007, **171**, 331–339

17 D. Muñoz Solano, P. Hoyos, M. J. Hernáiz, A. R. Alcántara and J. M. Sánchez-Montero, *Bioresour. Technol*., 2012, **115**, 196–207

18 W. Kroutil, H. Mang, K. Edegger and K. Faber, *Curr. Opin. Chem. Biol*., 2004, **8**, 120–126

19 L. Greiner, I. Schröder, D. H. Müller and A. Liese, *Green Chem.*, 2003, **5**, 697-700

20 P. Kwan, C. L. McIntosh, D. P. Jennings, R. C. Hopkins, S. K. Chandrayan, C. H. Wu, M. W. W. Adams and A. K. Jones, *J. Am. Chem. Soc*., 2015, **137**, 13556–13565

21 K. Lan Tee, J. Grinham, A. M. Othusitse, M. Gonz alez-Villanueva, A. O. Johnson and T. Seng Wong, *Biotech Method*, 2017, **12**, 170081

22 G. Grogan and N. J. Turner, *Chem. A Eur. J.*, 2016, **22**, 1900–1907

23 T. Huber, L. Schneider, A. Präg, S. Gerhardt, O. Einsle and M. Müller, *ACS Catal.*, 2018, **12**, 11534-11541

24 J. T. Wu, L. H. Wu and J. A. Knight, *Clinical Chem.*, 1986, **32**, 314-319

25 N. S. Scrutton, A. Berry and R. N. Perham, *Nature,* 1990, **343**, 38–43

26 J. K. B. Cahn, C. A. Werlang, A. Baumschlager, S. Brinkmann-Chen, S. L. Mayo and F. H. Arnold, *ACS ynth. Bio.,* 2017, **6**, 326-333

27 M. Capone, D. Scanlon, J. Griffin and P. C. Engel, *FEBS*, 2011, **14**, 2460-2468

28 H. A. Reeve, L. Lauterbach, O. Lenz and K. A. Vincent, *ChemCatChem*, 2015, **7**, 3480–3487

29 S. Chandra and M. Naiker, Compr. Anal. Chem., 2022, **98**, 77–90

Evaluation of electrochemical flavin recycling

4.1 Introduction

Joseph Srinivasan *et al*. previously demonstrated a system for using hydrogenase to recycle flavin mononucleotide (FMN) and used this reduced flavin as a cofactor to drive a reaction of interest using Johnson Matthey's ENE-reductase enzymes.[1] Electrons released in the oxidation of H_2 travel along the iron-sulfur clusters at the heart of the Hyd1 to the surface of the protein where they are then available to reduce the FMN in solution to flavin mononucleotide hydroquinone ($FMNH_2$). $FMNH_2$ can then replace expensive nicotinamide cofactor NAD(P)H to drive asymmetric alkene reductions using Johnson Matthey's ENE-reductase enzymes as shown in Figure 4-1.

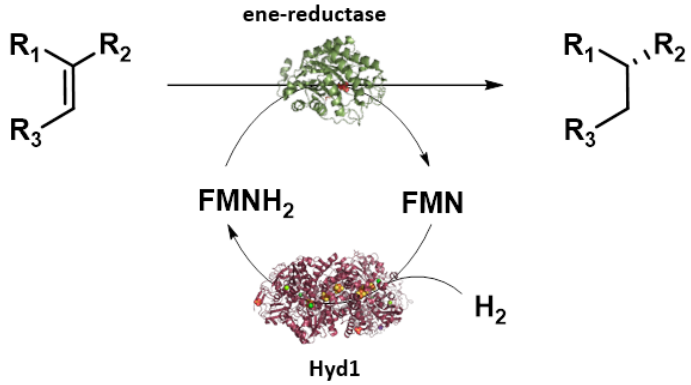


Figure 4-1 H_2-driven FMN reduction used to drive an asymmetric alkene reduction.

4.2 Electrochemical flavin reduction

Figure 4-1 shows the Hyd1 being used in this instance as an electron source for the reduction of the FMN. The first thing to establish was whether flavins could be reduced directly by a carbon electrode (Figure 4-2), which would simplify the process of cofactor recycling and eliminate the need for

hydrogenase enzymes as an electron source. This would minimise issues around separation and provide a cheaper and more sustainable way for biocatalytic synthesis.

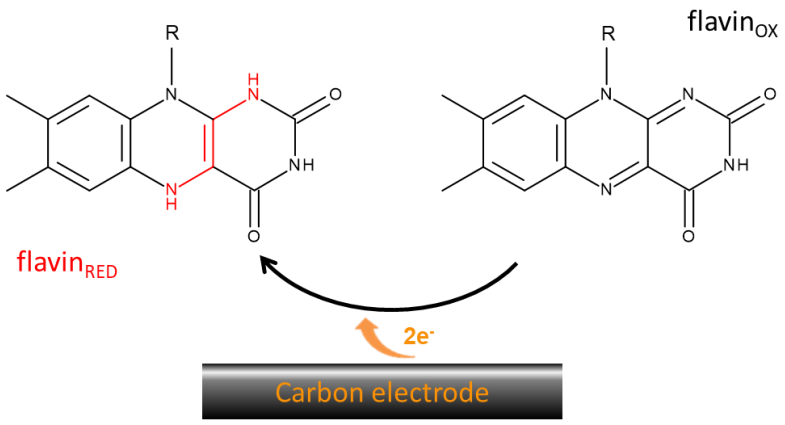


Figure 4-2: Reduction of flavins by direct transfer of electrons from a carbon electrode.

4.3 Preliminary flavin reduction

Unlike the nicotinamide cofactors used in Chapter 3, flavins can undergo both one and two electron transfer processes due to the isoalloxazine ring system which allows them to exist in several oxidation states as shown in the catalytic cycle in Figure 4-3. This versatility allows them to participate in many established reactions, both oxidation and reduction.[2] The redox states of interest in this chapter are; the oxidised form (**1**), and the fully reduced species (**3**) which is a two-electron reduction process, where the nitrogens shown in red are protonated.

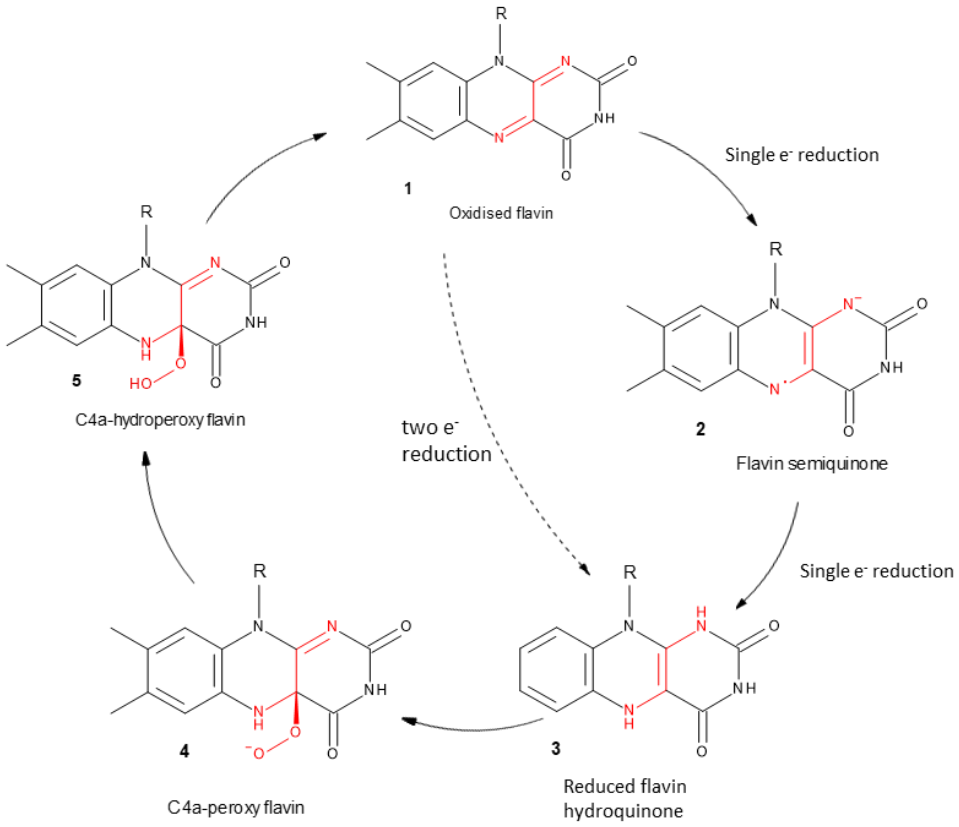


Figure 4-3: Catalytic cycle of flavins showing the redox states of flavin adapted from [3] with permission from Elsevier publisher: *Tetrahedron*, 2019, 75, 1115-1121. License number 5778260131031.

The flavins discussed in this chapter are:

- riboflavin (RF), the smallest flavin consisting simply of a heterocyclic isoalloxazine ring with a hydroxyl group at the end of the ribitol chain (shown in amber in Figure 4-4a). Section 4.10 will introduce RF together with preliminary electrochemistry experiments.

- flavin mononucleotide (FMN), which has the structure of RF attached to a phosphate group (magenta in Figure 4-4a).

- flavin adenine dinucleotide (FAD), which has an adenine is joined via a ribose and phosphate to the FMN structure (shown in purple in Figure 4-4a). The structural formula shown in Figure 4-4a is in its oxidised form.[4]

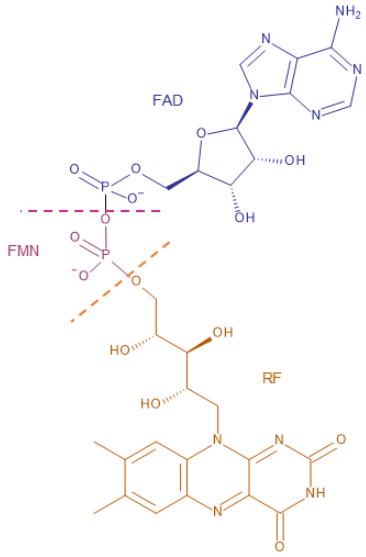


Figure 4-4: Structural formula of flavins used in this chapter shown in their oxidized state; riboflavin (RF) consists of a heterocyclic isoalloxazine ring (shown in amber), flavin mononucleotide (FMN) has the structure of RF with the addition of a ribityl phosphate group (magenta) and flavin adenine dinucleotide (FAD) includes the ribityl adenine diphosphate part of the molecule (shown in purple).

Initial electrochemistry experiments aim to establish whether the flavin could be fully reduced by the electrode and then determine if the reduced form was biologically active and able to drive a reaction of interest.

4.4 Preliminary electrochemical characterization of FMN and FAD

It has been previously established that both FMN and FAD can be reduced to $FMNH_2$ and $FADH_2$ respectively using Hyd1 under H_2,[1,5,6] however, it doesn't necessarily follow that the biologically active cofactor can be obtained electrochemically so this needs to be determined experimentally. The catalytic cycle shown in Figure 4-3 shows that five redox states of flavin exist. The species required to drive the alkene reduction (**3**) requires a 2-electron transfer to take place. When a potential is applied, electrons flow from the carbon electrode to reduce any flavin present at the surface of the electrode. Literature figures for flavin reduction are shown in Table 4-1.[7] Although

some variation is reported for the standard reduction potential of FMN with Shi *et. al*. reporting the more negative potential of -216 mV Vs SHE for FMN. [8]

Table 4-1: standard reduction potentials for the flavins used in this project[7]

Flavin	Standard Reduction Potential (mV)
FMN	-190
FAD	-220
RF	-210

Full details of the experimental procedures used for the cyclic voltammetry experiments can be found in Chapter 2, section 2.2.5. Preliminary electrochemistry experiments were performed using 0.1 mM flavin in 50 mM Tris HCl, pH 8. The electrochemical cell was covered in foil to exclude as much light as possible to avoid unwanted photo reactions. A potential was swept from 0.05 to -0.55 V vs SHE and the current recorded and this can be seen in Figure 4-5.

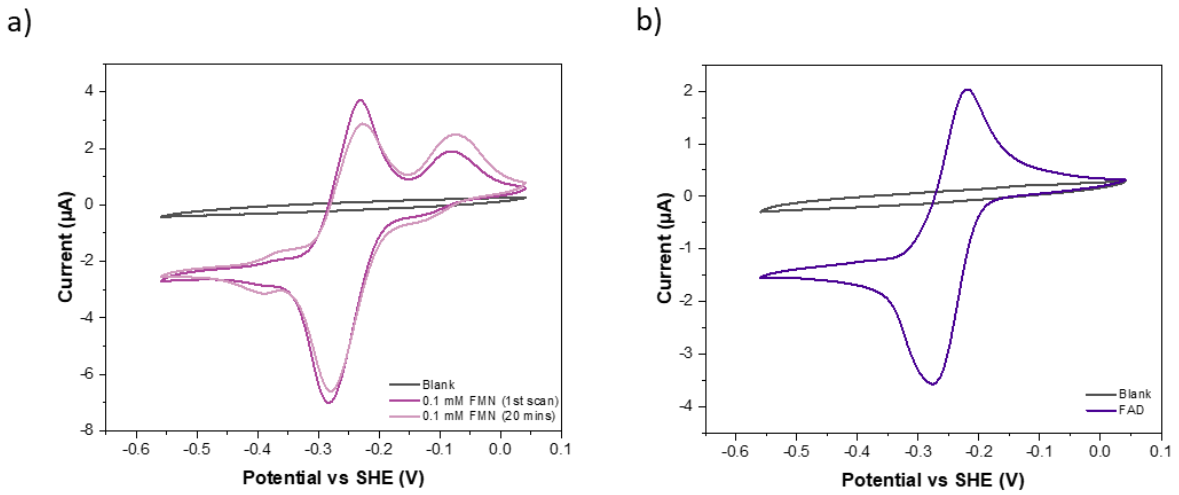


Figure 4-5: Cyclic voltammograms of a) FMN and b) FAD recorded at a freshly polished PGE RDE. Cell contained 7 mL Tris-HCl, pH 8, 25 °C with 0.1 mM flavin in solution. Cell was covered with foil to exclude as much light as possible. No rotation. Scans performed at 10 mV s^{-1}, no rotation.

The graphs in Figure 4-5 show a large reversible peak in both CV's is indicative of both surface-adsorbed and diffusion control redox. The onset potential for FMN is approximately -0.19 V vs SHE, with FAD having a slightly more negative onset potential of around -0.2 V vs SHE. The reduction potentials cannot be directly compared to the literature values shown in Table 4-1, as the diffusion layer is at a different concentration to the bulk solution. This causes a change in current. The graph in Figure 4-5a shows some other peaks which could be the possible formation of radical species formed by single-electron transfer from the electrode to the flavin. These peaks increase over time which is consistent with surface adsorption of the species on the carbon electrode. The formation of these species would be undesirable and therefore when selecting a reduction potential for any further experiments, it would be necessary to avoid the potentials at which these peaks occur.

4.5 Chronoamperometry experiments to determine if electrochemically $FMNH_2$ and $FADH_2$ are biologically active.

The results of the CV's in Figure 4-5 are consistent with the electrochemical oxidation and reduction of both (a) FMN and (b) FAD. To establish whether the electrochemically reduced flavin is biologically active and capable of driving an alkene reduction a chronoamperometry experiment was performed on both flavins and the results can be seen in Figure 4-6. A fixed potential of -0.26 V vs SHE was selected as it is in the catalytic region of the CV shown and avoids the formation of any unwanted radical species. The freshly polished RDE was spotted with a 40 mg mL^{-1} solution of ENE-107 and allowed to adsorb for a few minutes without drying completely. The electrode was then placed into the cell containing 8 mL Tris HCl, pH8 with 1% v/v DMSO and an overall flavin concentration of 0.1 mM and rotated at 3000 rpm to avoid any mass transport limitations. The potential was then applied and time allowed for the double layer to equilibrate (Chapter 2, section 2.3.2. After 200 seconds a 0.5 µL aliquot of 4-phenylbut-3-en-2-one was injected and any current

response recorded. After approximately 400 seconds another aliquot of substrate was injected. It can be seen that the current response in Figure 4-6b (FAD) is significantly larger to that observed in Figure 4-6b (FMN) for both injections indicating that the reduced flavin is being consumed and further flavin reduction is taking place due to the flow of electrons from the electrode to the system.

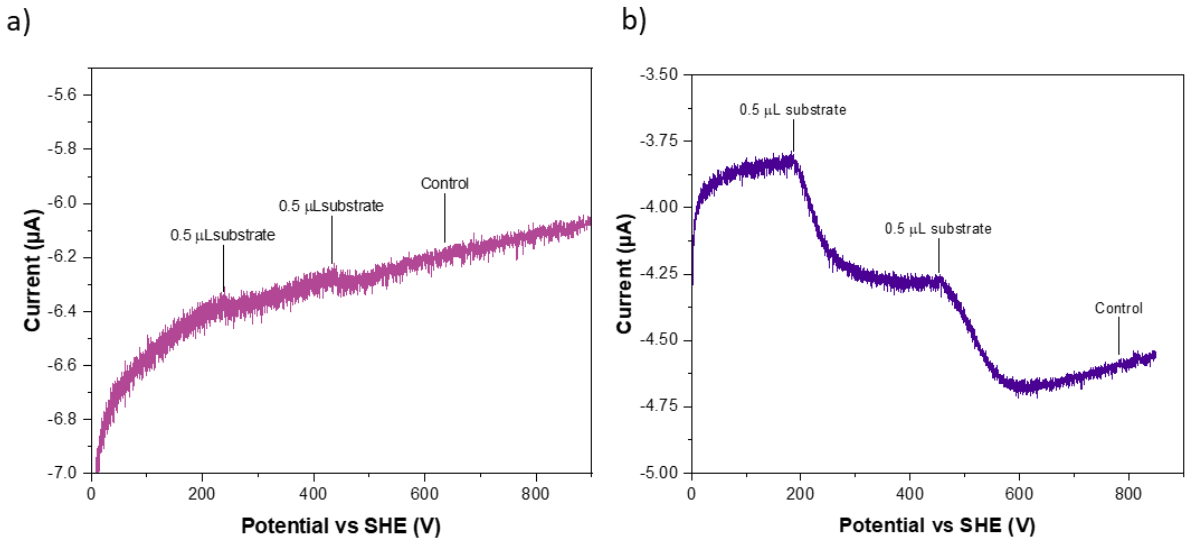


Figure 4-6: chronoamperometry experiments using (a) FMN and (b) FAD in solution. A freshly polished RDE was spotted with 0.8 µL ENE-107 (concentration 40 mg mL^{-1}) and allowed to almost dry. Cell contained 8 mL Tris-HCl, pH8 with 1% DMSO and 0.1 mM FMN/FAD. Aliquots of 4-phenylbut-3-en-2-one stock solution 10 mM in DMSO were added as indicated on the graphs, with an aliquot of 0.5 µL DMSO added as a control where indicated. Rotation 3000 rpm.

A control injection of 0.5 µL of DMSO was added to the cell where indicated on the graph to ensure that any current change was due to the enzyme's response to substrate and not just electrochemical disturbance due to the injection of a liquid. The lack of current response indicates that there is no catalytic activity upon addition of the control injection. These experiments were performed in triplicate.

4.6 Evolution of the crude electrochemical cell

Having established from the results of 4.4 that there was a flow of electrons from the electrode into the system, it was necessary to establish that firstly the flavin was being reduced and secondly that

the reduced flavin was biologically active and able to drive the alkene reduction. In order to do this, a crude electrochemical cell was constructed that would allow a larger volume of solution to be reduced electrochemically than the RDE cell used for the preliminary electrochemical experiments described in 4.4. It would also be necessary to use a carbon WE with a larger surface area than the RDE used in 4.4 so that the flavin in solution could be fully reduced in a reasonable time frame. The WE was constructed from a length of carbon felt 15 mm x 40 mm that was connected to the potentiostat using a length of carbon wool to allow electrons to flow whilst avoiding any unwanted side reactions taking place.

Figure 4-7 shows the evolution of the design of this crude cell over several initial experiments. Cell 1 was constructed from a 25 mL glass beaker; a pipette tip holder was placed on top to hold each of the electrodes in place. The problem with this cell was that the majority of the WE was sitting out of the solution, and the cell volume was quite large, so this took some time to reduce. Cell 2 consisted of a small RDE cell with a maximum volume of 7 mL. The design of the cell allowed the carbon felt electrode to curve around the inside of the cell so that it was completely submerged below the solution. However, the side-arm (see schematic drawing in 4-7(d)) that held the RE was partially blocked by the WE. This side-arm filled with some of the solution from the cell that then did not integrate with the rest of the bulk solution, preventing it from being fully reduced.

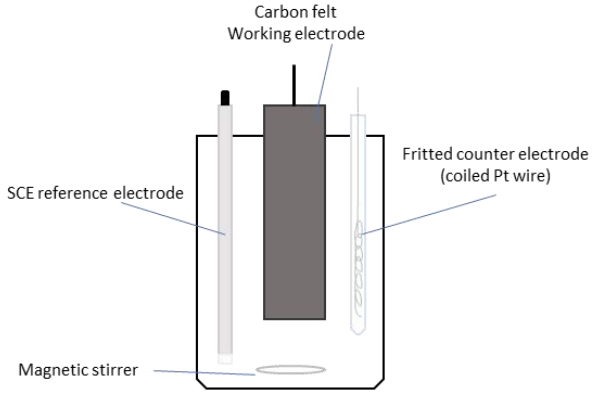
Finally, Figure 4-7(e) and (f) show the design of cell 3, which was constructed using a 10 mL three-arm round bottom flask. The design of this allowed for the WE to sit curved around the inside of the cell submerged below the solution with both the RE and CE sitting inside the WE. The curve of the flask allowed the stirring bar to sit at the bottom and move relatively freely. Whilst this design still had its limitations, which will be discussed in Chapter 5 when a bespoke cell was purchased, for the purpose of these initial experiments, this cell was adequate for the purpose of these experiments.

Cell 1

a)



b)

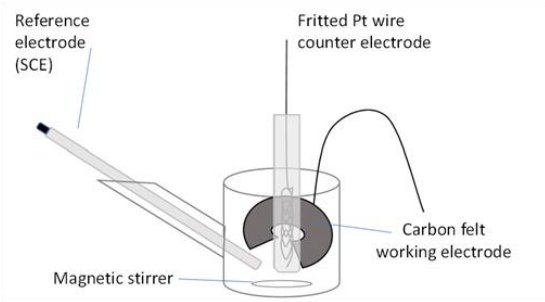


Cell 2

c)



d)



Cell 3

e)



f)

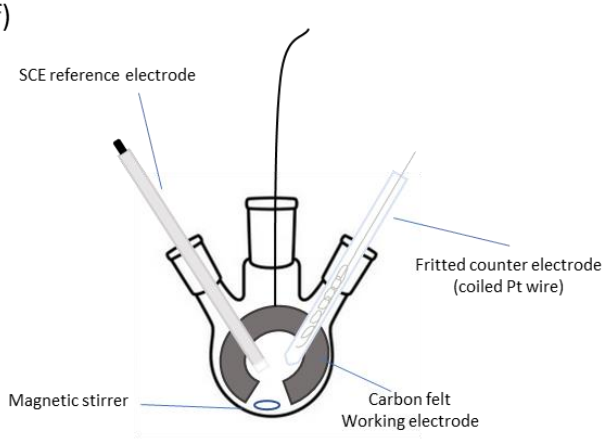


Figure 4-7: Crude electrochemical cell used for the flavin reduction experiments. (a) photograph of 'cell 1' (b) diagram of the cell shown in (a). (c) Cell 2 was a small RDE cell with side arm and design allowed WE to be submerged under solution. (d) diagram of cell shown in (c). (e) the final design of the crude cell constructed from a 3-arm round bottom flask. (f) diagram of cell 3.

4.7 Electrochemical FAD reduction on carbon felt with ex situ spectroscopy

Encouraged by the results of the FAD experiments in 4.4 and 4.5, this was initially selected for further investigation as the results of FMN experiments suggested the formation of radicals on the CV and the chronoamperometry experiments didn't seem to show much activity when tested with ENE-red for biological activity. The next step was to fully reduce a solution of FAD electrochemically. Oxidised flavin absorbs UV-Vis in the regions 365 nm and 460 nm whereas reduced flavin is spectroscopically inactive in these regions.[9] Therefore it would be easy to establish whether the FAD had been reduced by taking aliquots of the cell solution and analysing it by UV-Vis.

Using cell 2 shown in Figure 4-7(e) and (f,) a 10 mL solution of 0.5 mM FAD was made up with 1% v/v DMSO and placed into the electrochemical cell which had been covered with foil to exclude as much light as possible. A potential of -0.266 V vs SHE was applied, this was determined by selecting a potential approximately 50 mV more negative than the onset potential within the catalytic region of the CV shown in Figure 4-5. This figure that is chosen as a starting point for the experiments; the reduction of FAD is both surface-adsorbed and diffusion control, so the catalytic region of the CV is only an indication of the reduction potential, and may require some trial and error to establish the optimum potential.

The chronoamperometry was then left to run until the current reached 0 V (Figure 4-8a), indicated by the dotted red line). This indicates that electrons are no longer flowing and that the species in the cell has been fully reduced. This was achieved in under 2 hours. This plot can then be integrated

to determine the current passed, and the number of electrons transferred during the reaction can be calculated by equation 4-1 below:

$$\frac{\text{current passed (C)}}{\text{Faradays constant (C mol}^{-1})} = \text{e}^{-}\text{ passed (mol)} \qquad \text{Eqn. 4-1}$$

Conversion to FAD is a $2e^-$ process, so dividing the moles of electrons by 2 will give the predicted moles of $FADH_2$ that have been generated. From this it was predicted that more >99% of the FAD was converted to $FADH_2$.

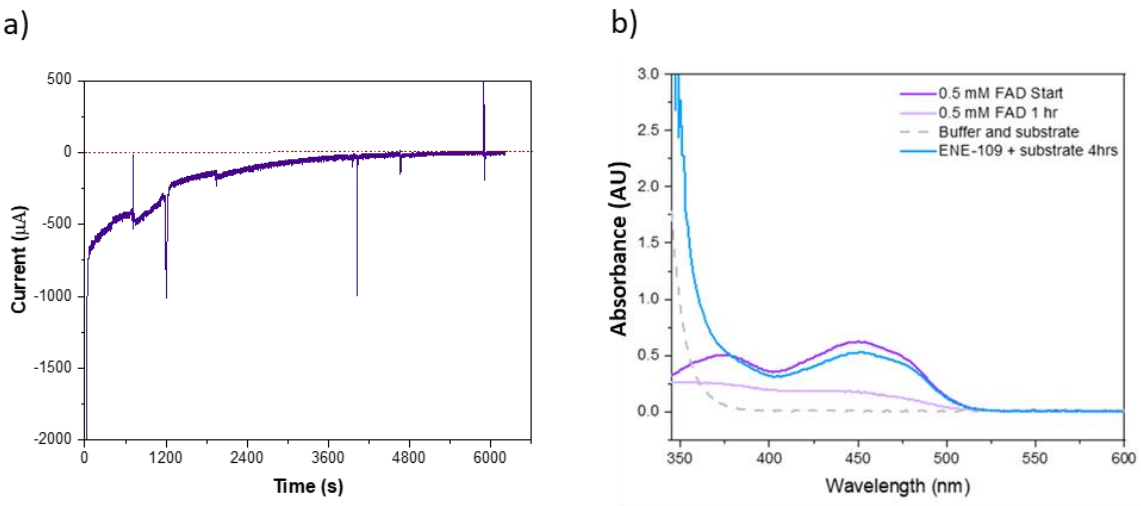


Figure 4-8 (a) chronoamperometry experiment to completely reduce a 0.1 mM solution of FAD electrochemically by applying a fixed potential of -0.266 V vs SHE and allowing to run for 2 hours. Cell contains 8 mL Tris-HCl pH8 with 0.1 mM overall concentration of FAD. Stirred constantly 400 rpm (b) UV-Vis analysis showing FAD at the start (dark purple) and after 1 hour (light purple) showing peak at 460 nm is much smaller indicating that species is reduced. To establish that the $FADH_2$ was biologically active, an aliquot of enzyme and substrate are added and a final UV-Vis specta is shown in blue after 4 hours which indicates that the $FADH_2$ has been consumed.

Upon complete reduction of the FAD, the chronoamperometry was stopped and the electrodes removed. A quantity of ENE-108 (0.5 mg mL^{-1}) was then added together with 4-phenyl-3-buten-2-one stock solution that gave an overall concentration of 0.5 mM with 1% v/v DMSO. If the $FMNH_2$ was biologically active, it would be consumed as the alkene is reduced by ENE-108. This was left to

react for 4 hours before being analysed by UV-Vis, this is shown as the blue trace on Figure 4-8b. This sample absorbs in the 460 nm region which indicates that the $FADH_2$ has been re-oxidised back to FAD and therefore suggested that the electrochemically generated $FADH_2$ was biologically active. It is important to note that the peak at 365 nm cannot be observed due to the strong solvent peak at this wavelength. This is confirmed by analysis of a sample of just the 4-phenyl-3-buten-2-one substrate dissolved in buffer (shown as the grey dashed trace in Figure 4-8b) which shows strong absorption at this wavelength. Therefore, the peak at 460 nm should be used as a diagnostic peak in these experiments.

Unfortunately, GC analysis of the solution after 4 hours showed no product. The experiment was repeated several times with the same result. Each time the UV-Vis after 4 hours showed a peak at 460 nm. One possible reason for this could be that the top of electrochemical cell was open once the electrodes had been removed and it is possible that the $FADH_2$ is reoxidised upon exposure to light rather than being regenerated by the alkene conversion.

Further experiments were carried out to fully reduce the FAD and then leave the potentiostat running after the ENE-red and substrate had been added, so that any regenerated FAD could be re-reduced. However, GC analysis showed that none of these yielded any alkane.

4.8 Considerations for recycling FMN

The electrochemical reduction of FMN was initially not pursued due to the possible formation of the radical species shown in catalytic cycle (Figure 4-3). However, the FAD experiments in section 4.7

indicated that electrochemically reduced FAD is not biologically active. This together with the significant cost difference between FAD and FMN shown in Table 4-2 prompted further investigation of FMN as an option.

Table 4-2: Comparative costs of flavins used in this project

Flavin	Cost Estimate	
	As Available	Per Gram
FMN	£196 per 50 g	£3.92 (MW: 478.33)
FAD	£615 per 1 g	£615 (MW: 829.51)
RF	£749 per 1 kg	£0.75 (MW: 376.36)

Cost estimate from Sigma-Aldrich with lowest price (and pack size), prices correct as of 2nd Oct 2023. Costs given per weight but molecular weights are given in brackets.

Section 4.3 introduced the five redox states of flavins which were shown in the catalytic cycle in Figure 4-3. The species shown as **2**, is the one-electron reduced form known as a semiquinone which can exist in two forms (shown in Figure 4-9):

- The neutral semiquinone which is protonated and shown in blue in Figure 4-9, which absorbs in the UV-Vis region 580-620 nm as shown by the dotted blue line
- The anionic semiquinone (shown in red) which absorbs around 380-400 nm as shown by the dotted red line.[9]

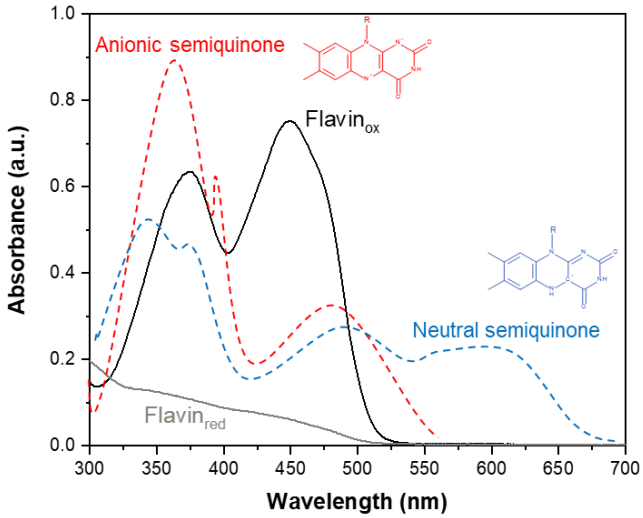


Figure 4-9: UV-Visible spectra showing oxidized and reduced flavin overlaid with dotted lines showing approximately where peaks would be expected to be observed for the neutral semiquinone (blue) and the anionic semiquinone (red). Adapted from information in Su *et.al.* 2019. [10]

Both species of radical semiquinone have a distinctive spectrum on the UV-Vis that could be detected by analysing electrochemically reduced FMN. The reduction potential of the semiquinone is -0.313 V so at the potential selected (-0.266 V vs SHE) for electrochemical reduction it is possible to avoid forming these radical species.[11] This is something that will need to be determined experimentally though as the FMN is dissolved in the bulk solution of the electrolysis cell and so it's reduction potential can be influenced by temperature, pH and also the rate at which the species diffuses to the electrode.

4.9 Electrochemical reduction of FMN

The process described in 4.7 was also used for the electrochemical reduction of FMN with a few modifications. The crude electrochemical cell was modified to allow a smaller volume, see cell 3 from Figure 4-7. This cell was constructed from a 3-arm round bottom flask which also allowed more efficient stirring due to the shape. The RE and CE sat in the arms of the flask allowing the carbon felt WE to curve around the inside of the flask, completely submerged in the solution. Foil could also be

placed around the flask to exclude light more effectively than cell 2, which avoids unwanted photo reactions.

The electrochemical experiment performed in 4.7 was performed using 0.5 mM FAD, so for comparison this experiment was repeated using 0.5 mM FMN. The UV-Vis spectra shown in Figure 4-10 shows the trace at the start of the experiment (dark pink) with clear peak at 460 nm, this peak is no longer visible after 1 hour (light pink trace). This would indicate that the FMN has successfully been reduced to $FMNH_2$.

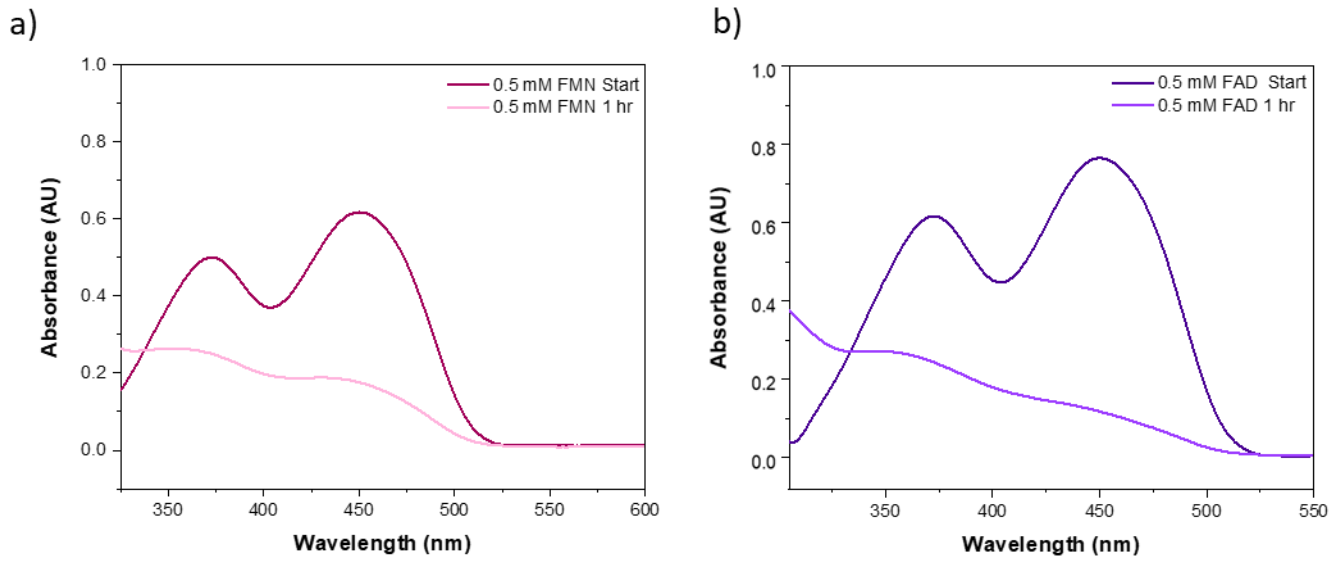


Figure 4-10: UV-Vis spectroscopic analysis of (a) FMN electrochemical reduction, showing 0.5 mM FMN solution at the start of the experiment (dark pink) and after 1 hour (light pink) and (b) FAD electrochemical reduction, showing 0.5 mM FAD solution at the start of the experiment (dark purple) and after 1 hour (light purple). Both graphs show peak at 460 nm is much smaller indicating that both species have been reduced.

Due to the UV-Vis spectrophotometric results in 4.7 indicating that the $FADH_2$ was biologically active, which then transpired not to be the case. A separate experiment was performed to couple the electrochemical generation of $FMNH_2$ to a continuous electrochemical alkene reduction, so that the results could be confirmed by GC-FID.

4.9.1 Coupling electrochemical $FMNH_2$ regeneration to a biocatalytic hydrogenation using ENE-108

Following on from the successful electrochemical reduction of FMN to $FMNH_2$ carried out in 4.9, it was necessary to determine that the generated species was biologically active and able to drive a biocatalytic reaction. An experiment was performed using 10 mL of 0.5 mM FMN in cell 3 Figure 4-7) and 0.5 mg mL^{-1} with 0.1 mM 4-phenyl-3-buten-2-one as substrate. A fixed potential of -0.27 V vs SHE was applied and the resulting current over time graph is shown in Figure 4-11(a). An aliquot (200 µL) was removed for analysis after 3 hours and the experiment left to run overnight. After 22 hours it was observed that the current has reached 0 A after approximately 15 hours, which indicated full conversion. At this point another 200 µL sample was removed for analysis and the contents of the cell stirred vigorously, then the stirring speed increased to 600 rpm. It can be seen in the graph that at this point there is an increase in the magnitude of current. The experiment was then left to run for another 2 hours before taking analysis of the solution at the end of 24 hours. The GC-FID results can be seen in Figure 4-11(b) which shows that after 22 hours only a 74 % conversion to product was achieved. This would indicate that there are stirring inefficiencies in the cell so that the substrate is not delivered to the electrode effectively for reduction. The increased stirring at 22 hours seems to have resolved this. One of the issues seems to be the position of the carbon felt WE was obstructing the stirrer bar, so car needed to be taken to avoid this in future experiments.

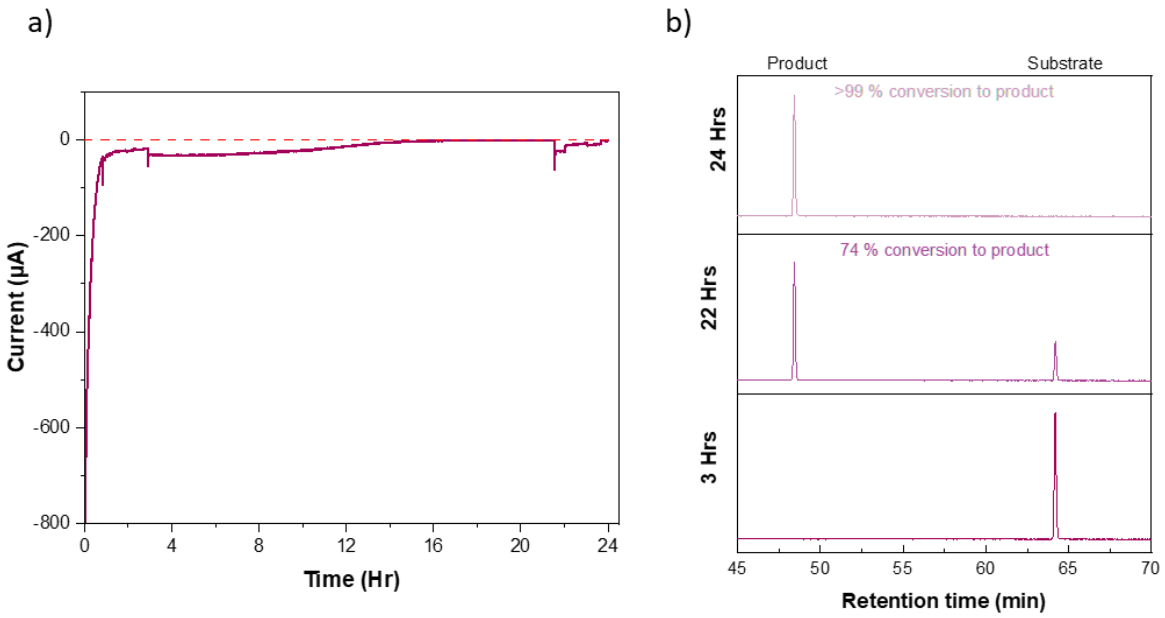


Figure 4-11: (a) chronoamperometry of the electrochemically regenerated $FMNH_2$-driven ENE-108 reduction of 4-phenyl-3-buten-2-one. Cell contained 0.5 mM FMN in KP_i, pH7 with 0.1 mM 4-phenyl—buten-2-one and 1% DMSO v/v. Potential -0.27 V vs SHE, stirred constantly 400 rpm until 22 hours when this was increased to 600 rpm. (b) GC-FID analysis of aliquots from experiment (a) taken at time points, showing full conversion to product was achieved in 24 hours.

The results of this experiment showed that the electrochemically produced $FMNH_2$ was biologically active and able to drive the ENE-108 hydrogenation. The experiment achieved full conversion of a 0.1 mM substrate within 24 hours.

4.9.2 Increasing the concentration of substrate

After promising results of the electrochemically generated $FMNH_2$-driven ENE-reduction in 4.9.1, the experiment was repeated, this time using 0.5 mM 4-phenyl-3-buten-2-one to give a stoichiometric ratio of cofactor: substrate. After noting the stirring inefficiency of the previous experiment; the cell was slightly modified to support the electrodes and prevent them obstructing the stirrer bar, and increasing the stirring speed to 600 rpm. Time points were taken more frequently in the earlier stages of the experiment and analysed using GC-FID. These results can be seen in Figure 4-12 which indicates full conversion to product takes place in less than 4 hours.

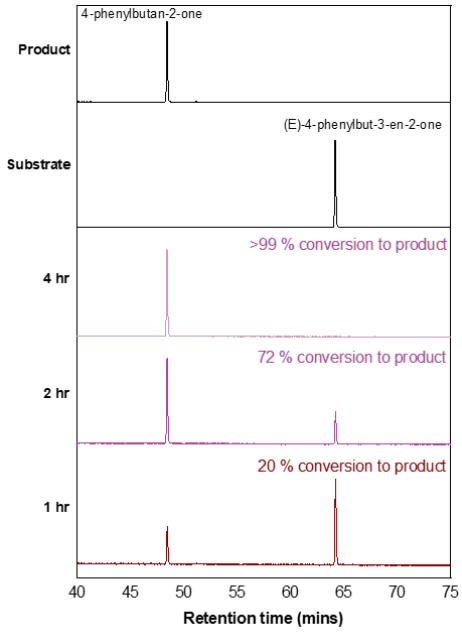


Figure 4-12: GC-FID results of reduction of (E)-4-phenylbut-3-en-2-one by $FMNH_2$-driven ENE-108. Aliquots taken over various time points throughout the experiment show that full product conversion was achieved somewhere between 2 and 4 hours.

After achieving full conversion of stochiometric quantities of substrate to FMN, the next step was to increase the concentration of substrate to show that the FMN was turning over and wasn't just consumed after the first reduction. An experiment was carried out starting with 1 mM substrate (4-phenyl-3-buten-2-one with 1 % DMSO v/v) applying a fixed potential of -0.27 V vs SHE. After 6 hours an aliquot of substrate was added which increased the overall substrate concentration to 5 mM. The experiment was then left to run initially for 24 hours. However, GC analysis after 24 hours showed a conversion to product of only 25% so the experiment was left for a further 48 hours, taking samples for analysis at 36 hrs, 48 hrs and 72 hours. These are shown in Table 4-3.

Table 4-3: Results of experiment to increase concentration of substrate to 10 times the concentration of FMN. Cell contained 50 mM KP_i with 1 mM 4-phenyl—buten-2-one and 1% DMSO v/v to start, increasing after 6 hours to 5 mM 4-phenyl—buten-2-one and 5% DMSO v/v. Samples were taken at the time points listed and analysed by GC-FID and the conversion to product shown, together with the predicted conversion calculated from the charge passed in Coulombs. From these the Faradaic efficiency has been calculated to approximately 100% throughout the reaction. The FMN turnover (TN) is calculated from the number of moles of product divided by the number of moles of $FMNH_2$

Time (hrs)	[FMN] (mM)	Conversion to product -CG (%)	Conversion to product - charge passed (%)	Faradaic efficiency (%)	FMN TN
2	1	48	48	~100	2
4	1	59	58	~100	2
6	1	73	70	~100	2
24	5	23	22	~100	10
36	5	40	35	~100	10
48	5	56	49	~100	10
72	5	71	66	~100	10

These results confirm that the FMN was being turned over and not just consumed in the reaction. This can be seen by the total turnover number (TN) in the final column, which is calculated by dividing the number of moles of product by the number of moles of $FMNH_2$. The conversion was quite low considering the time scale of the reaction. However, there were many parameters that could be altered to improve conversion, and these will be discussed in Chapter 5. It was encouraging to see a high Faradaic efficiency throughout the reaction, and confirmation that the FMN was being turned over. Next, using riboflavin as a cheaper alternative to FMN will be considered.

4.10 Riboflavin

Riboflavin, also known as vitamin B_2 is biologically essential for metabolic energy production, and is used for the formation of FMN and FAD in the body. Due to its importance for human health it liver and it is also added to foods such as flour, bread and pasta during the manufacturing process.

Industrially it is produced by fermentation and the production increased from 4000 to 9000 tonnes per annum between 2002 and 2015 when the data was last updated.[12] As riboflavin is so widely used, it is readily available and comparatively cheap in comparison to FMN and FAD (see Table 4-2). This could result in a significant cost saving when scaled up, which is an important consideration for industrial processes.[13]

4.10.1 Preliminary electrochemical testing of riboflavin

Riboflavin is similar in structure to FMN as shown earlier in this chapter in Figure 4-4a. Electrochemical experiments carried out by Kormanyos *et al.* showed in oxygen reduction electrochemical experiments that RF had similar catalytic behaviour to other flavins.[14] RF can be reduced by either a single- or two-electron process to produce the species shown in Figure 4-13b. Interestingly, the reduced species is colourless whereas the oxidised form is bright yellow.

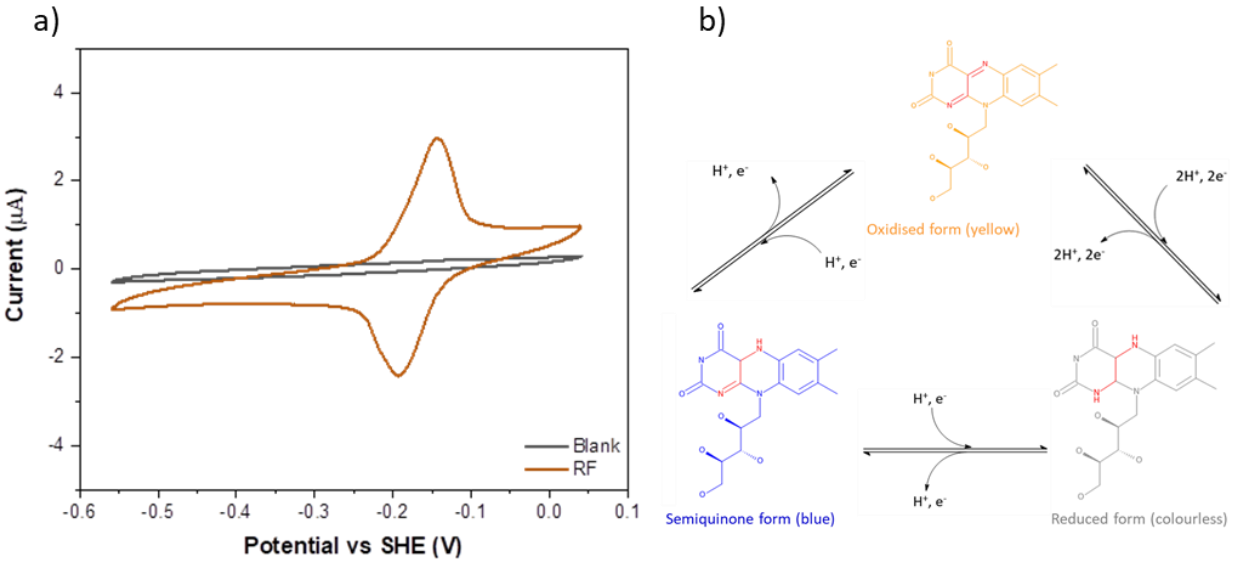


Figure 4-13: (a) Cyclic voltammogram of RF. Cell contained 7 mL potassium phosphate buffer, pH 7 with 0.1 mM RF in solution. Cell was covered with foil to exclude as much light as possible. No rotation. Scans performed at 10 mV s^{-1} (b) structural formula of RF showing the three species. The oxidised form (RF^{2-}) is yellow whereas the reduced form (RF) is colourless. The semiquinone can also be formed by a single e^- and H^+ transfer and this is bright blue in colour.

The formation of each species not only dependant on the applied potential, but also the solution pH.[15] In flavoproteins, hydrogen bonding stabilises the semiquinone to both single- and two-electro transfers to take place. However, in solution, the semi-quinone is a short-lived species and at the pH and potential used in this work, the two-electron transfer process should be favoured. The solubility of RF is only 2.2 g L^{-1} in water at 25 °C, therefore it is less soluble than both FMN and FAD so the 0.5 mM used in FMN experiments would not be suitable.[16]

A CV was recorded at the surface of a PGE RDE in 0.1 mM RF and this can be seen in Figure 4-13 which shows a reversible redox response, so the RF is able to be directly reduced by the electrode.

4.10.1 Complete electrochemical reduction of riboflavin

To determine whether a solution of RF could be directly reduced, a fixed potential of -0.356 V vs SHE was applied to the carbon felt WE. Using cell 3 Figure 4-7 which contained a solution of 0.1 mM RF. The cell was covered in foil to exclude as much light as possible to avoid unwanted photo reactions.

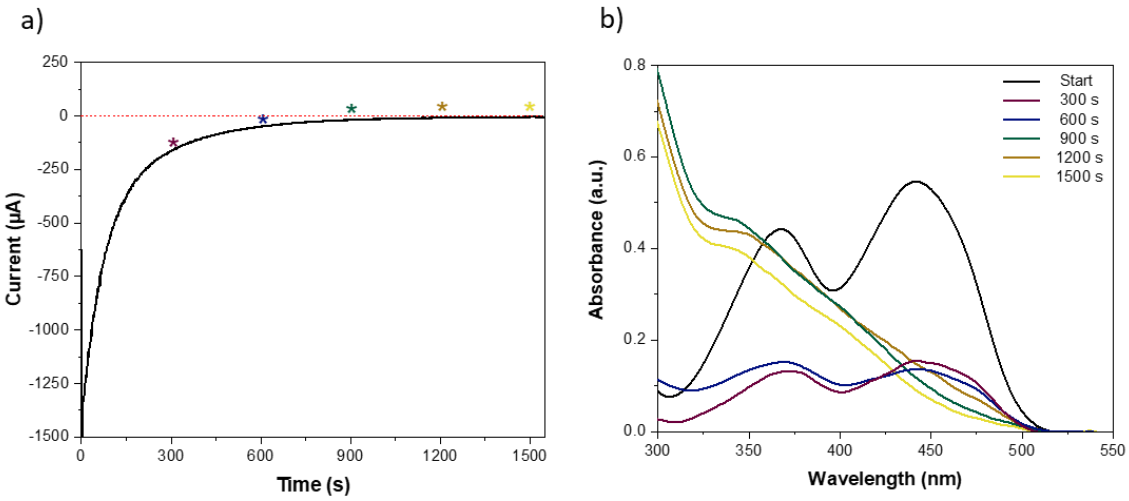


Figure 4-14:(a) complete electrochemical reduction of 0.1 mM riboflavin by poising electrode at -0.356 V vs SHE, coloured arrows indicate where aliquot was taken for UV-Vis analysis before being replaced in the cell. Cell contained 10 mL PBS with 0.1 mM riboflavin in solution. Stirred constantly 400 rpm. (b) UV-Vis analysis of aliquots taken from chronoamperometry experiment in (a). The colour of the UV-Vis corresponds with the colour of the star on the graph in (a) to indicate where the time points were taken.

The chronoamperometry trace for this reaction is shown in Figure 4-14(a). Aliquots were taken at 5 min intervals (indicated by the coloured stars on the graph) and these correspond to the coloured spectra on the UV-Vis shown in (b). These results indicate that the RF was fully reduced within 20 minutes. Note the potential used in this case was more negative than those previously used in the FMN and FAD experiments

4.11 Coupling electrochemical riboflavin reduction to ENE-red

The results of the electrochemical reduction of RF were promising, so the next step was to couple this reaction to the reduction of 4-phenyl-3-buten-2-one by ENE-108, as had been done in 4.9.1 with FMN.

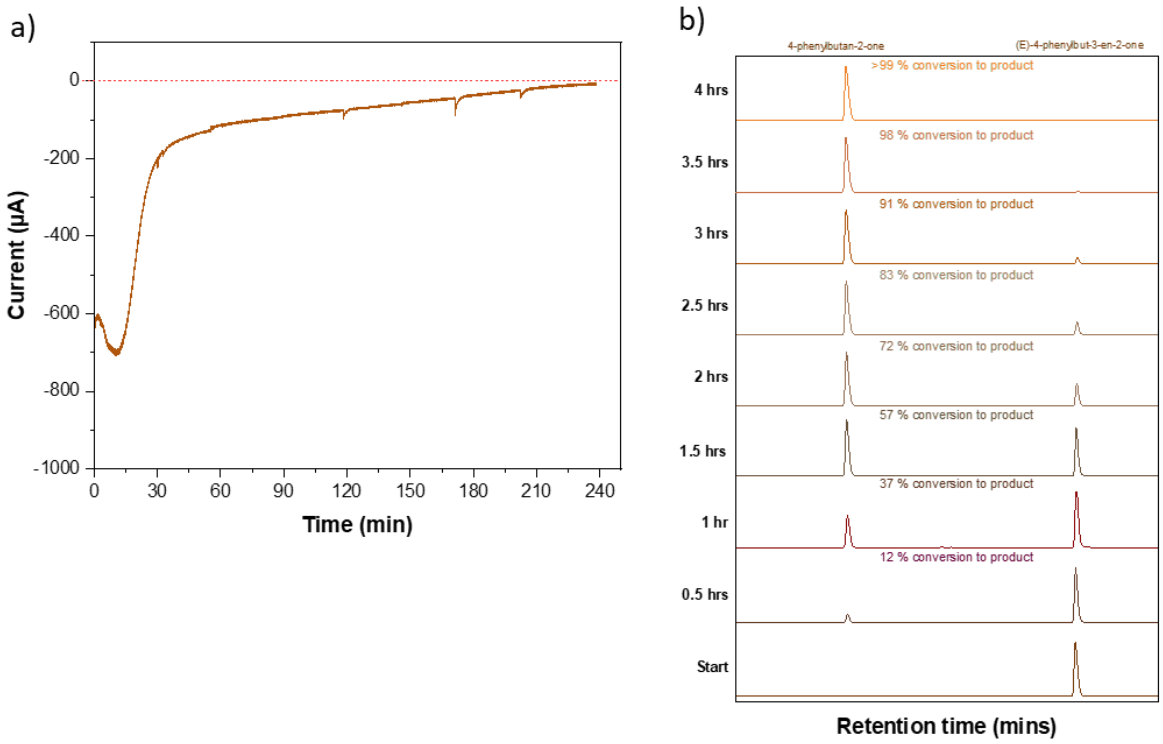


Figure 4-15: (a) chronoamperometry experiment to demonstrate the electrochemically-reduced riboflavin driven hydrogenation of 4-phenyl-3-buten-2-one by ENE-108. The cell contained 7 mL 0.1 mM riboflavin in 50 mM KP_i, pH 7 with 0.5 mg mL^{-1} ENE-108 and 0.5 mM substrate (4-phenyl-3-buten-2-one) with 1% v/v DMSO. New carbon felt electrode poised -0.356 V vs SHE. Stirred constantly 400 rpm. (b) GC-FID analysis of aliquots taken every half an hour from experiment (a) shows full conversion to product in under 4 hours.

The electrochemical cell (cell 3 Figure 4-7)contained 0.5 mM of 4-phenyl-3-buten-2-one, 0.1 mM RF, ENE-108 (0.5 mg mL^{-1}) and 1 vol% DMSO as a cosolvent in KP_i, pH7. The high surface-area carbon felt WE was poised at -0.366 V vs SHE (Figure 4-15(a) shows the current over time graph of this experiment). Aliquots (200 µL) were taken every 30 mins for GC analysis.

The results from this analysis are shown in Figure 4-15(b) where the retention time for the known standards is shown at the top of the graph. This shows that full conversion to product was achieved in under 4 hours.

The RF was also being turned over as the concentration of RF was 0.1 mM and the concentration of substrate was 0.5 mM, which represents a turnover (RF TN) of 10 (number of moles of product

divided by the number of moles of RF^{2-}). This is comparable to the results of the FMN experiment detailed in 4.9.2.

4.12 Summary

The results shown in this chapter demonstrate that each of the flavins studied in these reactions was able to be reduced at the surface of a carbon electrode. Unfortunately, the electrochemically generated FAD did not seem to be biologically active when coupled to biocatalytic reductions. The decision was made not to continue with this as a cofactor and instead look at the other flavin FMN which had previously been used in the group in an H_2-driven recycling system. Preliminary electrochemical investigations were also carried out on RF as another possible flavin for electrochemical regeneration.

Initial results from both the FMN and RF experiments were promising and show that both of these can be used to electrochemically regenerate the reduced flavin. When coupled to a biocatalytic hydrogenation, both FMN and RF were able to be turned over and supply reducing equivalents for the duration of the experiment, and achieved full conversion to product.

These results will now be extended to scaling up these reactions.

Chapter 4 Bibliography

1 S. Joseph Srinivasan, S.E. Cleary, M.A.Ramirez, H.A. Reeve, C.E.Paul, K.A.Vincent, *Angewandte Chemie*, 2021, **60**, 13824-13828

2 D. Leys, and N.S. Scrutton, *Curr. Opin. Struct. Biol.,* 2016, **41**, 19–26

3 S. A. B. Dockrey and A. R. H. Narayan, *Tetrahedron*, 2019, **75**, 1115–1121

4 Y. T. Kao, C. Saxena, T. F. He, L. Guo, L. Wang, A. Sancar, D. Zhong, *J. Am. Chem. Soc.* 2008, 39, 130

5 Ramirez, M. A., Joseph Srinivasan, S., Cleary, S. E., Todd, P. M. T., Reeve, H. A., and Vincent, K. A., *Frontiers in Catalysis*, 2022, **2**, 15

6 Joseph Srinivasan, S., DPhil Thesis, University of Oxford, 2022

7 C. Greening, F. H. Ahmed, A. E. Mohamed, B. M. Lee, G. Pandey, A. C. Warden, C. Scott, J. G. Oakeshott, M. C. Taylor and J. Jackson, *Am. Soc. Microbiol*., 2016, **80**, 451–493

8 Z. Shi, J. M. Zachara, L. Shi, Z. Wang, D. A. Moore, D. W. Kennedy and J. K. Fredrickson, Environ. Sci. *Technol*., 2012, **46**, 11644–11652

9 H. Hirsch-Kreinsen, *World*, 2003, **3**, 53–60

10 D. Su, M. Pabel Kabir, Y. Orozco-Gonzalez, S. Gozem, G. Gadda, D. Su, M. P. Kabir, Y. Orozco-Gonzalez, S. Gozem and G. Gadda, *ChemBioChem*, 2019, **20**, 1646–1652.

11 S. G. Mayhew and S. G. Mayhew, *Eur. J. Biochem*, 2001, 265**, 678-702**

12 S. K. Schwechheimer, E. Y. Park, J. L. Revuelta, J. Becker and C. Wittmann, *Appl. Microbiol. Biotechnol.*, 2016, **100**, 2107–2119

13 W. F. Liu and P. Wang, *Biotechnol. Adv*., 2007, **25**, 369–384

14 A. Kormányos, M. S. Hossain, F. W. Foss, C. Janáky and K. Rajeshwar, *Catal. Sci. Technol*., 2016, **6**, 8441–8448

15 M. R. Bailey and Z. D. Schultz, *Analyst*, 2016, **141**, 5078

16 A. Kormányos, M. S. Hossain, G. Ghadimkhani, J. J. Johnson, C. Janáky, N. R. de Tacconi, F. W. Foss, Y. Paz and K. Rajeshwar, *Chem. – A Eur. J.*, 2016, **22**, 9209–9217

Scale-up of flavin recycling

5.1 Introduction

In chapter 3 and 4 of this thesis methods for the successful electrochemical regeneration of cofactors were introduced. The results from these chapters showed promise for developing a more sustainable way to regenerate expensive cofactors using electrons as a clean reductant. In order to be considered as industrially relevant, the total turnover number (TTN) of cofactor needs to be high; typically in the region of 10^3 to 10^5 would be sufficient to make the process economically viable.[1] This turnover could not be achieved at lab scale, but it is important to demonstrate the scalability of the regeneration system. This work in this chapter looks to increase the turnover (TN = number of moles of product divided by number of moles of flavin) to achieve a TN of at least 100. In order to increase TN of the cofactor, there were a number of parameters that can be investigated on a lab scale (Figure 5-1) and these will be addressed throughout this chapter:

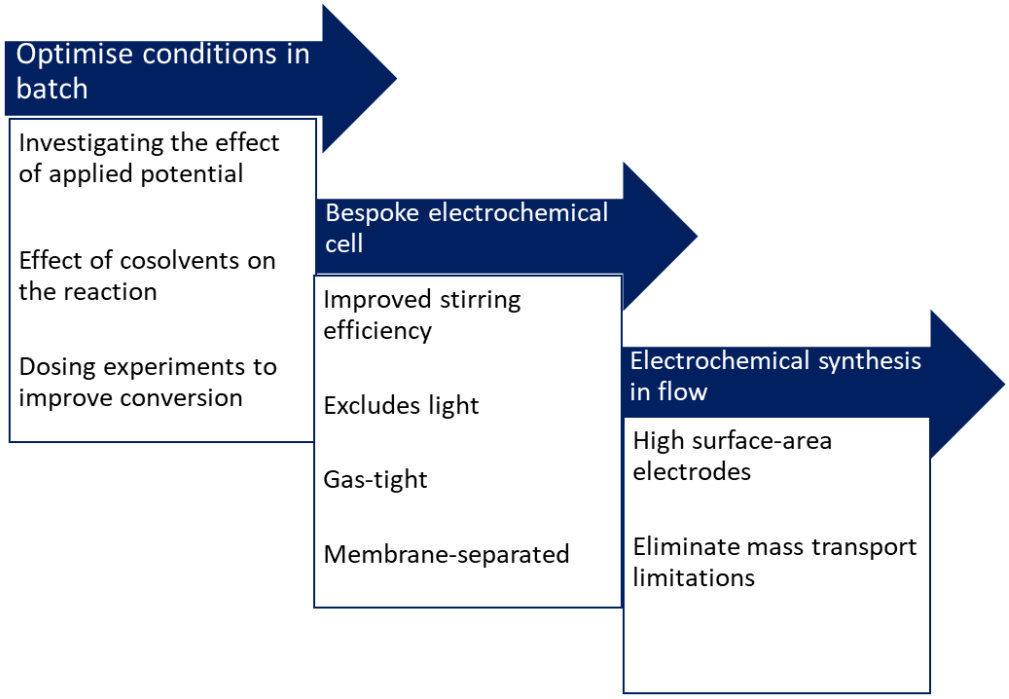


Figure 5-1: Overview of the experimental work carried out in this chapter.

5.2 Optimise conditions in batch

It was apparent from the preliminary results of electrochemical flavin recycling seen in Chapter 4 that conversion to product took a long time, and this would not be feasible for industrial applications. The crude electrochemical cell had been developed to overcome some of the problems that had been encountered, but it was clear that a more bespoke electrochemical synthesis cell would need to be purchased for more consistent results. This will be discussed in section 5.4.

Prior to this, a number of parameters were investigated to see their influence on the biocatalytic reaction. These were looked at in the home-built cell, and will be discussed next. Due to limitations with mixing and electrode geometry, a commercial cell was tested later in the chapter.

5.3 Solvent control experiments.

Experiments were performed to observe the effect of cosolvents on the electrochemical riboflavin recycling system. The Johnson Matthey ENE-red enzymes have been shown to perform well with up to 30% v/v of both MeCN and DMSO, so their performance with a cosolvent present was not in doubt.[2] However, during the dosing experiments (which will be discussed in section 5.3.2) a decrease in the magnitude of the current had been observed upon addition of an aliquot of substrate. Upon injection of substrate, an increase in current is expected, due to the extra demand for reduced cofactor by the enzyme.

(a)



(b)

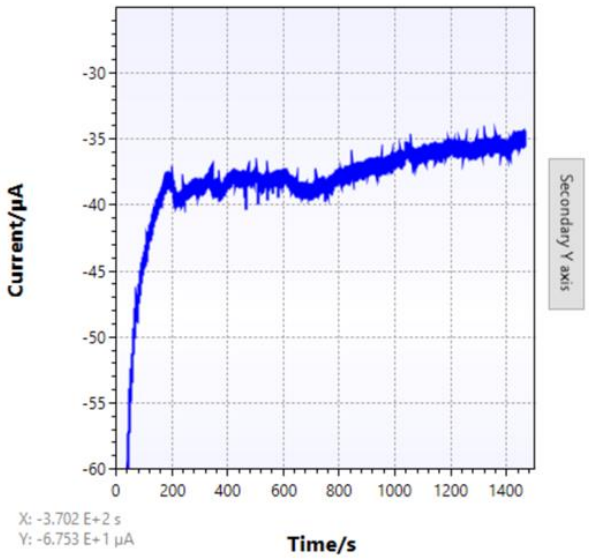


Figure 5-2: (a) photo of a vial containing the electrolyte for an electrochemical flow experiment. Here the substrate (acetophenone) dissolved in DMSO was added in doses throughout the duration of the experiment and colloid particles can be clearly seen where the substrate has not disolved. (b) This caused noise and disruption due to bubbles of undissolved cosolvent/substrate in the solution, this can be seen on the chronoamperometry trace in this screenshot.

It had been previously observed in some of the earlier experiments carried out in chapter 3, that the addition of organic solvents/substrate during an experiment, caused some disruption to the electrochemistry. The photo in Figure 5-2a is a vial that was used for an electrochemical flow synthesis experiment. The substrate used on this occasion was acetophenone and was added throughout the experiment in doses. Bubbles of undissolved cosolvent/substrate can be observed in the vial. These did eventually dissolve, but caused disruption to the electrochemistry when bubbles would adhere to the surface of the electrode, causing the noisy chronoamperometry trace in (b).

To see the effect of the co solvent on the electrochemical reduction of riboflavin (without enzyme or substrate present) chronoamperometry experiments were carried out injecting (a) DMSO and (b)MeCN at intervals during the experiment. The current over time traces for these are seen in Figure 5-3.

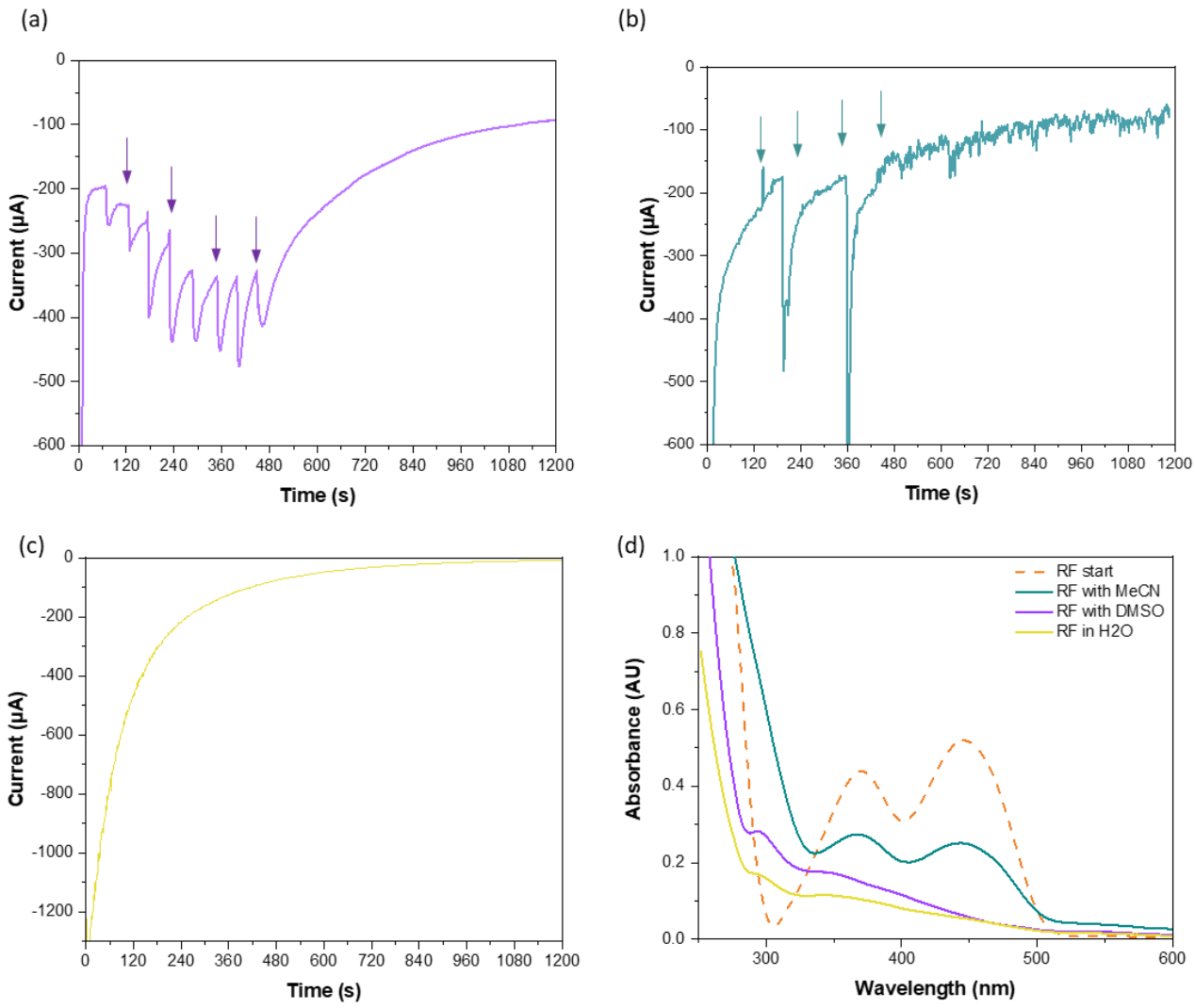


Figure 5-3: Chronoamperometry plots showing the electrochemical reduction of 0.2 mM RF in 50 mM KPi, pH 7 with (a) 2% v/v DMSO at the start of the experiment, then four further aliquots (indicated by arrows on graph) of DMSO added at 120 s intervals give a final 10% v/v DMSO after 1200 seconds. (b) 2% MeCN v/v at the start of the experiment with 4 further aliquots (indicated by arrows on graph) of MeCN to give a final concentration of 10% v/v MeCN after 8 mins. (c) control experiment to electrochemically reduce 0.2 mM RF with control injections of KP_i injected every 2 mins to give same final cell volume as experiments a and b, with continuous stirring at 400 rpm. (d) UV-Vis spectrophotometric analysis performed at the end of each of the experiments (a – c) spectra, colour of traces correspond to colour of current vs time plots. UV-Vis spectra of fully oxidised RF shown as dotted orange line.

Each of the cosolvent experiments were started with 2% cosolvent already in solution, then four further aliquots of the respective cosolvent was added approximately every 2 mins. The experiment was left to run for a total of 1200 s (20 minutes). At the end of the experiment, a sample was taken for UV-Vis analysis and the results are shown overlaid in Figure 5-3(d). A control experiment was

also carried out using just RF dissolved in KP_i. The graphs shown in (a) and (b) start with lower current than the control experiment, which is approximately 1200 μA. The control experiment trace is smooth and the current decreases in magnitude over time until it reaches 0 A which indicates the solute species is fully reduced. This is confirmed by the yellow trace on the UV-Vis spectra.

Each of the cosolvent experiments (a) and (b) show some disruption to the current with some sharp increases in the magnitude of the current. These increases do not necessarily correspond to the times when the aliquots were added. The current for each of these experiments decreases more slowly than the control experiment, and the current does not reach 0 A during the duration of the experiment. The UV-Vis traces at the end of each experiment show that the RF was not fully reduced in either case. Integrating the current-time graphs to give the charge passed can estimate the expected conversion of RF to RFH_2 (section 4.10.1). Calculating this gives the control experiment an expected conversion to RFH_2 of 93%, and for cosolvent experiments: DMSO 72% and MeCN 51%. These conversions seem to correspond qualitatively to the results of the UV-Vis analysis. Conversions were not quantified from the UV-Vis.

These results seem to suggest that the addition of a cosolvent slows down the rate at which the RF is reduced at the surface of the electrode. Flavins are known to adsorb well to carbon and it may be that the addition of the cosolvent somehow affects the interaction of the RF with the electrode. There seems to be less of an impact with DMSO, so for this reason, DMSO was selected as a suitable cosolvent for the rest of the experiments in this chapter.

5.3.1 Investigating the effect of applied potential on the reaction

The applied potential selected for the electrochemical experiments was discussed in chapter 4. This potential was in the catalytic reduction region of the CVs recorded of the three flavins in solution.

In general, a more negative potential than the thermodynamic redox potential will lead to the species being reduced. The more negative the applied potential, the bigger the driving force for reduction and therefore the faster the species will reduce. With the electrochemical reduction of flavins, care needed to be taken to avoid the formation of undesirable radical species. Therefore, a potential was selected of -0.27 V vs SHE and this potential was successful in reducing all three of the flavins studied in this thesis.

However, during one of the preliminary ENE-reductase experiments, the applied potential on the potentiostat was not adjusted after the previous user. This resulted in an electrochemical synthesis experiment being performed accidentally at the more negative potential of -0.366 V vs SHE. When the results of the experiment were analysed by GC, they showed full conversion to product of a stoichiometric quantity of substrate to RF within an hour; whereas the previous experiment under the same conditions had taken 4 hours. This prompted and investigation into the optimum potential for the synthesis experiments.

Three experiments were performed under the same conditions, each experiment used 5 mM 4-phenyl-3-buten-2-one with 0.1 mM RF (a ratio of 50:1 substrate: cofactor) carried out over 24 hours. This allowed the conversion to product to be quantified in order to compare. The results can be seen in

Table 5-1 below.

Table 5-1: The effect of applied potential on the conversion to product for the electrochemically-generated RFH_2-driven biocatalytic reduction of 4-phenyl-3-buten-2-one using ENE-108. Cell contained 7 mL 50 mM KP_i, pH 8, with 0.1 mM RF in solution, 0.5 mg mL ENE-108 and 10% DMSO v/v at 25 °C.

Applied potential (V vs SHE)	[RF] (mM)	Conversion to product charge passed (%)	Conversion to product GC (%)	RF TN
-0.27	0.1	35	34	17.5
-0.366	0.1	71	68	35.5
-0.41	0.1	24	21	12

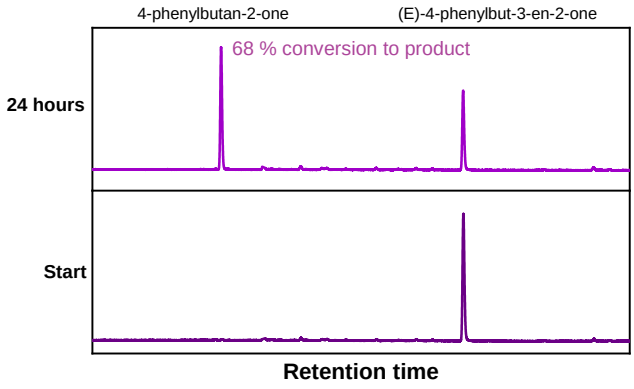


Figure 5-4: GC-FID ananlysis of the electrochemically-generated RFH_2-driven biocatalytic reduction of 4-phenyl-3-buten-2-one using ENE-108. Cell contained 7 mL 50 mM KP_i, pH 8, with 0.1 mM RF in solution, 0.5 mg mL ENE-108 and 10% DMSO v/v at 25 °C.

These results show double the conversion at the more negative potential of -0.366 V vs SHE (GC analysis shown in Figure 5-4). However, taking the potential more negative, to -0.41 V vs SHE resulted in a lower conversion. It is important to note that these experiments were only performed once at each potential due to time constraints. From these results the more negative potential of -0.366 V vs SHE was adopted for future experiments.

5.3.2 Dosing experiments to improve conversion

Although there were modifications required for the electrochemical set up (which will be discussed in sections 5.1.1 and 5.1.2) there were also steps that could be taken to optimise the conditions of the experiment to improve conversion. A suggestion from Johnson Matthey had been to add the substrate in doses, as this is done routinely on an industrial scale. This avoids enzyme inhibition due to high concentrations of substrate, allowing the enzyme to partially complete the conversion before adding fresh substrate.

A reaction was prepared to reduce 10 mM 4-phenyl-3-buten-2-one as substrate. The experiment was performed in cell 3 from the previous chapter and contained 7mL of 0.1 mM RF with 0.5 mg mL^{-1} ENE-108 in KP_i, pH7. An initial dose of 1 mM overall volume of substrate was added at the start of the experiment. A potential of -0.366 V vs SHE was then applied and the reaction left to run. Aliquots of 200µL were removed an analysed by GC at time points throughout the experiment and the results of this analysis are shown in red on the graph in Figure 5-5. Doses of substrate were added at intervals as shown on the graph in blue to give a final concentration of 10 mM substrate. The substrate aliquots were dissolved in DMSO and each 1 mM addition of substrate also increased the v/v percentage of DMSO by 1%.

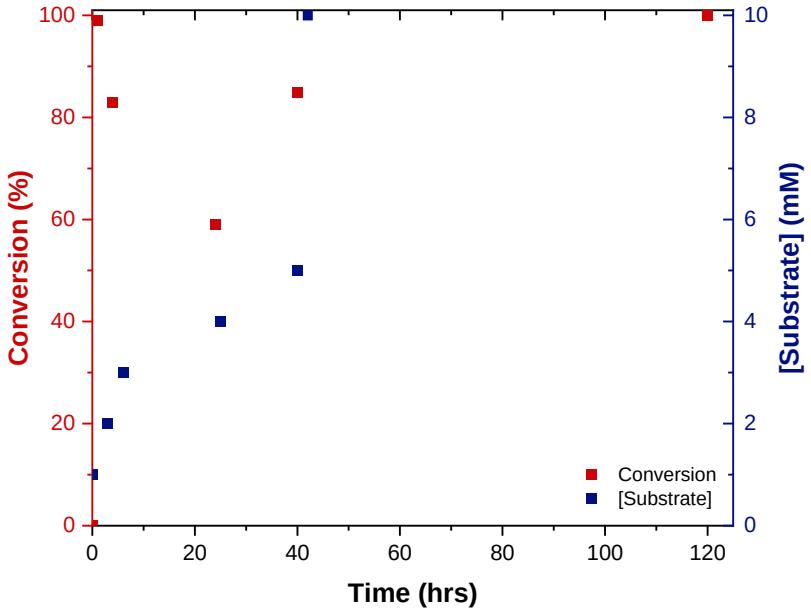


Figure 5-5: Conversion to product over time for the RF-driven hydrogenation of 4-phenyl-3-buten-2-one by ENE-108 adding substrate in doses as shown on right-hand axis in blue. Cell contained 0.1 mM RF in 50 mM KP_i, pH7 with 0.5 mg mL ENE-108 and a starting concentration of 1 mM 4-phenyl-3-buten-2-one with 1% v/v DMSO. Aliquots of substrate were added to take overall substrate concentration indicated on the right-hand axis of the graph. Each 1 mM of substrate added increased the DMSO by 1% v/v. Stirred constantly 400 rpm.

The results from this experiment show complete conversion of the first 1 mM substrate before the addition of the second aliquot was added. The experiment maintained good conversion throughout

and 85% conversion of 5 mM substrate had been achieved after 48 hours. The experiment was then left to run over the weekend, so it is likely that complete conversion of 10 mM substrate was achieved well before the 120 hours.

Although these results are not comprehensive, they do indicate the possibility of achieving full conversion of higher concentrations of substrate. The results do show good reasoning for adding the substrate in doses and this method was adopted for many of the subsequent experiments where appropriate.

5.4 Bespoke electrochemical cell

In order for more consistency with experiments, the purchase of a bespoke electrochemical synthesis cell was necessary. The crude electrochemical cells had served a purpose, but were not gas-tight and it was impossible to exclude all light (to avoid undesirable photo reactions involving the flavins). In order to try and increase the concentration of substrate, the size of the carbon felt WE had been increased. However, this meant that a larger surface-area CE was required, with with higher currents there would increase O_2 evolution on the surface of the CE. It was essential to avoid O_2 contamination that the CE and WE should be fritted (as had been used in the home-built cell) or in separate compartments.

The RedoxMe ECSynth Reactor D-series cell was purchased (Figure 5-6), which seemed suitable for the flavin experiments. The WE and CE are separated by an ion-exchange membrane to keep the oxidation and reduction reactions separate. The WE and CE are held in place by inert tantalum clips, and the WE and RE are close to the membrane to ensure a low potential drop throughout the electrolyte. The WE compartment where the reaction takes place seals completely to exclude all

light and is gas tight. Overall, these characteristics should bring more consistency to the experiments.

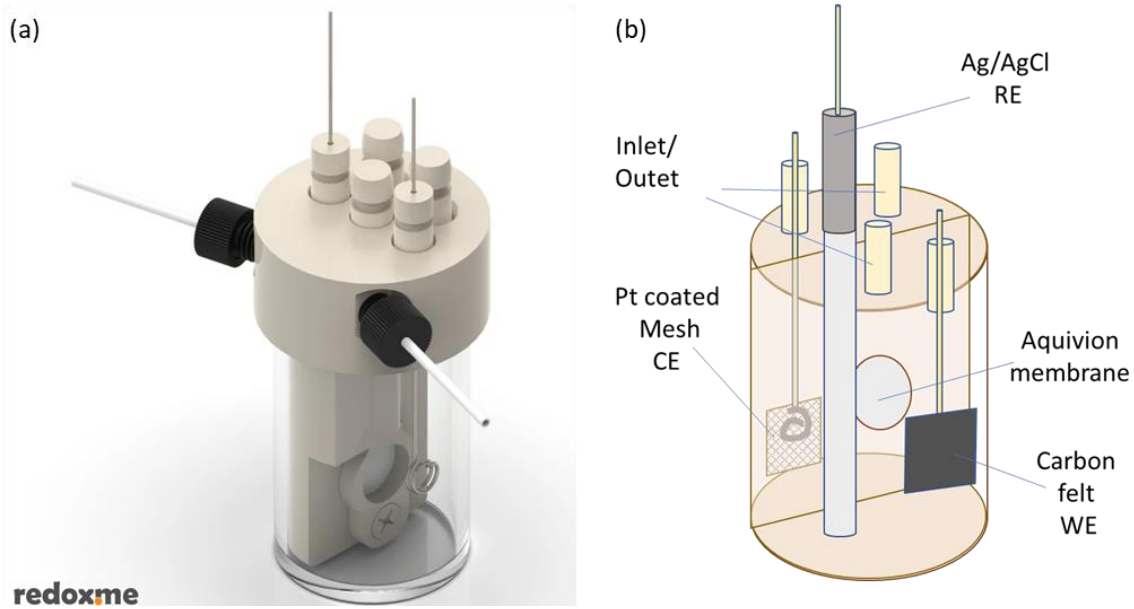


Figure 5-6 (a): RedoxMe electrochemical cell made from glass and polyether ether ketone (PEEK) with aquivion membrane-separated oxidation and reduction compartments. (b) Schematic representation of cell showing where electrode fit when the cell is assembled.

5.1.1 Results from RedoxMe cell experiments

With the experimental conditions having been somewhat optimised in previous experiments, the decision was made to take the best conditions from previous experiments and aim for an RF turnover of 100, which meant using a substrate concentration of at least 10 mM with 0.1 mM flavin (assuming full conversion). It had been previously established in the dosing experiment in section 5.3.2 that full conversion to product was possible. However, a time frame of 120 hours would not be relevant for industrial applications. With this in mind, all experiments would run for a maximum of 24 hours, to establish what conversion to product was achievable in that time frame.

The first experiment undertaken in the RedoxMe cell was another dosing experiment similar to that carried out in section 5.3.2, however, the experiment was set to run for 24 hours. The results from this experiment are shown in Figure 5-7. The conversion to product was much slower for this experiment, despite the same conditions as the previous one. The WE in the RedoxMe cell was geometrically smaller, which would result in less electrons being transferred. The cell does allow smaller volumes (as little as 2 mL reaction solution), so reducing the volume of the reaction could help mitigate the smaller surface-area electrode.

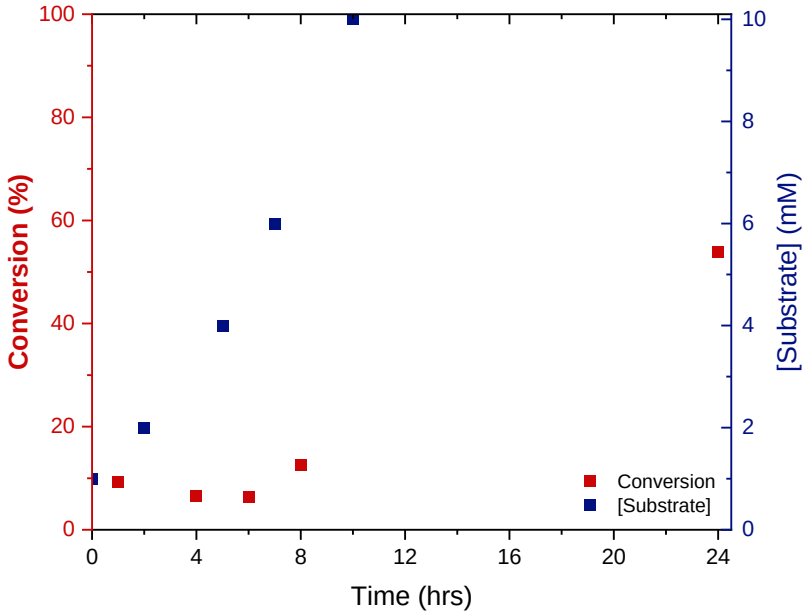


Figure 5-7: Conversion to product over time for the RF-driven hydrogenation of 4-phenyl-3-buten-2-one by ENE-108 adding substrate in doses as shown on right-hand axis in blue. Cell contained 0.1 mM RF in 50 mM KP_i, pH7 with 0.5 mg mL ENE-108 and a starting concentration of 1 mM 4-phenyl-3-buten-2-one with 1% v/v DMSO. Aliquots of substrate were added to take overall substrate concentration indicated on the right-hand axis of the graph. Each 1 mM of substrate added increased the DMSO by 1% v/v. Stirred constantly 400 rpm.

Another issue with the RedoxMe cell was the internal compartment for the reaction was semi-circular in shape, due to the CE compartment being separated. This seemed to cause more inefficient stirring. It required a very small stirrer bar to fit inside the compartment (4 mm x 10 mm) as anything larger caused the electrochemical trace to become very noisy. With such a small stirrer

bar and the irregular shape of the cell it was very difficult to stir the solution efficiently. This is especially important for an electrocatalysis experiment as without efficient stirring fresh substrate will not be delivered to the active site of the catalyst (and product removed), causing mass transport limitations.

The results from some of the most successful experiments carried out in the RedoxMe cell are shown in Table 5-2.

Table 5-2: Conversion to product from experiments using the RedoxMe cell for the electrochemically-generated RF-driven biocatalytic reduction of 4-phenyl-3-buten-2-one using ENE-108. All experiments used 50 mM KP_i, pH 8, 10% DMSO v/v with 0.1 mM RF in solution. Stirred constantly 400 rpm Enzyme loading was 0.5 mg mL^{-1} ENE-108 at 25 °C. [a] 5% DMSO v/v, [b] 800 rpm , [c] 1 mg mL^{-1} ENE-108, [d] 30% DMSO v/v. All conversions calculated after 24 hours. RF TN calculated from moles product divided by moles RF.

Entry	[RF] (mM)	[Substrate] (mM)	Conversion to product charge passed (%)	Conversion to product GC (%)	RF TN
1	0.1	5	28	23	11.5
2[a]	0.1	5	35	34	17.5
3[b]	0.1	10	33	35	33
4[c]	0.1	50	4	5	20
5[d]	0.1	10	25	25	25

The results from the RedoxMe experiments were disappointing. The best experiment in terms of RF TN was entry 3 which also achieved a 35% conversion to product by increasing the stirring. The increased stirring speed caused disruption to the electrochemistry though and on other experiments performed at this speed the WE was dislodged crashing the experiment. Entry 4 which used a high substrate loading was left to run for a week, although the results shown in Table 5-2 were after 24 hours. Even after 7 days the conversion to product was only 28% which represents an RF TN of 140.

Although the aim was to achieve a TN of over 100, running an experiment for this long would not be viable. The RedoxMe cell was not suitable for the purpose of this project.

5.1.2 Scale up of electrochemical flavin-driven ENE-reduction in batch

The following experiments were carried out using a bulk electrolysis cell from IJ Cambia that was borrowed for the purpose of scaling up the reaction. This cell is shown in Figure 5-8 and has a 100 mL capacity. The porous carbon electrode has an external diameter of 42 ±5 mm and an internal diameter of 27 ± 5 mm and the height is 50 mm. There are 20 pores per inch (PPI). The manufacturers state it is not possible to estimate the surface area as the porous material is not uniform, it is however significantly larger than the surface of the carbon felt WE that have been used in previous experiments. This can be seen by the large currents it achieved on the chronoamperometry traces in Figure 5-9 which are in mA whereas the earlier experiments achieved currents in µA.

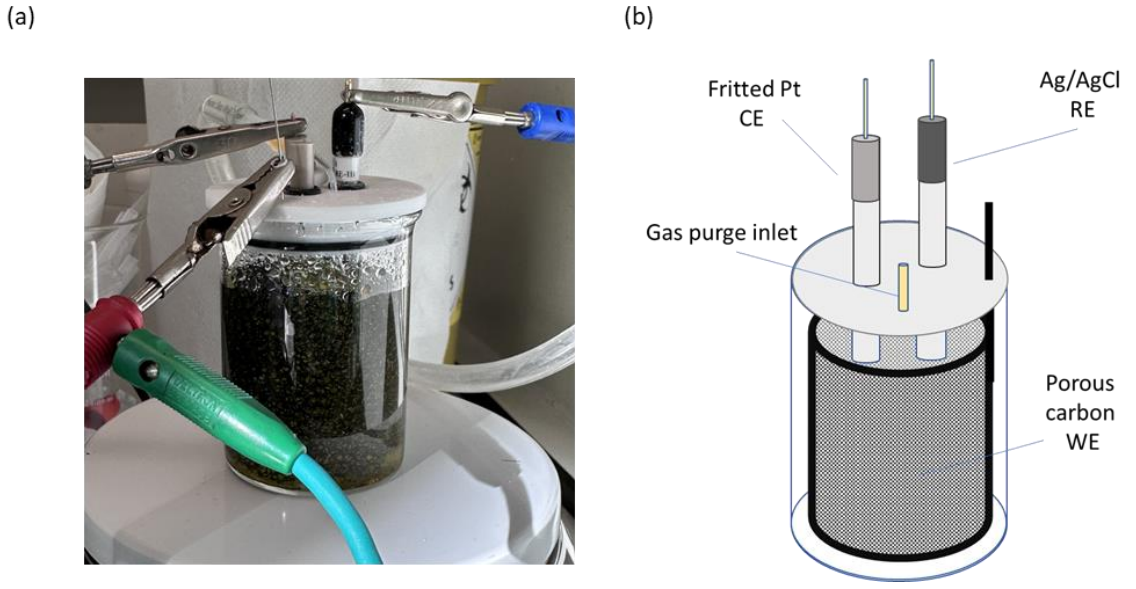


Figure 5-8(a): Bulk electrolysis cell with porous carbon electrode (b) schematic representation of SBC cell showing how electrodes fit.

Previous experiments had been performed in a glovebox, however, to demonstrate industrial relevance it was important to carry out some experiments in a fume hood, using an N_2 line to purge throughout the experiment. This would determine how sensitive the flavins were to atmospheric O_2. The electrolysis cell was filled with 63 mL of KP_i, pH7 which had been purged with nitrogen overnight to remove dissolved O_2. To this a measured amount of flavin (Figure 5-9(a) RF and Figure 5-9(b) FMN) to give a final concentration of 0.1 mM flavin with 0.5 mg mL^{-1} of ENE-108 also added to the solution. A stock solution of 4-phenyl—buten-2-one dissolved in DMSO was added to the cell to give a final cell volume of 70 mL with a concentration of 10 mM substrate and 10% v/v DMSO. The cell was constantly purged with nitrogen throughout the duration of the experiment to prevent O_2 contamination. A potential of -0.366 V vs SHE was applied to the cell and the current recorded for an hour for each experiment.

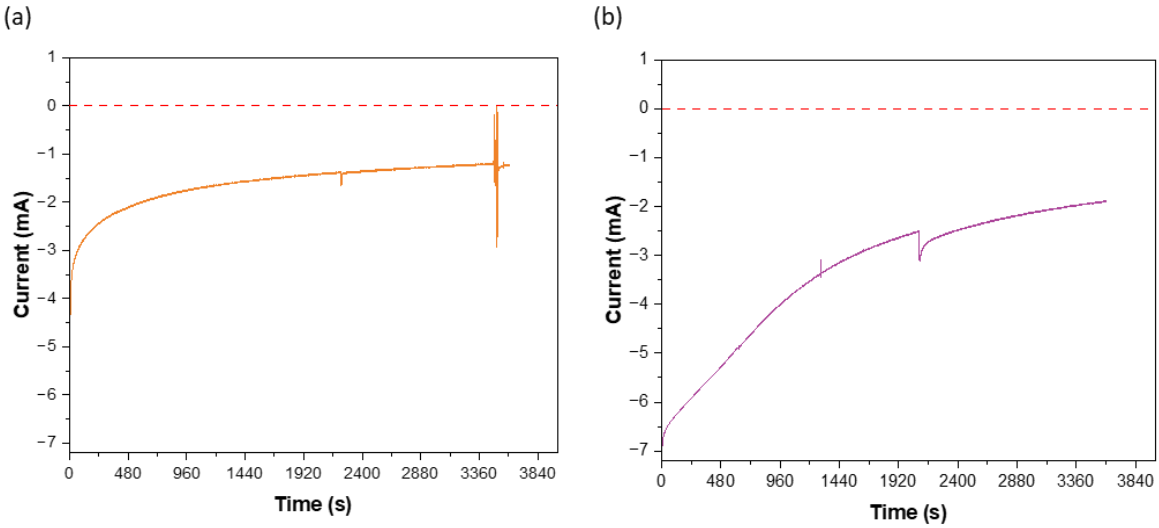


Figure 5-9: Chronoamperometry experiments performed using the bulk electrolysis cell from IJ Cambria. Cell contained 70 mL of 0.1 mM flavin in KP_i, pH 7 with 0.5 mg mL^{-1} ENE-108 and 10 mM 4-phenyl-3-buten-2-one with 10% v/v DMSO. Stirred constantly at 500 rpm and continuously purged with nitrogen throughout the duration of the experiment. Potential -0.366 V vis SHE.

What is immediately apparent from the graphs that the starting current for the FMN (b) is almost double that of the RF (a) at approximately 6.5 mA and 3.5 mA respectively. The magnitude of current decreases rapidly for the FMN experiment, suggesting that there is more reduction of FMN taking place at the surface of the electrode than there is in the RF experiment. Integrating the current to calculate the predicted conversion to product shows a 13% conversion for the FMN and only 4% for RF. After an hour the experiment was stopped and the results analysed by GC (results shown in Table 5-3).

Table 5-3: Results of electrochemical flavin reduction experiments using the bulk electrolysis cell from IJ Cambria. Cell contained 70 mL of 0.1 mM flavin in KP_i, pH 7 with 0.5 mg mL^{-1} ENE-108 and 10 mM 4-phenyl-3-buten-2-one with 10% v/v DMSO. Stirred constantly at 500 rpm and continuously purged with N_2 throughout the duration of the experiment.

Flavin used	[Flavin] (mM)	Conversion to product charge passed (%)	Conversion to product GC (%)	Flavin TN
RF	0.1	4	0	0
FMN	0.1	13	14	13

Interestingly there is no conversion to product for the RF, yet the integrated current suggests that some species in solution was being reduced. The charge passed accounts for 4 turnovers of the 0.1 mM RF in the reaction, but with no product detected it is clear that an undesirable side reaction was taking place.

The experiment was repeated under the same conditions but this time using 20 mM substrate and allowing the experiment to run for 4 hours. These results are shown in Table 5-4 and disappointingly still show no conversion for RF. Current was recorded on the chronoamperometry, so it can only be assumed that a species in solution was being reduced, but the electrode was not driving the

recycling of RFH_2. This could be due to traces of O_2 contaminating the experiment, as it is not possible to exclude all O_2 when working in a fume hood rather than a glovebox. Similar results were seen in some of the flow experiments which will be discussed in section 5.6 when the glovebox had traces of O_2 present.

Table 5-4: Results of electrochemical flavin reduction experiments using the bulk electrolysis cell from IJ Cambria. Cell contained 70 mL of 0.1 mM flavin in KP_i, pH 7 with 0.5 mg mL^{-1} ENE-108 and 20 mM 4-phenyl-3-buten-2-one with 10% v/v DMSO. Stirred constantly at 500 rpm and continuously purged with nitrogen throughout the duration of the experiment.

Flavin used	[Flavin] (mM)	Conversion to product charge passed (%)	Conversion to product GC (%)	Flavin TN
RF	0.1	5	0	0
FMN	0.1	50	51	102

The results from the FMN-driven ENE-reduction shown in Table 5-4 are much more promising. This shows a conversion to product of ~50% was achieved in 4 hours, and the results confirmed by GC analysis. This represents an FMN TN of 102 which was the aim of the scale up experiments. Unfortunately, time constraints prevented further experiments using this cell, but it is possible that these results could have been achieved with RF inside a glovebox.

5.5 Electrosynthesis in flow

Previous experiments carried out in batch looking to intensify the reduction of 4-phenylbut-3-en-2-one by ENE-108 with electrochemical flavin recycling had been unable to achieve more than 50% conversion to product within 24 hours. Flow chemistry, introduced in chapter 1, offers a more efficient alternative to batch production by pumping reagents through the flow cell where the biological catalyst is immobilised in a continuous reaction.[3–5] Problems with mass transport

limitation or inhibition of the enzyme can be overcome by the constant removal of reaction solution.[5–7] Incorporating electrochemistry into a flow system would offer a sustainable way to drive the biocatalytic reactions , as there is the opportunity to harvest solar and wind power. These reactions can be easily scaled up, which makes them desirable for industrial applications.

5.5.1 Electrochemical cofactor recycling in flow

In the early part of this project, during the development of the NAD(P)H recycling system, an electrochemical flow system was developed, and then set aside as the project focussed attention of flavin recycling. The work in the following section explores some of this early flow cell development and then later work in this chapter builds on this experience.

The analytical electrochemical experiments carried out in Chapter 2 and Chapter 3 were all performed using a pyrolytic graphite edge rotating disk electrode PGE RDE with very small quantities of enzyme. However, the aim was to achieve a high enough conversion of $NAD(P)^+$ to NAD(P)H to drive a biocatalytic reaction. For this it would be necessary to build high surface area electrodes which will be discussed next. These would be developed for use in a modified flow electrochemical cell that will be introduced in section 5.6

5.5.2 Development of high surface area electrodes

The concept of increasing the surface area of an electrode whilst maintaining its geometrical area was successfully introduced in Chapter 3, to increase the surface area of the RDE in order to synthesise a quantity of NADH. This can be adapted to other electrochemical systems by adsorbing he enzyme-modified particles onto carbon paper. The carbon paper can be cut to any shape or size necessary for the application. This is illustrated in Figure 5-10 where the enzyme-modified particles

dramatically increase the enzyme-loading on the surface of the electrode. The protocol for preparation of the enzyme-modified particles is given in (Chapter 2, section 2.4.2), and this was followed and the particles allowed to incubate in the fridge.

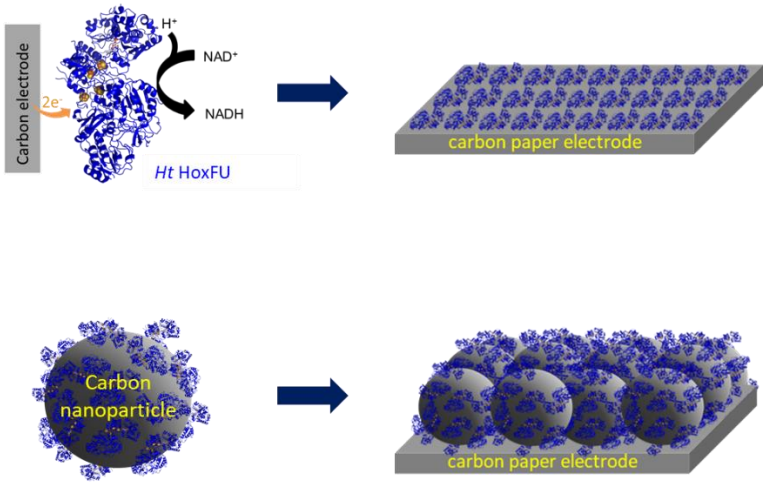


Figure 5-10: Schematic representation showing how the surface area of an electrode can be increased. The enzyme adsorbs directly to the electrode and accepts electrons for NAD(P)$^+$ reduction. In the top image the enzyme is immobilised on the surface of a carbon paper electrode. In the bottom of the image, the enzyme-modified particles are adsorbed to the surface of the same carbon paper electrode, but the carbon particles support much more enzyme which dramatically increases the surface area of the electrode.

To demonstrate the effect of increasing the surface area of the electrode. Cyclic voltammograms (CVs) were recorded of (a) *Ht* HoxFU on a freshly polished PGE RDE and (b) *Ht* HoxFU-modified particles on a freshly polished PGE RDE and these are shown overlaid in Figure 5-11.

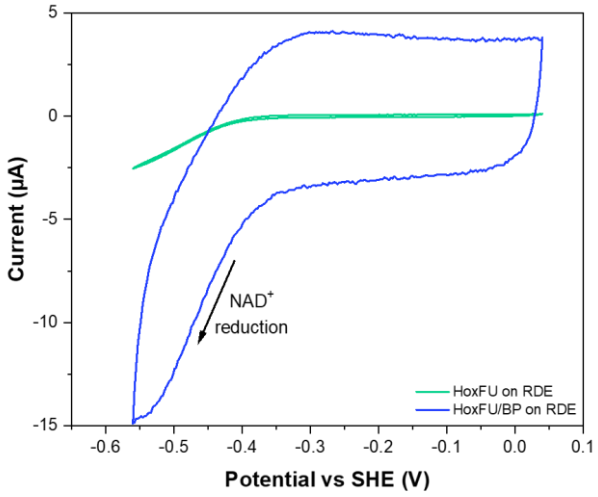


Figure 5-11: The effect of using BP2000 to increase the surface area of the electrode; 0.5 µL *Ht* HoxFU dropped onto the surface of a freshly polished PGE RDE (green trace) and 0.5 µL Ht HoxFU-modified BP2000 (ratio 1:1) dropped onto the surface of a freshly polished PGE RDE and allowed to almost dry for 120 s. Cell contains 8 mL Tris HCl, pH 8 with 1 mM NAD^+, Scan rate 10 mV s^{-1}, rotation 1000 rpm

It is clear from the graph that immobilising the enzyme on the Carbon particle BP2000 causes a significant increase in the magnitude of current due to the increased surface area, even taking into account the increased capacitance caused by the particles. The *Ht* HoxFU on the bare RDE (green trace) achieves a current of ~2.5 µA whereas the *Ht* HoxFU-modified particles (blue trace) achieve a current of ~11.4 µA after deducting the capacitive current, which represents more than a four-fold increase. Also worth noting is the curve of the blue CV as the potential gets more negative indicates mass transport limitations, so higher currents would likely be achieved in flow. The geometrical surface of the RDE is only 0.03 cm^2 and the internal dimensions of the electrochemical flow cell which is shown in Figure 5-12(a) were 0.2 cm^2 which could support approximately 6-7 times as many enzyme-modified particles as the RDE.

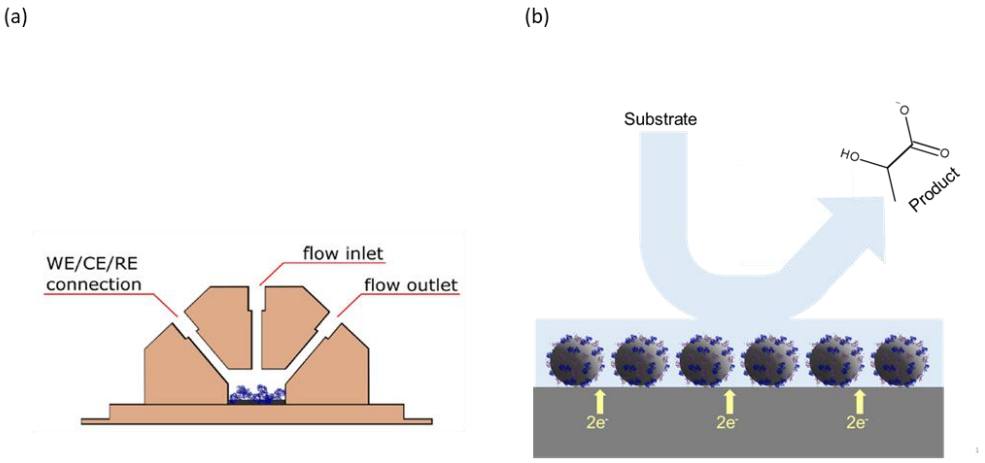


Figure 5-12: schematic representation of the flow system designed for electrochemically recycled NAD(P)H-driven biocatalysis. (a) cross section of the modified spectro-electrochemical cell which had been adapter for use an electrochemical flow cell. There are 5 holes in the top of the cell, one for each of the three electrodes and then a flow inlet where the substrate flows into the cell as shown in (b). The substrate flows over the immobilised catalyst where the reaction takes place. In this example *Ht* HoxFU has been co-adsorbed to the particles with another enzyme that performs the reaction of interest. The *Ht* HoxFU accepts electrons from the electrode to reduce the NAD^+ to NADH, and this drives the second enzyme to reduce the substrate. The product then flows out of the outlet.

Some initial experiments were carried out using *Ht* HoxFU to electrochemically recycle NAD^+ in the flow cell coupled to an alcohol dehydrogenase enzyme to reduce acetophenone. This is commonly used as a model reaction within the Vincent group as it has been well studied. The aim of these experiments was to develop the flow cell for electrochemical synthesis rather than to obtain results for the reduction of acetophenone, so these results will not be discussed here. As discussed in Chapter 3, the *m*HoxFU was not suitable as an electrocatalyst, so these experiments did not progress beyond this development stage.

The electrochemical flow cell could alleviate some of the problems experienced in the batch flavin recycling experiments, such as stirring inefficiencies preventing full conversion. The flow solution is constantly pumped through the cell delivering fresh substrate to the enzyme and removing product, which mitigates mass transport limitations.

5.5.3 Immobilising ENE-reductase enzyme on an electrode

The high surface area metalloenzyme electrodes developed in section 5.5.2 had the NAD^+-reductase enzyme adsorbed to the surface where the cofactor was reduced. The electrochemical flavin reduction requires electrons to be transferred directly from the electrode and this may be impeded by adsorbing the ENE-108 to the surface of the BP2000. Also, every enzyme has its own unique properties, so it was possible the ENE-108 would not adsorb to the BP2000 as readily as the *Ht* HoxFU and ADH-101 that had been previously trialled in this cell.

Particles were made up as following the procedure in (Chapter 2, section 2.4.2) to a concentration of 10 mg mL^{-1} and mixed with the same volume of ENE-108 10 mg mL^{-1} made up in KPi. The particles were then pipetted onto the surface of a carbon paper electrode and placed inside an Eppendorf tube to prevent drying out. They were then incubated in the fridge at 4°C for 1 hour (Figure 5-13a) and 10 mins (Figure 5-13b). The carbon paper electrode was then placed in a clean Eppendorf tube with 1 mL Milli-Q water and agitated gently (1st wash). The electrode was removed from the wash and placed in a clean Eppendorf tube with 1 mL Milli-Q water and agitated gently (2nd wash). These two washes were then placed in a clean cuvette for UV-Vis spectrophotometric analysis, and the A_{280} peaks are shown in Figure 5-13. This shows that when the enzyme that is incubated for longer it seems to adsorb better to the electrode. The black trace on each of the spectra is the analysis of initial the enzyme solution.

Flow experiments were then carried out using the ENE-108-modified particles pipetted onto a carbon paper electrode and left to incubate for an hour prior to use. A small sealed vial containing 10 mL of 0.1 mM riboflavin together with 5 mM 4-phenyl-3-buten-2-one as substrate with 10% v/v DMSO was used as reaction solution. This was recirculated during the experiment by flowing into the flow cell from the vial and then the resulting output solution being flowed back into the vial.

The reason for recirculating the solution is that it would be unlikely to achieve a high conversion in a single pass in this electrochemical flow cell. Small aliquots (200 µL) were taken at hourly intervals for GC analysis and the experiment left to run. Unfortunately, the conversion to product from the GC analysis was less than 13% after an hour, and then the conversion did not increase throughout the duration of the experiment. This indicated that the enzyme may not be well adsorbed to the electrode and had been washed off the electrode.

5.5.3.i Using polymyxin as co-adsorbate

In analytical electrochemistry it is sometimes necessary to add a co-adsorbate to attach a protein to the electrode in a more stable way.[8–10] One method is to use polymyxin, an antibiotic, as co-adsorbate, which forms strong interactions with both the protein and the electrode. To see if this would help the ENE-108 adsorb to the electrode, a solution of polymyxin (10 mg mL^{-1}) was added to the ENE-108 solution in a 1:1 ratio, before being mixed with the BP2000 (10 mg mL^{-1}) and pipetted onto a carbon paper electrode. The electrode was incubated for 4 mins at 4°C before being washed in the same way as the previous electrodes. The first and second washes were analysed by UV-Vis and the results shown in Figure 5-13

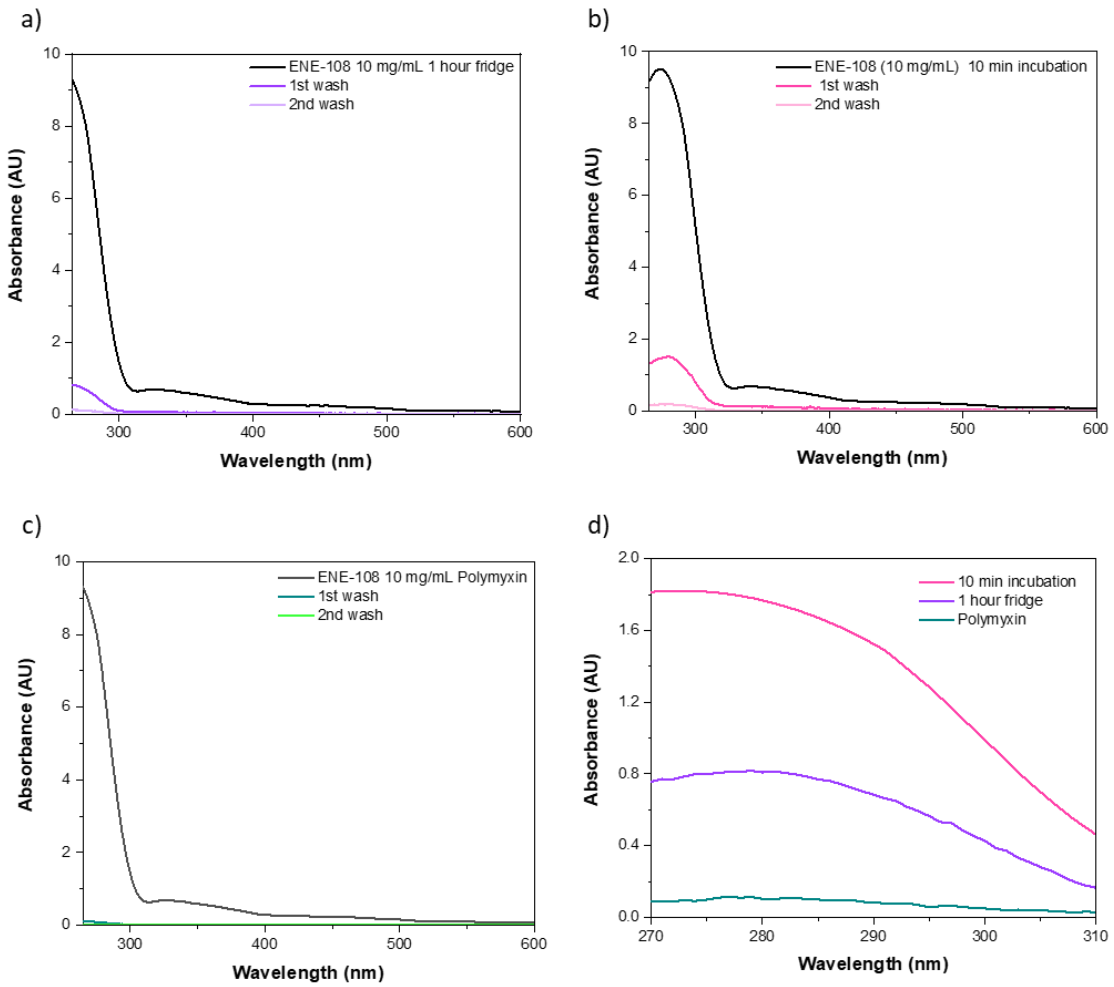


Figure 5-13: UV-Vis spectrophotometric analysis of different immobilisation techniques. All techniques used a 10 mg mL^{-1} solution of ENE-108 (black trace); (a) ENE-108 pipetted onto the surface of a carbon felt electrode and allowed to adsorb for 10 minutes before being washed. The purple traces show the 1st and 2nd wash. (b) ENE-108 pipetted onto the surface of a carbon felt electrode which was then placed into the fridge to incubate for 1-hour, pink traces show the 1st and 2nd wash. (c) A 10 mg mL^{-1} solution of ENE-108 was mixed with an equal volume of polymyxin (20 mg mL^{-1}) before being pipetted onto the surface of a carbon felt electrode and allowed to incubate for 10 mins. The green traces show the 1st and 2nd wash. (c) comparison of Abs$_{280}$ for the 1st wash from all three immobilisation techniques.

The results of the UV-Vis analysis shows that the amount of protein that washes off the electrode is negligible. This can be seen better when overlaid with the UV-Vis spectra from (a) and (b) in Figure 5-13(d) which is a close-up section of the A_{280}. Here it can be seen that the polymyxin (green trace) has no peak at all at 280 nm, indicating no protein was present in the wash. This is in contrast to the previous two experiments which show peaks of 0.8 AU for the 1-hour incubation and 1.8 AU for the

10-minute incubation. The polymyxin seems to help the ENE-108 adsorb to the enzyme, so this method was adopted for the initial experiments.

A repeat experiment of the one carried out in section 5.5.3was performed, this time using polymyxin to adsorb the ENE-108 to the electrode. All other conditions were kept the same. The GC analysis for this experiment indicated that 98% conversion to product was achieved in less than 3 hours.

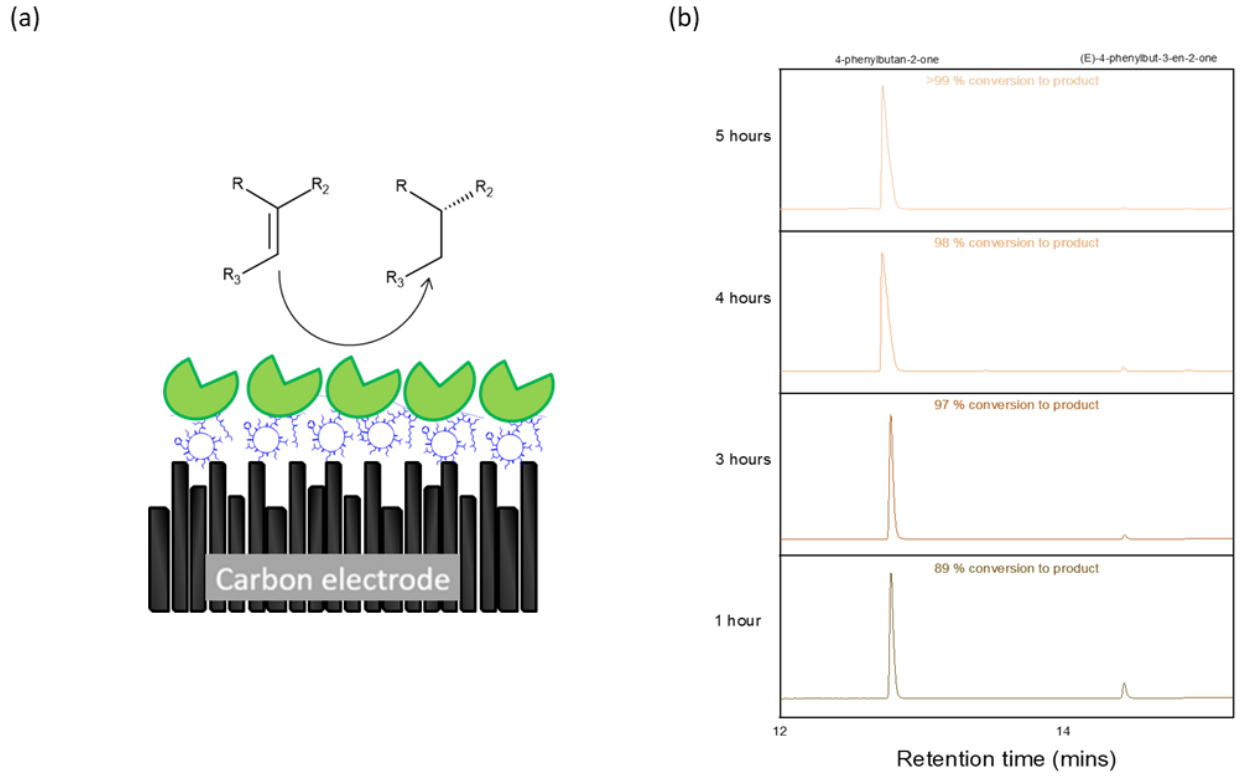


Figure 5-14:(a) Schematic representation of polymyxin being used as coadsorbant to attach enzymes (green) to carbon electrode (b) GC-FID analayis of one of the experiments using polymyxin as co-adsorbant, showing that 89% conversion to product was achieved in the first hour of the experiment with >99% conversion achieved in 5 hours. Flow experiments carried out using ENE-108 and polymyxin pipetted onto a carbon paper electrode and left to incubate for an hour prior to use. A small sealed vial containing 10 mL of 0.1 mM riboflavin together with 5 mM 4-phenyl-3-buten-2-one as substrate with 10% v/v DMSO was used as reaction solution and recirculated for the duration of the experiment

This result was promising, however, further experiments under the same conditions yielded varying results. Some achieved full conversion rapidly, whereas others did not achieve any conversion. This may be due to the enzyme orienting itself incorrectly and effectively blocking the active site. At this

point in the project, considering time constraints, the decision was made to carry out the flow experiments using both the RF and ENE-108 in solution.

5.6 Electrochemical recycling of riboflavin in flow

Due to the disappointing results from the high-surface area electrode experiments, the electrochemical flow system required some modification. It was not going to be possible to immobilise the enzyme onto the electrode. These experiments were using a recirculation system, with the substrate flowing through the cell and then the product/output being flowed back into the same vial to be recirculated through the flow cell. This allowed the flow solution multiple 'opportunities' for complete reduction as the same solution was pumped through the cell continuously for several hours.

A high surface-area electrode was still required, and the carbon paper without the BP2000 would not provide sufficient area, so a small piece of carbon felt 4 mm x 6 mm was cut to fit the internal dimensions of the cell. A glassy carbon rod WE connector connected the potentiostat to the carbon felt WE. A piece of Pt wire in a fritted electrode case was used as CE and a leak-free Ag/AgCl RE used, set up as shown in Figure 5-15.

a) b)

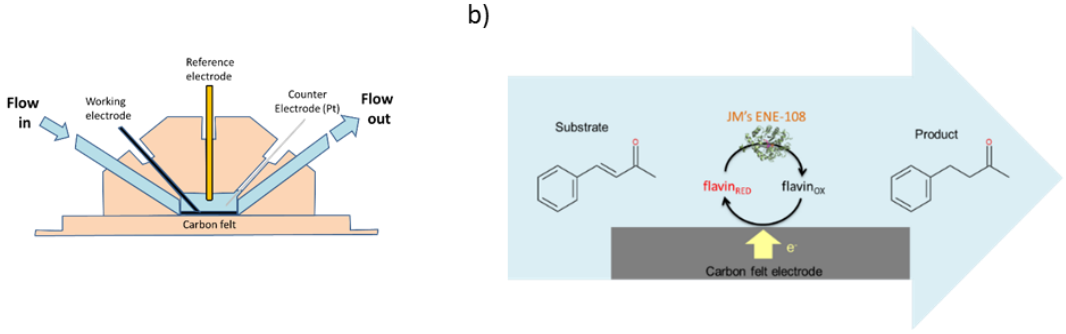


Figure 5-15: a) cross-section of the electrochemical flow cell showing b) schematic representation of flow reaction using ENE-108 in solution with 0.1 mM riboflavin and (E)-4-phenylbut-3-en-2-one with 10% DMSO as cosolvent passing over the carbon felt WE where the electrochemical reduction of RF takes place. The RFH_2 generated then drives the ENE-108 reduction, and the product is pumped out of the flow cell in a continuous reaction.

All reactions were carried out in a glovebox with an N_2 environment. The electrochemical flow cell is shown in Figure 5-16, showing the reaction solution in a small vial pumped through the flow cell by the attached syringe pump. A solution of 20 mM of 4-phenyl-3-buten-2-one was made up in a vial with 0.1 mM RF and ENE-108 (1.0 mg mL-1) and this was recirculated through the electrochemical flow cell whilst a potential of -0.40 V vs SHE was applied.



Figure 5-16: electrochemical flow cell and syringe pump used for flow experiments

The resulting current over time graph is shown in Figure 5-17(a). Integrating this graph, the charge passed predicted the conversion to product of 73% (from the number of $2e^-$ equivalents passed) after approximately 3 hours. These results were confirmed by the GC analysis of the final solution which is shown in Figure 5-17(b), referenced to the compound standards.

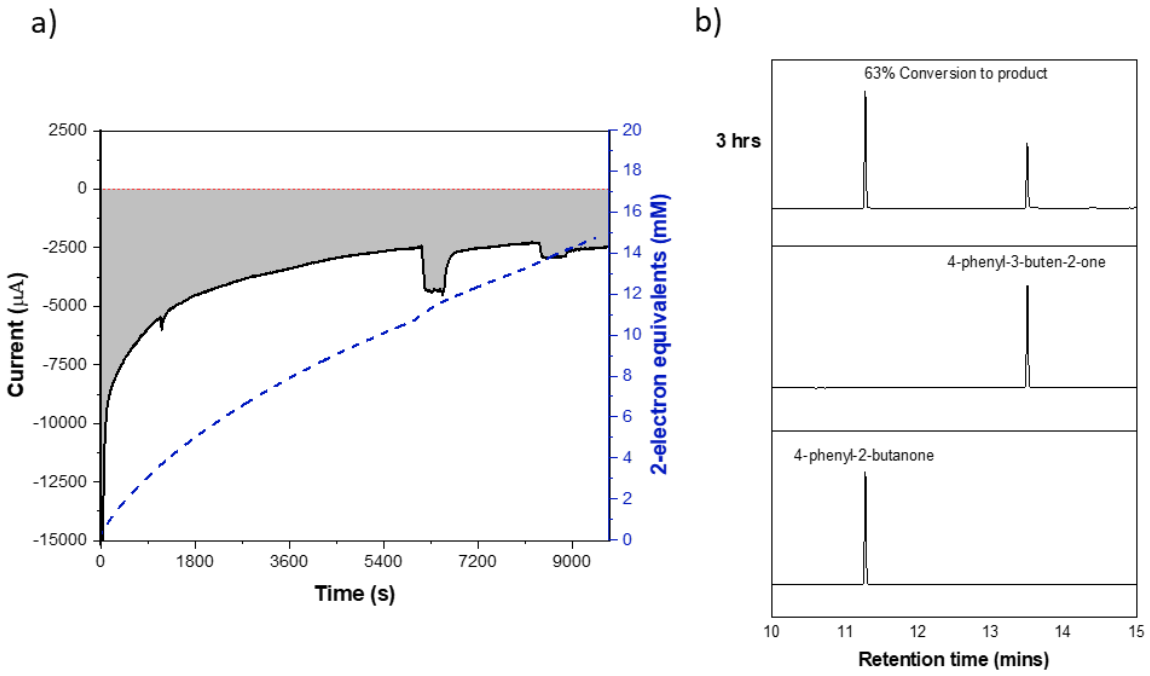


Figure 5-17: (a) Chronoamperometry experiment to reduce 12.7 mL of substrate 1 (20 mM) performed in continuous flow using RF (0.1 mM), and ENE-108 (1.0 mg mL-1) with the electrode poised at -0.40 V vs SHE. Area of shaded region shows the area integrated to calculate the charge passed in Coulombs used to calculate a Faradaic yield of 86%.

These results represent a RF TN of 126 which met the aim of these experiments to achieve a TTN > 100. Unfortunately, these results were not readily reproducible. However, the glovebox that the experiments were carried out in was experiencing some problems with the seal on the antechamber and this was causing higher than normal levels of O_2. It has been noted with other RF recycling experiments that even the smallest trace of O_2 can contaminate the reaction.

5.7 Summary and further work

The work carried out in this chapter has shown that both FMN and RF can be used in an electrochemical recycling system to drive a biocatalytic reaction of interest. This is particularly exciting in the case of RF which has not been used previously. In order to demonstrate its industrial relevance, it was necessary to achieve a TN of at least 100 within a reasonable time frame. This was achieved in flow with a 63% conversion to product of 20 mM substrate within 3 hours.

Similar results were achieved in batch with the electrochemical recycling of FMN to drive the reaction. However, these reactions were carried out on the bench under N_2 which was not a suitable environment for the RF experiments. It has been shown that RF is very sensitive to even low levels of O_2, and working on the bench yielded no desired product, indicating that possible undesirable side reactions are taking place.

The electrochemical flow system shows promise for further research. It is important to highlight that the flow cell used was not built for synthesis, but a modified spectro electrochemical cell used for analysis. With advances in 3D printing, it would now be possible to design a flow cell specific for electrochemical flavin recycling which would allow a larger area for the WE and a bigger compartment for a larger CE to scale up the reaction.

Chapter 5 Bibliography

1 Zhao, H. and Van Der Donk, W. A., *Curr. Opin. Biotechnol*., 2003, **14**, 583–589

2 Srinivasan, S. J. DPhil Thesis, University of Oxford, 2022

3 Plutschack, M. B., Pieber, B., Gilmore, K. & Seeberger, P. H. *Chemical Reviews,* 2017 **117** 11796–11893

4 Bogdan, A. R. and Dombrowski, A. W., *Journal of Medicinal Chemistry,* 2019, **62** 6422–6468

5 Thompson, M. P., Peñafiel, I., Cosgrove, S. C. and Turner, N. J., *Organic Process Research and Development*, 2019, **23** 9–18

6 Thompson, L. A., Rowbotham, J. S., Nicholson, J. H., Ramirez, M. A., Zor, C., Reeve, H. A., Grobert, N., Vincent, K. A., *ChemCatChem,* 2020, **12**, 3913-3918

7 Tamborini, L., Fernandes, P., Paradisi, F. and Molinari, F., *Trends in Biotechnology*, 2018, **36**, 73–88

8 Armstrong, F. A. and Wilson, G. S., *Electrochim. Acta,* 2000, **45**, 2623–2645

9 Armstrong, F. A., Hill, H. A. O. and Walton, N. J., *Acc. Chem. Res.*, 1988, **21**, 407–413

10 Blanford, C. F. and Armstrong, F. A., *J. Solid State Electrochem.*, 2006, **10**, 826–832

Library Building tool for Medicinal Chemists

This chapter is based on work carried out during a 16-week internship at HydRegen looking at an H2-driven bio-electro catalyst for the reduction of nitro comounds to their corresponding amine functionality.

6.1 Introduction

The reduction of nitroarenes to anilines is significant for the pharmaceutical industry as these serve as precursor molecules or active pharmaceutical ingredients (APIs) in the synthesis of many drugs.[1] The preferred method for nitro reductions uses hydrogenation over metal catalysts such as Pd/C, however the presence of additional functional groups on the nitroarene creates challenges around selectivity, and cleaner and more sustainable synthetic routes are desirable.[2] Often commercially available enzymes used in biocatalysis do not have a wide enough substrate scope to generate libraries for medicinal chemistry.

Bio2amine is a 'black powder' catalyst that consists of hydrogenase enzyme on a carbon black support as shown in Figure 6-1. The hydrogenase splits molecular hydrogen releasing electrons in this process that are carried via the carbon support to facilitate the reduction of nitro-groups. Sokolova *et al.* demonstrated full conversion of 30 nitroarenes in batch using this catalyst.[3] This project builds on some of this work by moving the reactions into flow using a commercially available flow system by ThalesNano with the catalyst supplied by HydRegen. The aim is to develop a system to allow selective reduction of a broad range of nitro substrates in flow, suitable for generating a compound library for medicinal chemists.

The Bio2Amine catalyst essentially acts as an electrocatalyst, coupling H_2 oxidation and nitro reduction half reactions. This widens the possible substrate scope as there is no requirement

for the substrate to fit the active site of the biocatalyst. The catalyst shows high selectivity for nitro-reduction over other unsaturated bonds in the compound.[4]

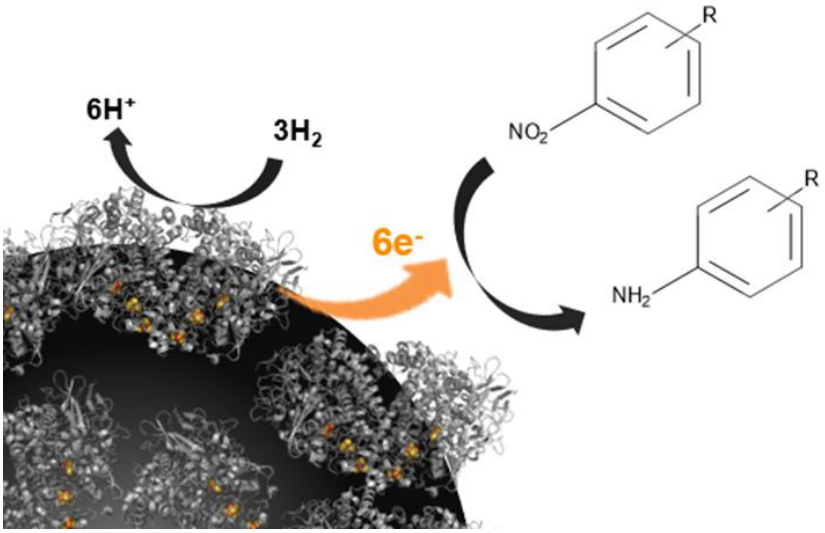


Figure 6-1: Bio2Amine catalyst spitting molecular hydrogen for use as an electron source to reduce nitro compounds to their amine derivatives by electron transfer from the carbon support to the species being reduced.

Over the last 15 years, the synthesis of APIs has been carried out increasingly in continuous flow systems[5] which can alleviate many of the issues seen with batch processes such as mass transport limitations. More recently this technology has expanded to flow biocatalysis where reactants are pumped though a reactor where enzyme is immobilised in a packed bed or column where the reaction takes place. The product then flows out. This simplifies separation and allows the catalyst to be reused whilst controlling temperature and allowing in-line reaction monitoring. [6,7]

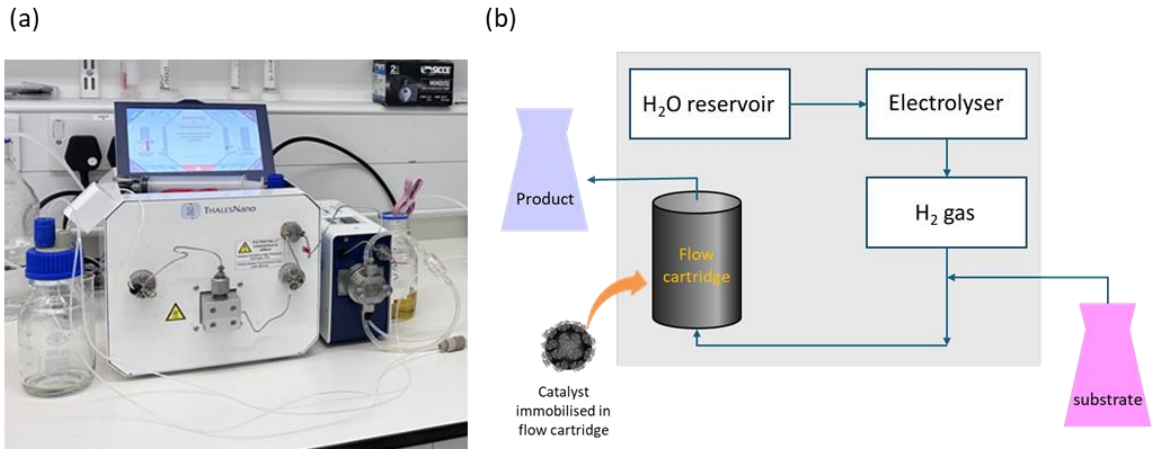


Figure 6-2: (a) ThalesNano H-cube being used as a flow reactor with the Bio2Amine catalyst packed into the flow cartridge (CatCart). (b) schematic representation of the H-cube; Electrolyser produces the hydrogen required from the water reservoir. The liquid feed is drawn into the flow reactor, and together with the H_2 passes through the flow cartridge where the catalyst is immobilised. The product flows out.

Poznansky *et al*. demonstrated H_2-driven hydrogenation reactions in the H-cube, a commercially available flow reactor (Figure 6-2) which was also used for the experiments in this chapter. The Bio2Amine catalyst was immobilised into a cartridge (CatCart) as shown and H_2 gas generated by the electrolyser was pumped through the system, together with the liquid feed which contains the substrate dissolved in buffer (and any necessary cosolvent). This flows through the cartridge where the enzyme is immobilised and the reduction takes place, the solution containing the product then flows out of the system into a collection vessel.

The aim of this industrial placement was to build a semi preparative screening tool for medicinal chemists, generating 2-10 mg amine fragments applicable to Medicinal Chemistry programmes. Often several compounds of interest are identified, and sometimes these molecules are very similar in structure. Only small quantities are required for preliminary cellular testing. In the event of one of these compounds showing promise, further synthesis

of up to 100 mg of this fragment would be useful and this system would allow for easy scale-up to that quantity, simply by flowing for longer.

One of the challenges faced in this project is with analytics; proving that one compound does not contaminate the next, showing if there are any intermediate species and quantifying conversion; these are discussed in detail in section 6.11.

Another challenge is solubility: many of these compounds are insoluble in water, so will require a co-solvent, which may vary depending on the compound. Ramirez *et.al.* demonstrated that Hyd1 tolerates DMSO and MeCN as cosolvent up to about 50% although with some loss of activity.[8] However, it is important to note that these experiments used Hyd1 in solution rather than supported on carbon. Solubility studies are discussed in 6.3.

6.2 Compound selection and analytics

6.2.1 Compound selection

Pharmacophores are important in medicinal chemistry due to the steric and electronic features of a molecule that allows them to interact with biological targets. Nitro groups are considered as excellent pharmacophores, as they can act as a hydrogen bond donor.[9] Early stage drug discovery involves the synthesis of small quantities of these pharmacophore molecules that may have familiar features but diversity in functional groups. They may contain interesting properties such as chloro or fluoro groups which are of interest to medicinal chemists due to being lipophilic such that they can interact with the phospholipid bilayer of a cell membrane. This is an essential characteristic if a drug is to have good absorption.[10]

When selecting compounds to use in this project, given that this was a 16-week internship, it was essential to use at least one compound that had been well studied within the company, so that the analytics were already developed and there were data available with which to compare results. Section 6.6 looks at the continuous synthesis of aminophenol (a precursor to paracetamol) as a model reaction.

The next compound that was selected for reduction was 5-nitrosalicylic acid. This is an interesting compound to study as the amine product, 5-aminosalicylic acid, is the drug mesalazine (Figure 6-3(b) **2** and **2a**), which is used to treat inflammatory bowel disease. One of the challenges with this particular compound is the presence of a carboxylic acid functional group on the aromatic ring which can affect pH in solution, this is discussed in detail in 6.17. Mechanistic studies into Hyd1 enzymes show good stability over a range of pH conditions from 3 – 10.8.[11,12] However, it is not known how drastic changes in pH may affect the stability of the catalyst in this flow system, as the enzyme is required to tolerate a number of conditions over a sustained period of time. This compound is a good example to test the effect of pH on the catalyst.

During drug discovery, compounds that are similar in structure are often synthesised, differing only in the position of a side-chain for example. For this reason, 3-nitrotoluene and 4-nitrotoluene were selected. Although seemingly similar compounds, the effect of the position of the methyl group has significant effect on the properties of the compound. Solubility, which is discussed in 6.12, generally decreases with a symmetrical compound, as the molecules are more tightly packed in a crystal lattice. This increases the melting point and lowers solubility for the *para*-substituted isomers. The positioning of the methyl group in the

para isomer results in 4 resonance structures which delocalise the charge in the structure and make the molecule more stable, compared to 3 resonance structures in the *meta*. This impacts the compound's absorbance of UV light, so the two compounds will require different analytical methods.

Finally, two halogenated compounds were selected; 3-nitrobenzotrifluoride and 5-chloro-2-nitropyridine. Fluoro and chloro-compounds are highly desirable in medicinal chemistry due to the lipophilic properties of these groups enhancing membrane permeation.[13] There are challenges with these molecules around solubility as the increased lipophilicity decreases the compounds solubility in water, so they may require a less polar cosolvent than DMSO (solubility is considered in 6.12). This in turn may affect the catalysts activity/stability.

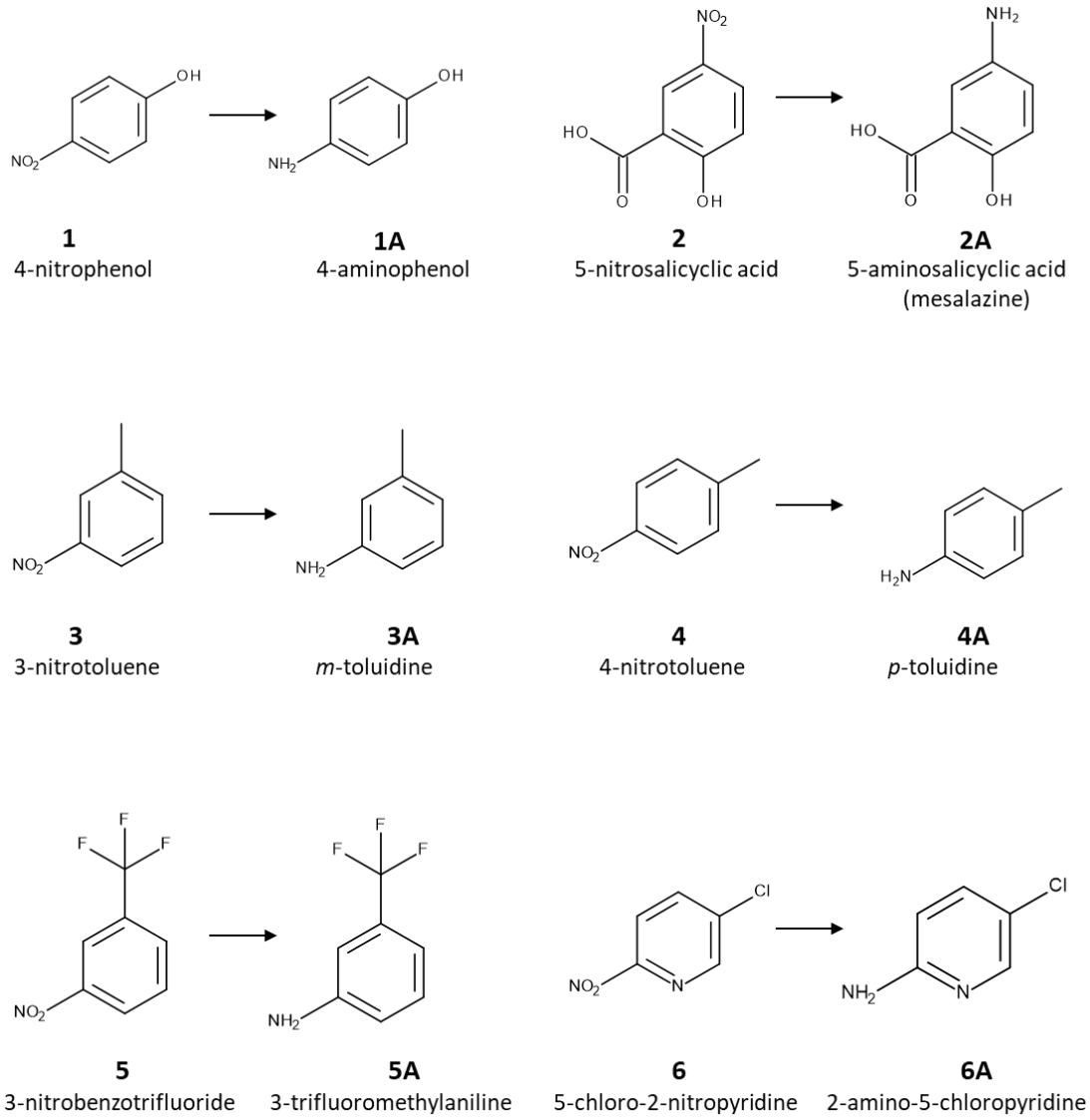


Figure 6-3: Nitro compounds used for this project together with their corresponding amine product. Numbers in bold are used throughout this chapter to reference the nitro substrate, letters in bold reference the amine product.

6.3 Solubility

Solubility in water is a challenge, particularly for compounds that have lipophilic groups attached. It is therefore necessary to identify a cosolvent that will improve the solubility of these compounds whilst being tolerated by the enzyme. This is particularly challenging for this system as the aim of the project is for use as a screening tool to flow successive compounds, and so requires the catalyst to be stable for an extended period of time. An ideal

scenario would be to use 10-30% DMSO for all compounds, which the catalyst is known to tolerate well.[8] Cosolvents are discussed in more detail in 6.12 along with increasing the solubility of hydrophobic compounds.

6.4 Analytical methods

One of the challenges of this project is in the analysis of products. There is no single standard method of analysing the range of compounds selected for this project as each compound has its own properties. The merits and drawbacks of available techniques will be discussed in the following sections:

6.4.1 UV-Vis spectroscopy for nitro-to-amine conversions.

All Ultra Violet Visible Spectroscopy (UV-Vis) analysis was carried out on a Thermoscientific Genesis 80 spectrophotometer. UV-Vis analysis can be rapidly and simply carried out during an experiment by diluting a small aliquot of the collection solution in a cuvette and analysing. This technique is simple and gives rapid results. Figure 6-4(a) shows the UV-Vis spectra for 3-nitrobenzotrifluoride (pink trace) which has two diagnostic peaks at 240 nm and 295 nm. The peak for the corresponding amine, 3-trifluoromethylaniline (purple trace), appears at 260 nm. Therefore in-situ analysis of the reduction of 3-nitrobenzotrifluoride would clearly show any amine present, and as the amine product absorbs strongly, a calibration curve can quantify the conversion. Conversely, UV-Vis analysis of 3-nitrotoluene (Figure 6-4(b)) shows that the nitro compound in this case absorbs UV light much more than the amine product, *m*-toluidine. As the amine peak is in the same region, this results in the nitro peak masking the amine.

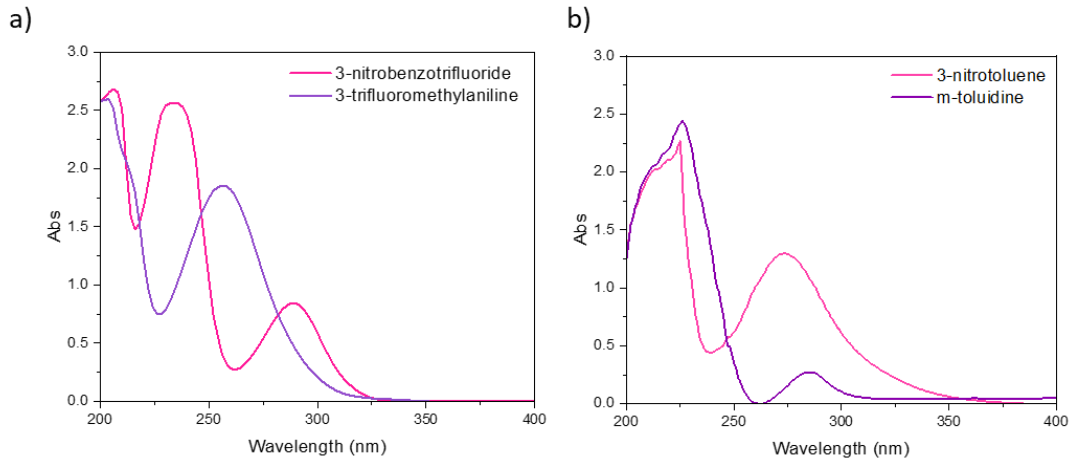


Figure 6-4: UV-Vis spectra for two of the nitro compounds used in this project, together with their aniline products: a) 3-nitrobenzotrifluoride (pink) which shows peaks at 230 and 280 nm and 3-trifluoromethylaniline (purple) which has a single peak at 260 nm. b) 3-nitrotoluene (pink) and *m*-toluidine (purple), both compounds have a peak in the region 275-280 nm.

6.4.2 High Performance Liquid Chromatography (HPLC)

High-performance liquid chromatography (HPLC) experiments were carried out on an Agilent 1100 HPLC system. HPLC enables identification of compounds in solution by comparison to known standards. It can also quantify the concentrations of each component by producing a calibration curve from these standards. Molecules are separated by their affinity to both the eluent used (mobile phase) and the HPLC column (stationary phase), which for the experiments in this chapter used a Zorbax Eclipse Plus C18 column. A UV-Vis absorbance detector that is set to a specific wavelength (selected as suitable for the analysis of the compounds being analysed) is used to detect the absorbance of the molecules as they are eluted. Samples are prepared for HPLC analysis by diluting an aliquot of collection solution with some of the mobile phase.

The main problem with HPLC analysis for the compounds selected is that the amines are often eluted early on in the analysis (and can often co-elute with the DMSO), whereas the nitro compounds are retained on the column. Altering the composition of solvents in the eluent enables both the nitro and the amine to be eluted in a reasonable time frame, whilst ensuring good separation of peaks. In some HPLC methods, the hydroxylamine can elute at a similar position to the amine, masking the amine. However, for each of the compounds chosen for this project, the HPLC method used ensured that any intermediates had their own clear retention time. Intermediates will be discussed fully in 6.11.

A standard protocol has been established within HydRegen which enables an HPLC method to be developed for most of the nitro/amine compounds they use. Standards of each nitro and amine are made up and an aliquot of the 100 µL of this solution is diluted with 900 µL of a 50: 50 ratio of MeCN: Ultrapure water with 1% formic acid added (H_2OFA). A 20-minute gradient method which starts with 90% H_2OFA and 10% MeCN and gradually alters the composition of eluents to 10% H_2OFA and 90% MeCN is used. Most of the compounds in this project will be eluted somewhere within this gradient. The composition of solvents together with the time taken to elute can then be used to develop an isocratic method for that combination of nitro/amine. The UV wavelength used for HPLC analysis is established by first running a UV-Vis of the standards and choosing a wavelength where both the nitro and the amine compounds absorb.

Once an isocratic method had been established for the compounds being analysed (both substrate and product), a calibration curve on the compound standards was produced. An

example of two such calibration curves are shown in Figure 6-5 for 3-nitrobenzotrifluoride (substrate) and 3-trifluoro methylaniline (product).

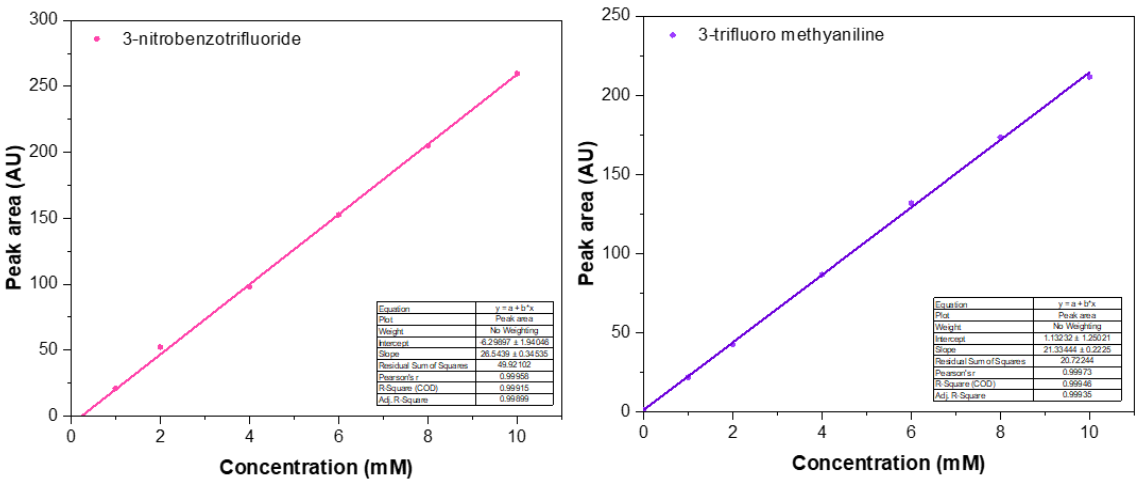


Figure 6-5: Calibration curves for 3-nitrobenzotrifluoride (pink) and 3-trifluoro methylaniline (purple). HPLC analysis was carried out of compound standards in varying concentrations from 1 – 10 mM. The concentration was then plotted against the peak area of the UV-Vis spectra recorded at 280 nm for these compounds. The resulting straight-line equation of the graph can be used to calculate the concentration of these compounds contained in any sample.

These are generated by running analyses of several different concentrations of the compound standard and then plotting the concentration against the peak area of the absorbance of the UV-Vis curve measured at 280 nm. This wavelength was selected as appropriate as both the nitro and the amine absorb in this region (see Figure 6-4a). Using the resulting equation of the straight line for the graph allows the concentration of any given peak area to be determined. This allows for a quantitative means of analysing the output.

6.5 NMR

NMR potentially may seem the best method to choose, as standards of both the substrate and the product can be taken to compare to, and any intermediate species generated during the reaction would be apparent. HydRegen have an in-line NMR that could analyse the flow throughout the experiment, further simplifying the analysis. However, the results are only clear with quite concentrated samples. To achieve this, the liquid feed would need to be at least 10 mM to give a clear result, and low conversions of product may not show. The water suppression feature allowed for aqueous samples to be run without the need for any deuterated solvent. This meant that no diluting of samples was required and also in-line analysis could be carried out.

NMR analysis was carried out using the Magritek Spinsolve 80 Ultra connected to a Baoding Longer BT100-3J peristaltic pump for in-line NMR analysis.

6.6 Continuous synthesis of aminophenol

The conversion of 4-nitrophenol to 4-aminophenol has been well studied, both in the Vincent group and at HydRegen. For this reason, this compound was selected as a model substrate to carry out in the initial flow experiments. The analytical methods have already been established at HydRegen and previous experiments show that 4-nitrophenol can be converted to 4-aminophenol using Bio2Amine with no intermediate species generated once the system has reached a steady-state (intermediates are discussed in 6.11). This made 4-nitrophenol hydrogenation an ideal model reaction to try in this project, as the results would be easy to

analyse, allowing us to focus on the parameters of the reaction, as these could potentially be applied to other compounds to establish a protocol for the experiment.

A starting concentration of 10 mM substrate was used with the H-cube set at 35°C and 2 bar H_2 pressure with an initial flow rate of 0.5 mL min^{-1} (column 1, Figure 6-7).

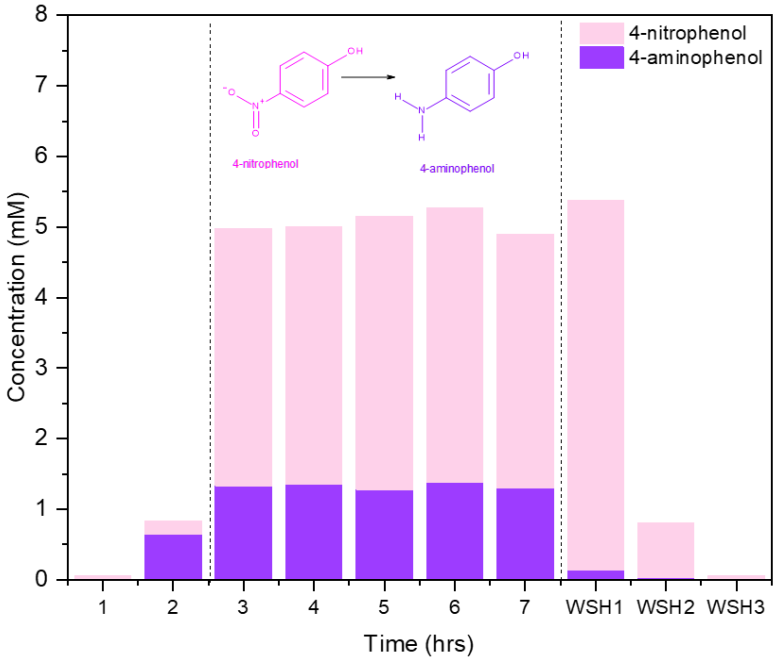


Figure 6-6: Results of the HPLC analysis of initial flow experiment to synthesize 4-aminophenol (purple) from a liquid feed of 4-nitrophenol (pink) in continuous flow using Bio2Amine catalyst in the H-cube.

All eluent solution was flowed into a collection vessel. Every hour, 500 µL was collected for analysis, this represents approximately 4-5 column volumes (see section 6.9 for important note on column volumes).

The graph in Figure 6-6 shows concentration of 4-aminophenol (purple) and 4-nitrophenol (pink) over time, analysed using HPLC. The early time points show low concentrations of 4-aminophenol and 4-nitrophenol, likely due to the compounds adsorbing onto the carbon-

based catalyst support. This phase is complete after approximately 2 hours. At this point, the data show that steady state has been reached, with approximately 1 mM product observed in the analysis of the collection solution for the following 5 hours.

The HPLC analysis of this experiment also detected the presence of an intermediate species eluted at around 6.8 mins retention time (RT) (amine RT 10.1 mins, nitro RT 21.3 mins) during the first two hours of this experiment. This is presumed to be the hydroxylamine (although lack of product standards mean that the species cannot be identified, but would be either the nitroso or hydroxylamine). This intermediate peak disappeared as the amine peak increased. Once the system reached a steady state the presence of the intermediate was negligible, this is discussed further in section 6.11.

A starting concentration of 10 mM substrate was applied. It is observed that the total concentration of 4-aminophenol and 4-nitrophenol in the analysis is much less than this concentration of the substrate. This suggests that some of the compound is adsorbed to the catalyst on the column. For this reason, a wash phase was included using a faster flow rate of 3 mL min^{-1}. Aliquots of the wash solution were collected for analysis every 15 minutes (shown on the graph in Figure 6-6 as WSH). This step is crucial to clean the column before any subsequent substrates are used. The wash was continued until the analysis of the collection showed no substrate or product was present to contaminate further experiments.

During the steady state phase of the experiment, a total of 30 mL was collected, with an average of 10% conversion to product. This gives an approximate collection of ≈ 3 mg, which would be the desired quantity for the purpose of preliminary cellular testing by medicinal chemists. Further optimisation of conditions should improve this conversion so that collecting

this amount of product can be achieved in a shorter time frame. These data highlight the need to include the wash phase in the collection, due to a small amount of product being present. It also gives preliminary evidence that the system can be used for semi-preparative screening. Next, the possibility of moving between reaction conditions / substrate is considered.

6.7 Continuous flow of successive compounds as a semi-preparative screening tool.

The aim of this project is to develop a tool for use by medicinal chemists who want to synthesise small quantities (2-4 mg) of multiple compounds of interest. Therefore, the main priority is not necessarily full conversion, but rather ensuring that the catalyst is robust enough to withstand the various conditions imposed during the synthesis of multiple compounds. Figure 6-7 shows the range of conditions explored during the experiments carried out in this project:

- Columns 1 and 2 were used primarily to optimise conditions for the flow system: to ensure good conversion of substrate to product, to ascertain a time frame for the system to reach steady state and establish a protocol for the wash phase to ensure no contamination between experiments.
- Experiments carried out using column 1 looked at varying the temperature, H_2 pressure and flow rate. Very low conversion was achieved at a flow rate of 0.5 mL min^{-1}, but conversion improved when the flow rate was decreased to 0.1 mL min^{-1} (which was the slowest rate this model of H-cube could use). It was also established during this experiment that an H_2 pressure of 4 bar achieved improved conversion.

- Column 2 was frozen for 2 weeks without loss of activity. This column also used a range of pH conditions to establish protocol for the synthesis of mesalazine from 5-nitrosalicylic acid. These results are discussed in section 6.17.

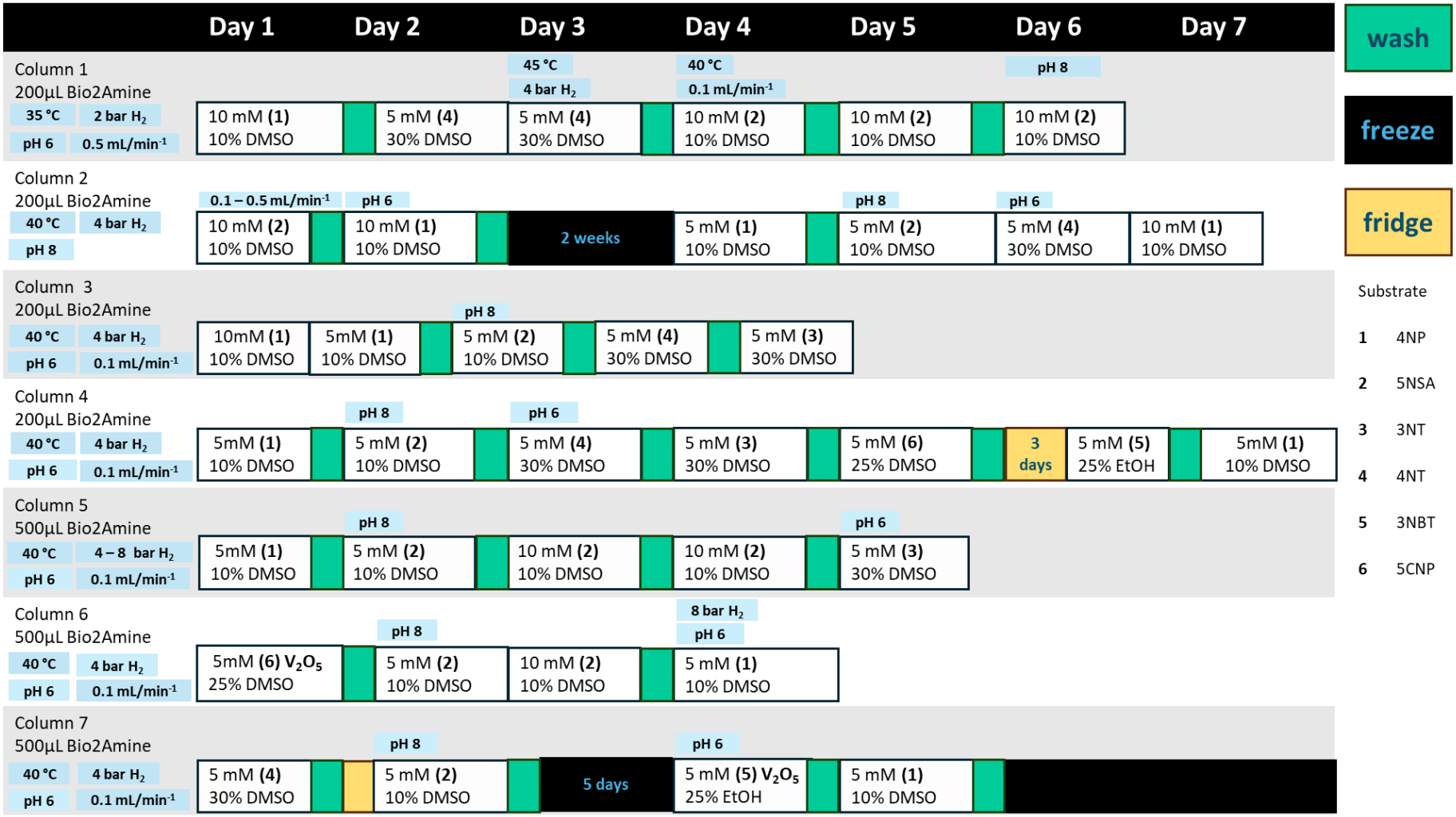

Day 1
Day 2
Day 3
Day 4
Day 5
Day 6
Day 7
wash
freeze
fridge
Column 1
200µL Bio2Amine
35 °C
2 bar H2
pH 6
0.5 mL/min-1
10 mM (1) 10% DMSO
5 mM (4) 30% DMSO
45 °C
4 bar H2
5 mM (4) 30% DMSO
40 °C
0.1 mL/min-1
10 mM (2) 10% DMSO
10 mM (2) 10% DMSO
pH 8
10 mM (2) 10% DMSO
Column 2
200µL Bio2Amine
40 °C
4 bar H2
pH 8
0.1 – 0.5 mL/min-1
pH 6
10 mM (2) 10% DMSO
10 mM (1) 10% DMSO
2 weeks
pH 8
5 mM (1) 10% DMSO
5 mM (2) 10% DMSO
pH 6
5 mM (4) 30% DMSO
10 mM (1) 10% DMSO
Column 3
200µL Bio2Amine
40 °C
4 bar H2
pH 6
0.1 mL/min-1
pH 8
10mM (1) 10% DMSO
5mM (1) 10% DMSO
5 mM (2) 10% DMSO
5 mM (4) 30% DMSO
5 mM (3) 30% DMSO
Column 4
200µL Bio2Amine
40 °C
4 bar H2
pH 6
0.1 mL/min-1
pH 8
pH 6
5mM (1) 10% DMSO
5 mM (2) 10% DMSO
5 mM (4) 30% DMSO
5 mM (3) 30% DMSO
5 mM (6) 25% DMSO
3 days
5 mM (5) 25% EtOH
5mM (1) 10% DMSO
Column 5
500µL Bio2Amine
40 °C
4 – 8 bar H2
pH 6
0.1 mL/min-1
pH 8
pH 6
5mM (1) 10% DMSO
5 mM (2) 10% DMSO
10 mM (2) 10% DMSO
10 mM (2) 10% DMSO
5 mM (3) 30% DMSO
Column 6
500µL Bio2Amine
40 °C
4 bar H2
pH 6
0.1 mL/min-1
pH 8
8 bar H2
pH 6
5mM (6) V2O5 25% DMSO
5 mM (2) 10% DMSO
10 mM (2) 10% DMSO
5 mM (1) 10% DMSO
Column 7
500µL Bio2Amine
40 °C
4 bar H2
pH 6
0.1 mL/min-1
pH 8
pH 6
5 mM (4) 30% DMSO
5 mM (2) 10% DMSO
5 days
5 mM (5) V2O5 25% EtOH
5 mM (1) 10% DMSO
Substrate
1 4NP
2 5NSA
3 3NT
4 4NT
5 3NBT
6 5CNP

Figure 6-7: Overview of the conditions used in the H-cube throughout the duration of the project. Each of the columns used for these experiments has been numbered 1-7 on the left-hand side of the table and indicates the volume of catalyst used (see section 6.9 for details), together with the starting conditions for that experiment. Where conditions were changed during the experiment, this is indicated by a blue box above the experiment details. The flow rate given is for the duration of the experiment after it has reached steady state. The first two hours of the experiment were carried out at a flow rate of 2 mL min^{-1} in order to saturate the column with substrate and achieve steady state. Wash cycles were performed at a flow rate of 3 mL min^{-1}. Substrate details are given in Table 6-1. Substrates are indicated by numbers in bold, details of which can be found in Figure 6-3.

The catalyst will be supplied to the customer and they will need to determine the conditions relevant for the compounds they are working with. The work described in sections 6.9 to 6.15 of this chapter explore the parameters that can be modified in order to optimise the conversion of a specific compound.

6.8 Control experiment

Before commencing any experiments using the Bio2Amine catalyst, it was first necessary to run a control experiment to ensure that the nitro compounds were not reduced in the absence of the catalyst and also to establish that each compound could be washed from the column and did not contaminate each successive experiment.

The H-cube uses a bespoke cartridge (CatCart) which consists of a stainless-steel tube into which a solid catalyst can be packed. There is a filter system at each end of the CatCart to prevent the catalyst escaping. The CatCarts used in this chapter were either 30 mm or 70 mm in length with respective void flow volumes of ~100 µL and ~250 µL respectively. The CatCarts are filled with catalyst then compressed and closed before use, so there will be some variation to the mass off catalyst and hence the exact void volume cannot be stated. The volume of the reactor and pump is comparatively large and therefore using these approximate values for the void flow volume will not introduce a huge uncertainty.

The control experiment was performed by packing the CatCart with 50 mg activated charcoal with a 100-mesh particle size (Sigma carbon) and loading into the H-cube. Buffer was then flowed through the H-cube at a flow rate of 1 mL min^{-1} for 10 minutes. This step is performed on experiments using the Bio2Amine catalyst, with aliquots of solution analysed by UV-Vis every 60 seconds. This step is to check that no protein has leached from the column. Flushing the column for

10 mins at the same flow rate mimics this step to ensure the same conditions for the control experiment.

Once the CatCart had been flushed with buffer, a 10 mM liquid feed was prepared for each of the nitro compounds selected for use in this project using the relevant quantity of co-solvent detailed in Table 6-1 below:

Table 6-1: Details of nitro compounds together with their corresponding amine product and conditions for the liquid feed. Substrate numbers correspond with those given in Figure 6-3.

Substrate	Nitro	Amine	Cosolvent	Buffer
1 /1a	4-nitrophenol	4-aminophenol	10% DMSO	KP_i pH6
2 /2a	5-nitrosalicylic acid	5-aminosalicylic acid	10% DMSO	Tris-HCl pH8
3/3a	3-nitrotoluene	*m*-toluidine	30% DMSO	KP_i pH6
4/4a	4-nitrotoluene	*p*-toluidine	30% DMSO	KP_i pH6
5/5a	3-nitrobenzotrifluoride	3-trifluoromethylaniline	25% EtOH	KP_i pH6
6/6a	5-chloro-2-nitropyridine	2-amino-5-chloropyridine	30% DMSO	KP_i pH6

Each compound was flowed through the H-cube under H_2 pressure of 2 bar and a flow rate of 0.5 mL min^{-1}. Samples of the collection solution were analysed by UV-Vis until the system reached a steady state. This occurs when the column has become saturated with the liquid feed, as some of the substrate/product is adsorbed to the surface of the column. For any output to be accurately analysed, a steady state must be achieved before this analysis is carried out. Once a steady state was achieved aliquots were collected every 15 mins (approximately for a total of 1 hour, and the results analysed by HPLC and UV-Vis.

At the end of each experiment, a wash phase was commenced using potassium phosphate buffer (KP_i) pH 6 and 10% DMSO at a faster flow rate of 3 mL min^{-1}. The increased flow rate allows this step to be completed as quickly as possible. Aliquots were taken every 15 minutes (equivalent to approximately 450 column volumes) for UV-Vis analysis until there was no trace of either substrate or product in the collection.

In all experiments the results showed that no conversion was observed for any of the substrates indicating that the blank carbon does not act as a catalyst for hydrogenation in the absence of enzyme.

6.9 Catalyst loading

A number of conditions can be modified in order to optimise conversion, however perhaps the most important is the catalyst loading. It stands to reason that if more catalyst is loaded into the column, there will be more enzyme available to the substrate. CatCarts are available in two lengths; 30 mm which can support approximately 200 µL enzyme and 70 mm which can support approximately 500 µL enzyme. However, due to the enzyme production process, each batch of enzyme can differ in its activity, so comparison of the volume of enzyme used is not useful. Table 6-2 gives details the activity of each aliquot of enzyme used during this project, listed by the column number for the experiment. The total loaded enzyme is calculated by dividing the enzyme activity (U mL^{-1}) but the column volume. This will give a figure in U which can be used for comparison purposes, and it is this figure that will be used for discussion in section 6.15.

Table 6-2: Activity of enzyme used in the experiments carried out in this chapter. The column numbers correspond with those in Figure 6-7. The number of enzyme units per mililitre is divided by the volume of enzyme used to give the total enzyme activity (U) which will be used when comparing columns.

Column number	Volume enzyme used (µL)	Enzyme activity (U mg^{-1})	Enzyme activity (U mL^{-1})	Total loaded enzyme activity (U)
1	200	2.65	10.65	2.13
2	200	1.27	2.63	0.53
3	200	11.20	6.70	1.34
4	200	11.40	9.20	9.2
5	200	8.36	11.79	4.6
	300	5.25	7.62	
6	500	20.32	14.62	7.31
7	500	20.32	14.62	7.31

For each column (1-7) a CatCart was loaded with the carbon support (50 mg Sigma carbon for a short column and 120 mg Sigma carbon for a long column) before pipetting the enzyme onto the carbon and allowing to disperse. The Column is then sealed and briefly vortexed before placing in the ThermoShaker for an hour at 450 rpm, 4°C to allow the enzyme to adsorb to the carbon.

Once the CatCart had been loaded with catalyst, it was placed into the H-Cube and KP_i, pH6 was flowed through at a flow rate of 1 mL min^{-1} with aliquots taken every 60 seconds for 10 minutes. These aliquots are then analysed by UV-Vis to ensure there is no loss of protein from the column. The results of this wash phase are shown in Figure 6-8. Protein absorbs ultraviolet light at 280 nm, so any protein lost would give a peak in this region. These results show no loss of protein from the CatCart, indicating that all of the enzyme loaded has been adsorbed to the surface of the carbon.

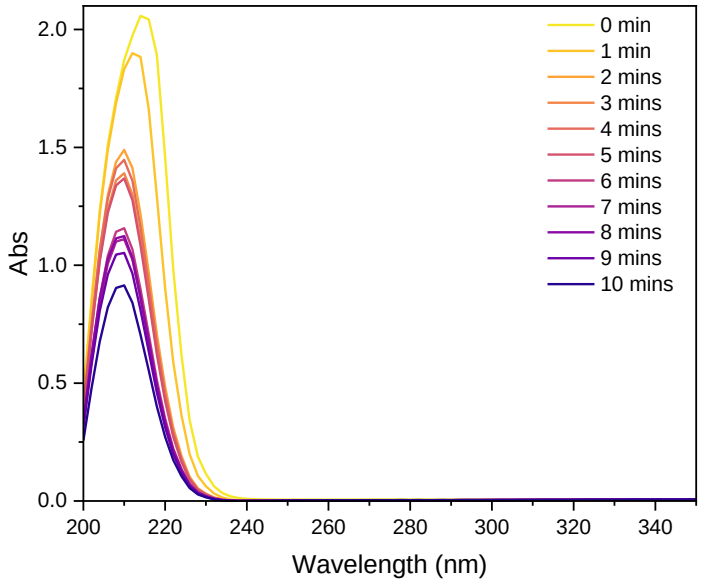


Figure 6-8: The collection solution from each experiment is analyzed by UV-Vis to check for any protein leaching from the column. Any adsorbed protein would show a peak at 280 nm.

The enzyme is the most expensive component of the experiment, so initial experiments were prepared with short columns to get an idea of conditions for subsequent optimisation experiments. Full conditions of catalyst loading for all experiments are detailed in Figure 6-7 .

6.10 Catalyst stability

Initial experiments performed were with the aim of running multiple successive compounds through the system to establish if the catalyst was stable over a period of time and could tolerate different substrates being flowed through and washed off. Each nitro compound selected has different solubility conditions and therefore need to be made up to a liquid feed using the appropriate buffer and cosolvent (see Table 6-3). For these reasons a short column was prepared so that if the catalyst was exposed to conditions that inactivated the enzyme, only a small quantity of enzyme was lost.

As discussed in section 6.7, columns 1 and 2 were used primarily to establishing conditions for each of the compounds such as flow rate, temperature and H_2. Using the optimised conditions from these experiments, column 3 was prepared (see Figure 6-7 for full details) with the aim of running multiple

successive compounds with a short wash phase between each. The results of this experiment are shown below in Figure 6-9.

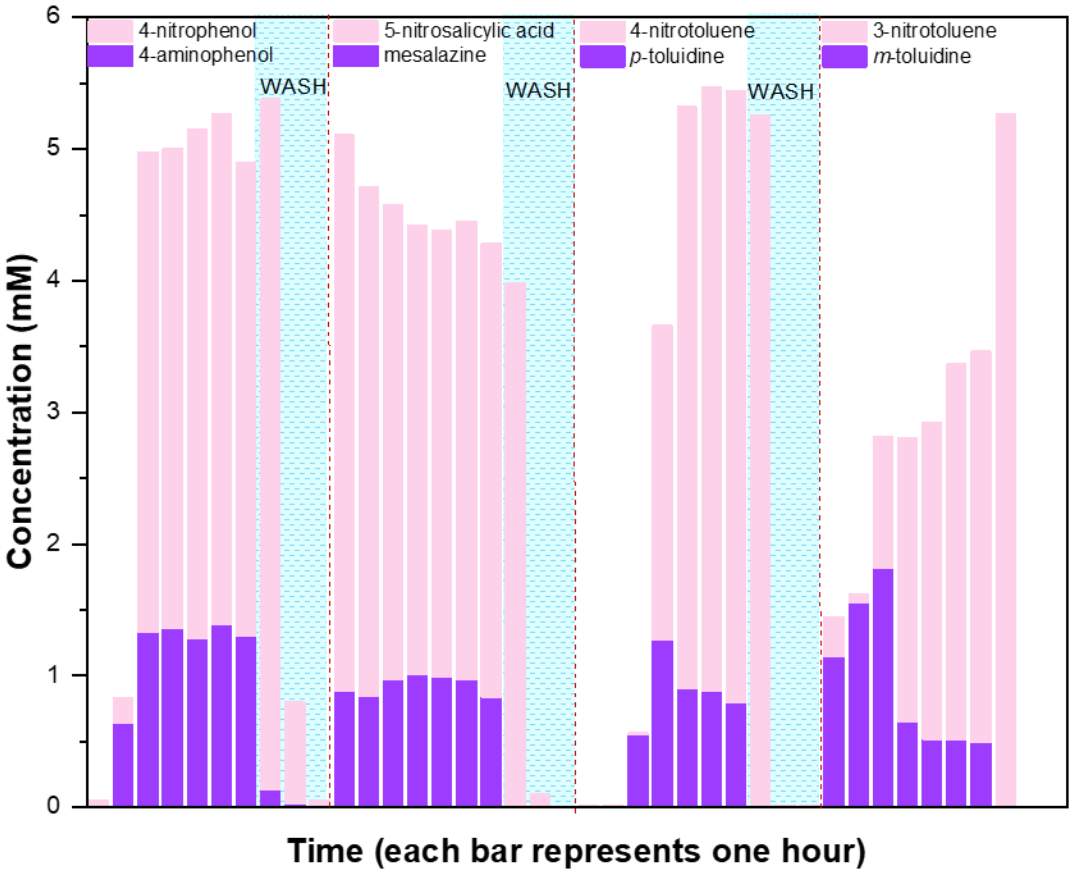


Figure 6-9: Results of H-cube reduction of nitro-compounds in flow; 5 mM 4-nitrophenol in KP_i pH 6, 10% DMSO, 10 mM 5-nitrosalicylic in Tris HCl pH 8, 10% DMSO, 5 mM 4-nirotoluene in KP_i pH 6, 30% DMSO and 5 mM 3-nitrotoluene in KP_i pH 6, 30% DMSO. Each bar of the graph represents one hour. The first two hours of each experiment were carried out at a flow rate of 2 mL min^{-1} to achieve steady state then the flow rate was lowered to 0.1 mL min^{-1}. A short wash phase was completed after each compound (shaded area). All experiments were at 4 bar H_2, 40°C.

The results of this experiment showed that the catalyst remained stable and active throughout the changes in pH and tolerated the DMSO cosolvent up to 30% v/v. Conversion to product was low across all substrates for this experiment, but it can be seen in Table 6-2 that the enzyme used in this experiment had quite a low activity compared with some of the other batches used.

6.11 Intermediates

The conversion from nitro to amine is a 6-electron reduction occurring via three main steps with the production of two intermediate species shown in Figure 6-10. Previous work carried out by Sokolova *et al.* on hydrogenation of nitro compounds using Hyd1/C detected no presence of the nitroso in any analysis.[4]

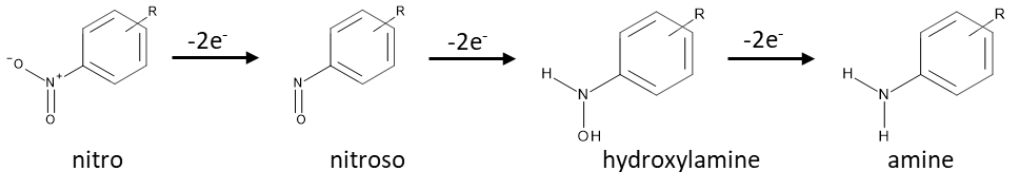


Figure 6-10: General mechanism for the 6-electron reduction of nitro to amine, proceeding via two intermediate steps

Solokova *et al.* detected no presence of nitroso in any of their batch reactions and determined that where the hydroxylamine was detected, this had been produced via a 4-electron transfer. Subsequently, any hydroxylamine produced was further reduced to the amine, and there was no evidence to suggest that accumulation of hydroxylamine hindered full conversion to product.

Experiments performed using columns 1 and 2 (Figure 6-7) displayed a large unknown peak in the HPLC analysis which was presumed to be the hydroxylamine. There is no standard for this species so it cannot be identified, but it was eluted close to the amine peak, in the region expected for the hydroxylamine. Columns 1 and 2 were primarily used to establish conditions for the experiments and it was noted that with a slower flow rate and increased temperature, this peak was much smaller.

Once conditions for any given experiment were optimised, it was possible to almost eliminate this peak altogether when the system reached a steady state. The HPLC trace in Figure 6-12a shows an

intermediate peak at RT 6.8 mins which does not correspond to either the amine (RT 10.1 mins) or the nitro (RT 21.1 mins) so is presumed to be due to the formation of hydroxylamine. This peak could be seen to gradually decrease in size as the system reached a steady state. It can be seen from the trace in Figure 6-12b that the peak at RT 6.8 was almost negligible, and the amine peak had increased, indicating the hydroxylamine was converting to product.

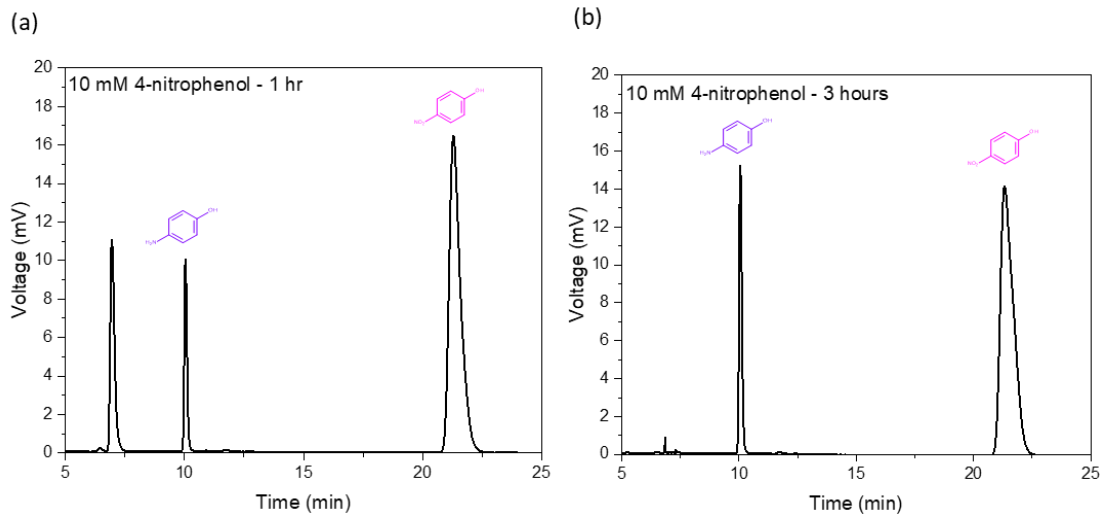


Figure 6-11: HPLC analysis of two samples taken at time points (a) 1 hour and (b) 3 hours of an experiment to synthesise 4-aminophenol from a 10 mM solution of 4-nitrophenol. Both graphs display a peak at 10.1 mins that corresponds to the amine product, and 21.1 mins that corresponds to the nitro substrate. Another peak can be seen at 6.8 mins which is an intermediate presumed to be the hydroxylamine, this peak can be seen to reduce over time as the experiment reaches a steady state.

It was not possible to quantify the hydroxylamine from the HPLC, due to lack of standards with which to produce a calibration curve. It was noted that for most of the compounds used in this project, the amount of hydroxylamine was not significant by the time the system reached a steady state, and did not impact conversion to product. There were exceptions with the halogenated compounds and these will be discussed in section 6.16.

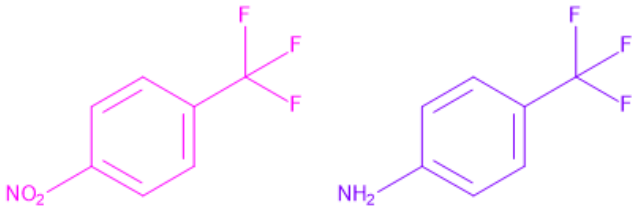
6.12 Increasing solubility of hydrophobic compounds

It was previously mentioned in 6.3 that many of the most of the compounds used in this project are not fully soluble in water, with the exception of 5-nitrosalicylic acid. The Bio2Amine catalyst is known to tolerate 10-30% DMSO well. [8] Protocol at HydRegen is to use 10% DMSO as standard in the H-cube, as this seems to help the compounds flow through the column and interact with the enzyme without adsorbing to the column. For this reason, 10% DMSO v/v was added to 5-nitrosalicylic acid. Solubility studies were carried out for the other compounds used in the project and it seemed that all but the halogenated compounds would dissolve in a solution containing 30% or less of DMSO. Therefore, DMSO was used as the cosolvent of choice, using the minimum percentage necessary to dissolve the compound fully.

Solubility studies for both 3-nitro toluene and 4-nitro toluene seemed to indicate that the substrates were fully dissolved in KP_i with 30% v/v DMSO. However, early experiments using both of these compounds showed low conversion to product. HPLC analysis indicated that the sum of the concentration of substrate and product did not equal the concentration of the starting material. There were no significant intermediate peaks on the HPLC, and the wash phase did not account for the shortfall. This indicated that perhaps the substrate was not fully dissolved and was being trapped in the column filter. Heating both of the substrate solutions to 40°C resolved this issue.

DMSO is a polar aprotic solvent and the halogenated compounds used in this project were shown to be insoluble in 30% DMSO, so an alternative cosolvent had to be found for these compounds.

Table 6-3: Results of solubility tests carried out on 5 mM 3-nitrobenzotriluoride and 5 mM 3-trifluoromethylaniline in potassium phosphate buffer (KPi) pH 6.



Cosolvent	3-nitrobenzotrifluoride	3-trifluoromethylaniline
10% DMSO	×	×
20% DMSO	×	×
30% DMSO	×	×
10% MeCN	×	×
20% MeCN	×	×
30% MeCN	×	×
10% EtOH	×	×
20% ETOH	✓	✓

Table 6-3 shows the results of the solubility tests for both 3-nitrobenzotriluoride and its corresponding aniline product, 3-trifluoromethylaniline. This was found to be insoluble in both 30% DMSO and 30% MeCN. Solubility tests on ethanol showed that the compound would dissolve in buffer with 20% EtOH, although the solution had to be heated to 35°C to dissolve.

Heating the solutions to aid solubility was not an issue as the experiments in the H-cube were carried out at 40°C.

6.13 Effect of flow rate on conversion.

One of the parameters that can be modified is the flow rate. The range on the ThalesNano H-cube is 0.1 mL min^{-1} to 3 mL min^{-1}, selecting a faster flow rate will allow more solution to flow through

the column and give a higher volume output over time. However, in order to achieve good conversion, the substrate requires contact with the catalyst so that electron transfer can take place. Figure 6-12b shows how a faster flow rate allows more substrate through the column, but this can overcrowd the column and not allow the substrate to come into contact with the catalyst. When the flow rate is slowed down, less substrate flows over the catalyst, but the substrate has sufficient residence time to allow the transfer of electrons and so the substrate is reduced. There is a balance to be achieved by selecting a flow rate slow enough to achieve good conversion but running each substrate for the shortest time possible; in order to allow multiple successive compounds to be synthesised from an active catalyst.

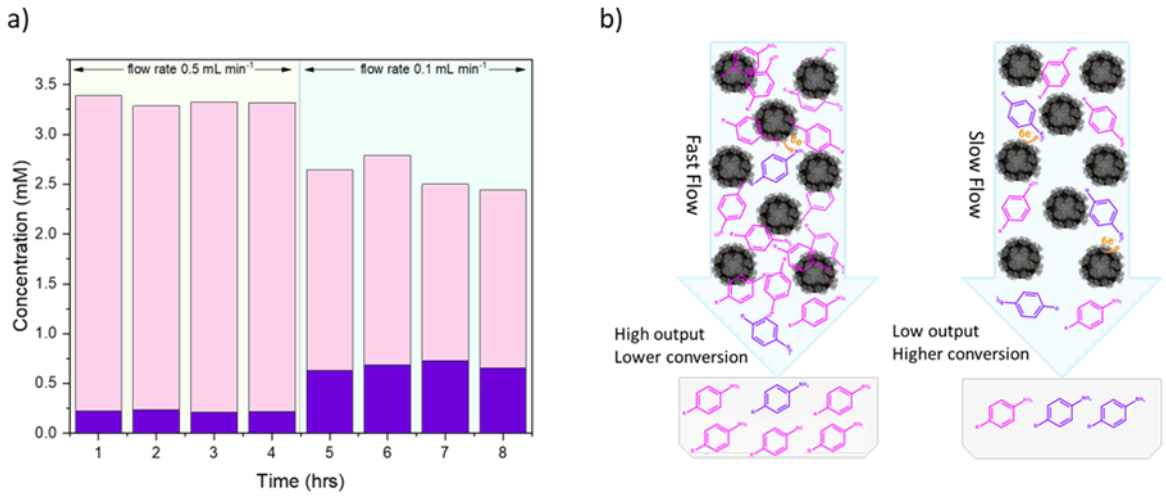


Figure 6-12: a) HPLC analysis of the output solution from experiment containing 5 mM 4-nitrotoluene solution with 30% v/v DMSO in KP_i pH 6. b) schematic representation of the effect of using different flow rates.

An experiment was performed to determine the effect of flow rate on conversion (Column 3 Figure 6-7). A 5 mM solution of 4-nitrotoluene was prepared in KP_i, pH 6 with 30% DMSO and heated to 40°C to allow the compound to fully dissolve. This was initially flowed through the H-cube at a rate of 2 mL min^{-1} to allow the system to reach a steady state. After this time the flow rate was slowed down to 0.5 mL min^{-1} for a period of 4 hours with aliquots taken for analysis each hour. The flow

rate was then slowed down further to 0.1 mL min^{-1} for another 4 hours and aliquots taken for analysis. The analysis is shown in the graph in Figure 6-12a shows that the output solution contains around 4-5% product in the first half of the experiment and this improves to around 14-15% when the flow rate is lowered, allowing the compound to have more residence time on the column. This experiment was one of the earlier experiments which used a short column, so the results were further optimised by increasing the column size and using more catalyst (Figure 6-7, column 7) where the conversion to product was improved to 25%.

6.14 Effect of concentration on conversion.

The effect the concentration of the liquid feed has on the conversion to product is similar to the effect of adjusting the flow rate. Just as an increased flow rate allows more molecules to pass through the column, so does increasing the concentration of the liquid feed. This can result in an overcrowding of substrate molecules that cannot access the catalyst for electron transfer to take place. Figure 6-13 shows the HPLC results of the output collection from an experiment that used two different concentrations of 5-nitrosalicylic acid (column 5, Figure 6-6). The conditions for the 5-nitrosalicylic acid experiments will be discussed fully in 6.17 which looks at the synthesis of mesalazine.

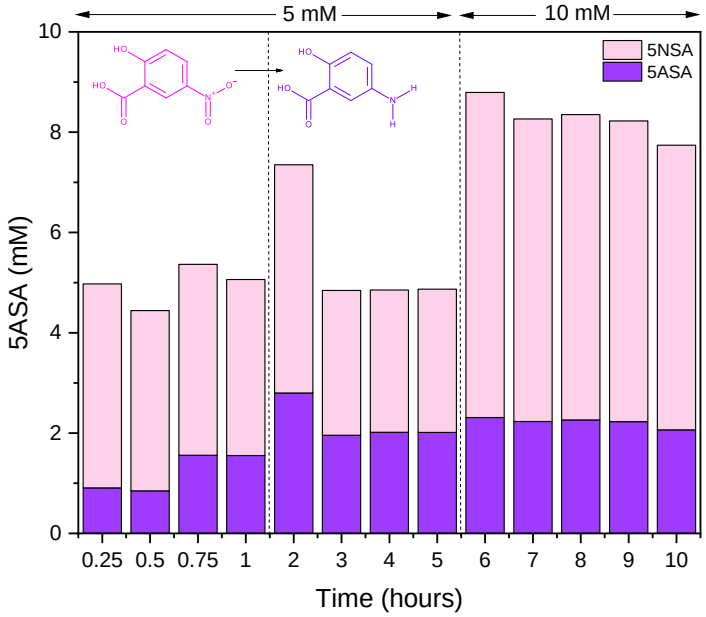


Figure 6-13: HPLC analysis of the output solution from experiment to determine the effect of concentration on the conversion to product. Liquid feed contained 5/10 mM 5-nitrosalicylic acid with 10% v/v DMSO in 100 mM Tris HCl, pH8.

The results here show that there was no improvement in the concentration of 5-amino salicylic acid in the output, after reaching steady state it can be seen that there is a concentration of approximately 2 mM product in the output from 5 mM liquid feed (2-5 hours on the graph). The concentration of the liquid feed was increased to 10 mM from 6-10 hours. Although there is a significant increase in the concentration of 5-nitrosalicylic acid in the analysis, the concentration of product remains constant at approximately 2 mM. This suggests that a lower concentration of substrate in the liquid feed is optimal for higher percentage conversion.

6.15 Increasing catalyst

Early experiments used small quantities of catalyst as the catalyst is expensive and during the optimisation phase the system was being put through changes in temperature, flow rate, pH and H_2 pressure. Any of these changes in parameters could cause have inactivated the enzyme, so small amounts were used for testing. Columns 1 and 2 from Figure 6-7 were used as optimisation

experiments, so will not be included here. For the purposes of comparing the catalyst, the synthesis of 4-aminophenol from a 5 mM solution of 4-nitrophenol will be used. This will compare the activity of the catalyst in columns 3, 4 and 5, as in each of these experiments all other conditions (temperature, H_2 pressure, pH, cosolvent) were the same.

Table 6-4: Details of column length, catalyst activity and conversion to product for the reduction of 4-nitrophenol to 4-aminophenol. All experiments used 5 mM starting concentration of 4-nitrophenol in KP_i, pH 8 with 10% v/v DMSO. All experiments were performed at 40°C, 2 bar H_2 using a flow rate of 0.1 mL min^{-1}.

Column	Column length (mm)	Total activity of enzyme loaded (U)	Conversion to product (%)
3	30	1.34	9
4	30	9.2	35
5	70	3.6	45

Table 6-4 gives the details of the total activity of enzyme loaded into each column (this was detailed in section 6.9). It can be seen that column 3 had a comparatively low activity and this was evident in the results which showed only 9% conversion to product. Column 4 had the highest activity loaded of any of the experiments in this chapter. This was due to a 1 mL aliquot of enzyme being condensed into 200 µL, which is the maximum volume that the 30 mm column can hold. The results from this experiment show almost four times the conversion to product for this experiment. This would suggest that the higher the catalyst loading, the greater the conversion to product.

In Experiment 5, a longer column was used, which can accommodate 500 µL of enzyme, the results of this are also shown in Table 6-4. This shows a conversion to product of 45% although the total enzyme activity loaded was only half that of column 4. This indicates that the catalyst loading is not the only important parameter and may suggest that loading too much catalyst into a column does not allow the substrate to access the catalyst efficiently. A longer column length allows for even

distribution of the enzyme and therefore the substrate can access the catalyst more effectively. The substrate has a greater retention time on a longer column, allowing more opportunity for electron transfer to take place.

Increasing the amount of catalyst used in an experiment seems to have a positive impact on conversion to product, but equally retention time is key to conversion. Due to the constraints of the model of H-cube used in this project, it was not possible to slow the flow rate to less than 0.1 mL min. This meant that the only way to increase the retention time on the column was to use a longer column. These results suggest that both the column length and the catalyst loading are important for good conversion, but more results are needed to establish optimum enzyme activity loading.

6.16 Optimising tricky compounds

As discussed in section 6.2.1, halogenated nitro amines are desirable compounds in medicinal chemistry due to lipophilicity. However, these compounds present challenges not just in their solubility (section 6.3) but also achieving complete conversion from the nitro to amine which requires a 6-electron transfer. As previously mentioned in section 6.11, one common problem when synthesising amines is the production of the undesirable intermediates. The accumulation of hydroxylamine can be quite significant, especially for compounds with an electron withdrawing group (EWG)[14] such as the halogenated compounds 5-chloro-2-nitropyridine and 3-nitrobenzotrifluoride used in this project. The conversion of hydroxylamine to amine is the slowest step of the 6-electron reduction of nitro to amine, and in some cases the reduction can stop at this stage.[14] Addition of vanadium salts has been shown to decrease the accumulation of hydroxylamine in Pt and Pd catalysis.[14] Bisagni *et al.* added vanadium pentoxide (V_2O_5) to their nitro reductase

reactions in order to achieve full conversion to amine for reactions that were stuck at the hydroxylamine species.[2]

Figure 6-14a shows the HPLC analysis of the collection solution from one experiment (column 4 Figure 6-7) using a liquid feed of 5 mM 3-nitrobenzotrifluoride. The graph shows no trace of 3-trifluoro methylaniline product in the analysis of the collection solution. There was however an unknown peak (RT 7.37 mins) in the HPLC analysis that did not correspond with either the nitro (RT 9.65 mins) or amine (RT 5.33 mins) standards. Figure 6-14 shows there was only approximately 1 mM of the 3-nitrobenzotrifluoride starting material present in the collection solution. This suggests that reduction was taking place and most of the liquid feed was being converted to the hydroxylamine intermediate and the reaction was stopping there.

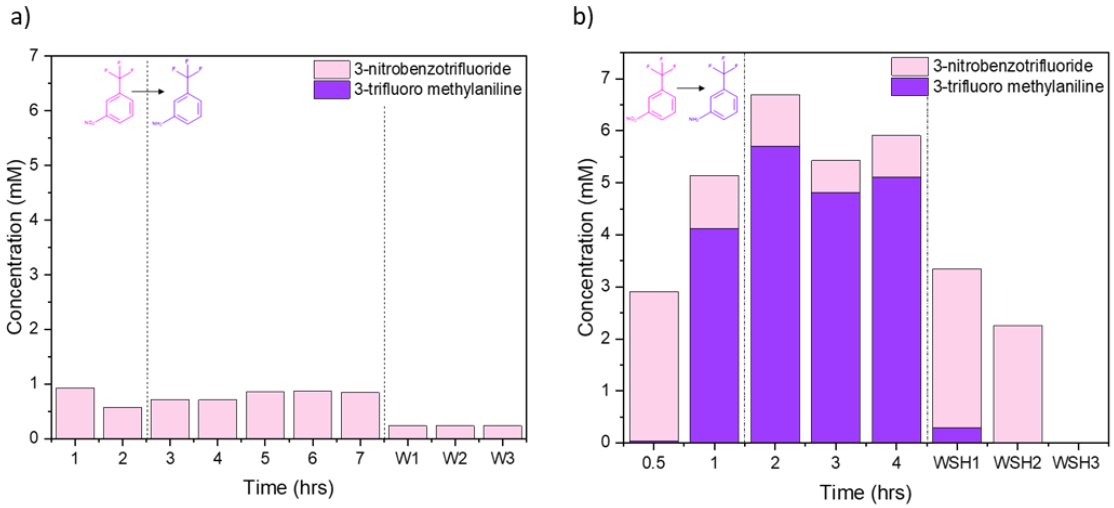


Figure 6-14: HPLC analysis of collection solution. a) liquid feed contains 5 mM 3-nitrobenzotrifluoride with 25% EtOH v/v made up in 10 mM phosphate buffer, pH6. b) liquid feed contains 5 mM 3-nitrobenzotrifluoride with 25% EtOH v/v made up in 10 mM phosphate buffer, pH6 with ~ 0.1 mM vanadium pentoxide.

Bisagni *et. al* reported improved conversion of nitro to aniline in flow with the addition of 2 mM co-catalyst vanadium pentoxide.[2] A suspension of 1 mM V_2O_5 was prepared and mixed thoroughly before adding an aliquot to the liquid feed which would give an overall concentration of ~ 0.1 mM

V_2O_5 in the 5 mM 3-nitrobenzotrifluoride liquid feed. Vanadium pentoxide is sparingly soluble in buffer, despite the 25% v/v EtOH required to dissolve the 3-nitrobenzotrifluoride small crystals of undissolved salt could be observed in the feed which suggests that the final concentration of V_2O_5 was much lower than 0.1 mM. The liquid feed has to pass through a frit into the H-cube, so any undissolved salt would be removed. The results are shown in Figure 6-14b, and show that even a small amount of co-catalyst present in the feed can have quite an effect, which in this instance has increased from no amine product to 85% conversion. The proposed mechanism is shown in Figure 6-15, the addition of V_2O_5 acts as a disproportionation catalyst to the hydroxylamine and allows complete reduction to the amine to take place.

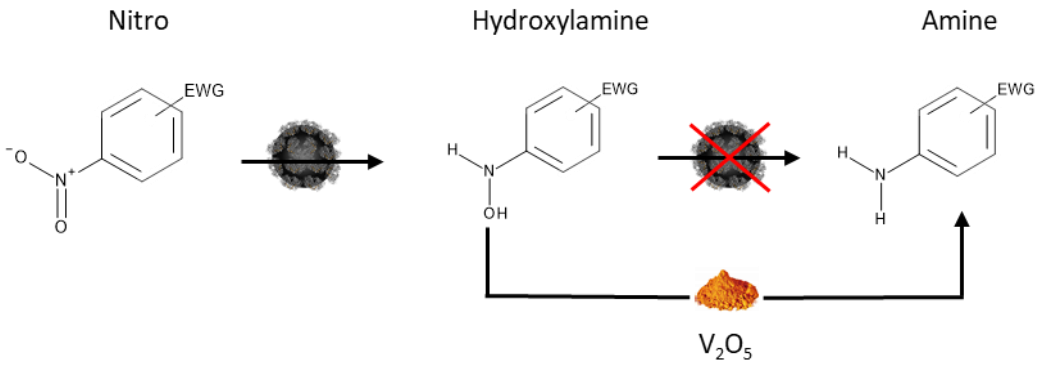


Figure 6-15: Proposed reaction mechanism for vanadium-catalyzed reduction of a nitroarene containing an electron withdrawing group (EWG) such as a halogen. The V_2O_5 acts as a disproportionation catalyst which disproportionates the hydroxylamine in the reaction completing the reduction to amine.

Another compound that was difficult to reduce in the H-cube was 5-chloro-2-nitropyridine. Figure 6-16a shows the HPLC analysis of the collection solution from one of the earlier experiments (column 4 Figure 6-7) that used a liquid feed of 5 mM 5-chloro-2-nitropyridine with 25% DMSO as cosolvent. It can be seen from the graph that a steady state is achieved after 2-3 hours, but only a small amount of the 2-amino-5-nitropyridine (purple) can be seen in the analysis of the collection

solution. The 5-chloro-2-nitropyridine (pink) can be seen in the analysis seeming to pass through the column without converting. The HPLC analysis indicated no intermediate species after the system reached a steady state, just low levels of amine representing poor conversion. Figure 6-16Figure 6-14b shows that the addition of V_2O_5 as co-catalyst dramatically improves the conversion to the aniline.

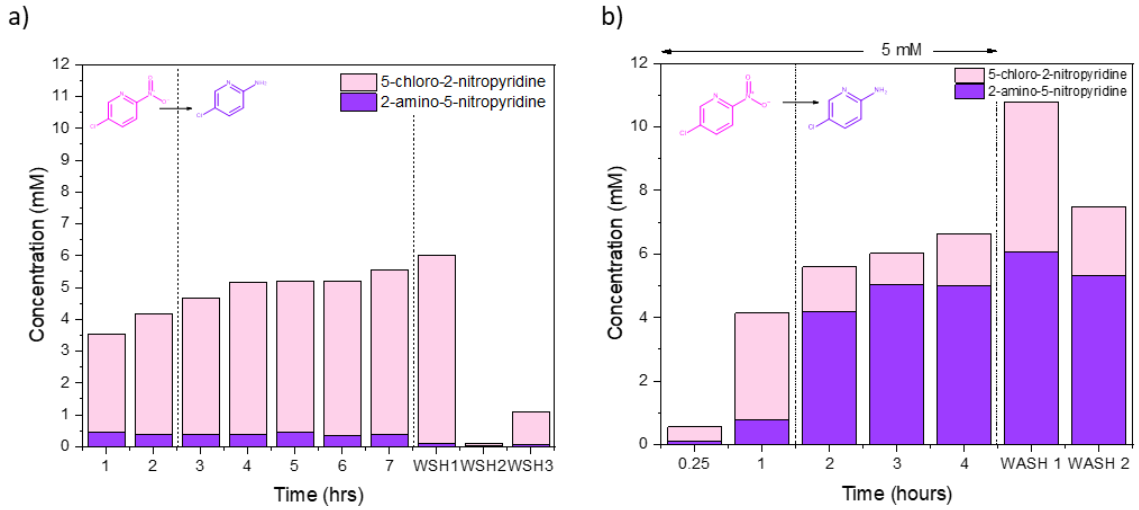


Figure 6-16: HPLC analysis of collection solution. A) liquid feed contains 5 mM 5-chloro-2-nitropyridine with 25% DMSO v/v made up in 10 mM phosphate buffer, pH6. b) liquid feed contains 5 mM 5-chloro-2-nitropyridine with 25% DMSO v/v made up in 10 mM phosphate buffer, pH6 with ~ 0.1 mM vanadium pentoxide

This analysis suggests that for compounds that are difficult to convert, especially those with an EWG, show that the addition of a small amount of a metal co-catalyst such as V_2O_5 can improved the conversion to amine.

6.17 Mesalazine

There were two main aims to this project. The first being the development of a screening/library-building tool to reduce small quantities (2-4 mg) nitro compounds to their corresponding amine for use on a cellular scale. The second aim was to be able to scale up any reduction of interest to

synthesise ~100 mg of product. To demonstrate this, the compound 5-nitrosalicylic acid has been chosen as a case study, as reduction of this compound produces the drug mesalazine.

This compound presented a particular challenge, due to the properties of the molecule, which affected its pH when in solution. The NO_2 group in the *meta* position on 5-nitrosalicylic acid, has an electron-withdrawing effect. There is no resonance when the nitro is in the meta position, so it cannot stabilise the carboxylate ion through resonance. This makes it harder to deprotonate the carboxylic acid which helps keep the solution more basic. Upon reduction to the amine, the electron-withdrawing effect is lessened, however, the issue of resonance remains. This means the EDG will not destabilise the carboxylic acid, and the solution turns more acidic as the concentration of amine is increased in the output. This can cause a significant change in the pH of the solution. Although the enzyme is tolerant to a range of pH conditions, as mentioned previously, it was unknown how the enzyme would behave when exposed to significant fluctuations in pH over a sustained period of time.

6.18 Selecting an appropriate buffer

Initial experiments for all compounds using column 1 (Figure 6-7) were carried out using 10 mM KP_i, as this was known to work well in the H-cube for a number of nitro compounds that had previously been used at HydRegen. A 10 mM solution of 5-nitrosalicylic acid was prepared in 10 mM KP_i with 10% DMSO and flowed through the H-cube under the conditions shown in Figure 6-7. After flowing for 3 hours, the H-cube became blocked and upon investigation it was observed that the collection solution had thickened to a gel-like substance and had blocked the flow tubes. HydRegen had been running their batch experiments using this compound in 50 mM Tris HCl, pH8, as this would allow any decrease in pH to stay within the range suitable for the enzyme.

A fresh solution 5-nitrosalicylic acid was prepared in 10 mM Tris-HCl, pH 8 with 10% DMSO and set to run overnight. In the morning, it was apparent that the flow tubes had once again become blocked and the collection solution was once again a gel like substance. The pH of this was checked and found to be 2.4, this is out of the pH range that the enzyme is known to work well at.[8] The H-cube was flushed through to clean the column and then a solution of 4-nitrophenol was flowed through to check the activity of the enzyme. There was no conversion, which indicated that the enzyme had denatured and was no longer active.

A further experiment was run using column 2 (Figure 6-7) this time using 100 mM Tris-HCl, pH8. HydRegen always select the lowest concentration possible for their buffers in order to minimise issues around product separation. However, it was clear that the buffering capacity of 50 mM Tris-HCl was insufficient to buffer against the decreasing pH caused by the 5-amino salicylic acid product.

6.19 Optimisation experiments

Further experiments involving 5-nitrosalicylic acid were carried using columns 1-3 (Figure 6-7) to establish optimum temperature, H_2 pressure and flow rate, and these have been discussed earlier in this chapter. The effect of concentration on conversion was also explored and this was discussed in 6.14. The rest of this chapter will consider the scale-up experiments, carried out with the aim of synthesise 50-100 mg mesalazine.

6.20 Scale up of mesalazine synthesis

These experiments used columns 4-6 (Figure 6-7) and were set up with the in-line NMR so that overnight analysis could be carried out. It was shown in section 6.14 that a lower concentration of substrate produced equally good conversion to product. However, for the in-line NMR analysis, it

was felt that a higher concentration would give more accurate analysis, so a 10 mM solution of 5-nitrosalicylic acid was made up in 100 mM Tris HCl, pH8 with 10% DMSO. The flow system was connected to the NMR as shown in Figure 6-17, with the output solution from the H-cube being pumped continuously through the NMR. This was set to analyse the output every hour. The output solution was then collected into a vessel for purification.

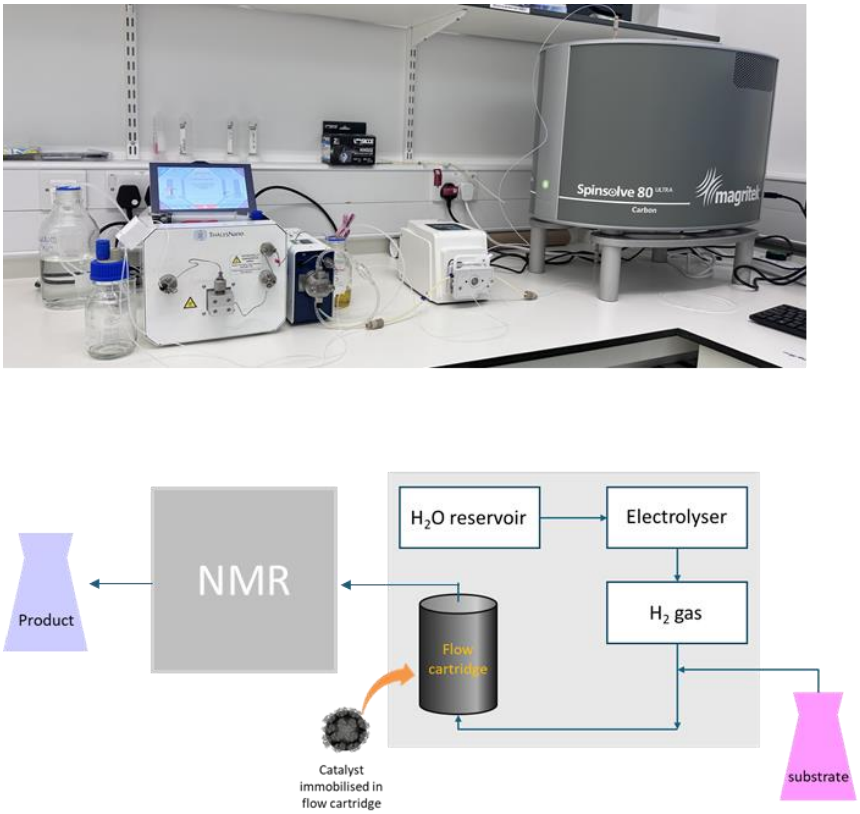


Figure 6-17: (top) In-line NMR analysis set-up showing output from H-cube flows directly through NMR to allow real time analysis of product. (bottom) schematic representation of flow set-up with in-line NMR analysis.

In-line NMR analysis was carried out over a period of 12 hours and the results of a diagnostic peak for each compound (Figure 6-18b) were integrated to calculate the concentration in the output solution. The results of these concentrations over time are shown in Figure 6-18a. This shows a steady decrease in the concentration of the substrate, 5-nitrosalicylic acid (shown in pink) from 10 mM at the start of the experiment to approximately 8 mM by the time the system reached a steady

state after 4 hours. The concentration of 5-aminosalicylic acid (mesalazine) increased over the same time period to reach a concentration of approximately 2 mM by the time the system is at a steady state. It is important to note that the system takes longer to reach a steady state than in previous experiments described in this chapter. This is because the flow rate was set to 0.1 mL min^{-1} from the start of the experiment due to the in-line analysis requiring a steady flow rate.

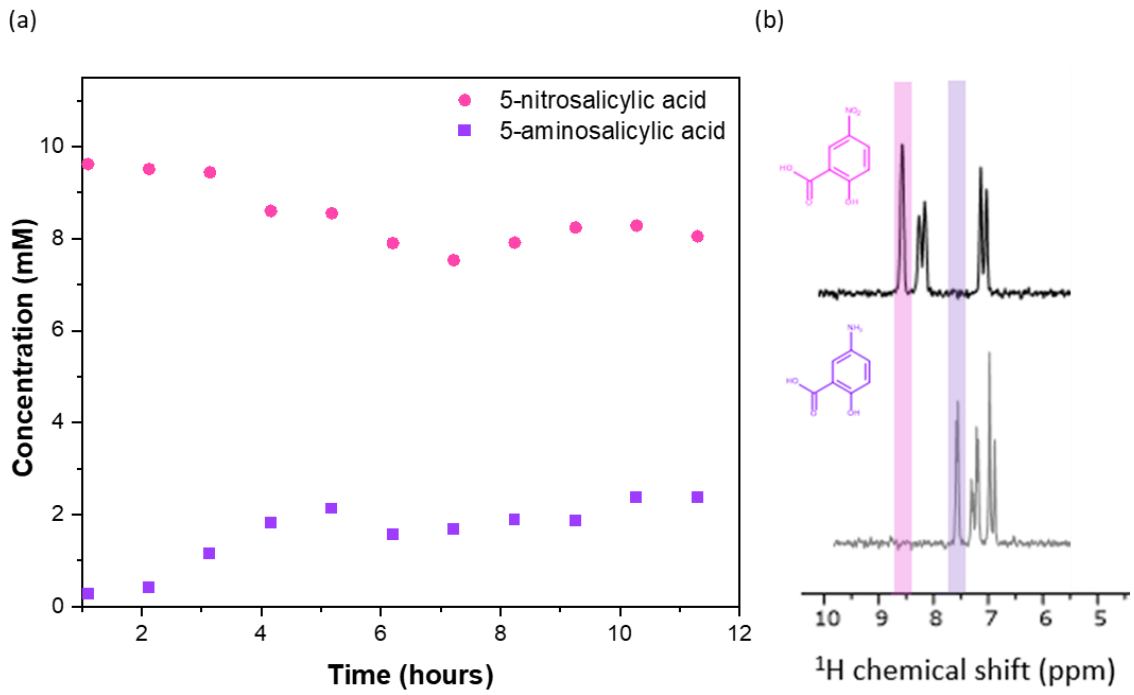


Figure 6-18: (a) Graph to show concentration of substrate, 5-nitrosalicylic acid and product 5-aminosalicylic acid over time determined by in-line ^{1}H-NMR analysis and calculated by integrating diagnostic peaks shown in (b) 5-nitrosalicylic acid (pink) and 5-aminosalicylic acid (purple)

Whilst conversion to product is only around 20%, this has been consistent for all of the 5-nitrosalicylic acid experiments carried out during this project. Higher conversions were achieved with other nitro compounds, indicating that optimal conditions had possibly not been established for this compound. It was reassuring to observe that the concentration of substrate plus the concentration of product equalled the concentration of the feed, indicating that no intermediate species were formed in the process. The low conversion did not affect the subsequent isolation of product which will be described next.

6.21 Isolated yield of mesalazine

A total of 102 mL of the output collection was collected overnight. HPLC analysis of this collection solution showed a concentration of 2.2 mM product present in the collection. A wash cycle was also carried out at the end of the experiment, and from this 180 mL output collection was collected. HPLC analysis of this showed a concentration of 2.3 mM 5-aminosalicylic acid so these two solutions were combined when isolating the product.

A total of 282 mL of the output collection was adjusted to pH 2 by dropwise addition of 1M HCl. The solution was then combined with an equal quantity of ethyl acetate in a separating funnel to separate the nitro from the amine. The 5-aminosalicylic acid remains in the aqueous layer whilst the 5-nitrosalicylic acid goes into the organic layer. The aqueous layer was then dried using a Biochromato Smart Evaporator. The dry solid was then weighed (303 mg). Calculation to determine yield of product from a 2.2 mM solution of 5-aminosalicylic acid when flowed over the time period of the experiment show a maximum yield of 94 mg of product could be obtained. This indicates that impurities remain. ^{1}H-NMR analysis of the isolated product is shown in Figure 6-19, this confirms that the product is 5-aminosalicylic acid and has been successfully separated from the 5-nitrosalicylic acid. However, it is clear from the ^{1}H-NMR spectra that there are impurities in the sample, probably tris salts from the buffer.

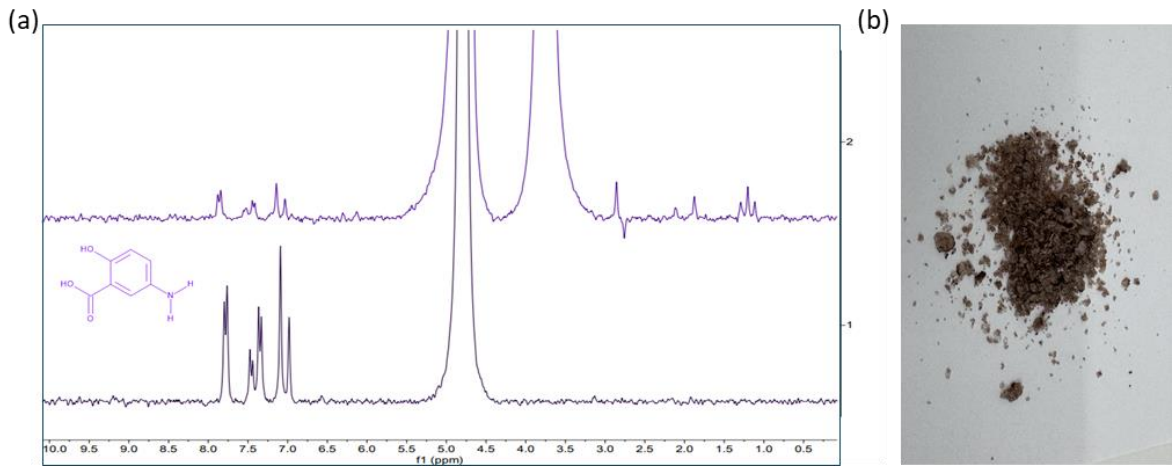


Figure 6-19: (a) ^{1}H-NMR spectra (80 MHz, 298 K, 10% D_2O in H_2O) of 10 mM standard solution 5-aminosalicylic acid (bottom trace) and isolated yield diluted in water (top trace). (b) photo of dried, isolated product.

Several solvents including acetone, dichloromethane (DCM) and dimethylformamide (DMF) were used to try to separate out the tris salts from the isolated product. If a solvent could be found that the 5-aminosalicylic acid was soluble in but tris was insoluble (or vice versa) then it would be possible to purify the 5-aminosalicylic acid. Unfortunately, either both compounds were soluble or both insoluble, so separation could not be achieved. It would be possible to separate by column chromatography, but time constraints prevented further investigation of this.

6.22 Conclusion and future work

The aim of this project was to demonstrate a biocatalytic flow system for use as a library building tool for medicinal chemistry programmes. It was demonstrated that it is possible to reduce multiple successive compounds using the Bio2Amine catalyst in flow with only a short wash phase necessary to clean the column completely ready for the next compound.

Conditions such as temperature, H_2 pressure, flow rate and pH were explored within the constraints of the ThalesNano H-cube model used for the project. A set of parameters were established as a starting point for most nitro compounds. However, it was clear from the results that each compound has its own unique properties, and it may be necessary to use alternative cosolvents to increase solubility. Future work could explore the enzymes tolerance of other cosolvents, as well as more comprehensive studies into the effect of pH and temperature.

The reduction of some nitro compounds can produce intermediates which stop the reaction. Conversion to amine can be achieved by the addition of a small quantity of V_2O_5 as co-catalyst.

The synthesis of mesalazine was used as a case study to investigate scaling up the reaction to allow larger quantities of product to be synthesised. Due to time constraints, full purification of this product was not achieved so it is uncertain the final yield of product. However, analysis of the collection solution showed a product concentration of 2.2 mM, equivalent to 94 mg in sample collected during one overnight experiment. This demonstrates a simple method of synthesising larger quantities of product. Some of the nitro compounds used in this project achieved significantly better conversions than the mesalazine reaction, and would therefore produce higher yields in a shorter time frame.

It was shown that the quantity of catalyst together with retention time are key parameters to good conversion. However, further work is required to optimise these conditions. It is possible that simply slowing the flow rate further would increase conversion, as this allows the substrate longer residence time on the column. The model of H-cube used for this project had a minimum flow rate of 0.1 mL min^{-1} but other models are available with slower flow rates.

Overall, this short project demonstrated a versatile biocatalyst capable of synthesising amines by hydrogenating of aromatic nitro compounds in flow. The catalyst was stable under a range of conditions (including freezing and defrosting cycles) for up to 8 days, allowing multiple successive compounds to be reduced. With more time it would be interesting to extend the substrate scope and further optimise the system to achieve higher conversion.

Chapter 6 Bibliography

1 Song, J. *et al. Appl. Catal. B Environ.* 2018, **227**, 386–408

2 Bisagni, S. *et al. Curr. Res. Chem. Biol.,* 2022, **2**, 100026

3 Sokolova, D. *et al. Nat. Commun.,* 2024 **15**, 7297–7306

4 Britton, J. and Raston, C. L., *Chemical Society Reviews,* 2017 **46** 1250–1271

5 Zor, C. *et al. Chem. Commun.*, 2017 **53**, 9839–9841

6 Thompson, L. A. *et al. ChemCatChem,* 2020, **12**, 3913-3918

7 Ramirez, M. A. *et al., Front. Catal.,* 2022, **2**, 15

8 Nepali, K., Lee, H. Y. and Liou, J. P., *J. Med. Chem.,* 2019, **62**, 2851–2893

9 Fang, W. Y. *et al., Eur. J. Med. Chem.*, 2019, **173**, 117–153

10 Evans, R. M. *et al.,* JACS*,* 2018, **140**, 10208-10220

11 Murphy, B. J., Sargent, F. and Armstrong, F. A., *Energy Environ. Sci.,* 2014, **7**, 1426–1433

12 Shah, P. and Westwell, A. D., *J. Enzyme Inhib. Med. Chem.,* 2007, **22**, 527–540

13 Studer, M., Neto, S. and Blaser, H. U., *Top. Catal.,* 2000, **13**, 205–212

Conclusion

7.1 Conclusion

The work presented in this Thesis has demonstrated a novel approach to electrochemically recycle cofactors to drive a biocatalytic reaction. The methods described could easily scale up for industrial application and have a range of benefits over existing cofactor recycling systems; on an industrial scale these recycling systems could employ the use of greener energy sources such as solar and wind power. Using electrons as a clean reductant minimises issues around product separation and the associated costs.

Electrochemical cofactor recycling has not yet been widely adopted on an industrial scale, however as companies look for more sustainable synthesis methods, this would be an obvious choice. The work in this thesis has demonstrated a scalable and sustainable method for driving biocatalytic reactions. In chapter 3 characterisation is described for an enzyme moiety from a thermophilic organism, *Ht* HoxFU expressed in *E. coli,* which has the advantage of enabling introduction of mutations. This enzyme worked well over a range of temperature and pH conditions, also with up to 30% cosolvent it maintained its activity. The K_M determined for Ht HoxFU compared well to biological literature values and showed a high affinity for NAD^+ making it a good electrocatalyst. Based on these results a mutation was introduced that allowed the enzyme moiety to increase its selectivity to accept $NADP^+$ as well as NAD^+. This would be advantageous for our electrochemical biocatalysis reactions as it would widen the scope of available enzymes to use for these reactions. The results from the H_2-driven experiments showed promise as full conversion of an IRED reaction was achieved with >99 *ee*. Unfortunately, however, the mutated enzyme moiety mHoxFU did not work well as an electrocatalyst, and would require further mutations to achieve this. This work was beyond the scope of this project, but this could be adopted for a future DPhil student to take up.

The electrochemical cofactor recycling system was then adapted for chapter 4 to look at recycling flavins, after the success a previous DPhil student had with an H_2-driven recycling system. The preliminary electrochemistry for FAD reduction looked promising, but it seemed that the reduced cofactor was not biologically active and could not be used to drive a biocatalytic reaction of interest. The CV of FMN had multiple peaks suggesting the formation of radical species, and it was initially thought that these may form undesirable side-products. However, electrochemically-generated $FMNH_2$ was shown to be biologically active and capable of driving the ENE-RED enzymes to hydrogenate alkenes. This success prompted the exploration of riboflavin as a cheap alternative. Riboflavin is readily available and produced at scale for the food industry, and would be an attractive option for industrial application if successful. The preliminary results for riboflavin showed that it performed as well as FMN in experiments and was a successful electrocatalyst.

The results from chapter 4 were exciting but the time scale of the experiments made them unattractive for industrial application. In order to be considered as a viable cofactor recycling system the experiments would have to achieve a TN of at least 100 (ideally higher) in a significantly shorter time scale. The first step was to optimise the conditions in the homebuilt electrochemical cell by exploring the best applied potential to drive the reaction, it was established that a slightly more negative potential doubled the TN of the RF. Experiments were carried out to determine whether the cosolvent had an effect on the riboflavin conversion. While the results of this were difficult to interpret quantitavely, they did suggest that the presence of a cosolvent could slow down the RF reduction. This could be due to a change of polarity at the surface of the electrode, each electrolyte will have different properties and will affect the RF TN. However, the cosolvents improve the solubility of some of the organic substrates, so are a necessary addition.

In a bid to improve the conversion to product, it was suggested that the substrate was added in doses to prevent inhibition of the enzyme from high concentrations of substrate in solution. Allowing smaller doses to convert to product before the addition of the next dose did improve the results and was adopted in many of the later experiments.

Once the parameters of the electrochemical experiments had been somewhat optimised, it was apparent that the main thing hindering conversion was the electrochemical set-up. To address this, a bespoke electrochemical cell was purchased with the aim of making the experiments more consistent and alleviating some of the issues that such as the crude cell not being gas tight and difficulty excluding light. Unfortunately, the results from this cell did not show any improvement from those achieved in the crude cell.

Later in chapter 5 the scale-up experiments were discussed. Some success was achieved with a large electrolysis bulk cell that used a porous carbon working electrode. These experiments were performed on the bench under a constant flow of N_2, rather than in the anaerobic environment of the glovebox. The FMN experiments achieved 50% conversion to product within 4 hours, achieving the desired FMN TN >100. However, the RF experiments achieved no conversion to product, despite reaching high currents on the chronoamperometry trace. This suggests that the RF is very sensitive to even small amounts of O_2 and is either generating a biologically inactive form, or is generating some undesirable side products. Time was a limiting factor with these experiments, but this electrochemical cell shows real promise for scale up; the earlier electrochemistry experiments used a cell volume of approximately 7 mL and the bulk electrolysis cell used 70 mL, increasing the scale by an order of magnitude. This demonstrated the simplicity of scaling up the electrochemical flavin recycling system which has industrial relevance.

Finally, the electrochemical flavin recycling experiments concluded with a move into flow chemistry. The advantages of flow chemistry which include eliminating mass transport limitations were discussed in chapter 1. Flow chemistry is being increasingly adopted for industrial processes and incorporating electrochemistry into a flow system has the advantage of using electrons as a clean reductant. It is important to note that these experiments were performed on a modified spectrochemical cell rather than a cell designed for synthesis. One of the first challenges was to build an electrode that could support lots of enzyme to achieve the higher currents necessary to scale up the reactions. For industrial processes it would be necessary for the reactions to take place in a single pass rather than the recirculated system that was demonstrated in chapter 5. However, the aim of these experiments was to achieve a high TN and good conversion, and with the limitations of the flow cell a recirculation system was necessary.

High currents were achieved for flow experiments to electrochemically recycle NADH using high surface area electrodes. This shows promise for an electrochemical cofactor recycling system in flow for future work on the NAD(P)H experiments. Disappointingly the ENE-RED enzymes that were being used with the flavin recycling system did not adsorb well to the BP2000, and experiments using the ENE-RED particles had very inconsistent results. It may be possible for future work to look at covalently attaching these enzymes, but due to time constraints it was decided to use these enzymes in solution for the flow experiments.

The RFH_2 driven ENE-RED experiments in flow achieved a 63% conversion to product in only 3 hours, with a Faradaic efficiency of 86%. This represented a RF TN of 126 which met the desired threshold. Issues with O_2 contamination meant that these results were not reproducible. The results from the bulk electrolysis experiments suggested that RF was very sensitive to O_2, so designing a bespoke flow system that would be anaerobic could overcome this issue and make it a viable option.

Chapter 6 moved on to work carried out during an industrial placement at HydRegen, with the aim of developing a biocatalytic flow system for use as a library building tool for medicinal chemistry programmes. This was a good opportunity to build on the experience gained from the results of chapter 5 and contextualise these results with an industrial project.

Medicinal chemists often want to synthesise small quantities of multiple compounds, often similar species, to test on a cellular level. The Bio2Amine catalyst has shown great success at reducing various nitro compounds to their respective amine analogues. For this project, the aim was to be able to reduce multiple successive compounds in a commercially available flow system. The results from Chapter 6 showed that this was possible with a short wash phase necessary to clean the column completely ready for the next compound.

The catalyst would be supplied as a black powder catalyst for use in the ThalesNano H-cube. A set of standard protocol was established to provide the customer with a starting point for most nitro compounds. Conditions such as temperature, H_2 pressure, flow rate and pH were explored; however, it was clear from the results that each compound has its own unique properties, so conditions may need modification to suit a compounds' properties. The project was limited to the 16-week internship, but further work could explore the tolerance of the catalyst to other cosolvents, as well as more comprehensive studies into the effect of pH and temperature.

Also discussed in chapter 6 was the conversion to amine being hindered or even prevented when intermediate species form and stop the reaction. Conversion to amine can be achieved by the addition of a small quantity of V_2O_5 as co-catalyst.

The synthesis of mesalazine was used as a case study to investigate scaling up the reaction to generate larger quantities of product. This is desirable to medicinal chemists when they find a compound that they want to investigate further. The simplicity of the flow system allows more product to be generated by simply flowing for longer. This allowed a quantity of mesalazine to be synthesised overnight which was equivalent to 94 mg. Some of the nitro compounds investigated achieved significantly better conversions than the mesalazine reaction, and would therefore produce higher yields in a shorter time frame.

Further work is required to optimise conditions for the flow system and also increase the substrate scope, but the results were promising. The model of H-cube used in this project had a minimum flow rate of 0.1 mL min^{-1} but other models are available with slower flow rates. It is possible that simply slowing the flow rate further would increase conversion, as this allows the substrate longer residence time on the column

This internship project demonstrated a versatile application of a biocatalyst capable of synthesising amines by hydrogenating of aromatic nitro compounds in flow. The catalyst was stable under a range of conditions which allowed multiple successive compounds to be reduced with a short wash phase between compounds.

The approaches in this thesis have outlined simple scalable ways of using electrons as a clean reductant for biocatalytic reactions. The offer promising ways of incorporating electrochemical cofactor recycling into industrial processes to increase implementation of biotechnology and develop more sustainable routes for organic synthesis.